INVESTIGATION OF THE ADAPTIVE IMMUNE RESPONSE IN MULTIPLE SCLEROSIS

BY

EMMA RATHBONE

A thesis submitted to the University of Birmingham for the degree of

DOCTOR OF PHILOSOPHY

Institute of Inflammation and Ageing

College of Medical and Dental Sciences

University of Birmingham

May 2018

Abstract

In multiple sclerosis (MS), clonally-expanded brain-resident B cells may sustain chronic disease, however their relative contributions versus recently recruited B cells is unclear. Furthermore, pro-inflammatory CD20+ T cells may also be involved in MS pathogenesis. This study aimed to characterise the cerebrospinal fluid (CSF) B cell response in MS and investigate the features of CD20+ T cells.

CSF B cells and antibody-secreting cells (ASC) displayed an activated phenotype and were identified in MS CSF at a higher frequency than controls. In contrast to the periphery, CSF ASC almost exclusively expressed IgG and were strongly Igκ-biased, whereas memory B cells displayed similar immunoglobulin expression profiles in both compartments. MS CSF antibodies were frequently reactive towards EBNA-1, which preferentially induced an Igκ-biased antibody response. Finally, CD20+ T cells displayed a highly activated effector phenotype and were present in the CSF, although their frequencies were no different between MS and other neurological disease groups.

These findings suggest that most CSF B cells result from non-specific recruitment, whereas ASC are involved in a persistent Igκ-biased antigen-driven immune response, which may primarily be directed towards EBNA-1. Despite their highly activated phenotype, a role for CD20+ T cells in MS pathogenesis, if any, remains to be determined.

Acknowledgements

Birmingham – it's been a blast! Firstly, I would like to express my gratitude to my excellent supervisors, Dr John Curnow and Professor Mike Douglas, for support and encouragement over the years. Being in the Curnow Lab gave me the confidence to believe in myself as a scientist and I'm lucky to have been part of the group. Special thanks to the inspirational Dr Graham Wallace for motivation and mentorship during my time at Birmingham.

There are so many people within the Institute of Inflammation and Ageing and the wider College who offered their support and friendship over the years and I'm incredibly grateful for the time and kindness people have shown me on my journey. On a professional and a personal level I'd especially like to thank Lindsay Durant - I miss you and your cakes! I'm also particularly thankful to Dr David Gardner, Dr Matt McKenzie, Scott Davies and Kalvin Sahota for technical help and useful discussions. Thanks to Dr Heather Long for the tetramer staining and to Graham and Dr Zania Stamataki for helpful feedback on my annual progress reviews. A huge thanks to Professor Peter Nilsson and everyone at the SciLife Lab in Stockholm for their kindness and hospitality and for making the 'antigen search' project possible – I'm very lucky I got to do this and really enjoyed my time here. I am also hugely grateful to the Medical Research Council, British Society for Immunology (BSI), European Committee for Treatment and Research in Multiple Sclerosis (ECTRIMS) organisers and the University of Birmingham for financial support and for giving me some fantastic opportunities to present my work at conferences around the world.

Finally, a massive thanks to my wonderful family and friends. Thanks to my home friends, especially Sarah, for positivity and always having time for me. Thanks to my Uni friends, especially Scott – we've got this! Thanks to Sudipta, for being my rock and keeping me sane. And thanks to my amazing mum, for her endless support and for always believing in me.

Publications

The following publication is derived from elements of this thesis:

Rathbone, E., Durant, L., Kinsella, J., et al. 2018. Cerebrospinal fluid immunoglobulin light chain ratios predict disease progression in multiple sclerosis. *J Neurol Neurosurg Psychiatry*, doi: 10.1136/jnnp-2018-317947.

Table of Contents

List of Figures and Tables

Abbreviations

ADCC	Antibody-dependent cellular cytotoxicity
ADCP	Antibody-dependent cell-mediated phagocytosis
ADEM	Acute disseminated encephalomyelitis
AID	Activation-induced cytidine deaminase
AIRE	Autoimmune regulator
ANO2	Anoctamin 2
APC	Antigen presenting cell
APRIL	A proliferation inducing ligand
ASC	Antibody-secreting cell
ATP	Adenosine triphosphate
BAB	Blood-arachnoid barrier
BAFF	B cell activating factor
BBB	Blood-brain barrier
BCL10	B cell lymphoma/leukaemia 10
BCMA	B cell maturation antigen
BCR	B cell receptor
BCSFB	Blood-cerebrospinal fluid barrier
Blimp-1	B lymphocyte-induced maturation protein-1
CCDC85C	Coiled-coil domain containing 85C
CCR/L	CC chemokine receptor/ligand
CD	Cluster of differentiation
CDC	Complement-dependent cytotoxicity
CDR	Complementarity-determining region
CIS	Clinically isolated syndrome
CLP	Common lymphoid progenitor
CLR	C-type lectin receptor
CNS	Central nervous system
CSF	Cerebrospinal fluid
CSR	Class-switch recombination

Ct	Cycle threshold
CTLA-4	Cytotoxic T lymphocyte-associated protein 4
CXCL	Chemokine CXC ligand
CXCR	Chemokine CXC receptor
DC	Dendritic cell
DISC	Death-inducing signalling complex
DMT	Disease modifying therapy
DNA	Deoxyribonucleic acid
EAE	Experimental autoimmune encephalomyelitis
EBNA-1	Epstein-Barr nuclear antigen-1
EBV	Epstein-Barr virus
EDSS	Expanded disability status scale
EMA	European Medicines Agency
ER	Endoplasmic reticulum
Fab	Fragment antigen binding
FACS	Fluorescence-activated cell sorting
FADD	Fas-associated death domain
Fc	Fragment crystallisable
FcRn	Neonatal Fc receptor
FDA	Food and Drug Administration
FDC	Follicular dendritic cell
FLC	Free light chain
GM-CSF	Granulocyte macrophage colony-stimulating factor
GWAS	Genome-wide association study
HERV	Human endogenous retrovirus
His_6-ABP	Hexahistidyl-albumin binding protein
HLA	Human leucocyte antigen
HPA	Human Protein Atlas
HSC	Haematopoietic stem cell
ICAM	Intercellular adhesion molecule
IFI27	Interferon-α inducible protein 27

IFNγ	Interferon gamma
Ig	Immunoglobulin
IL-	Interleukin
IL-7R	Interleukin-7 receptor
ILC	Innate lymphoid cell
Irf-4	Interferon regulatory factor 4
IRIS	Immune reconstitution inflammatory syndrome
ITAM	Immunoreceptor tyrosine-based activation motif
ITIM	Immunoreceptor tyrosine-based inhibition motif
JCV	John Cunningham virus
LMPP	Lymphoid-primed multipotential progenitor
MAC	Membrane attack complex
MAD	Median absolute deviation
MBP	Myelin basic protein
MCL1	Myeloid cell leukaemia 1
MFI	Median fluorescence intensity
MHC	Major histocompatibility complex
MMP	Matrix metalloproteinase
MOG	Myelin oligodendrocyte protein
MPP	Multipotential progenitor
MRI	Magnetic resonance imaging
MRZ	measles, rubella and zoster
MS	Multiple sclerosis
MZ	Marginal zone
NMO	Neuromyelitis optica
NPW	Neuropeptide W
OCB	Oligoclonal band
OND	Other neurological disease
ONID	Other neurological inflammatory disease
PAMP	Pathogen-associated molecular pattern

Pax5	Paired box 5
PBMC	Peripheral blood mononuclear cell
PD-1	Programmed cell death receptor 1
PGAM5	Phosphoglycerate mutase family member 5
PLP	Myelin proteolipid protein
PML	Progressive multifocal encephalopathy
PPMS	Primary progressive multiple sclerosis
PrEST	Protein epitope signature tag
PRR	Pattern recognition receptor
PSGL-1	P-selectin glycoprotein ligand 1
QTRT1	Queuine tRNA-ribosyltransferase 1
RAG	Recombination-activating gene
RLR	Retinoic acid-inducible gene-1 like receptor
ROS	Reactive oxygen species
RRMS	Relapsing-remitting multiple sclerosis
RSS	Recombination signal sequence
S1P	Sphingosine-1-phosphate
S1P1	Sphingosine-1-phosphate receptor-1
SLE	Systemic lupus erythematosus
SNP	Single nucleotide polymorphism
SPMS	Secondary progressive multiple sclerosis
T_{CM}	Central memory T cell
TCR	T cell receptor
TD	T-dependent
T_{EM}	Effector memory T cell
T_{EMRA}	Revertant effector memory T cell
T_{FH}	T follicular helper cell
TGFβ	Transforming growth factor beta
Th	T helper cell
TI	T-independent
TIM-3	T cell immunoglobulin mucin-3

TIMP-1	Tissue inhibitor of metalloproteinase-1
TLR	Toll-like receptor
TNFR	tumour necrosis factor receptor
TNFα	Tumour necrosis factor alpha
TRADD	TNF receptor type 1-associated death domain
TRAIL	TNF-related apoptosis-inducing ligand
Treg	Regulatory T cell
UPR	Unfolded protein response
VCA	Viral capsid antigen
VCAM-1	Vascular cell adhesion molecule-1
VLA-4	Very late antigen-4
Xbp-1	X-box binding protein-1
ZAP-70	Zeta-associated protein kinase-70
ZBTB20	Zinc finger and BTB-containing domain protein 20
2,3-CNPase	2',3'-cyclic nucleotide 3'-phosphodiesterase

CHAPTER 1

GENERAL INTRODUCTION

Chapter 1: General Introduction

1.1 Overview

The ability of the human immune system to recognise and protect against an almost limitless range of antigens whilst simultaneously maintaining tolerance to self is a crucial property of adaptive immunity. Though mechanisms to prevent loss of tolerance exist, these checkpoints may be breached by autoreactive lymphocytes, and the failure to control aberrant responses by these cells can result in autoimmune conditions such as multiple sclerosis. The distinction between the instigators and propagators of autoimmune conditions, and the identification and characterisation of immune cell populations that are involved, can provide important information on the pathological mechanisms, along with the dynamics, of a disease course. In this thesis, I explore the possible contributions of B cells and T cells to the pathogenesis of multiple sclerosis.

1.1.1 Innate Immunity

The innate immune system is an ancient and evolutionary conserved system representing the first immunological line of defence following breach of a physical barrier such as the skin or mucosa. Cells of this system include macrophages, neutrophils, eosinophils and basophils. Innate immune cells utilise pattern recognition receptors (PRRs) to recognise structural pathogen components, termed pathogen-associated molecular patterns (PAMPs), which includes fungal and bacterial cell wall components and viral nucleic acids (Iwasaki and Medzhitov, 2015). PRRs divide into several families including toll-like receptors (TLR), C-type lectin receptors (CLR) and retinoic acid-inducible gene-1 like receptors (RLR) which recognise both extracellular and intracellular microbial components (Thompson et al., 2011).

PAMP recognition induces numerous effector functions such as increased phagocytosis, increased antigen presentation and pro-inflammatory cytokine secretion; a response that is tailored to the type of pathogen recognised (Turvey and Broide, 2010). Importantly, PAMP recognition also leads to activation of the adaptive immune response.

In addition to these cellular components, the innate immune system comprises the complement system, a collection of serum proteins which enhances pathogen removal. These proteins exist as inactive zymogens that are activated in the presence of bacterial products (alternative and lectin pathways) or in the presence of IgG or IgM immune complexes (classical pathway) (Sarma and Ward, 2011). Activation of either pathway results in a proteolytic cascade, which ultimately leads to formation of the membrane attack complex (MAC) and subsequent pathogen lysis (Tegla et al., 2011).

1.1.2 Adaptive Immunity

In many circumstances, innate immunity alone is not sufficient to fully eradicate pathogens from the body. Cells of the adaptive immune system are highly specialised in clearing pathogens by mounting a sophisticated antigen-specific response. In contrast to innate cells, adaptive cells utilise one type of antigen-recognition receptor, each with a single specificity that collectively can recognise an almost limitless number of antigens; this is achieved by gene segment recombination (see section 1.2.2).

In addition to sophisticated antigen recognition, a hallmark of adaptive immunity is the ability of adaptive immune cells to provide long-lived protection by developing ‘memory’, allowing more rapid and efficient responses to previously encountered antigens. These properties, which are normally under strict regulation, are also responsible for the chronic nature of autoimmune conditions.

1.2 B cell biology

1.2.1 B cell lineages

B cells can be divided into two major lineages, B1 cells and B2 cells, which differ in ontogeny, phenotype and anatomical location. B1 cells are a self-renewing population generated in the foetal liver and are enriched in the peritoneal and pleural cavities (Lund, 2008). B1 cells constitutively secrete high levels of IgM in the absence of infection, known as natural antibody, which is rapidly increased following activation. These antibodies are germ-line encoded with limited diversity, they display high polyreactivity and autoreactivity and can recognise repeating non-protein antigens such as microbial components (Nagele et al., 2013).

B2 cells arise from bone marrow progenitors and are made up of follicular B cells and marginal zone (MZ) B cells. MZ B cells express the integrins $\alpha_L\beta_2$ and $\alpha_4\beta_1$ and the sphingosine-1-phosphate receptors S1P1 and S1P3, which retain them in the marginal sinuses of the spleen, permitting continual surveillance for blood-borne pathogens (Weill et al., 2009). Like B1 cells, marginal zone B cells can respond rapidly when activated, differentiating into antibody-secreting cells (ASC) in just one to two days following stimulation (Lund, 2008). B1 and MZ cells express TLR and can respond to PAMPs including carbohydrates and lipid antigens with or without B cell receptor (BCR) ligation (Cerutti et al., 2013). Thus, both B1 and MZ cells possess innate-like features and are ideally located and equipped to rapidly respond to T-independent (TI) antigens.

The other B2 lineage cell type, follicular B cells, are the predominant B cell population in the body and are considered the conventional B cells of adaptive immunity. These cells use the blood and lymph to re-circulate between the follicles of secondary lymphoid organs, where

the majority of these cells are located. Follicular B cells primarily respond to T-dependent (TD) antigens, processing proteins and presenting them to CD4+ T cells loaded onto Major Histocompatibility Complex (MHC) class II molecules, although they can respond to TI antigens (Hoffman et al., 2016; Nutt et al., 2015).

1.2.2 B cell development and V(D)J recombination

The extraordinary range of foreign antigens that the immune system may encounter during an individual's lifetime demands a highly diverse antibody repertoire able to recognise more than $5x10^{13}$ different antigens (Pieper et al., 2013). This diversity is achieved by V(D)J recombination, in which variable (V), diversity (D) and joining (J) germline gene segments are spliced and rearranged to generate antibodies with almost endless specificities from a limited set of pre-existing gene segments. This process is carried out by enzymes encoded by recombination-activating genes (RAG1 and RAG2) which introduce breaks in conserved regions of DNA expressed adjacent to each segment, known as recombination signal sequences (RSS). The segments are liberated and re-joined using DNA repair mechanisms to yield a contiguous V(D)J region, where additional diversity is created through nucleotide deletion and the addition of palindromic (P-) or non-template encoded (N-) nucleotides (Market and Papavasiliou, 2003; Nadel and Feeney, 1997).

The generation of mature naïve B cells expressing functional BCRs is summarised in Fig. 1.1. Following migration of common lymphoid progenitors (CLP) to the bone marrow and expression of Paired box protein 5 (Pax5) to determine B lineage commitment, RAG expression is induced in progenitor (pro)-B cells to rearrange heavy chain V, D and J segments on the first chromosome (Cobaleda et al., 2007). Another enzyme, terminal deoxynucleotidyl transferase (TdT), is also expressed at this stage. TdT helps to generate diversity by adding N-nucleotides to the V, D and J segments and like RAG-1 and RAG-2

enzymes is expressed only during somatic mutation (Melchers, 2015). If gene segment rearrangement is unsuccessful, the B cell attempts to rearrange segments on the second chromosome and if it fails, the cell dies. If successful rearrangement occurs, RAG genes are down-regulated and the heavy chain is expressed on the cell surface with surrogate light chain proteins λ5 and VpreB, marking the start of the pre-B cell phase (Grawunder et al., 1995). At

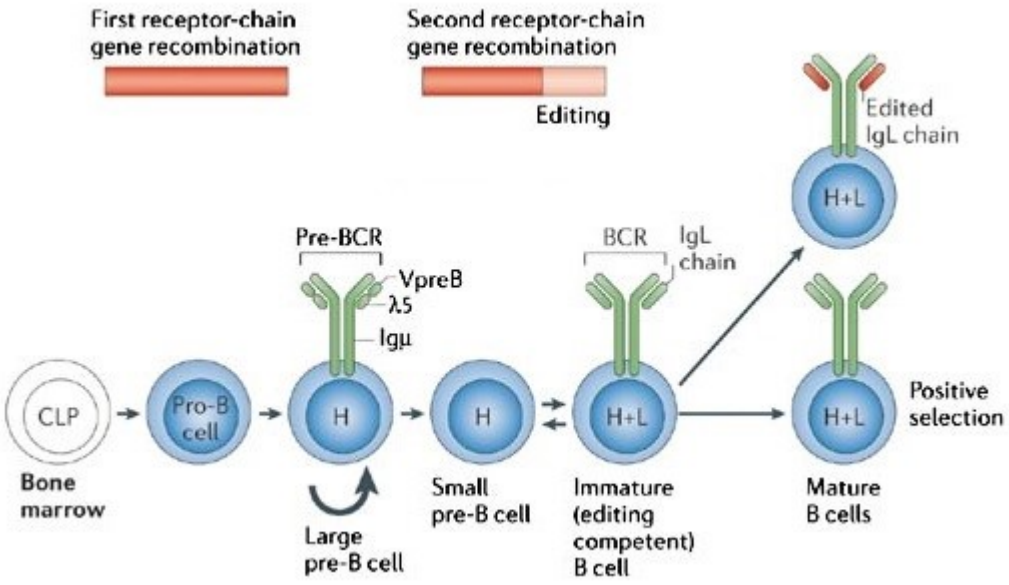

Figure 1.1. B cell development and the generation of a functional B cell receptor. Within the bone marrow, B cells undergo a series of developmental stages marked by gene rearrangement and editing of heavy and light chains. This either results in apoptosis or expression of a unique and fully functional BCR which does not recognise self-antigens. Adapted from (Nemazee, 2006). Reproduced with permission of the copyright owner.

this stage, B cells undergo their first central tolerance checkpoint to eliminate potentially autoreactive B cells, and any pre-B cell receptor with strongly reactive heavy chains are deleted (Basten and Silveira, 2010). Following a proliferative phase in which pre-B cells become large pre-B cells, these cells exit the cell cycle to become small pre-B cells; at this stage, the light chain gene loci are opened, and RAG genes are re-expressed (Nemazee, 2006). Immunoglobulin light chains may be either kappa (Igκ) or lambda (Igλ) isotypes. V and J

segments of the kappa light chain are rearranged first, however if this produces a non-functional product, the kappa locus is removed by the kappa deleting element (KDE) and rearrangement of the lambda light chain commences (Das et al., 2009). If successful, the light and heavy chains associate and the BCR is expressed on the cell surface; the cell is now an immature B cell. Here, cells are met by another central tolerance checkpoint. Immediate apoptosis would be a biologically costly and energy demanding process at this late developmental stage, therefore immature B cells with moderate to high avidity for their cognate antigen undergo receptor editing, in which RAG genes are reactivated and immunoglobulin (usually light chain) gene segments are further rearranged in an effort to generate a non-self-reactive BCR (Basten and Silveira, 2010). Despite these stringent central tolerance checkpoints, resulting in the elimination of over 85% of immature B cells in the bone marrow, some autoreactive B cells still evade these processes (Gururajan et al., 2014; Melchers, 2015).

Recently generated immature B cells migrate from the bone marrow to the spleen and undergo transitional stages (T1 and T2) where they encounter self-antigens that may not have been present in the bone marrow (Basten and Silveira, 2010). These peripheral tolerance checkpoints are essential for B cells considering their ability to hypermutate their receptors following activation and their ability to respond to antigens in the absence of T cell help. B cells binding to their cognate antigen with high avidity undergo clonal deletion, whereas those binding with low avidity undergo a state of non-responsiveness, characterised by desensitised BCR signalling, known as anergy (Goodnow et al., 1988; Nemazee and Bürki, 1989). Upon BCR ligation, these cells migrate to the T cell zone in search for T cell help, but do not receive the necessary co-stimulation required for full activation (Basten and Silveira, 2010). At this stage, B cell survival is dependent upon BAFF, and greater BAFF responsiveness is

achieved by BAFF receptor upregulation following BCR stimulation; however, weak BCR signalling and insufficient BAFF responsiveness in anergic B cells leads to cell death (Lesley et al., 2004; Stadanlick and Cancro, 2008). Peripheral tolerance is also achieved through the action of the B cell siglecs CD22 and Siglec-G. These inhibitory receptors bind sialic acids commonly expressed on mammalian but not microbial cells, thus dampening reactivity by setting a 'threshold' to self-antigens (Macauley and Paulson, 2014).

1.2.3 B cell activation

B cells can acquire soluble or particulate antigens from macrophages or follicular dendritic cells (FDC) within the secondary lymphoid organs via the BCR (Yuseff et al., 2013). The BCR comprises membrane-bound immunoglobulin molecules coupled with Igα (CD79a) and Igβ (CD79b) heterodimers, which transmit intracellular signals through immunoreceptor tyrosine-based activation motifs (ITAMs) in their cytoplasmic tails. A co-receptor complex comprising CD19, CD21 (complement receptor 2) and CD81 also plays a role by augmenting signal transduction (DeFranco, 1996; Fujimoto et al., 2000). Antigen binding and BCR cross-linking results in ITAM phosphorylation and activation of kinases including Lyn, Syk and Btk that mediate an intracellular signalling cascade and activate downstream signalling pathways affecting differentiation, survival and proliferation (Harwood and Batista, 2010; Hobeika et al., 2015). The BCR-antigen complex is internalised and processed in endocytic vesicles where the antigen is digested and the resulting peptides are loaded onto MHC class II molecules and expressed on the cell surface. Antigen-loaded B cells migrate towards the T cell zone of the lymphoid follicle, where they distribute alone the B/T border (Pereira et al., 2010). On recognition by their cognate T follicular helper (T_{FH}) cell, B cells are activated through MHC class II engagement, co-stimulation via CD40-CD40L and the provision of cytokines such as interleukin (IL)-4 (IL-4) and IL-21 (Yuseff et al., 2013). Some of these B

cells will immediately differentiate into early plasmablasts to provide low-affinity antigen-specific antibody in the early phases of the immune response, and a small fraction will be released into the periphery as germinal centre -independent memory B cells, possibly to maintain a broad range of antigen-specific B cells (Kurosaki et al., 2015). Alternatively, B cells enter the germinal centre reaction, where they are referred to as centroblasts. Germinal centres (GC) are specialised structures within secondary lymphoid organs that develop over several days following antigen encounter, with the goal of producing large numbers of clonal B cell populations and high affinity antibodies (Fig. 1.2). Entry of activated B cells into the germinal centre is controlled to favour high affinity B cells expressing the most antigen, whilst the entry of low affinity B cells is restricted (Crotty, 2014; Schwickert et al., 2011). Here, B cells undergo repeated rounds of proliferation and somatic hypermutation of their immunoglobulin genes within the dark zone, before migrating to the light zone, where FDCs select those with the highest affinity and allow their survival (Allen et al., 2007; Schwickert et al., 2011). B cells may also change their antibody isotype during class switching, following interaction with their cognate T_{FH} cell (Zhang et al., 2016). Following the germinal centre reaction, centroblasts may re-

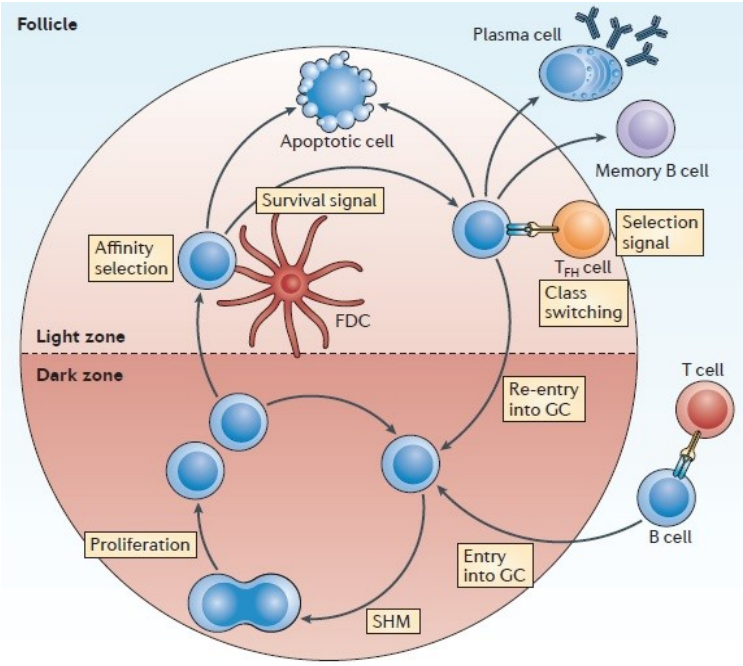

Figure 1.2. The germinal centre reaction. Repeated rounds of proliferation and somatic hypermutation in the dark zone followed by affinity selection and class switching in the light zone generates B cells with a high affinity for antigen (Heesters et al., 2014). Reproduced with permission of the copyright owner.

enter the germinal centre to allow further affinity maturation, or they may exit as memory B cells or ASC (Heesters et al., 2014).

1.2.4 Affinity Maturation

Affinity maturation is an essential component of adaptive humoral immunity and involves secondary diversification of the antibody repertoire to produce higher affinity antibodies; this is achieved following repeated exposure of the B cell to its cognate antigen as described above. Somatic hypermutation occurs when point mutations are introduced into the V regions by the enzyme activation-induced cytidine deaminase (AID), that converts C:G base pairs into U:G mismatches, which may then be excised, replicated or repaired (Muramatsu et al., 1999; Luo et al., 2004). The mutational frequency induced by AID activity is reportedly 1,000,000 times higher than the rate of spontaneous mutations in other genes (Briney and Jr, 2013).

In addition to modifying the V regions through somatic hypermutation, B cells can further modify antibody function by switching the C region in a process known as isotype switching, which alters the effector function of the antibody. Isotype switching is achieved through class-switch recombination (CSR) in which heavy chain encoding sequences are looped out and deleted by a process involving AID and re-joined by DNA repair enzymes (Stavnezer and Schrader, 2014). The decision of an activated B cell to undergo isotype switching is governed by CD4+ T cell-derived cytokines, particularly IFNγ (IgG2a and IgG3), IL-4 (IgE, IgG1 and IgG4) and TGFβ (IgA and IgG2b), and in the presence of multiple cytokine signals there is a hierarchy (IFNγ>IL-4>TGFβ) which allows the B cell to make logical decisions in a complex milieu (Tangye et al., 2002; Deenick et al., 2005). B cells may also undergo isotype switching in the absence of T cell help; this is best characterised in the gut, where intestinal epithelial

cells and FDC stimulated by commensal bacteria secrete cytokines that induce isotype switching to IgA (He et al., 2007; Suzuki et al., 2010; Chorny et al., 2010).

1.2.5 Antibodies

A unique feature of B cells is the production of antibodies. Antibodies are the secreted form of the BCR and are exclusively produced by ASC. Antibodies contain two identical heavy chains and two identical light chains linked by disulphide bonds. Five antibody isotypes exist based on their heavy chain class (IgG, IgM, IgA, IgD, IgE), and IgG (IgG1, IgG2, IgG3, IgG4) and IgA (IgA1, IgA2) may be further subdivided into several subclasses. The heavy and light chain V regions collectively form the antigen-binding (Fab) region of the antibody, composed of two identical antigen binding sites, and the C regions form the fragment crystallisable (Fc) region, which induces effector mechanisms by activating components of the innate immune system (Hoffman et al., 2016). The Fc region can activate the classical

Table 1.1. Properties and functions of immunoglobulin isotypes.

	Immunoglobulin Isotype						
	IgG1	**IgG2**	**IgG3**	**IgG4**	**IgM**	**IgA**	**IgE**
Adult serum levels (mg/dl)	900	300	100	50	150	300	0.03
Heavy chain	γ1	γ 2	γ 3	γ 4	μ	α	ε
Molecular Mass (kDa)	146	146	165	146	970	160	188
Serum half-life (days)	21	2	7	21	10	6	2
Polysaccharide antigens	+	+++	+/-	+/-	++	++	++
Protein antigens	++	+/-	++	++	+	+	+
Complement activation	++	+	+++	-	++++	-	-
Fc receptor binding	+	-	+	+/-	-	+	+
Mast cell/basophil activation	+	-	+	-	-	-	++++

– to +++ indicates the relative absence or presence of activity or response. (Hoffman et al., 2016). Reproduced with permission of the copyright owner.

complement pathway, resulting in lysis of bacterial cell walls, and bind Fc receptors expressed by macrophages, leading to phagocytosis of opsonised pathogens (Wang et al., 2007; Hoffman et al., 2016).

The heavy chain is responsible for antibody effector functions and different heavy chain isotypes possess different properties (summarised in table 1.1). For example, IgM is a strong activator of the complement pathway due to its pentameric structure and low avidity, whereas IgE is excellent at binding FcεR1 on mast cells and basophils (Hoffman et al., 2016).

1.4 B cell subsets: characteristics and phenotypic features

1.4.1 Naïve and memory B cells

In humans, naïve B cells comprise a large proportion (60-70%) of the circulating B cell pool and co-express IgM and IgD on the surface (Perez-Andres et al., 2010). Naive and memory B cells express high levels of BCR-associated molecules such as CD19, CD20 and CD45, and molecules associated with a T-dependent response such as CD40 and MHC class II (Perez-Andres et al., 2010). During the generation of memory B cells, intrinsic developmental changes occur that enable a more rapid secondary response to antigen compared to naïve B cells encountering antigen for the first time, with enhanced magnitude and proliferative capacity (Tangye and Tarlinton, 2009). These properties can be attributed to the selection of higher affinity B cells during the primary response, the placement of memory B cells at antigen-draining sites that allows earlier antigen contact than naïve B cells, and a higher expression of co-stimulatory markers that facilitates rapid T cell help (Good and Tangye, 2007). Around 50% of circulating memory B cells have undergone CSR, with around half of the memory B cell pool expressing unswitched IgM+IgD+ or IgM alone (Perez-Andres et al., 2010). As with class-switched memory B cells, unswitched memory B cells can be

phenotypically distinguished from naïve B cells by the high expression of CD27, a tumour necrosis factor receptor (TNFR) family member involved in B cell differentiation into ASC (Klein et al., 1998).

1.4.2 Antibody-secreting cells

1.4.2.1 Characteristics and identification

Antibody-secreting cell (ASC) is an umbrella term encompassing plasmablasts and plasma cells. Plasmablasts are highly proliferative, recently generated cells peaking at day 7 following infection; nonetheless, around 90% of these cells will die within 2-3 weeks (Fink, 2012). Regardless of their origin, any activated B cell, including naïve, marginal zone or memory, may become a plasmablast, though it is unclear whether cells from all these origins have the capacity to become plasma cells (Radbruch et al., 2006). Despite low steady-state levels, plasmablasts can be detected in the peripheral blood of healthy humans at approximately 2 cells/µl and typically represent 1-3% of the total B cell pool (Morbach et al., 2010; Caraux et al., 2010; Perez-Andres et al., 2010).

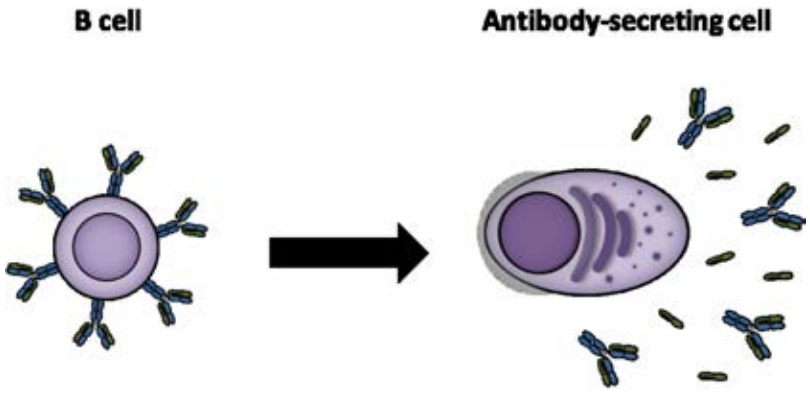

Figure 1.3. Morphological features distinguishing B cells and antibody-secreting cells. B cells are small round cells which express surface-bound immunoglobulin and display a high nucleus to cytoplasm ratio (left image). Antibody-secreting cells display eccentric (non-central) nuclei with condensed chromatin, and abundant cytoplasmic constituents (such as golgi apparatus and endoplasmic reticulum) involved in rapid antibody synthesis (right image).

Morphologically, ASC display eccentric (non-central) nuclei, condensed chromatin and abundant golgi apparatus and endoplasmic reticulum (ER; Fig. 1.3), making them well equipped for secreting large quantities of antibody (Miller, 1931). ASC display a distinct phenotype that coincides with their progressive differentiation from short-lived plasmablasts to long-lived plasma cells. This includes gradual downregulation of molecules involved in B cell receptor signalling and antigen presentation, and upregulation of activation markers (e.g. CD27 and CD38) and homing molecules (e.g. CXCR4 and CD138; table 1.2). Steady-state circulating plasmablasts express CD19 and are CD27+CD38+, with up to half expressing CD138 (Syndecan-1), a heparin sulphate associated with a more mature phenotype compared to CD138- plasmablasts (Caraux et al., 2010). The requirement of CD138 for long-term survival suggests that CD138- plasmablasts are destined to remain short-lived, whereas CD138+ plasmablasts have the potential to become plasma cells if a suitable niche is found.

Table 1.2. Summary of antibody-secreting cell maturation.

	Naïve B cell	**Plasmablast**	**Immature plasma cell**	**Mature plasma cell**
Lifespan	++	+	+	++++
Proliferation	-	++	-	-
CD27, CD38, CD138* and CXCR4 expression	-	+	++	+++
CD19, CD20, CD45, MHC class II and sIg expression	+++	++	+/-	+/-
Location	L.O.	L.O., P.B.	L.O., B.M.	B.M.
BLIMP1 expression	-	+	+	++

+/- indicates low or heterogeneous expression. sIg = surface immunoglobulin, L.O. = lymphoid organs, P.B. = peripheral blood, B.M. = bone marrow. *CD138 expression is heterogeneous within the plasmablast population. Adapted from (Nutt et al., 2015). Reproduced with permission of the copyright owner.

Different ASC populations have been identified and characterised within human lymphoid tissues. Based on phenotypic markers (see table 1.2), CD19- ASC are the most terminally differentiated and have been shown to maintain a long-lived antibody response to mumps and measles viruses over 40 years after infection, and thus can be considered long-lived plasma cells (Halliley et al., 2015). Consistent with these observations, Landsverk et al (2017) showed that within a year of transplanting human duodenal tissue, the CD19- ASC population remained stable, indicating substantial longevity, whereas a third of donor CD19+ ASC had been replaced by recipient CD19+ ASC, indicating that CD19+ ASC represent short-lived plasmablasts (Landsverk et al., 2017). This group also measured carbon-14 levels from the genomic DNA of ASC subsets in intestinal biopsy samples and showed that CD19- but not CD19+ ASC were extremely long-lived, with a median age of 22 years (Landsverk et al., 2017). Long-lived plasma cells are not replenished by the memory B cell pool, as their long-term depletion does not affect ASC frequency, but their longevity could be achieved by low levels of homeostatic proliferation, as despite being regarded as terminally differentiated, low levels of the proliferation marker Ki-67 has been observed in these cells (Ahuja et al., 2008; Macallan et al., 2005). As such, the ASC pool represents a heterogeneous population of short-lived (i.e. plasmablasts) and long-lived (i.e. plasma cells) ASC which can largely be distinguished based on CD19 and CD138 expression.

1.4.2.2 Survival niches

The majority of survival niches are found in the bone marrow; however, a proportion of niches are found within the spleen, lymph nodes or inflamed tissues (Radbruch et al., 2006). Arrival at a survival niche is a critical stage for plasmablast differentiation into plasma cells. Survival niche homing is governed by chemokines which direct plasmablasts to different anatomical locations. For example, CXCR4 is important for homing to the bone marrow,

which is the largest plasma cell niche in the body; however, CXCR3, which binds inflammatory chemokines such as CXCL9 and CXCL10, can direct plasmablasts to ectopic sites of inflammation (Radbruch et al., 2006; Hauser et al., 2002).

Niches are served by several accessory cells that contribute to the survival and maintenance of the plasma cell pool (Fig. 1.4) such as dendritic cells (DC), macrophages and eosinophils, which secrete important growth factors including BAFF, a proliferation inducing ligand (APRIL), IL-6 and CXCL12 (Chu et al., 2011; Jego et al., 2001; Nutt et al., 2015). Plasma cells are retained within the niche via adhesion molecules, including CD44, which binds hyaluronic acid and other extracellular matrix components, very late antigen-4 (VLA-4; CD49d), the ligand for vascular cell adhesion molecule-1 (VCAM-1; CD106) which is expressed by stromal cells, and CD138, which mediates adhesion to several extracellular matrix components, and is also a receptor for APRIL (Ingold et al., 2005; Radbruch et al., 2006; Nutt et al., 2015). As the number of niches within the body is finite, recently generated plasma cells compete for survival by dislodging long-lived plasma cells from their niche (Odendahl et al., 2005).

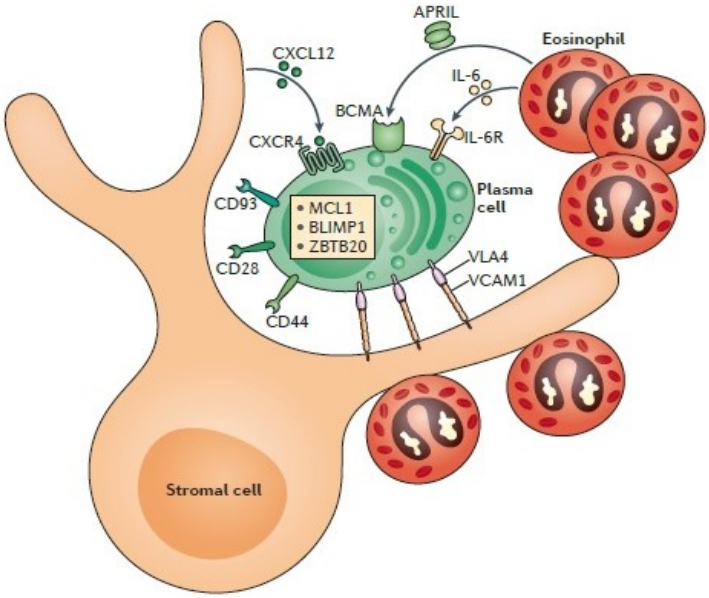

Figure 1.4. The plasma cell survival niche. Antibody-secreting cells are dependent on a range of survival factors, which includes chemokines and adhesion molecules, secreted by stromal cells and accessory cells (Nutt et al., 2015). Reproduced with permission of the copyright owner. APRIL; a proliferation inducing ligand, BCMA; B cell maturation antigen, MCL1; myeloid cell leukaemia 1, ZBTB20; zinc finger and BTB-containing domain protein 20, VLA4; very late antigen 4, VCAM1; vascular cell adhesion molecule 1

1.5 T cell biology

1.5.1 T cell development

Like B cells, T cells undergo a series of distinct differentiation stages to produce mature, fully functional naïve cells that are released into the periphery (summarised in Fig. 1.5). Developing thymocytes undergo VDJ recombination in a similar fashion to B cells,

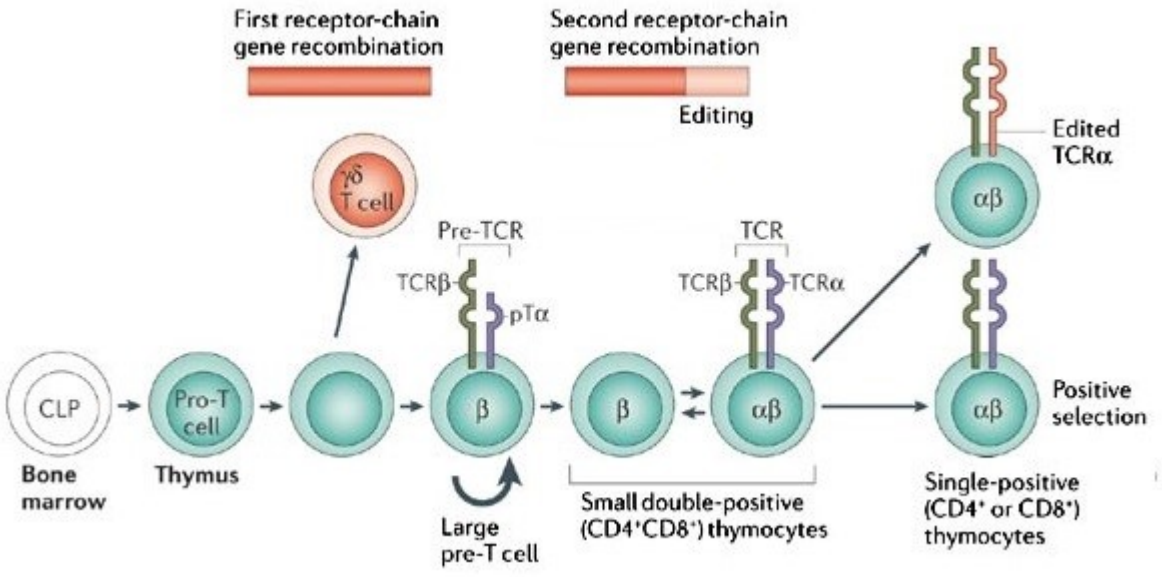

Figure 1.5. T cell development and generation of the T cell receptor. T cells rearrange their V, D and J segments to produce a functional antigen-specific TCR which is associated with single positive CD4+ or CD8+ cells following positive selection. Gene recombination of the first receptor chain often gives rise to αβ T cells but can also give rise to γδ T cells. Adapted from (Nemazee, 2006). Reproduced with permission of the copyright owner.

rearranging gene segments to produce a functional T cell receptor (TCR) before receiving important selection signals before their release into the periphery. Lymphoid progenitors from the bone marrow migrate to the cortico-medullary junction of the thymus, where they are referred to as CD4-CD8- double negative thymocytes (Zuniga-Pflucker, 2004). These cells migrate through the cortex, interacting with cortical thymic epithelial cells whilst undergoing a number of developmental stages which results in expression of the pre-T cell receptor (TCR) complex; in the majority of T cells this consists of the TCRβ chain and the pre-TCRα

chain. Loss of IL-7 and notch ligand signals allows differentiation into double positive (CD4+CD8+) thymocytes with expression of a complete TCR (Rothenberg et al., 2008). The thymocytes then migrate to the medulla where they undergo central tolerance checkpoints to assess TCR affinity towards self-proteins. These proteins, referred to as tissue-specific self-antigens, are promiscuously expressed by medullary thymic epithelial cells, and their expression is mediated by the autoimmune regulator (AIRE) transcription factor, which is thought to act by opening chromatin to allow the transcription of normally-repressed genes, thus allowing ectopic expression of self-proteins (Derbinski et al., 2001; Anderson et al., 2002). Strong binding to self-peptide-MHC complexes results in elimination (negative selection), whereas T cells displaying intermediate affinity towards self-peptide-MHC-complexes are allowed to mature into single positive CD4+ or CD8+ T cells (positive selection) and are released into the periphery (Germain, 2002; Klein et al., 2014).

1.6 T cells in the immune response

1.6.1 The T cell receptor and T cell subsets

The TCR is a heterodimeric structure consisting of two peptide chains linked together by a disulphide bond, and is anchored to the cell surface by a hydrophobic transmembrane domain. Around 95% of T cells express TCRs with an α and β chain and are thus referred to as αβ T cells; most of these recognise peptide fragments bound to MHC molecules, but a minority of unconventional αβ T cells recognise antigens via alternative methods. These cells, though not well characterised, display limited diversity and recognise bacterial components and lipid antigens (Attaf et al., 2015).

Another group of T cells express γ and δ polypeptide chains to form the TCR- these are referred to as γδ T cells and, like the unconventional αβ T cell subsets, do not recognise

peptide antigens. δ T cells constitute 1-10% of the peripheral T cell pool but are considerably enriched in epithelial tissues; this reflects their function as rapid responders using restricted TCR as pattern recognition receptors to recognise bacterial antigens entering the skin (Attaf et al., 2015; Vantourout and Hayday, 2013).

The αβ TCR is associated with four invariant membrane-bound accessory chains on the cell surface, comprised of two ε, one δ and one γ chain, which collectively make up the CD3 complex. The cytoplasmic domains of each CD3 accessory chain, along with an intracellular homodimer of ζ chains, contain ITAMs which are phosphorylated following TCR engagement, allowing zeta-associated protein kinase (ZAP)-70 binding and a subsequent signalling cascade (Wang et al., 2010).

1.6.2 States of T cell differentiation

Circulating T cells can be identified based on their differentiation status, allowing them to be split into naïve, central memory (T_{CM}), effector memory (T_{EM}) and revertant effector memory (T_{EMRA}) subsets.

Naïve T cells circulate between secondary lymphoid organs in search for their cognate antigen. These cells extravasate through high endothelial venules and enter the lymph nodes using the adhesion molecule L-selectin (CD62L) and CCR7 (Brinkman et al., 2013). Within the T cell zones of the lymph nodes, recognition of antigen presented by DC leads to T cell activation. Naïve T cells can be distinguished by the expression of CD45RA, a protein tyrosine phosphatase involved in cell signalling. On differentiation, memory T cells express an alternatively spliced isoform, CD45RO, which alters the sensitivity of the cell to external stimuli and improves the efficiency of TCR signalling (Earl and Baum, 2008).

T_{CM}, which are responsible for maintaining the memory pool, also home to secondary lymphoid organs where they rapidly proliferate and differentiate into T_{EM} on antigen recognition (Sallusto et al., 2004). T_{EM}, which downregulate CD62L and CCR7 to prevent re-entry to the lymph nodes, migrate to peripheral tissues using alternative homing receptors such as CXCR3, where they elicit their effector functions in the presence of inflammation (Sallusto et al., 2004; Willinger et al., 2005). T_{EMRA} are terminally differentiated memory T cells that retain their potent effector functions but have switched back to expressing CD45RA to limit their activation. Mainly found in the CD8+ T cell compartment, T_{EMRA} are pre-senescent and lack proliferative capacity, displaying the shortest telomeres amongst T cells, which marks their end-stage differentiation status (Henson et al., 2012; Mahnke et al., 2013).

1.6.3 Limiting T cell activation

In addition to TCR ligation (signal 1), T cells require co-stimulation, typically via CD28 (signal 2) which binds CD80 or CD86 on the antigen presenting cell (APC), and cytokine priming (signal 3). These events result in T cell activation, proliferation and differentiation (Smith-Garvin et al., 2009). However, because of their potential damaging consequences, these functions are highly regulated. T cells may be subjected to several peripheral tolerance mechanisms such as suppressed activation by regulatory T cells (Treg), peripheral deletion following high affinity self-peptide engagement, or conversion to Treg following low-affinity self-peptide engagement (Xing and Hogquist, 2012). Anergy may also be induced in peripheral T cells, in which TCR ligation is received in the absence of co-stimulation, rendering the cell non-responsive. This may occur in the absence of inflammation due to a lack of pro-inflammatory cytokines, which are required for the expression of co-stimulatory molecules on DC (Mueller, 2010). In addition, activated or autoreactive T cells can be inhibited by the expression of inhibitory receptors, which induce a non-responsive state

within peripheral tissues. These include programmed cell death receptor 1 (PD-1), T cell immunoglobulin mucin 3 (TIM-3) and cytotoxic T lymphocyte-associated protein 4 (CTLA-4) which block intracellular activation signals through immunoreceptor tyrosine-based inhibition motifs (ITIMs) (Fuertes Marraco et al., 2015).

1.7 T cell subsets

The TCR co-receptors CD4 and CD8 promote signal amplification during antigen recognition (Artyomov et al., 2010). CD4 is expressed by T helper (Th) cells and interacts with peptides bound to MHC class II molecules expressed by antigen presenting cells, which have been sampled from exogenous proteins (Blum et al., 2013). CD8 is expressed by cytotoxic T cells and interacts with MHC class I molecules, which are expressed by all nucleated cells. MHC class I molecules bear endogenous peptides derived from cytosolic proteins, such as viral components, permitting identification of infected host cells that require elimination (Blum et al., 2013).

1.7.1 CD4+ T cells

Naïve CD4+ T cells are uncommitted precursors with a high level of plasticity, playing a central role in T cell-mediated immunity through their proliferation and differentiation into distinct subsets following activation. This process is governed by cytokines which induce specific transcription factors, leading to a switch in the gene expression profile that is responsible for the subsequent phenotype of that cell. The original model involved differentiation into Th1 cells or Th2 cells (Murphy and Reiner, 2002). Th1 cells predominantly secrete IFNγ and are responsible for cell-mediated immunity, responding to intracellular pathogens such as viruses and bacteria; conversely, Th2 cells secrete IL-4 (amongst other cytokines) and contribute to humoral immunity, providing protection against

extracellular parasites such as intestinal helminths (Murphy and Reiner, 2002). Both subsets also play a role in pathological responses, with Th1 cells associated with autoimmune diseases and Th2 cells associated with allergy and asthma (Murphy and Reiner, 2002).

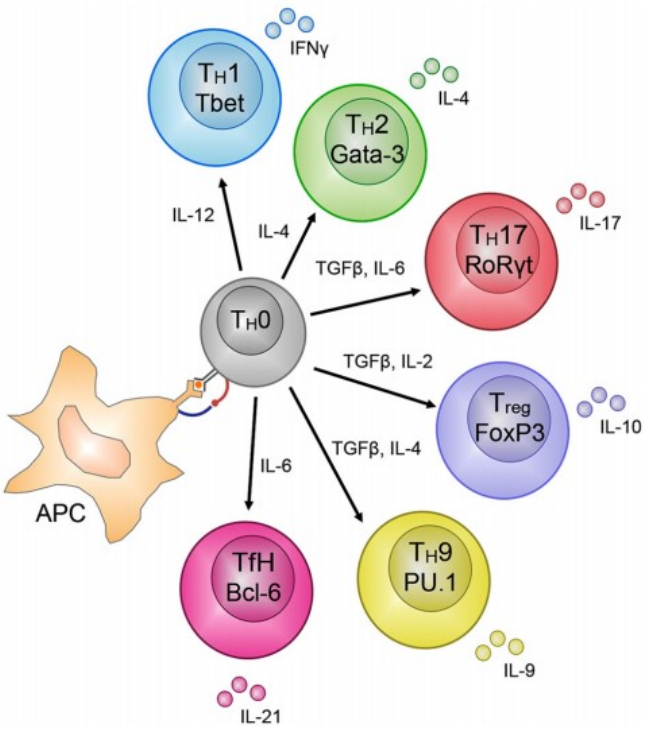

Figure 1.6. CD4+ T cell differentiation. Naïve CD4+ T cells (Th0) can differentiate into a variety of T helper subsets following activation (Russ et al., 2013). Reproduced with permission of the copyright owner.

Besides Th1 and Th2, naïve CD4+ T cells can follow alternative differentiation pathways (Fig. 1.6). Contrary to conventional T helper cells, Tregs modulate the immune response by downregulating T cell activation, predominantly through IL-10 secretion and the expression of CTLA-4, a homologue of CD28, which acts through the co-stimulatory molecules CD80 or CD86 (Corthay, 2009).

Th17 cells play a role in pathogen clearance at mucosal surfaces predominantly through secretion of IL-17, IL-21 and IL-22 (Crome et al., 2010). Previously believed to be a distinct subset for their inability to secrete other lineage-defining cytokines, it is now appreciated that Th17 cells can produce IFNγ, a Th1-associated cytokine, or IL-10, a Treg-associated cytokine, depending on the pathogen encountered (Zielinski et al., 2012). Aberrant Th17 cell responses have been linked to several chronic inflammatory conditions including psoriasis, multiple sclerosis and rheumatoid arthritis (Crome et al., 2010).

1.7.2 CD8+ T cells

Cytotoxic CD8+ T cells eliminate target cells through direct cell-cell contact via death receptor signalling or perforin-mediated killing, or indirectly through the production of pro-inflammatory cytokines (Andersen et al., 2006).

The primary mechanism by which CD8+ T cells exert their cytotoxicity is through the perforin pathway. This rapid-acting mechanism, which is calcium-dependent, involves the secretion of pre-formed effector molecules within cytoplasmic granules, namely perforin and granzymes (granule enzymes). Following target cell identification, an immunological synapse is formed and the CD8+ T cell becomes polarised, transporting secretory granules to the cell surface through the action of microtubules. These granules fuse with the cell membrane and release their contents into the synaptic cleft, where perforin assembles into multimeric complexes and form pores in the target cell membrane (Voskoboinik et al., 2015). Granzymes then diffuse into the target cell, translocate to the nucleus and initiate cell death through proteolytic cleavage of substrates that induce apoptosis (Chowdhury and Lieberman, 2008). Granzymes are stored in an inactive form due to the acidity of the granules, which is lost on degranulation; however, the CD8+ T cell is protected from self-damage by expression of protease inhibitors known as serpins (Regner and Mullbacher, 2004; Ashton-Rickardt, 2012).

Granzymes are a family of five of serine-proteases homologous to trypsin, constituting five members in humans. Granzymes A and B are the most abundant and well-studied, while granzymes K, H and M are less understood and are referred to as orphan granzymes (Voskoboinik et al., 2015). Granzyme A-mediated cell death is independent of caspase recruitment, involving reactive oxygen species (ROS) generation and subsequent recruitment of ER-associated nucleases, leading to DNA cleavage (Beresford et al., 2001). Unlike other granzymes, granzyme B can cleave after aspartate residues in the same way as caspases and

can therefore activate cell death through direct cleavage of caspase substrates, although it can also act through caspase-dependent mechanisms (Pinkoski et al., 2001; Chowdhury and Lieberman, 2008). As well as granzymes, granulysin, a small protein that targets bacteria by rupturing their membranes, may also be delivered into target cells (Stenger et al., 1998).

The death receptor pathway is mediated by TNF-family members, namely Fas ligand (FasL), which binds Fas on target cells, or TNF-related apoptosis-inducing ligand (TRAIL), which binds its receptors TRAIL-R1 or TRAIL-R2 (Falschlehner et al., 2009). Trimerisation of the signalling complex leads to formation of the death-inducing signalling complex (DISC) and recruitment of Fas-associated death domain (FADD), which initiates an intracellular caspase cascade leading to apoptosis (Falschlehner et al., 2009).

Triggering of pro-inflammatory cytokine release by CD8+ T cells, such as TNFα and IFNγ, is induced on TCR ligation and promotes resolution of infection through multiple mechanisms. TNFα binds its receptor on the target cell and initiates an intracellular signalling cascade involving the adaptor protein TNF receptor type 1-associated death domain (TRADD), leading to apoptosis (Pobezinskaya and Liu, 2012). IFNγ acts on host cells by upregulating Fas expression and antigen presentation through MHC class I, increasing the likelihood of recognising infected cells and allowing faster eradication (Andersen et al., 2006). IFNγ also induces the transcription of proteins involved in the inhibition of viral replication, and recruits macrophages to promote enhanced effector function (Samuel, 2001; Rauch et al., 2013).

1.8 Multiple sclerosis

1.8.1 General overview

'Why this deliberate, slow-moving malignity? Perhaps it is a punishment for the impudence of my desires. I wanted everything so I get nothing ... I am not offering up my life willingly – it is being taken from me piece by piece, while I watch the pilfering with lamentable eyes.'

~ W.N.P. Barbellion, The Journal of a Disappointed Man (early 20th century)

Personal accounts of multiple sclerosis (MS), including those documented in W.N.P. Barbellion's journals published in 1919 following his death from the disease aged just 30 years old, offer some insight into the plight of sufferers where detailed medical knowledge was limited and effective treatments absent. The first medical descriptions of MS have been traced back to around the 14th century, but it is the famous French neurologist Jean-Martin Charcot, often referred to as the father of modern neurology, who is largely credited with the first comprehensive description of MS in 1868. Charcot's details of the pathological changes that occur in the MS brain and spinal cord, described as 'la sclérose en plaques disseminées', as well as recognising the disease course, symptoms and the correlation of clinical features with post-mortem findings, led to the recognition of MS as a distinct disease (Pearce, 2005; Kumar et al., 2011).

Today, MS is the most common chronic inflammatory disease of the central nervous system (CNS) and is the primary cause of neurological disability affecting young adults in the Western world (Rodriguez et al., 1994). MS most often presents between 20 and 40 years of age and affects more women than men at an approximate ratio of 2:1 (Bostrom et al., 2013). Though the clinical course can vary considerably between affected individuals, the disease is

degenerative in most cases and in time generally progresses to irreversible disability of varying degrees (De Jager, 2011).

1.8.2 Clinical features and disease phenotypes

Most individuals initially present with a single acute neurological attack known as clinically isolated syndrome (CIS), representing the earliest symptomatic demyelinating event suggestive of MS (Fig. 1.7). A CIS may present in a wide range of clinical scenarios, including optic neuritis, transverse myelitis, a brainstem syndrome and sometimes diffuse cerebral dysfunction, causing a range of symptoms from visual disturbances to muscle weakness and sensory disturbance, depending on the site of demyelination (Polman et al., 2011; Marcus and Waubant, 2013). A diagnosis of MS is generally made when a second clinical event (a relapse) is experienced. Initially these episodes spontaneously resolve

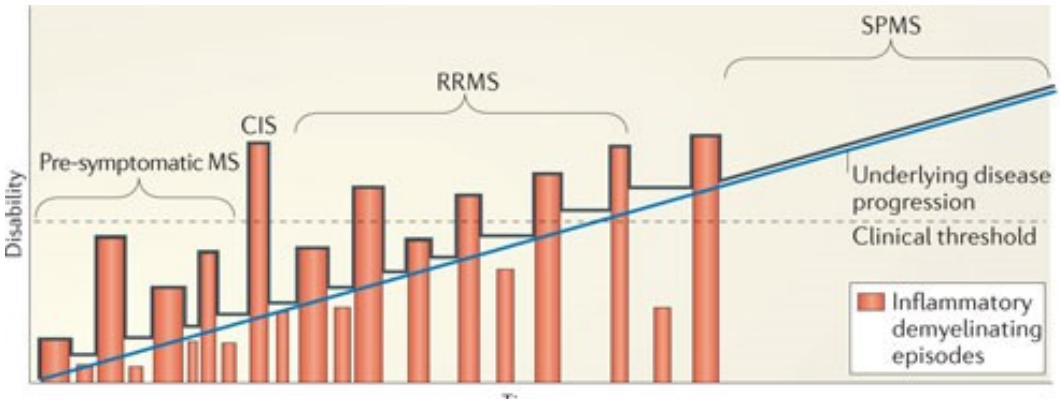

Figure 1.7. The major clinical phenotypes of multiple sclerosis. Though MS is highly variable in nature, several common features have allowed the disease to be divided into subtypes (Stys et al., 2012). Reproduced with permission of the copyright owner.

(remit), with apparent improvement of disability and return to normal CNS function between episodes, thought to represent resolution of inflammation. 80-90% of these individuals will experience further future relapses at a variable rate, generally (but not necessarily) equating to around 0.5-2 per year; this is referred to as relapsing-remitting MS (RRMS) and is the most common form of the disease (Compston and Coles, 2008).

With increasing disease duration, recovery following relapses is less complete and increasing disability and a gradual decline in neurological function is often experienced; this disease state, termed secondary progressive MS (SPMS), affects around 70-80% of those with RRMS (Disanto et al., 2011; Nylander and Hafler, 2012). A subset of people with MS (10-15%) experience progressive disability from the onset of diagnosis without periods of remission, a form known as primary progressive MS (Miller and Leary, 2007). In addition, some individuals experience a comparatively benign disease course, and although the definition of benign MS has been varied, it is characterised by minimal disability accumulation as measured by the expanded disability status scale (EDSS) (Hawkins and McDonnell, 1999; Pittock et al., 2004). In a 10-year follow-up study of 161 cases, 17% of individuals had an EDSS of 2 or less with a <10% chance of developing significant disability (Pittock et al., 2004). The variable manifestations of MS are testament to the heterogeneity of the disease, and underpin the difficulties with predicting prognosis, particularly early in the disease. This principle was demonstrated in a large follow-up study in which 42% of individuals had developed significant disability 20 years from disease onset with a median EDSS of 6.5, whereas 38% experienced a less severe outcome with a median EDSS of less than 3 (Fisniku et al., 2008).

1.8.3 Risk factors

Like many autoimmune conditions, MS is a complex disease with multiple contributing factors. It is important to note that some factors may play a more important role than others and the presence or absence of all the factors associated with MS does not guarantee disease occurrence nor confer absolute protection.

1.8.3.1 Genetics

Despite variable outcomes, twin studies suggest a positive influence of heritability in MS. A British Isles survey of MS in 105 pairs of twins found concordance in 25% of monozygotic twins compared to 3% of dizygotic twins, however a weaker genetic link was found in a large North American study of over 1,100 twins, which found a concordance rate of 13% for monozygotic and 5% (same sex) and 3.7% (opposite sex) for dizygotic twins (Thorpe et al., 1994; Islam et al., 2006).

Genome-wide association studies (GWAS) have consistently revealed a link between several HLA genes (particularly HLA-DRB1*1501) and associated single nucleotide polymorphisms (SNPs) with MS, implicating immune function as a disease-contributing mechanism (Lincoln et al., 2005; Alcina et al., 2012; Schmidt et al., 2007). Some MHC class I risk alleles are also associated with MS, including the HLA-A SNP rs6457110, which is also linked to increased susceptibility for infectious mononucleosis (Jafari et al., 2010). Aside from the strong HLA association, many of the 110 non-MHC risk variants identified are also immune related, notably the interleukin-2 receptor alpha (IL-2Ra) and interleukin-7 receptor alpha (IL-7Ra) encoding regions, and epigenetic mechanisms that regulate gene expression have also been suggested to play a role (Sawcer et al., 2011; Beecham et al., 2013; Didonna and Oksenberg, 2015; Miyazaki and Niino, 2015).

1.8.3.2 Infectious agents

Of the many infectious agents linked to MS pathogenesis, Epstein-Barr virus (EBV) is the most strongly associated. Over 90% of adults have been infected with EBV, however the seropositivity in MS is thought to be over 99%, or even 100% where two independent EBV detection methods are used (Pakpoor et al., 2013; Burnard et al., 2017). In addition, most

studies have found a higher seroprevalence of anti-Epstein-Barr Nuclear Antigen 1 (EBNA-1) and anti-Viral Capsid Antigen (VCA) antibodies in MS compared to non-MS controls (Fernandez-Menendez et al., 2016; Almohmeed et al., 2013; Santiago et al., 2010). The presence of cerebrospinal fluid (CSF) antibodies towards EBV-related proteins, and of EBV-infected B cells in the brain, has also been described in MS (Cepok et al., 2005b; Serafini et al., 2007). Using a highly sensitive *in situ* hybridisation technique, a recent study identified EBV in 90% of MS cases compared to 24% of controls with non-MS neurological disease (Hassani et al., 2018). Possible scenarios explaining the association of EBV with MS are molecular mimicry, where cross-reactivity results from sequence similarity of foreign and self-peptides, bystander damage, in which an EBV-specific CNS immune response causes inflammation and damage to host tissues, and the EBV-infected autoreactive B cell hypothesis, where defective T cell control of autoreactive EBV-infected B cells leads to their accumulation in the CNS (Márquez and Horwitz, 2015; Pender, 2003).

1.8.3.3 Other environmental factors

Lack of sunlight exposure and the associated reduction in vitamin D and melatonin levels in countries further from the equator is linked to an increased prevalence of MS (Ascherio and Munger, 2007; Farez et al., 2015). Support for the contribution of vitamin D comes from identification of four SNPs involved in vitamin D synthesis or metabolism, and both vitamin D and melatonin play roles in immune regulation (Mokry et al., 2015; Berge et al., 2016). Smoking, low testosterone levels and dysbiosis of the gut microbiota have also been linked to an increased risk of MS (O'Gorman and Broadley, 2016; Pakpoor et al., 2016; Chen et al., 2016b).

1.8.4 Diagnosis

A diagnosis of MS is made based on medical history and physical examination using the regularly revised McDonald criteria, with the aid of clinical testing (Thompson et al., 2018). Magnetic resonance imaging (MRI) is useful in demonstrating CNS lesions disseminated in space (lesions affecting separate regions of the CNS) and in time (indicating chronic disease), and both conditions must be met to fulfil a formal diagnosis of MS (Inglese, 2006; Polman et al., 2011).

For a more immediate indication, CSF analysis is useful in identifying inflammatory activity which along with clinical indications can provide strong support for a diagnosis of MS. Oligoclonal band (OCB) testing is considered the gold standard CSF test and detects the electrophoretic migration properties of free immunoglobulin in the CSF. Around 60-70% of CIS samples and more than 90% of clinically definitive MS samples demonstrate two or more OCB that are specific to the CSF, with more bands reportedly indicating a worse prognosis (Franciotta et al.; Marcus and Waubant, 2013). Similarly, the measurement of CSF free light chains (FLC), which are made in excess of heavy chains during rapid intrathecal antibody production, provide superior sensitivity and specificity than OCB and might also provide prognostic information, with high levels predicting earlier conversion from CIS to MS (Solling et al., 1981; Villar et al., 2012; Hassan-Smith et al., 2014).

1.8.5 Disease management

The variable and largely unpredictable disease course combined with a multitude of therapeutic options presents a challenge for the treatment of MS. Treatment may be restricted to symptomatic management of acute relapses using steroids, which may eventually involve additional treatment with a more potent therapy as the disease progresses; conversely,

individuals affected by MS may be started on the more potent disease-modifying therapies (DMT) from the onset in an effort to reduce disease severity in the long term, at the expense of potentially experiencing serious side effects (Gajofatto and Benedetti, 2015). Several DMTs are approved by the FDA Food and Drug Administration (FDA) and European Medicines Agency (EMA) for use in MS, all of which are immunomodulatory or immunosuppressive, including interferon beta (1a and 1b), glatiramer acetate, fingolimod, mitoxantrone, natalizumab and ocrelizumab (Vargas and Tyor, 2017). Some DMTs (e.g. fingolimod, natalizumab) block lymphocyte trafficking, whereas others (e.g. glatiramer acetate, interferon beta) induce a switch in the inflammatory response to a regulatory phenotype (Groves et al., 2013; von Glehn et al., 2012; Aharoni, 2013).

Following its approval in 1997 for the treatment of non-Hodgkin Lymphoma, rituximab was the first anti-CD20 therapy to be successfully used in MS (Maloney et al., 1994; Hauser et al., 2008; Bar-Or et al., 2008). By targeting CD20, which is expressed by mature B cells from the pre-B cell to plasmablast stage, these therapies deplete B cells via antibody-dependent cellular cytotoxicity (ADCC), complement-dependent cytotoxicity (CDC) and antibody-dependent cell-mediated phagocytosis (ADCP), leading to significant reductions in relapse rates and lesion formation (Sorensen and Blinkenberg, 2016; Agahozo et al., 2016; Geland et al., 2017). For example, in the first B cell-depleting trial, rituximab led to a 91% reduction in the total number of gadolinium-enhancing lesions and a 50% reduction in the annualised relapse rate compared to placebo controls at 24 weeks (Hauser et al., 2008). More recent trials with ocrelizumab, a humanised anti-CD20 antibody, and ofatumumab, a fully human anti-CD20 antibody, have also shown beneficial results (Sorensen et al., 2014; Kappos et al., 2011; Montalban et al., 2017). For example, lower rates of disease activity and disease progression was recently demonstrated in two identical phase 3 trials in RRMS (Hauser et al., 2017).

Additionally, ocrelizumab recently became the first DMT approved for treating PPMS (Montalban et al., 2017).

Though the efficacy of anti-CD20 therapies have largely been attributed to the elimination of antigen presenting properties of B cells, a small population of CD20+ T cells is present in the blood of MS and healthy control groups which is also depleted by anti-CD20 therapies (Wilk et al., 2009; Palanichamy et al., 2014b). CD20+ T cells, which appear to exhibit an activated pro-inflammatory profile, have also been detected in chronic MS brain lesions and as such, their possible contribution to MS cannot be disregarded without further investigation (Holley et al., 2014; Schuh et al., 2016).

1.9 Immunopathology of multiple sclerosis

1.9.1 Pathogenesis

MS is widely considered an autoimmune disease which is thought to occur when peripherally activated T cells infiltrate the CNS and are re-activated upon encountering their cognate antigen, leading to activation of mononuclear phagocytes such as macrophages and microglia with subsequent inflammation and tissue damage (Weissert, 2013). Though CD4+ T cells are considered central to MS pathogenesis, other immune cell subsets such as CD8+ T cells, B cells and ASC are thought to play a role (Dendrou et al., 2015).

CNS lesions are a hallmark of MS and represent sites of demyelination which are associated with inflammatory immune cell infiltrates. Demyelination and lesion formation is more likely to occur in the myelin-rich white matter areas of the CNS, particularly those with a high venous density such as the perivasclular and periventricular regions, although grey matter damage also occurs (Calabrese et al., 2015; Haider, 2015). Influx of inflammatory cells is an

early feature the disease, which likely begins many months or years prior to the onset of symptoms, but with disease progression the inflammatory component gradually subsides and neurodegenerative effects become more apparent as the mechanisms promoting neuronal plasticity become overwhelmed (Compston and Coles, 2008; Ksiazek-Winiarek et al., 2015). Key to the degenerative process is the accumulation of ROS and glutamate, inducing mitochondrial injury, which in turn leads to energy failure and neuronal cell death (Haider et al., 2011; Macrez et al., 2016).

1.9.2 Lymphocyte migration into the CNS

1.9.2.1 The concept of CNS immune privilege

The concept of biological barriers between the blood and CNS was established over 100 years ago by Paul Ehrlich, who observed that a water-soluble dye infused into the circulation was unable to stain brain tissue, but that the same dye infused into the CSF could stain brain tissue (Liddelow, 2011). CNS barriers have since been well characterised, and their unique features combined with the limited CNS immune interactions have led to consideration of the CNS as an immunologically specialised site. Whilst this remains true, historical findings are constantly being challenged and redefined. Notably, the importance of CNS immune responses and the presence of a lymphatic drainage system connecting the CNS to the periphery have advanced the understanding of immune interactions in the CNS (Louveau et al., 2015a; Louveau et al., 2015b; Engelhardt et al., 2017).

1.9.2.2 Anatomy of CNS barriers

Three major access sites for leucocytes have been distinguished for CNS entry; the blood-arachnoid barrier (BAB), the blood-brain barrier (BBB) and the blood-CSF barrier (BCSFB). These are eloquently summarised in Fig. 1.8.

1.9.2.3 Lymphocyte trafficking in health and disease

Homeostatic lymphocyte trafficking is largely considered to occur across the BCSFB, where selectins and adhesion molecules necessary for migration are constitutively expressed, rather than across the BBB, where endothelial cells lack the necessary adhesion molecules required by T cells in the absence of inflammation (Goverman, 2009; Shechter et al., 2013).

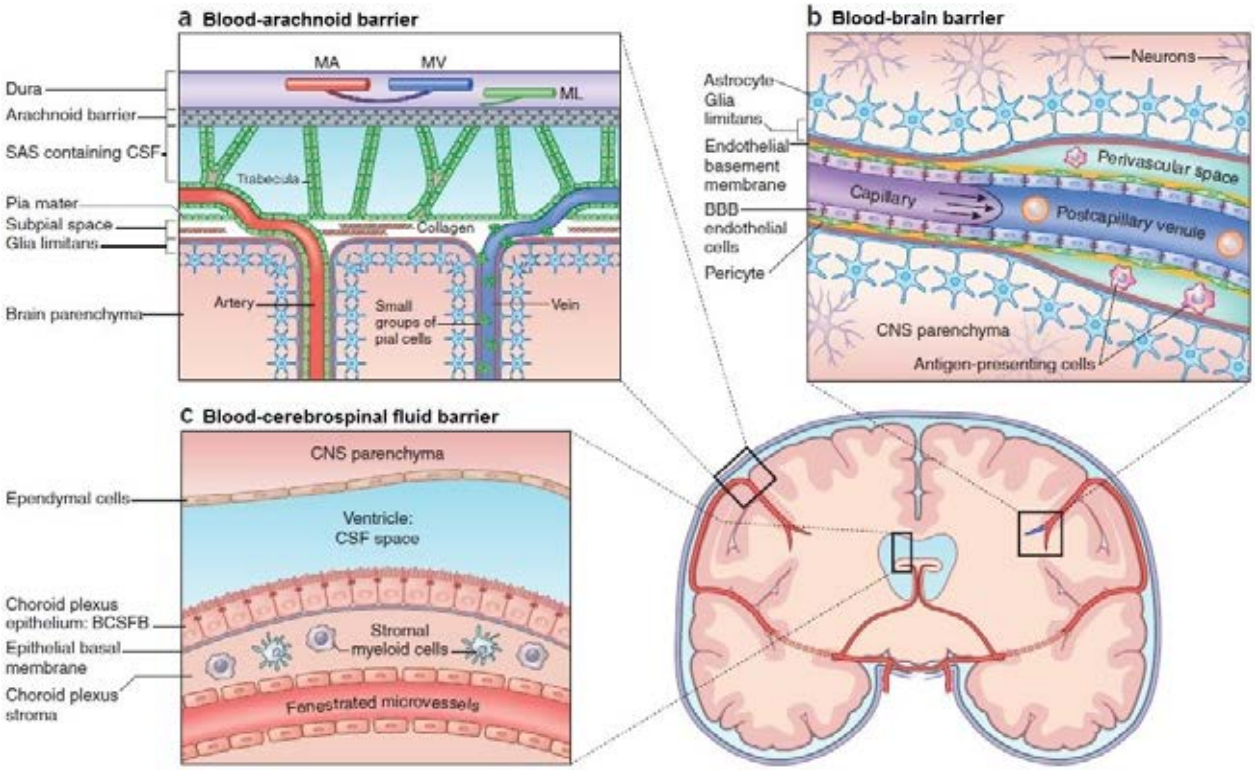

Figure 1.8. Anatomy of CNS barriers. The blood-arachnoid barrier **(A)** surrounds the entire CNS parenchyma and contains meningeal arteries (MA), meningeal vessels (MV) and meningeal lymphatics (ML). The BAB is composed of the arachnoid barrier and the pia mater, forming the inner two layers of the meninges known as the leptomeninges, which are separated by the CSF-filled sub-arachnoid space (SAS). Meningeal vessels traverse the sub-pial and sub-arachnoid spaces, which may provide opportunities for lymphocyte migration. The blood-brain barrier **(B)** is composed of tightly packed endothelial cells linked by tight junctions to form CNS microvessels, which are surrounded by pericytes. Astrocytic foot processes and the endothelial basement membrane form the glia limitans, which opens up at the post-capillary venules to form a perivascular space, where professional APC await migrated lymphocytes. The blood-CSF barrier **(C)** lines the cerebral ventricles and is composed of specialised choroid plexus epithelial cells that help maintain brain homeostasis and secrete CSF into the ventricles. The capillaries of the choroid plexus, which are fenestrated and lack tight junctions, are surrounded by a stromal network containing APC and a substantial vasculature. Adapted from (Englehardt et al., 2017). Reproduced with permission of the copyright owner.

In a P-selectin-dependent manner T cells extravasate from the blood into the choroid plexus parenchyma, where they can subsequently traverse the choroid plexus epithelium to enter the CSF (Engelhardt and Ransohoff, 2012). The precise mechanisms governing these processes are unclear, as adhesion molecules such as vascular cell adhesion molecule (VCAM)-1 (CD106) and intercellular adhesion molecule (ICAM)-1 (CD54) are expressed on the apical surface of the choroid plexus and are not available to T cells. In terms of chemokine receptor requirements, animal models have shown that CCR6-expressing Th17 cells may traverse the BCSFB through binding CCL20, which is constitutively expressed by the choroid plexus epithelium (Vajkoczy et al., 2001; Laschinger et al., 2002; Reboldi et al., 2009). The importance of immunosurveillance is highlighted in those individuals with MS who develop progressive multifocal leukoencephalopathy (PML) following prolonged natalizumab treatment, which inhibits leucocyte trafficking into the CNS by targeting α4-integrin. PML is a rare and often fatal infection caused by John Cunningham virus (JCV), a common virus that is reactivated during immunosuppression; however, symptoms may be further exacerbated by rapid restoration of CNS trafficking which can lead to immune reconstitution inflammatory syndrome (IRIS), a condition associated with high morbidity and mortality rates (Metz et al., 2012; Barber et al., 2012; Purohit et al., 2016).

During inflammation, activated endothelial cells of the BBB or BAB upregulate selectins, including P-selectin, which interact with their glycosylated ligands, such as P-selectin glycoprotein ligand-1 (PSGL-1), expressed by lymphocytes. Subsequent tethering and rolling allows the lymphocyte to bind to chemokines expressed by the endothelium (such as CXCL12, the ligand for CXCR4, and CCL19/CCL21, the ligands for CCR7), increasing their binding capacity for endothelial adhesion molecules by causing conformational changes in the integrins expressed by the lymphocyte. Key molecules mediating lymphocyte arrest include

VCAM-1, which binds VLA-4, and ICAM-1 and -2 (CD102), which binds leucocyte function-associated antigen (LFA)-1 (CD11a). Firm arrest allows diapedesis, via either transcellular or paracellular routes, where they extravasate into the leptomeningeal or perivascular spaces (Shechter et al., 2013; Engelhardt and Ransohoff, 2012).

Unless they re-encounter their specific antigen expressed by APC, T cells are unable to cross into the CNS parenchyma proper; this phenomenon has been elegantly demonstrated using intravital imaging of a rat model of experimental autoimmune encephalomyelitis (EAE), the animal model for MS, where T cells specific for brain antigens could enter the CNS but activated brain antigen-ignorant T cells were not permitted (Bartholomaus et al., 2009). Interaction with cognate APC induces pro-inflammatory cytokine secretion such as IFNγ, TNFα and IL-17; this increases endothelial barrier permeability, allowing influx of additional immune cells, and induces matrix metalloproteinase (MMP) secretion, allowing breach of the glia limitans and access to the CNS parenchyma (Shechter et al., 2013; Engelhardt and Ransohoff, 2012).

In contrast to T cells, very few B cells enter the healthy CNS for immune surveillance, however, B cell numbers are increased during neuroinflammation (Anthony et al., 2003; Cepok et al., 2005a). Although the specific molecules used by B cells are less well understood, it appears that many receptors and chemokines that facilitate T cell trafficking can also be used by B cells; these include ICAM-1, VLA-4 ligands, CXCL12 and CXCL13, with the latter considered a major player in CNS B cell recruitment (Alter et al., 2003; Lehmann-Horn et al., 2015; Blauth et al., 2015). CXCL13 is significantly elevated in the CSF during MS and other neuroinflammatory conditions, is expressed on inflamed endothelium and is strongly associated with B cell-related parameters (Krumbholz et al., 2006; Kowarik et al., 2012; Puthenparampil et al., 2017).

Though the mechanisms for B cell migration into the CNS are not fully clear, it has recently been demonstrated that B cells can undergo bidirectional exchange across the BBB in MS (Fig. 1.9C). This was achieved using advanced high-throughput sequencing, known as deep repertoire sequencing, of Ig heavy chain variable region genes. In matched CSF and peripheral blood samples, five of six donors with MS were found to harbour related clones in the CSF and periphery, although this was also true for some of the control samples (von Budingen et al., 2012). By analysing B cell antibody repertoires from matched CNS and peripheral tissues, related B cell clones were found between CNS compartments and the cervical lymph nodes, however most founding B cell clones were from the cervical lymph nodes, implicating the latter as the primary site of maturation for CNS B cells (Stern et al., 2014). Applying deep sequencing to CSF cells and sorted peripheral blood B cell populations, Ig class-switched memory B cells were identified as the major B cell population involved in bidirectional exchange, although in some individuals, IgG+ plasma cells and CD27-IgD- B cells were also connected to both compartments (Palanichamy et al., 2014a).

1.9.3 T cell involvement in MS

Autoreactive T cells are a major player in the pathogenesis of MS. The active or passive induction of EAE in animals, by immunisation with myelin peptides or adoptive transfer of myelin-specific T cells, demonstrates the ability to induce a CNS demyelinating disease with the immunological, pathological and histological features of MS from a peripheral immune response (Kabat et al., 1948; Constantinescu et al., 2011; Legroux and Arbour, 2015). In addition, the association of several genes with MS pathogenesis that are involved in T cell responses, such as MHC class II, IL-2 and IL-21, suggests an important role for these cells in MS pathogenesis (Sawcer et al., 2011; Weissert, 2013).

Th1 and Th17 cells are considered the dominant T cell populations involved in MS pathogenesis. The Th1/Th17 phenotype shows an exaggerated inflammatory profile in MS, with elevated IFNγ and IL-17 secretion following *ex vivo* stimulation or in response to myelin-associated peptides (Edwards et al., 2010; Cao et al., 2015). Despite these findings, EAE studies suggest that there is no absolute requirement for either cytokine phenotype, although the presence of IL-23 does appear to be necessary as its deficiency in mice confers resistance to disease (Ferber et al., 1996; Haak et al., 2009; Langrish et al., 2005; Lovett-Racke et al., 2011; Gyülvészi et al., 2009; Fletcher et al., 2010). In EAE, IL-23 permits homing of myelin oligodendrocyte protein (MOG)-specific T cells to the CNS, where recruitment into the CNS is regulated by CCR6 and its ligand CCL20 (Gyülvészi et al., 2009; Reboldi et al., 2009).

In humans, CCR6+ T cells in the CSF are largely ex-Th17 (non-classic) Th1 cells that predominantly secrete IFNγ and GM-CSF, which activates CNS-resident microglia and infiltrating macrophages and causes polarisation to a pro-inflammatory M1 phenotype (Restorick et al., 2017; Mazzoni et al., 2015; Shiomi et al., 2016). Interestingly however, infiltrating lymphocytes are predominantly CD8+ T cells, with frequencies consistently dominating that of CD4+ T cells, sometimes by up to 50 times; this increased frequency has been observed in the parenchyma, perivascular cuffs, normal appearing white matter and CSF (Hauser et al., 1986; Salou et al., 2015; Jilek et al., 2007).

In MS the majority of CD8+ T cells show high clonal expansion in lesional/non-lesional brain tissue and CSF, with identical clones found in different brain regions; related CD8+ T cell clones in MS CNS have also been identified in the peripheral blood (Skulina et al., 2004; Junker et al., 2007). Up to 35% of CD8+ T cells within the parenchyma are clonally related, whereas the CD4+ T cell infiltrate is more heterogeneous (Babbe et al., 2000). Infiltrating

CD8+ T cells show biased TCR V-β chain usage, which has also been identified in the peripheral blood T cell repertoire, where there is more skewing in the CD8+ compared to the CD4+ compartment (Babbe et al., 2000; Salou et al., 2015; Gran et al., 1998; Laplaud et al., 2004). CD8+ T cells from MS peripheral blood exhibit exaggerated responses to myelin-derived peptides, and their pathogenicity is supported by EAE studies where MOG-reactive CD8+ T cells induce severe clinical features throughout the disease course following adoptive transfer (Zang et al., 2004; Crawford et al., 2004; Sun et al., 2001; Ford and Evavold, 2005).

1.9.4 B cell involvement in MS

It has been shown that current MS therapies, which were believed to suppress disease activity by depleting T cells, also deplete memory B cells (Baker et al., 2017b). For example, cladribine induces a more marked depletion of B cells than any other immune subset, and anti-neoplastic agents such as mitoxantrone, teriflunomide and cyclophosphamide preferentially target B cells due to their enhanced proliferative capacity compared to T cells (Baker et al., 2017a; Gandoglia et al., 2017; Hurd and Giuliano, 1975; Fidler et al., 1986). In conjunction with the limited efficacy of CD4+ T cell depletion in RRMS, this implicates a strong pathogenic role for B cells in MS (van Oosten et al., 1997; Samijn et al., 2006). B cells have been identified within distinct CNS compartments including the meninges, cortex, normal-appearing white matter and CSF; they have also been observed in MS lesions, where their immunoglobulin proteomes and transcriptomes strongly overlapped with those in the CSF, indicating an active and dynamic B cell component (Lucchinetti et al., 2000; Owens et al., 2003; Lovato et al., 2011; Obermeier et al., 2011). The presence of B cell aggregates, referred to as ectopic lymphoid-like follicles, have been reported in the meninges of some SPMS post-mortem brain specimens (Fig. 1.9B). Though devoid of mantle zones, these structures display features of germinal centres and contain proliferating B cells organised

around a stromal niche, with FDC secreting the B cell chemoattractant CXCL13 (Serafini et al., 2004). These follicles appear to be functional structures containing a number of AID-expressing B cells, providing evidence for class switching and somatic hypermutation; features of a sustained T cell-dependent B cell response (Serafini et al., 2007). Furthermore, detailed analysis of post-mortem tissue suggests that the development and maintenance of these follicles is associated with local neurodegeneration and cell loss, correlating clinical disability with B cell activity (Magliozzi et al., 2010). As such, these findings implicate the CNS as an environment conducive to long-term B cell survival.

1.9.4.1 CSF analysis

Class-switched CD27+, IgM-IgD- memory B cells accumulate in MS CSF, and short-lived plasmablasts have been identified as the main effector B cell subset in MS, constituting up to 30% of the CSF B cell pool (Cepok et al., 2001; Cepok et al., 2005a; Winges et al., 2007). CSF plasmablasts correlate with intrathecal IgG levels and parenchymal inflammation, and are present throughout the disease course, in contrast to those with infectious neurological diseases where CSF plasmablasts disappear rapidly following resolution of inflammation (Cepok et al., 2005a). Some studies have also identified CSF ASC with a mature CD19- phenotype, implicating a continuum of CNS B cell differentiation that is detectable in the CSF (Corcione et al., 2004; Winges et al., 2007). In contrast, other groups have failed to identify these cells in the CSF (Cepok et al., 2005a; Kuenz et al., 2008).

Several markers of B cell activity have been identified within the MS CSF. Notably, CXCL13 shows the strongest association and is significantly elevated in the CSF but not the serum of individuals with CIS, RRMS and PPMS compared to non-inflammatory controls, also correlating with B cell counts, intrathecal IgG synthesis, MRI activity and relapse rate (Kuenz et al., 2008; Kowarik et al., 2012). Although other markers of B cell activity have also been

implicated, they are often associated with contradictory findings. BAFF levels are elevated in MS CSF compared to controls, with higher levels in those with progressive disease and during relapse, and shows positive correlations with CXCL13, IL-6, IL-10 and APRIL (Ragheb et al., 2011; Wang et al., 2012). In contrast, a recent study found significantly decreased BAFF levels in MS CSF, with the authors speculating the absorption of BAFF by local ASC in the earlier stages of disease (Puthenparampil et al., 2017). In addition, IL-15 and CXCL12 were elevated in some studies, but as a hallmark of MS, OCB remain the most consistent immunological feature of the disease (Krumbholz et al., 2006; Rentzos et al., 2006).

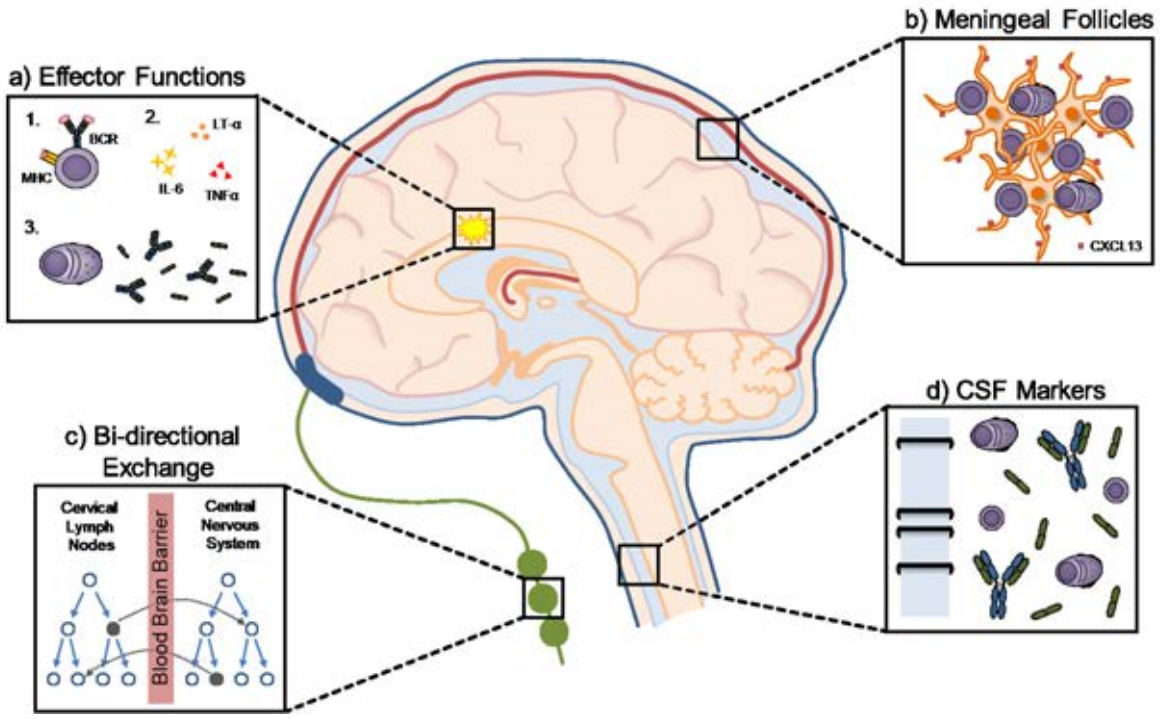

Figure 1.9. The involvement of B cells in multiple sclerosis. B cells may contribute to MS pathogenesis through various effector functions, such as antigen presentation, cytokine secretion and antibody production (A). B cells and antibody-secreting cells may survive in ectopic follicles within the CNS (B) and may undergo bidirectional exchange across the blood-brain barrier (C). In addition, the presence of CSF B cell markers, including antibodies and free light chains, is suggestive of B cell activity in MS (D).

1.9.4.2 Cytokine profiles of B cells in MS

B cells may contribute to MS pathogenesis through several mechanisms (Fig. 1.9). The defining feature of B cell biology is the production of antibodies; however, the immediate benefits of anti-CD20 treatment, combined with the persistence of long-lived ASC and OCB, suggests that antibodies may not play a substantial role in MS pathology (Piccio et al., 2010). B cell-derived cytokines may contribute to disease pathology and are reportedly perturbed in MS. B cells from people with MS display elevated capacity to secrete pro-inflammatory cytokines including IL-6, lymphotoxin-α, TNFα and GM-CSF, and demonstrate a diminished capacity to secrete IL-10 compared to healthy controls (Barr et al., 2012; Duddy et al., 2007; Li et al., 2015).

1.9.4.3 Antigen presentation by B cells in MS

Since B cells are strong presenters of antigen, this function could be their major contribution to MS pathogenesis (Fig. 1.9A). Memory B cells from RRMS blood can induce activation and proliferation of cognate T cells in response to myelin-associated antigens (Harp et al., 2010). B cells from the blood and CSF of those with MS express higher levels of co-stimulatory molecules compared to controls, and express higher levels of HLA-DR, suggesting a stronger propensity for antigen presentation (Fraussen et al., 2016; Mathias et al., 2017). In addition, mice with a B cell-specific defect in MHC class II molecules are resistant to EAE induction, and B cell-mediated antigen presentation enhances EAE severity and is required for maximal disease (Molnarfi et al., 2013; Parker Harp et al., 2015).

1.9.4.4 The contribution of antibodies to MS

A hallmark of MS is the presence of CSF antibodies (Fig. 1.9D). Demyelinating type II lesions, which are associated with substantial IgG and complement deposition, are the most

common lesion type in MS (Lassmann et al., 2007). Antibodies in the brain are thought to bind Fc receptors expressed by phagocytes, which process and present the antigen in the context of MHC class II molecules which can subsequently activate cognate CD4+ T cells. In B cell-dependent EAE models, where disease is sub-clinical in B cell-deficient animals, autoreactive CD19+ plasmablasts contributed to disease pathology by producing autoreactive antibodies, and transfer of MOG-primed B cells is sufficient to induce disease in MOG-immunised B cell-deficient mice (Chen et al., 2016a; Lyons et al., 2002). In humans, antibodies are prominent in active MS lesions where they associate with areas of myelin degeneration (Lucchinetti et al., 2000).

1.9.4.5 Possible autoantigens associated with MS

Candidate targets of MS antibodies have been extensively investigated over the years, with myelin sheath components such as MOG and myelin basic protein (MBP) frequently identified (Pittock et al., 2007; von Budingen et al., 2008; Menge et al., 2011). These proteins, along with several others, are distributed amongst lipids in the myelin sheath and their exposure allows them to be targeted by antibodies (Podbielska et al., 2013). In animals, antibodies towards myelin components are capable of inducing demyelination and augmenting T cell-mediated EAE (Linington et al., 1988; Schluesener et al., 1987). Elevated reactivity of serum and CSF immunoglobulin towards myelin proteins has been observed in MS but not controls, and B cells specific for MOG and MBP have been identified in the periphery of those with MS (Xiao et al., 1991; Markovic et al., 2003; Reindl et al., 1999; Harp et al., 2010). Conversely, using various technological methods, several other studies have shown that CSF antibodies were either not reactive to myelin antigens, or were characterised by very low affinity binding; these included histological analysis of MS brain sections, western blotting, protein arrays and immunoprecipitation, using serum or CSF antibodies or

recombinant antibodies produced from CSF-derived ASC (O'Connor et al., 2003; Kuhle et al., 2007; Owens et al., 2009; Ayoglu et al., 2016; Levin et al., 2013). Additionally, the presence of equivalent levels of functional anti-MBP antibodies in healthy individuals, and the presence of anti-MOG antibodies in several other CNS conditions such as neuromyelitis optica (NMO) and acute disseminated encephalomyelitis (ADEM), indicates that myelin is not the primary autoimmune target for B cells in MS (Xiao et al., 1991; Hedegaard et al., 2009; Mader et al., 2011; O'Connor et al., 2007).

Many other candidate autoantigens have been described in MS; these include those directed towards structural and molecular components, including neurofilament light chain, anoctamin 2 and neurofascin, small molecules, such as alpha-B crystallin, and microbial antigens, such as EBV, measles, rubella and zoster (MRZ) viruses and *Chlamydia pneumoniae* (Amor et al., 2014; Ayoglu et al., 2016; Mathey et al., 2007; van Noort et al., 1995; Felgenhauer et al., 1985; Nociti et al., 2010; Sriram et al., 1999). The search for MS target antigens has also been extended to lipids. It has been reported that up to 60% of people affected by MS demonstrate serum and CSF reactivity towards myelin-derived lipids, particularly sulfatide, ganglioside and cerebroside (Brennan et al., 2011; Ilyas et al., 2003; Kanter et al., 2006). Lipid reactivity is also associated with IgM, which correlates with a more aggressive disease course (Villar et al., 2015). However, the inconsistent reproducibility between studies, and the generally low proportion of individuals with autoantibodies of a given specificity, implicate a real need for further investigating the antibody response in MS, especially considering the potential impact of identifying common autoantigens that are specific to MS.

1.9.4.6 Features of the antigen-driven B cell response

Irrespective of their antigen specificities, evidence suggests an antigen-driven B cell response in MS. Extensive somatic hypermutations of IgG heavy and light chain V regions, particularly

in the complementarity-determining region (CDR)3, with overrepresentation of VH4 and VH2 gene segments, is a key feature of B cells in MS brain lesions (Baranzini et al., 1999; Owens et al., 1998) and in the CSF (Owens et al., 2007; Colombo et al., 2000; Qin et al., 1998). VH4 and VH2 germline sequences share related sequence homology and since the VH4 bias appears earlier than the VH2 bias in MS, this could represent an evolving immune response from one to several antigenic targets (Bennett et al., 2008; Kirkham et al., 1992). Though less frequently studied, CSF light chain sequences also demonstrate high levels of homology, with remarkably similar V_{κ} regions identified in CSF B cells from three out of three MS CSF samples; this was particularly evident within the kappa light chain CDR, which forms part of the antigen binding site (Blalock et al., 1999). In addition to suggesting a restricted antigen response that is shared between affected individuals, this study also supports the contribution of light chains to MS pathogenesis.

Light chains have long been associated with MS pathogenesis. Studies spanning nearly 50 years have reported elevated FLC in MS CSF, with preferential bias towards kappa light chain usage (Link and Zettervall, 1970; Zeman et al., 2012; Presslauer et al., 2014; Hassan-Smith et al., 2014). A normal serum kappa to lambda light chain ratio is approximately 1.6:1 in favour of kappa light chain but can be skewed in either direction during persistent immunological challenges such as chronic inflammation or autoimmunity (Barnidge et al., 2014). This bias presumably relates to a restricted antigen response, caused by monoclonal or oligoclonal expansion of antigen-specific B cell clones. An immunohistochemistry study using post-mortem MS brain tissue demonstrated biased expression of kappa light chains in active ASC-containing lesions at a ratio of 2.3:1, compared to a ratio of 1.6:1 in non-active lesions (Esiri, 1977). A more recent study identified a kappa light chain bias of over 10:1 in blast-like CD19+ B cells in three MS CSF samples from individuals who went on to develop

MS (Vafaii and DiGiuseppe, 2014). This evidence points to the phenomenon of a kappa light chain bias in MS patients, indicative of a clonal B cell response.

1.10 Project Aims

It is appreciated that B cells play a role in MS pathogenesis, but their precise features in MS CSF remain to be determined. B cells and ASC have been identified in MS CSF, and some studies have reportedly identified mature ASC, indicative of a sustained B cell response, although this has been disputed by others. Additionally, the identification of clonal B cell populations in MS brain compartments, and their ability to traffic between the CNS and periphery, raises questions as to the relative contributions of CNS-expanded B lineage cells, which may sustain disease, versus peripheral B cells, which may gain access to the CNS through an inflamed BBB. The presence of clonally expanded B cell populations, in addition to the elevated ratio of kappa light chains (Igκ) to lambda light chains (Igλ) in MS CSF, implicate the involvement of a dominant autoantigen capable of inducing an Igκ-biased antibody response. As such, the initial aims of this thesis were to:

1) **Identify, characterise and quantify B cells and ASC in the CSF and peripheral blood of CIS, established MS and control groups.**
2) **Investigate the heavy and light chain isotypes on B cells and ASC in the CSF and peripheral blood of CIS, established MS and control groups.**

Despite extensive investigations, the antigen specificity of CSF antibodies in MS remains elusive and not well-characterised, however the availability of increasingly sophisticated applications allows the use of high-throughput approaches to investigate potential autoantigens in autoimmunity. With the assumption that CSF antibodies are pathogenic,

identification of the antigen responsible for inducing an Igκ-biased antibody response, which is a key feature of MS CSF, could have important implications for understanding how MS is triggered and how it could be treated. The antigen specificities of antibodies bearing Igκ versus those with Igλ light chains have not before been investigated, therefore, using high-density protein arrays, the next aim of this investigation was to:

3) **Investigate the antigen specificities of CSF antibodies from CIS, established MS and control groups and investigate whether certain antigens induce a skewed kappa light chain response.**

In addition to the ongoing interest in CSF antibody specificity, the rapid and sustained clinical benefits of anti-CD20 therapeutics in reducing inflammatory brain lesions and relapse rates has been attributed to the removal of antibody-independent functions mediated by CD20+ B cells, since CSF antibody remains largely unaffected (Hauser et al., 2008; Bonnan, 2014). Intriguingly, while CSF B cells are almost fully eliminated by anti-CD20 therapeutics, CSF T cell numbers also show a marked reduction in frequency (Cross et al., 2006). One possibility for this phenomenon is the contribution of CD20-expressing T cells to MS pathogenesis. These cells, which are reportedly increased in MS blood versus controls and are present in MS brain tissue, were shown to be removed following rituximab treatment, implicating possible involvement in disease (Wilk et al., 2009, Palanichamy et al., 2014b; Holley et al., 2014). In addition, the elusive nature of this pro-inflammatory T cell population warrants further investigation into their phenotype and function in health and disease (Schuh et al., 2016). Therefore, the final aim of this thesis was to:

4) **Investigate the frequency and phenotype of CD20+ T cells in the peripheral blood and CSF of MS and OND groups, and characterise these cells in healthy donors *in vitro.***

CHAPTER 2

MATERIALS AND METHODS

Chapter 2: Methods

2.1 Materials

Table 2.1 Common laboratory reagents.

Description	Components
PBS	Phosphate buffered saline (8g/l NaCl, 0.26g/l KCl, 1.15g/l Na_2HPO_4, 0.2g/ml KH_2PO_4); prepared as 1 tablet in 100ml distilled H_20 (Oxoid, Basingstoke, UK)
FACS buffer	PBS with 2% Bovine Serum Albumin (BSA; Sigma Aldrich, Dorset, UK)
RPMI medium	RPMI 1640 medium (Sigma Aldrich) with 1% GPS (2mM L-glutamine, 100U/ml penicillin, 100ug/ml streptomycin; HyClone, Northumberland, UK) and 1% HEPES (Sigma Aldrich)
RPMI + 10% FCS	RPMI-1640 medium with 10% heat-inactivated foetal calf serum (FCS; Biosera, Ringmer, UK)
MACS buffer	PBS, 0.5% BSA and 2mM ethylenediaminetetraacetic acid (EDTA; Sigma Aldrich)
Sort buffer	1:1 RPMI-1640 medium with heat-inactivated foetal calf serum
Planar array assay buffer	PBS + 0.1% tween + 3% BSA + 160µg/ml His_6-ABP
Planar array wash buffer	PBS + 0.1% tween
Suspension bead array assay buffer	PBS + 0.1% tween + 3% BSA + 160µg/ml His_6-ABP
Suspension bead array wash buffer	PBS + 0.05% tween

2.2 Antibodies

Table 2.2 Primary monoclonal antibodies used to detect surface and intracellular proteins by flow cytometry.

Specificity	Fluorochrome	Company	Cat. No	Clone	Dilution
CD19	Alexa Fluor 488	BioLegend	302219	HIB19	1/20
	Bv605	BioLegend	302244	HIB19	1/320
CD20	Bv421	BioLegend	302330	2H7	1/40
	Bv711	Biolegend	302342	2H7	1/80
	PE	Biolegend	302306	2H7	1/20
CD27	APC-Cy7	BioLegend	302816	O323	1/40
CD138	PE	BioLegend	356504	MI15	1/20
	Alexa Fluor 700	Biolegend	356511	MI15	1/20
CD38	PE-Cy7	BioLegend	356608	HB-7	1/200
Igκ	PerCP-Cy5.5	BioLegend	316516	MHK-49	1/10 (surface) 1/33 (IC)
Igλ	APC	BioLegend	316610	MHL-38	1/5 (surface) 1/50 (IC)
IgA	VioBright FITC	Miltenyi Biotec	130-104-726	IS11-8E10	1/80
IgG	PE-CF594	BD Biosciences	562538	G18-145	1/80
IgM	Bv650	BioLegend	314526	MHM-88	1/320
CD3	Bv510	BioLegend	317332	OKT3	1/100

CD4	Pe-Cy7	Miltenyi Biotec	130-096-552	VIT4	1/80
CD8α	APC eFluor 450	eBioscience eBioscience	17-0087 48-0087-42	SK1 SK1	1/1000 1/100
CD54RA	PE-Texas Red	BD Biosciences	562298	HI100	1/800
CCR7	Alexa Fluor 488	BioLegend	353206	G043H7	1/20
IFNγ	PE	eBioscience	12-7319	4S.B3	1/20
IL-17A	PerCP-Cy5.5	eBioscience	45-7179	eBio64DEC17	1/40
CCR6	APC	Biolegend	353416	G034E3	1/20
CD25	PerCP-Cy5.5	eBioscience	45-0259	BC96	1/20
CD69	APC-Cy7	Biolegend	310914	FN50	1/40
CD107a	FITC	Biolegend	328606	H4A3	1/20
Perforin	PE	Biolegend	308106	dG9	1/20
Granulysin	PE	eBioscience	12-8828	DH2	1/20
Granzyme A	PE-Cy7	eBioscience	25-9177	CB9	1/20
Granzyme B	PE	Biolegend	561142	GB11	1/20
FASL (CD178)	PE	BD Biosciences	NOK-1	564261	1/20
CTLA-4 (CD152)	PE	Biolegend	349906	L3D10	1/20
PD-1	PE	Biolegend	329906	EH12.2H7	1/20
TIM-3	PE	Biolegend	345006	F38-2E2	1/20
GM-CSF	PE	BD Biosciences	554507	BVD2-21C11	1/160

IL-4	PE	eBioscience	12-7049-42	8D4-8	1/20
IL-5	PE	Biolegend	500904	JES1-39D10	1/20
IL-10	PE	eBioscience	12-7108	JES3-9D7	1/1000
IL-13	PE	BD Biosciences	340508	JES10-5A2	1/20
IL-2	PE	eBioscience	12-7029	MQ1-17H12	1/3000
LTα	PE	BD Biosciences	554556	359-81-11	1/50

Table 2.2 Primary monoclonal antibodies used to detect surface and intracellular proteins by flow cytometry. Shown for each antibody is the antigen specificity, fluorochrome, order details, clone and dilution used. Abbreviations: Brilliant violet (Bv), phycoerythrin (PE), fluorescein isothiocyanate (FITC), allophycocyanin (APC), peridinin chlorophyll protein cyanine 5.5 (PerCP-Cy5.5), cyanine 7 (Cy7), intracellular (IC).

Table 2.3 Isotype controls used for flow cytometry.

Specificity	Fluorochrome	Company	Cat. No
Mouse IgG2b	Bv421	BioLegend	400342
Mouse IgG2b	PE	BioLegend	400314
Mouse IgG1κ	PE	Biolegend	400112
Rat IgG2aκ	PE-Cy7	Biolegend	400521
Rat IgG2aκ	PE	Biolegend	400508
Rat IgG1κ	PE	eBioscience	12-4031

Appropriate isotype controls were used on the same fluorochrome and at the same concentration of their matched antibody. On occasions where no appropriate isotype control was available, gates were set using a fluorescence minus one (FMO) panel, in which the antibody of interest was omitted. Flow cytometry gates were set at 1% positivity on the isotype control/FMO, except for when gating on CD20+ T cells, which were set at 0.5% positivity or less.

2.3 Samples and Ethics

Individuals undergoing elective diagnostic lumbar puncture with a suspected or confirmed diagnosis of MS, or control patients undergoing diagnostic or therapeutic lumbar puncture, were prospectively recruited from the Queen Elizabeth Hospital, University Hospitals Birmingham NHS Foundation Trust (QEHB) for matched peripheral blood and CSF. For studies requiring large numbers of cell-free CSF samples (i.e. the antigen arrays), historical banked CSF was used, which was collected between 2011 – 2016.

Individuals were stratified into the following groups according to clinical criteria based on the diagnosis of MS: clinically isolated syndrome (CIS), relapsing-remitting (RRMS), primary progressive (PPMS) and those with MS recently ceasing natalizumab therapy (NAT). A combination of RRMS and PPMS was collectively referred to as clinically definitive MS (CDMS). Individuals with other neurological diseases (OND) and other neurological inflammatory diseases (ONID) were also included in the study. The OND cohort consisted of individuals diagnosed with headaches and headache-related disorders, hydromyelia, non-epileptic attacks, anxiety and diabetic neuropathy. The ONID cohort were more heterogeneous, with diagnoses including autoimmune neuropathy, Behcet's syndrome, neurosarcoidosis and transverse myelitis.

Individuals were recruited after obtaining informed written consent and ethical approval was provided under study 'Molecular and Cellular Studies on Inflammation in Multiple Sclerosis' (UKCRN ID 13585). For healthy controls, peripheral blood was taken from donors recruited at the University of Birmingham, with ethical approval under 'Immune mechanisms in the ocular microenvironment' (UKCRN 4654) or 'Adaptive immunity in multiple sclerosis'

(ERN_15-1608A). For each results chapter within this thesis, the clinical information can be found within Appendices I-III.

2.4 Preparation of Cerebrospinal fluid

CSF was collected following non-traumatic diagnostic or therapeutic lumbar puncture from consenting individuals at the QEHB. CSF was centrifuged at 600x*g* for 8 min and the cell-free CSF was collected and stored at -80°C for later analysis. The CSF cell pellet was stained for surface and/or intracellular markers, either directly or following *in vitro* stimulation.

2.5 Peripheral blood mononuclear cell (PBMC) isolation

Peripheral blood was collected into EDTA-containing tubes (Greiner Bio-One, Gloucestershire, UK) and was diluted 1:1 with serum-free RPMI. Up to 18ml blood was layered onto 7ml Ficoll-paque (GE Healthcare Bio-Sciences, Uppsala, Sweden) and centrifuged at 400x*g* for 30 min with no brake applied. For PBMC isolation from lymphocyte cones (National Blood Service, Birmingham), blood was diluted to a volume of 30ml and 15ml was layered onto 15ml Ficoll-paque in two 50ml falcon tubes. Mononuclear cell layers were harvested and washed in RPMI at 300x*g* for 8 min, then at 200x*g* for 8 min to remove platelets. For PBMC isolation from lymphocyte cones, red cell lysis buffer (Sigma Aldrich; 3-4ml for up to 5 min) was used to deplete red blood cells present in the pellet. PBMC were re-suspended in 10ml RPMI + 10% FCS and counted with the addition of trypan blue dead cell exclusion dye (Sigma Aldrich). PBMC were washed a final time at 300x*g* for 8 min and were resuspended at the required volume for further applications.

2.6 Fluorescence Activated Cell Sorting (FACS)

Prior to isolating CD20- and CD20+ CD8+ memory T cells by fluorescence activated cell sorting (FACS), PBMC from lymphocyte cones were first stained with eFluor™ 450 Cell Proliferation Dye (eBioscience, Leicestershire, UK). PBMC were twice centrifuged in 10ml PBS at 300x*g* for 4 min and were resuspended in an appropriate volume of PBMC to yield $20x10^6$ cells/ml. This was added 1:1 to a 1/500 dye solution, to yield a final dye concentration of 10μM. The cell suspension was thoroughly mixed and incubated at 37ºC for 10 min in the dark. The labelling reaction was quenched by adding a 4-5x volume of cold RPMI + 10% FCS and incubating on ice for 5 minutes. Cells were then centrifuged 3 times at 300x*g* for 4 min. PBMC were then pre-enriched for CD8+ memory T cells using a negative selection magnetic isolation kit (Miltenyi Biotec, Surrey, UK) following the manufacturer's instructions. For 10^7 cells, PBMC were incubated in 40μl MACS buffer with 10μl biotin-antibody cocktail against CD4, CD11c, CD14, CD15, CD16, CD19, CD34, CD36, CD45RA, CD56, CD57, CD61, CD123, CD141, TCR γ/δ, and CD235a for 10 min at 4ºC. PBMC were washed in 1-2ml MACS buffer and incubated with 80μl MACS buffer plus 20μl anti-biotin microbeads for 15 min at 4ºC. PBMC were resuspended at the recommended volume and were passed through a pre-rinsed LS column (Miltenyi Biotec) on a magnetic MidiMACS™ separator. The unlabelled CD8+ memory T cell fraction was eluted and stained with surface markers for 20 min on ice, along with the appropriate single colour compensation controls. Cells were washed and resuspended in 2ml RPMI + 10% FCS. Cell sorting was performed on a MoFlo Astrios Flow Cytometer Cell Sorter (Beckman Coulter, High Wycombe, UK) using the gating strategy established in Chapter 5, Fig. 5.10B.

2.7 Cell culture

In vitro cell culture assays were carried out in 96 well round-bottom plates, using RPMI + 10% FCS as the assay media, with a total volume of 200µl per well.

2.7.1 T cell stimulation assays

For assessment of cytokine secretion by T cells from MS (CIS, RRMS or PPMS) and OND groups, samples were prepared as described above and both PBMC (adjusted to $1x10^6$ cells per well) and CSF cells were resuspended in RPMI + 10% FCS and stimulated at 37ºC for 3 hours with phorbol 12-myristate 13-acetate (PMA; 50ng/ml) and ionomycin (750ng/ml) in the presence of brefeldin A (0.1µg/ml; all from Sigma Aldrich) to inhibit intracellular protein transport. These were subsequently prepared for flow cytometry (section 2.8).

For longer term T cell stimulation, isolated CD20+ and CD20- T cells were prepared as in section 2.6 and seeded at $2x10^4$ cells per well in RPMI + 10% FCS with the addition of recombinant human IL-2 at 25U/ml (PeproTech, London, UK). Where required, $1.8x10^5$ PBMC were added to give a 10:1 ratio. Cultures were stimulated with Dynabeads® Human T-Activator CD3/CD28 beads (Life Technologies, Paisley, UK) at a 1:1 cell to bead ratio, or ImmunoCult™ Human CD3/CD28 T cell activator (StemCell Technologies, Cambridge, UK) using 25µl per 1ml cell suspension, as instructed by the manufacturer. Alternatively, cells were left unstimulated. Cultures were incubated for 4 days at 37 ºC and were subsequently stained for CD8 and CD20, with a corresponding FMO/isotype control used, and analysed by flow cytometry (section 2.8).

2.7.2 Degranulation assays

To assess the ability of T cells to release cytotoxic molecules in response to stimulation, expression of CD107a (also known as lysosomal-associated membrane protein-1 or LAMP-1)

and perforin were analysed simultaneously on an hourly basis for a total of 3 hours. PBMC were stimulated as described in the presence of FITC-conjugated anti-human CD107a and brefeldin A. PBMC were then stained for surface markers to allow the identification of CD20+ T cells within T cell subsets, fixed and stained for intracellular perforin. Flow cytometry gates were set on stimulated control wells in the absence of CD107a and perforin.

2.8 Multi-colour Flow Cytometry

2.8.1 Surface staining

1-5x10^6 cells (depending on application) were washed in FACS buffer by centrifugation at 300x*g* for 4 min. Where required, cells were first stained with Zombie Aqua™ Fixable Viability dye diluted in cold PBS (1/400; BioLegend, London, UK) on ice for 20 min and washed in FACS buffer at 300x*g* for 4 min. Cells were stained with 50µl fluorescently labelled antibodies to detect surface markers for 20 min on ice in the dark. 100µl FACS buffer was added and cells were centrifuged at 300x*g* for 4 min. For immediate analysis by flow cytometry, cells were resuspended in a final volume of 300µl FACS buffer, or were alternatively fixed, either for later analysis or for intracellular staining (see below).

2.8.2 Intracellular staining

Cells were fixed in medium A (FIX & PERM® cell fixation kit, Life Technologies) for 15 min at room temperature (RT) and washed in FACS buffer by centrifugation at 300x*g* for 4 min. Cells for surface marker staining only were re-suspended in 100µl FACS buffer and stored at 2-8°C for later analysis. Cells were resuspended in 50µl permeabilisation buffer (medium B), containing fluorescently labelled antibodies to detect intracellular markers, for

20 min at RT. Cells were washed in 100µl FACS buffer by centrifugation at 300x*g* for 4 min, and were resuspended in 300µl FACS buffer for immediate analysis, or were resuspended in 100µl and stored at 2-8°C for later analysis.

Table 2.4 Antibody panels used for flow cytometry analysis.

Panel	Description	Antibodies
B cell phenotyping	CSF and peripheral blood, MS/control groups	CD19, CD20, CD27, CD38, CD138, Igκ, Igλ, IgG, IgM, IgA
CD20+ T cell cytokine secretion – 3h stimulation	CSF and peripheral blood, MS/control groups	CD3, CD8a, CD20, CD45RA, CCR7, IFNγ, CCR6, IL-17A
CD20+ T cell phenotyping - resting or 3h stimulation	Peripheral blood, healthy donors	CD3, CD8a, CD45RA, CCR7 plus various surface or intracellular markers for phenotyping
CD20+ T cell sort/post-culture panel	Peripheral blood, healthy donors	CD8a, CD45RA, CD20
CD20+ T cell degranulation assay	Peripheral blood, healthy donors	CD3, CD8a, CD45RA, CD107a, perforin
Tetramer panel	Healthy donors	APC-labelled tetramer, CD3, CD8, CD20

Shown are antibody panels used throughout the thesis along with a description of samples they were used for, to identify and characterise various cell populations.

2.8.3 Tetramer staining

Tetramer staining was performed using APC-labelled tetramers towards two common EBV lytic cycle peptides, GLC (amino acid sequence: GLCTLVAML) or YVL (amino acid

sequence: YVLDHLIVV) (Moosmann et al., 2010). Frozen PBMC from three HLA-A*02-positive donors were thawed, washed in 15ml RPMI + 10% FCS and counted. PBMC were resuspended at 2-3x10^6 cells per well and were stained with the APC-labelled tetramers for 30 min at 37ºC at a dilution of 1/25 in FACS buffer. PBMC were washed in FACS buffer at 300x*g* for 4 min and were stained with surface antibodies towards CD3-Bv510, CD8-eFluor™ 450 and CD20-PE for 20 min at RT, washed at 300x*g* for 4 min and resuspended in 300µl FACS buffer. Cells were then analysed using flow cytometry.

PBMC and tetramers were kindly donated by Dr Heather Long, Institute of Immunology and Immunotherapy, University of Birmingham.

2.8.4 Flow cytometry data analysis

Samples were ran on a BD LSR Fortessa™ flow cytometer (BD Biosciences, Oxford, UK) or a Cyan ADP flow cytometer (Beckman Coulter, High Wycombe, UK). Single colour compensation was achieved using surface-stained PBMC or OneComp eBeads (eBioscience). Data was analysed using Kaluza Flow Cytometry Analysis Software v1.2 (Beckman Coulter).

2.9 Free light chain quantification

FLC concentrations were measured by nephelometry using the latex particle-enhanced, Freelite® κ and λ immunoassays on a Dade-Behring BN ™ II Analyser (Bradwell et al., 2001). Assays were performed by The Binding Site Group Ltd (Birmingham, UK), using anonymised coded samples. The limit of detection for the κ FLC assay was 0.06 mg/l and 0.05 mg/l for the λ FLC assay.

2.10 CXCL13 Luminex assay

A Luminex assay for CXCL13 was performed using the Bio-Plex Pro™ reagent kit III (cat.no 171304090M) following manufacturer's instructions. All reagents were purchased from Bio-Rad Laboratories Ltd, Hertfordshire, UK. The standard (Bio-Plex Pro™ human chemokine standard, cat.no 171-DK0001) was reconstituted and serially diluted four-fold to produce eight standards. Blank wells containing wash buffer were also included. 50µl neat CSF from a OND and MS groups were incubated with 50µl coupled magnetic beads (Bio-Plex Pro™ human chemokine BCA-1/CXCL13 set, cat.no 171BK12MR2) for 1 hour on a shaker at RT. The plate was washed 3 times with 100µl wash buffer before adding 25µl of the detection antibody to each well. The plate was incubated for 30 min on a shaker in the dark and washed 3 times with 100µl wash buffer. 50µl of streptavidin-PE antibody was added to each well and the plate was incubated as previously for 10 min. The plate was washed 3 times with 100µl wash buffer and each well was resuspended in 125µl assay buffer. The plate was covered and placed on a shaker for 30 seconds prior to running on a Bio-Rad Bio-Plex 200 machine.

2.11 Quantitative Polymerase Chain Reaction (qPCR)

2.11.1 mRNA isolation from sorted lymphocyte subsets

Sorted cell subsets (B cells, CD20- T cells and CD20+ T cells) were washed in cold PBS at 400x*g* for 8 min. Cell sorts yielding <1,000 cell equivalents per reaction were discarded.

mRNA was isolated using µMACS mRNA Isolation kit (Miltenyi Biotec, Surrey, UK) following the manufacturer's instructions. Cells were lysed by vigorously vortexing in lysis buffer, and cell lysate was removed by centrifuging in LysateClear columns at 13,000x*g* for 3

min. The cleared lysate was mixed with Oligo(dT) MicroBeads and magnetically retained in a MACS column placed in the magnetic field of a µMACS Separator, retaining the magnetically-labelled mRNA within the column. The column was washed with Lysis Buffer and Wash Buffer.

2.11.2 cDNA synthesis from mRNA

cDNA was synthesised using µMACS One-Step cDNA Synthesis Kit (Miltenyi Biotec) following the manufacturer's instructions as follows: the column was washed twice with Equilibration/Wash Buffer and reconstituted Enzyme Mix was added to the column, followed by sealing solution to avoid evaporation, and incubated for 1 hour at 42°C. The column was rinsed twice in Equilibration/Wash Buffer and cDNA Release Solution was added to the column for 10 min before eluting the cDNA with 50µl cDNA Elution Buffer. cDNA was stored at -20°C until further analysis.

2.11.3 qPCR assay

qPCR was performed on a LightCycler 480 PCR machine (Roche, Basel, Switzerland) in 384 well plates. The reaction mix was prepared with 2.5µl LightCycler 480 probes mastermix (Roche), up to 1.8µl cDNA, 0.35µl primer-limiting glyceraldehyde 3-phosphate dehydrogenase (GAPDH) Taqman probe and 0.35µl CD20 Taqman probe (Life Technologies), made up to a total reaction volume of 5µl with DEPC-treated water (Life Technologies). Cycle steps included a pre-incubation cycle at 95ºC for 10 min, 40 amplification cycles at 95ºC (10 seconds), 60 ºC (1 min) and 72ºC (1 second), and a cooling cycle at 40ºC for 10 seconds.

2.11.4 Determination of relative gene expression

Following qPCR, amplification curves were analysed using the LightCycler 480 software (Roche). The cycle threshold (Ct) values for the housekeeping gene (GAPDH) and the gene of interest (CD20) was determined and the difference between them calculated to generate the ΔCt value; this normalises the Ct value for each sample based on the level of GAPDH expression and accounts for variation in cDNA concentrations. The difference in ΔCt values was determined to obtain the ΔΔCt, using sorted B cell cDNA as a positive control for CD20 expression. Finally, the fold change in CD20 expression (2^-ΔΔCt) was calculated to determine the relative gene expression for each sorted T cell subset.

2.12 Antigen arrays

The antigen arrays were conducted in Stockholm, Sweden within Professor Peter Nilsson's laboratory (Science for Life Laboratory, Tomtebodavägen 23a, 171 65 Solna, Sweden). Antigen arrays used in this study were either on glass slides (planar arrays) or magnetic beads (suspension bead arrays) and the arrays were generated in-house. For an overview of the assay methodology see Fig. 2.1, and for an overview of the assay workflow see Fig. 2.2.

2.12.1 Antigens

The antigens used this study, also known as PrESTs (protein epitope signature tags), were generated as part of the Human Protein Atlas (HPA) project using a whole genome bioinformatics approach. Antigens of 25-150 amino acids long (average length of 80 amino acids) representing predicted human proteins were designed based on the lowest sequence homology to other proteins (<60%), with transmembrane regions and signal peptides

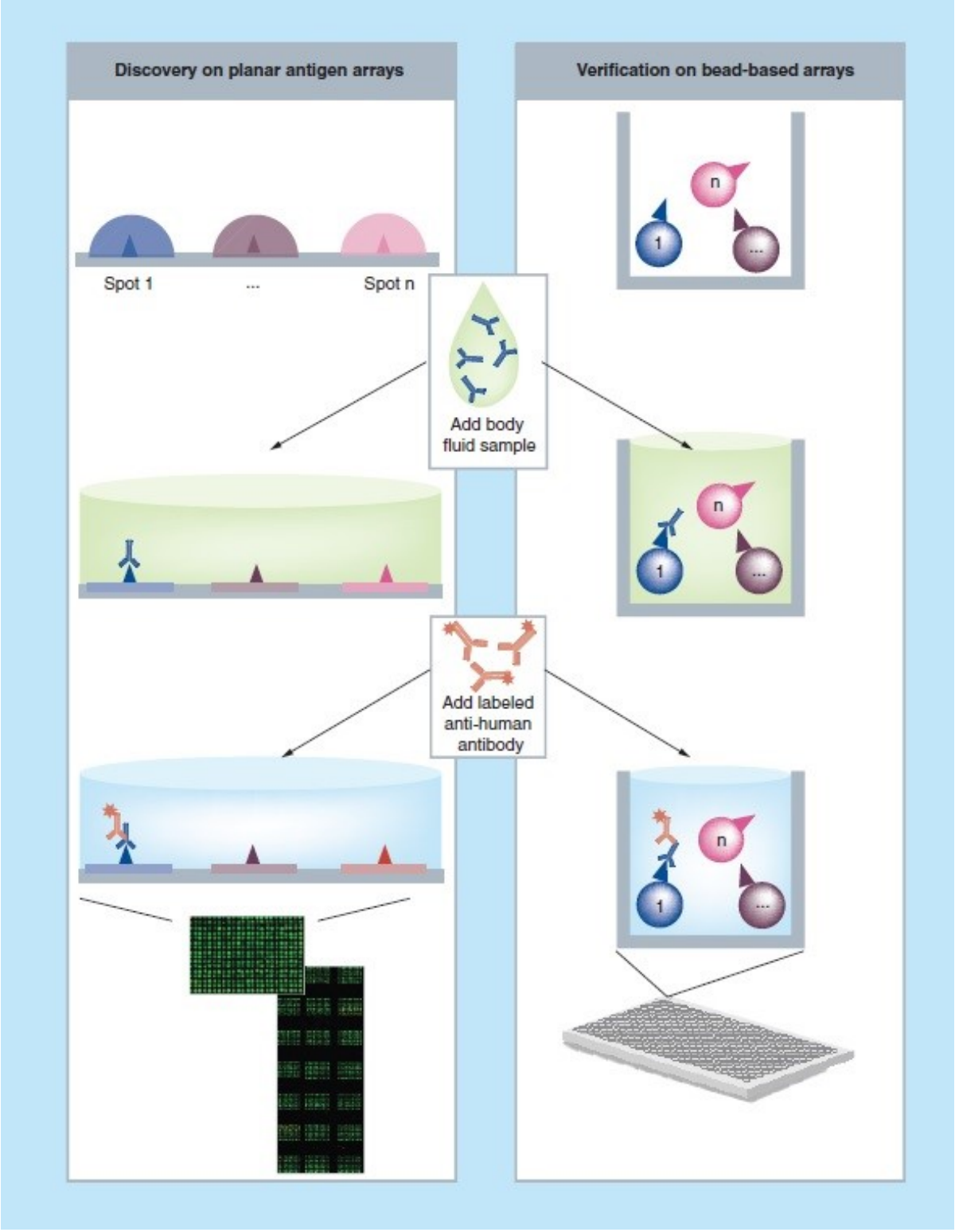

Figure 2.1 An autoantibody profiling assay workflow using planar or bead-based antigen arrays. Antigens representing human proteins are immobilised onto glass slides (planar) or magnetic beads (bead-based). The primary antibody is applied in the form of a biological fluid such as CSF, and bound antibody is detected using a fluorescently labelled anti-human secondary antibody. Adapted from (Ayoglu et al., 2016). Reproduced with permission of the copyright owner.

excluded. The antigens were expressed in *Escherichia coli* Rosetta DE3 strain as fusion proteins with a His_6-ABP tag, consisting of a hexahistidyl (His_6) and albumin binding protein (ABP), to allow the antigens to be purified.

2.12.2 Planar antigen arrays

Planar antigen arrays, hosting 21,120 protein fragments immobilised onto glass slides, were used for unbiased screening of CSF from 6 individuals with CIS, and pooled CSF from RRMS or OND groups (6 CSF samples per pool). A smaller array hosting 384 protein fragments potentially linked to MS (such as CNS antigens) was also used for further exploration using the same samples individually rather than pooled.

CSF samples diluted 1/4 (384 array) or 1/10 (21k array) in assay buffer (PBS + 0.1% tween + 3% BSA + 160µg/ml His_6-ABP; generated in-house) with chicken anti-His_6-ABP IgY (1/40,000 dilution; Agrisera, Vannas, Sweden), were incubated for 30 min on a plate shaker (Grant Instruments, Cambridge, UK). Slides hosting immobilised protein fragments were washed in distilled H_20 (dH_20), 60µl of CSF was added and slides were incubated for 2 hours on a shaker at RT. Slides were washed in wash buffer (PBS + 0.1% tween, 2x5 min) and incubated in AlexaFluor 647 goat anti-human (H+L) IgG diluted 1/15,000 (life technologies, cat. A21445) on a shaker for 1h to detect bound human antibodies. To aid grid alignment prior to scanning, slides were co-stained with AlexaFluor 555 goat anti-hen IgG diluted 1/60,000 (Molecular Probes, OR, USA) to detect bound His_6-ABP tag-specific chicken antibodies. Slides were washed 2x5 min in wash buffer, 1x5 min in PBS and were rinsed in deionised water prior to spinning dry. Slides were scanned to 10µm resolution in a microarray scanner (G2565BA; Agilent Technologies, Santa Clara, CA, USA) and analysed using

GenePix Pro v.5.1 (Molecular Devices, Sunnyvale, CA, USA). The top reactive antigens from the planar arrays, along with several potential autoantigens from the literature, were investigated further using suspension bead arrays (see Appendix IV for a list of antigens selected for further investigation using suspension bead arrays, and Appendix V for a list of established candidate autoantigens selected from the literature).

2.12.3 Sample preparation for the suspension bead arrays

A total of 235 banked CSF samples, diluted 1/50 in assay buffer (PBS + 0.1% tween + 3% BSA + 160µg/ml His_6-ABP), were aliquoted into randomised destination wells using a liquid handling system (Freedom EVO150, Tecan, Männedorf, Switzerland). Three blank wells and three pooled wells (containing pooled CSF from every sample) were included on each plate. Plates were stored at -20ºC until required.

2.12.4 Generation of suspension bead arrays

Antigens of interest, determined by both previous assays on planar arrays and potential disease relevance based on previously published literature, were covalently conjµgated to the free carboxyl groups on carboxylated microspheres as per manufacturer's instructions (MagPlex-C, Luminex Corporation, Austin, TX). For each of the 301 unique bead IDs, 750,000 beads per bead ID were brought to room temperature and distributed across 96 well plates (Greiner BioOne, Longwood, FL). Beads were washed and resuspended in phosphate buffer (0.1M NaH2PO4, pH 6.2) using a magnetic plate (Dexter) and a plate washer (EL406, Biotek, Winooski, VT). To activate the carboxyl sites on the beads, 50µl of activation solution, containing a 10mg/ml solution (0.5mg/well) of N-hydroxysµlfosuccinimide (NHS; Pierce, Rockford, IL) and 1-ethyl-3-(3-dimethylaminopropyl)-carbodiimide hydrochloride (EDC; Pierce), was added to the microspheres. Following 20 min incubation on a plate shaker

(Grant Bio), beads were washed twice in MES buffer (0.05M, pH 5.0). For the coupling reaction, 100µl of each antigen, diluted to 60µg/ml in MES buffer, were added to the microspheres and incubated for 2h on a plate shaker. The following control proteins were also coupled to beads: 4µg rabbit anti-human IgG, 4µg recombinant EBNA-1 protein (Tebu-Bio, Roskilde, Denmark) and 4µg His_6-ABP.

2.12.5 Sample and coupling test

A sample pool, generated by combining 1µl of each CSF sample, was used to test the conditions of the suspension bead array. Goat F(ab')2 fragment anti-human IgG R-PE (5µg/ml; Invitrogen) was used at 1/750, but because the goat anti-human kappa (cat. no: 2060-09) and lambda light chain R-PE antibodies (cat. no: 2070-09; Southern Biotech, Birmingham, UK) had not been tested, two dilutions of 1/100 and 1/500 were first assessed.

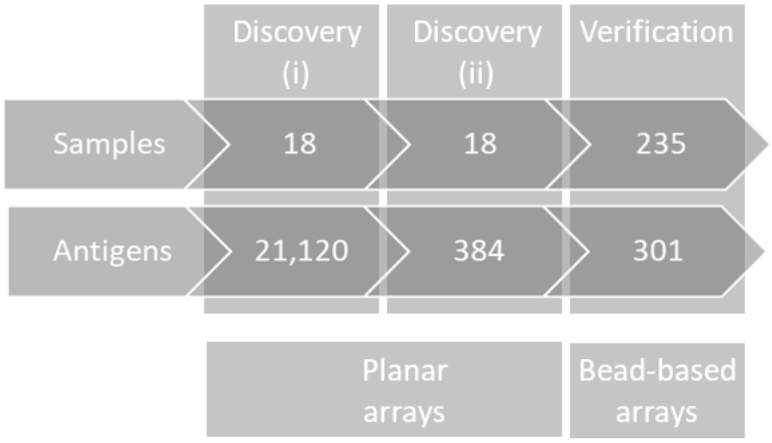

Figure 2.2 Overview of assay workflow on planar and bead-based arrays. An initial unbiased discovery approach targeting 21,120 antigens, followed by a screen of 384 potential target antigens, allowed a selection of potential autoantigens to be generated. These were further investigated using bead-based arrays in a verification phase using a larger sample size.

For the sample test, pooled CSF was diluted in assay buffer containing 160µg/ml His_6-ABP with or without 5% milk and incubated for 1h on a shaker. Pooled CSF was incubated with 5µl bead stock and primary antibodies (with a total volume of 50µl per well) for 1h on a shaker, and were washed 3x in 100µl wash buffer (PBS + 0.05% tween) using a magnetic plate and plate washer. The pooled CSF was then incubated with secondary antibodies for 30 min on shaker and washed 3 times as previously described. Samples were resuspended in 50µl and ran on a Luminex FlexMap 3D (Luminex Corporation, Austin, Texas, USA).

For the coupling test, conjugation of the antigens to the beads was confirmed by detecting the His_6-ABP tag on the antigens using chicken anti-His_6-ABP (1/20,000 dilution; Agrisera) followed by R-PE-conjugated F(ab)2 fragment donkey anti-chicken IgY (1/1000; Jackson Immunoresearch Laboratories, West Grove, PA, USA). This allowed bead IDs with a median fluorescence intensity (MFI) below 30 to be excluded from further analysis, on the assumption that the conjugation step was unsuccessful. Some antigens such as EBNA-1 were purchased commercially rather than generated within the HPA; as such these proteins did not have a His_6-ABP tag so no signal was expected. To ensure that the antigens were coupled to the correct bead IDs in the correct order, anti-human HPA antibodies against two antigens (MBP and anoctamin 2; ANO2) were used (1/1000) with a secondary R-PE anti-rabbit IgG antibody (1/2000; Jackson Immunoresearch Laboratories).

2.12.6 Assays on suspension bead arrays

Plates containing randomised CSF samples, pre-diluted in assay buffer, were thawed and incubated for 1h on a shaker. Following thorough sonication, 5µl of bead solution was added to each CSF sample and incubated on a shaker overnight. Beads were washed 3 times in wash buffer using a magnetic plate and plate washer, and were incubated in 0.2% paraformaldehyde (PFA; Sigma Aldrich) for 10 min to allow antibody cross-linking. Beads were washed and

incubated in anti-human IgG (1/750), anti-human kappa light chain (1/100) or anti-human lambda light chain (1/100) antibodies diluted in assay buffer (no milk) for 1h on shaker. Plates were washed 3 times in wash buffer with a final volume of 50µl per well and were ran on a Luminex FlexMap 3D.

2.12.7 Analysis of antigen array data

Data were analysed in Microsoft Excel and GraphPad prism v7.0. Following quality control checks, involving evaluation of positive and negative controls and exclusion of beads and their corresponding protein conjugates with bead counts of less than 30 per well, an arbitrary cut-off threshold was applied to each sample, which was calculated as the MFI across the sample plus 0.5x, 4x or 10x median absolute deviation (MAD), depending on the assay. This accounted for variable background levels across samples.

2.13 Statistics

Statistical analyses were performed using GraphPad Prism v7.0 (GraphPad Software Inc., CA, USA). For analysis of *ex vivo* human data sets, median values were determined, and non-parametric testing was used as these data were not normally distributed, although normal distribution was not tested for. Parametric testing was used for the analysis of *in vitro* cell culture data. Statistical comparisons with a P-value of $P<0.05$ or below were considered significant.

CHAPTER 3

CHARACTERISING THE B CELL RESPONSE IN MULTIPLE SCLEROSIS

Chapter 3: Characterising the B cell response in multiple sclerosis

3.1 Introduction

The evidence for a B cell-mediated component in MS pathogenesis is strong. B cells, plasmablasts and their antibody products are present in CNS compartments throughout the disease course where they correlate with pathogenesis and disease progression (Cepok et al., 2005a; Winges et al., 2007). Despite this knowledge, the finer features of B cell biology in MS warrants further exploration. ASC have been identified within MS brain tissue, including in ectopic meningeal follicles; in an EAE model, long-lived EdU-labelled ASC were shown to persist in the inflamed CNS for up to five weeks, indicating that the CNS can provide ASC survival niches for extended periods of time (Serafini et al., 2007; Pollok et al., 2017). The clinical benefits of anti-CD20 therapies, mediated by depletion of mature B cells, suggest an active peripheral component, and it is known that B cells can exchange across the blood-brain barrier in either direction, potentially receiving stimulation in the periphery and in the CNS (von Budingen et al., 2012; Palanichamy et al., 2014a; Hauser et al., 2008; Kappos et al., 2011). As such, the relative contributions of recently recruited peripheral B cells versus locally expanded B cells remains unclear.

CSF analysis has identified an accumulation of IgM-IgD- class-switched B cells in MS, implicating selective memory B cell recruitment to the CNS, however, specific immunoglobulin isotypes of CSF B cell subsets have not been investigated (Cepok et al., 2006). This may help to shed light on the origins of CSF B cells. ASC have also been identified in the CSF, and it has been reported that short-lived CD19+CD138+ASC are the major B cell effector subset during the course of MS (Cepok et al., 2005a). In contrast,

another study identified mature ASC as the major ASC population in MS CSF (Corcione et al., 2004). In addition to these inconsistencies, Cepok et al found that the frequency of CD19+ ASC, but not CD19- ASC, correlates with intrathecal IgG synthesis; however, several studies have identified clonal relationships between CSF ASC populations, implicating a continuum of B cell differentiation rather than the presence of distinct B cell pools (Ritchie et al., 2004; Winges et al., 2007). So, although the CSF B cell compartment in MS has been widely studied, further investigation may help to clarify the involvement of these populations with disease.

In contrast to the widely reported peripheral blood Igκ:Igλ ratio of approximately 1. 6:1, Igκ light chains are elevated in MS CSF (Zeman et al., 2012; Perez-Andres et al., 2010). This bias may have prognostic significance, as a lower ratio has recently been linked to increased conversion from CIS to CDMS (Voortman et al., 2017). Though a handful of studies have identified a biased Igκ:Igλ ratio on MS CSF B cells, the prevalence of this bias within and between MS groups is unclear, and its expression by CSF ASC, which are presumably responsible for their secretion, has not been investigated (Nowakowski et al., 2005; Vafaii and DiGiuseppe, 2014).

The hypothesis of this chapter was that clonally expanded B lineage cells can be detected in MS CSF, and that the humoral response in MS begins with a restricted Igκ response, which spreads to both Igκ and Igλ specificities as the disease progresses.

3.1.1 Chapter Objectives

1. Characterise B cells and ASC from the peripheral blood of MS and healthy control groups
2. Identify ASC in the CSF of individuals with different subtypes of MS (CIS, clinically definitive MS, MS on natalizumab treatment) in comparison to OND and ONID groups
3. Determine immunoglobulin heavy and light chain expression in B cells and ASC in matched CSF and peripheral blood
4. Determine the extent of Igκ:Igλ bias on B cells and ASC, and compare this ratio between disease groups

3.2 Results

3.2.1 Characterisation of B cells and ASC in the blood and CSF

Matched peripheral blood and CSF were received from individuals undergoing diagnostic or therapeutic lumbar puncture (LP), except for those coming off natalizumab, who were undergoing LP for JCV testing. The other individuals were stratified into disease groups following a formal diagnosis (**Appendix I**) with the following classifications: OND (n=17), ONID (n=7), CIS (n=10), MS (n=14) and NAT (n=14).

PBMC from peripheral blood and cell pellets from the CSF were stained *ex vivo* for a series of characterisation markers and activation markers, to identify B cells and ASC, which were analysed by flow cytometry. For this, an appropriate gating strategy was determined. In the

peripheral blood, B cells were identified as CD19+CD20+ and ASC identified as $CD27^{high}CD38^{high}$ within the CD19+ gate (**Fig. 3.1A**, blue arrows). The absence of circulating CD19- ASC was confirmed by gating on $CD27^{high}CD38^{high}$ within the CD19- gate (**Fig. 3.1A**, red arrows), allowing CD19 to be used as a marker of peripheral blood ASC, in accordance with the literature, and for cleaner gating to be achieved (Mei et al., 2009; Yoshida et al., 2010). Though CD138 is sometimes regarded as a plasma cell-specific marker, its expression is heterogeneous in peripheral blood plasmablasts and therefore cannot be used for their identification. This set of markers allowed subsequent gating for immunoglobulin light and heavy chain expression within these subsets.

In the CSF, B cells were again identified as CD19+CD20+ (**Fig. 3.1B**). Based on previous studies that have identified heterogeneous CD19 expression on CSF ASC, CD19 was not used to identify these cells in the CSF; ASC were defined as $CD27^{high}CD38^{high}$CD138+, Despite the heterogeneous CD138 expression by peripheral blood ASC, previous reports have identified CSF ASC as CD138+, therefore this marker was included in the CSF ASC phenotyping panel.

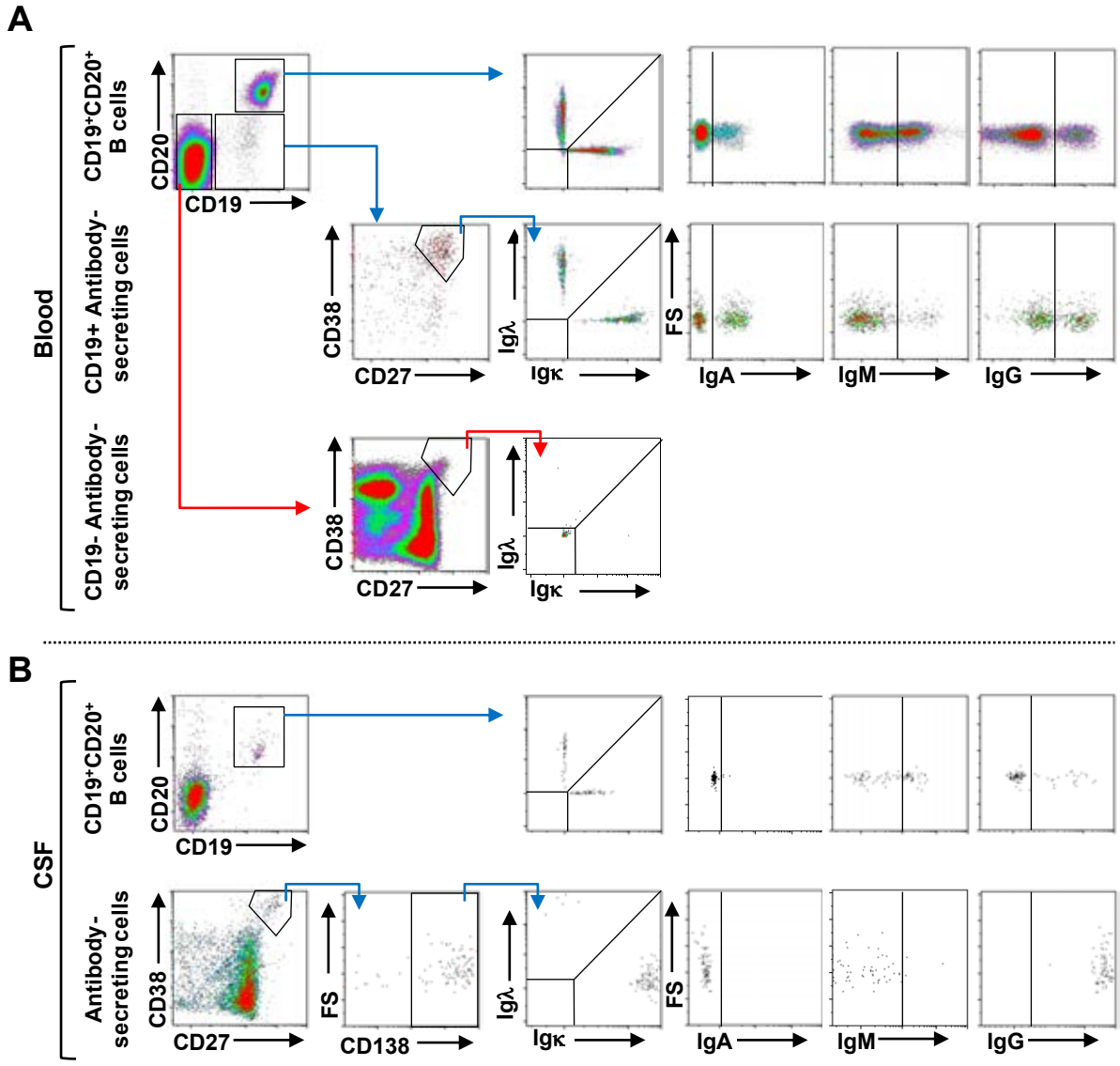

Figure 3.1. Gating strategy to identify B cells and antibody-secreting cells in the peripheral blood and CSF. In the peripheral blood, B cells were identified as CD19+CD20+ (upper panel) and antibody-secreting cells identified as $CD27^{high}CD38^{high}$ within the $CD19^{+}$ gate (middle panel) due to the absence of CD19- antibody-secreting cells (lower panel) **(A)**. In the CSF, B cells were identified as CD19+CD20+ (upper panel) whereas antibody-secreting cells were defined as $CD27^{high}CD38^{high}CD138^{high}$ (lower panel) **(B)**. Gated on viable cells with doublets excluded. Blue arrows represent gating used throughout, red arrows represent example gating. FS; forward scatter.

The gating strategy was validated by comparing marker expression between B cells and ASC (**Fig. 3.2**). Comparisons were made between those cells in the peripheral blood, rather than the CSF, since they were present at higher frequencies. This was achieved by gating on B cells and ASC respectively, and then creating a histogram for each marker to derive the MFI values. Although these MFI values were obtained from established gates, since these was required to first distinguish B cells and ASC prior to MFI analysis, comparison of MFI values for both cell populations allowed the relative expression levels of each marker to be determined and compared between populations. ASC expressed significantly lower levels of CD19 and CD20, and significantly higher levels of CD27, CD38 and CD138 compared to B cells (**Fig. 3.2A, B**). A strong distinguishing feature of ASC is their low surface and high intracellular Ig levels, with correspondingly high surface and low intracellular Ig in B cells; this phenomenon was observed using this gating strategy, thus confirming the ability to successfully distinguish B cells and ASC using these methods (**Fig. 3.3A, B**).

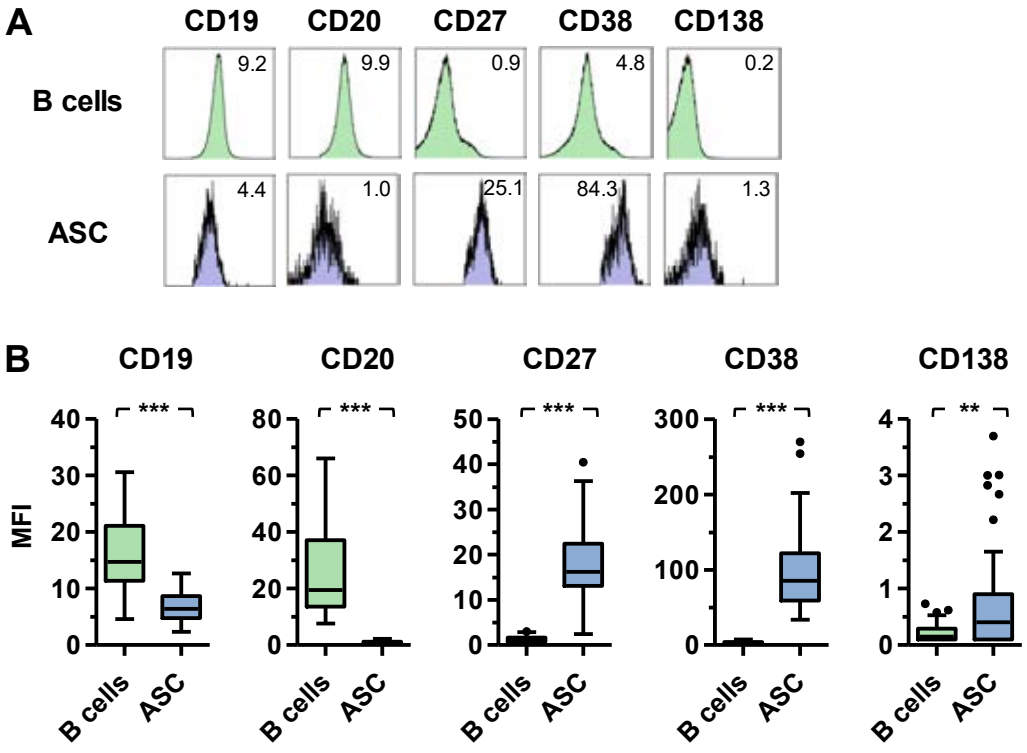

Figure 3.2 Features distinguishing ASC from CD19+CD20+ B cells in the peripheral blood (i). Representative histograms **(A)** and analysis **(B)** of marker expression intensity by peripheral blood B cells and ASC. Data are significant to *** (P<0.001) or ** (P<0.01) using Mann-Whitney test (n=62)**.** Values from all disease groups. Tukey box and whisker plot showing median values. MFI; median fluorescence intensity.

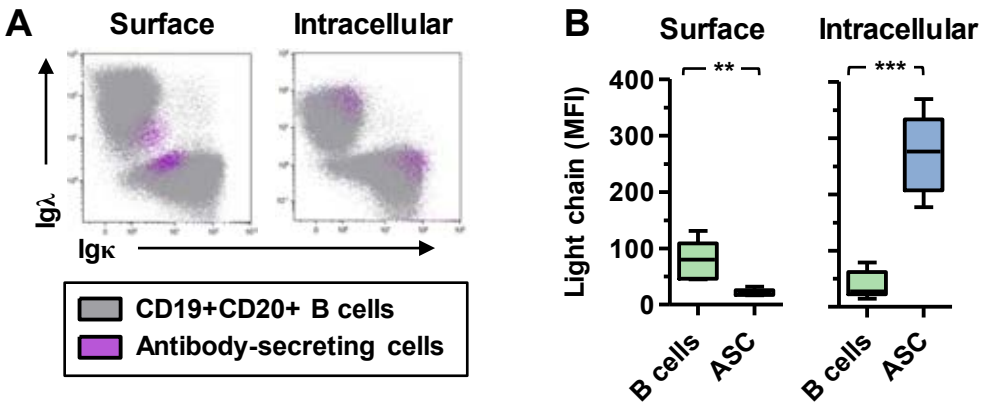

Figure 3.3 Features distinguishing ASC from CD19+CD20+ B cells in the peripheral blood (ii). Flow plots **(A)** and quantification **(B)** of surface (n=5) and intracellular (n=9) Igκ and Igλ expression in CD19+CD20+ B cells and ASC**.** Data are significant to ** ($P<0.01$) and *** ($P<0.001$) using Mann-Whitney test. Values from all disease groups. Tukey box and whisker plot showing median values.

3.2.2 B cells and ASC were elevated in MS CSF

No significant differences were observed in the frequency of CD19+CD20+ B cells between OND (9.5%), ONID (13.4%), CIS (8.7%) and MS (9.9%) groups (**Fig. 3.4A**). However, the natalizumab (anti-α4 integrin) group had significantly elevated frequencies (16.4%) compared to OND, CIS and MS groups. In the CSF, CIS (0.99%) and MS (1.07%) groups displayed elevated B cells compared to OND (0.33%) but not ONID (1.06%). In contrast, CSF B cells in the natalizumab group (0.16%) were significantly reduced compared to other MS groups.

Frequencies of peripheral blood ASC were no different between groups, but in the CSF were significantly elevated in CIS (0.065%) compared to OND (0%), and MS (0.25%) compared to OND and natalizumab-treated individuals (0%) (**Fig. 3.4B**). CSF ASC appeared more elevated in MS than CIS, though this comparison was not statistically significant.

In an effort to identify whether B cells and/or ASC in MS can be distinguished from OND/ONID control groups on the basis of marker expression, the expression of CD38 and CD27, both considered markers of activation, was compared between these groups. In the blood, there was no significant difference in CD38 or CD27 expression in B cells or ASC between groups (**Fig. 3.5A**). Similarly, analysis of these markers on CSF cells revealed little difference between groups, except in the post-natalizumab group, who demonstrated significantly elevated CD38 expression on B cells (**Fig. 3.5B**). Comparison of marker expression in CSF ASC between groups was difficult due to limited cell numbers (an arbitrary minimum of 5 cells were required for analysis of MFI values).

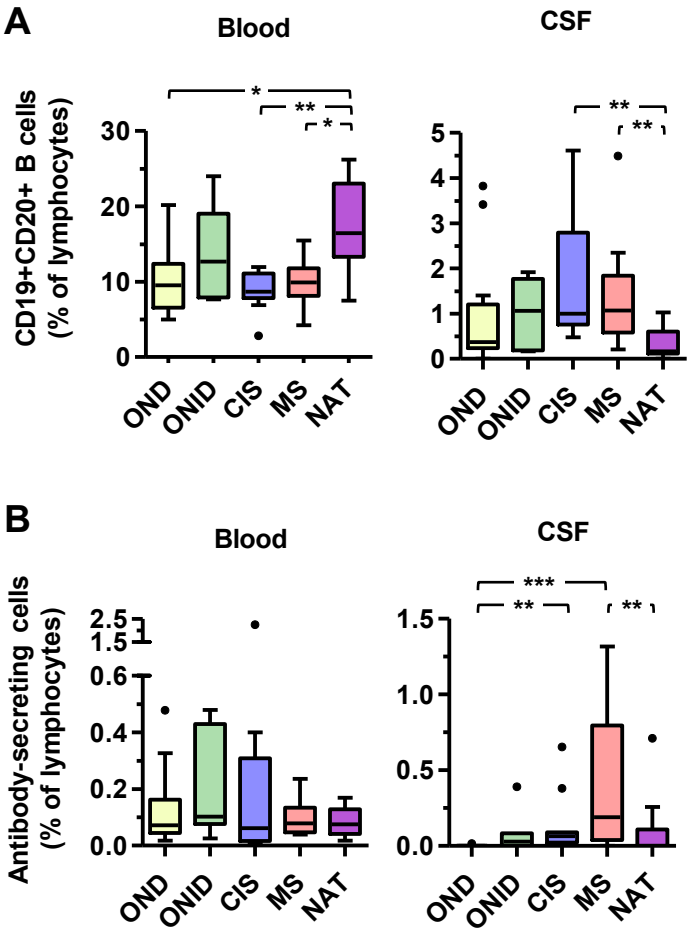

Figure 3.4 CD19+CD20+B cell and ASC frequencies in the blood and CSF of individuals with neurological diseases. Investigation of the frequency of CD19+CD20+ B cells **(A)** and ASC **(B)** as a percentage of total lymphocytes in the blood and CSF of MS and control groups. Data are significant to * ($P<0.05$), ** ($P<0.01$) or *** ($P<0.001$) using Dunn's multiple comparisons test. Tukey box and whisker plot showing median values. OND; other neurological disease (n=17); ONID; other neurological inflammatory disease (n=7), CIS; clinically isolated syndrome (n=10), MS; multiple sclerosis (including relapsing-remitting and primary-progressive, n=14), NAT; MS coming off natalizumab therapy (n=14).

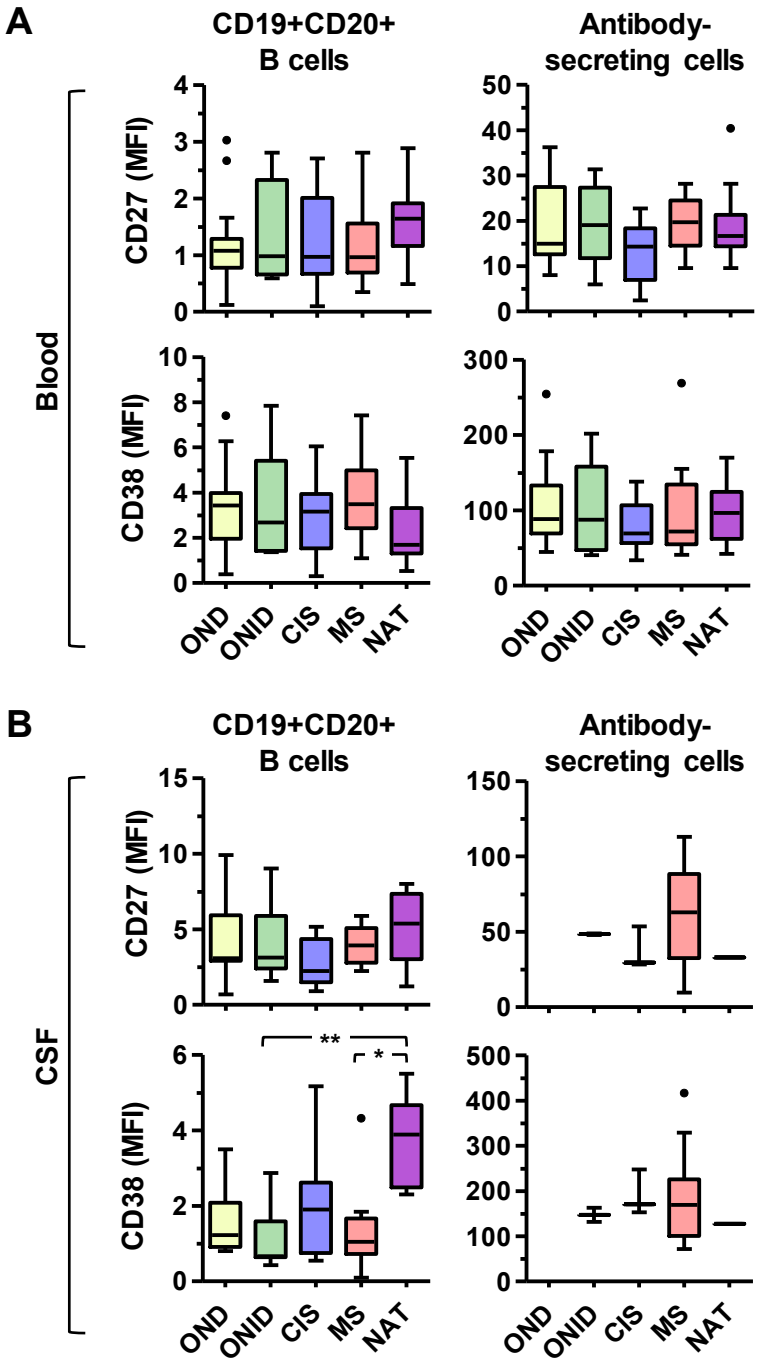

Figure 3.5 Marker expression in MS B cells and ASC. MFI of CD38 and CD27 expressed by CD19+CD20+ B cells and ASC in the blood **(A)** and CSF **(B)** of MS and control groups. Data are significant to * ($P<0.05$) and ** ($P<0.01$) using Dunn's multiple comparisons test. Tukey box and whisker plot showing median values. OND (n=17), ONID (n=7), CIS (n=10), MS (n=14), NAT (n=14).

3.2.3 CSF B cells and ASC show features of recent activation

Since there was little difference in CD27 and CD38 expression between groups, I investigated whether the expression of these markers, in addition to the expression of IgG, may differ on B cells and/or ASC in the CSF compared to the peripheral blood (**Fig. 3.6A**). The results showed that both populations expressed significantly higher levels of CD27 (1.18 vs 3.39 for B cells, 17.6 vs 47.7 for ASC), and IgG (35.9 vs 78.9 for B cells, 145.5 vs 416.7 for ASC) in the CSF compared to those in the periphery (**Fig. 3.6B**). Interestingly however, levels of CD38 were decreased in CSF (1.28) vs peripheral (3.18) B cells but increased in CSF (161.6) vs peripheral (87.4) ASC. Finally, both B cells and ASC were significantly larger in size, measured by forward scatter, in the CSF compared to those in the periphery (**Fig. 3.6C, D**).

3.2.4 Characterisation of CSF ASC populations

Within the CSF, distinct ASC populations were identified based on differential expression of CD19 (**Fig. 3.7A**). This was performed by gating on total CSF ASC, as in Fig. 3.1B, and then gating on CD19. As a proportion of total ASC, CD19+ ASC were more common than CD19- ASC (64% vs 31%), though these proportions varied widely (**Fig. 3.7B**). This analysis was performed on CSF samples containing 10 or more ASC, as too few cells could easily bias the analysis (e.g. the presence of one CD19+ ASC would give an CD19+ ASC frequency is 100%, whereas analysing samples containing a larger cell population would provide more reliable data). Though no difference was identified between the two ASC subsets in terms of frequencies, CD19- ASC expressed higher levels of CD138 compared to CD19+ ASC (**Fig. 3.7C**). CD19- ASC also showed a trend for increased levels of CD27, CD38 and IgG compared to their CD19+ counterparts, although this was not significant (**Fig. 3.7D**).

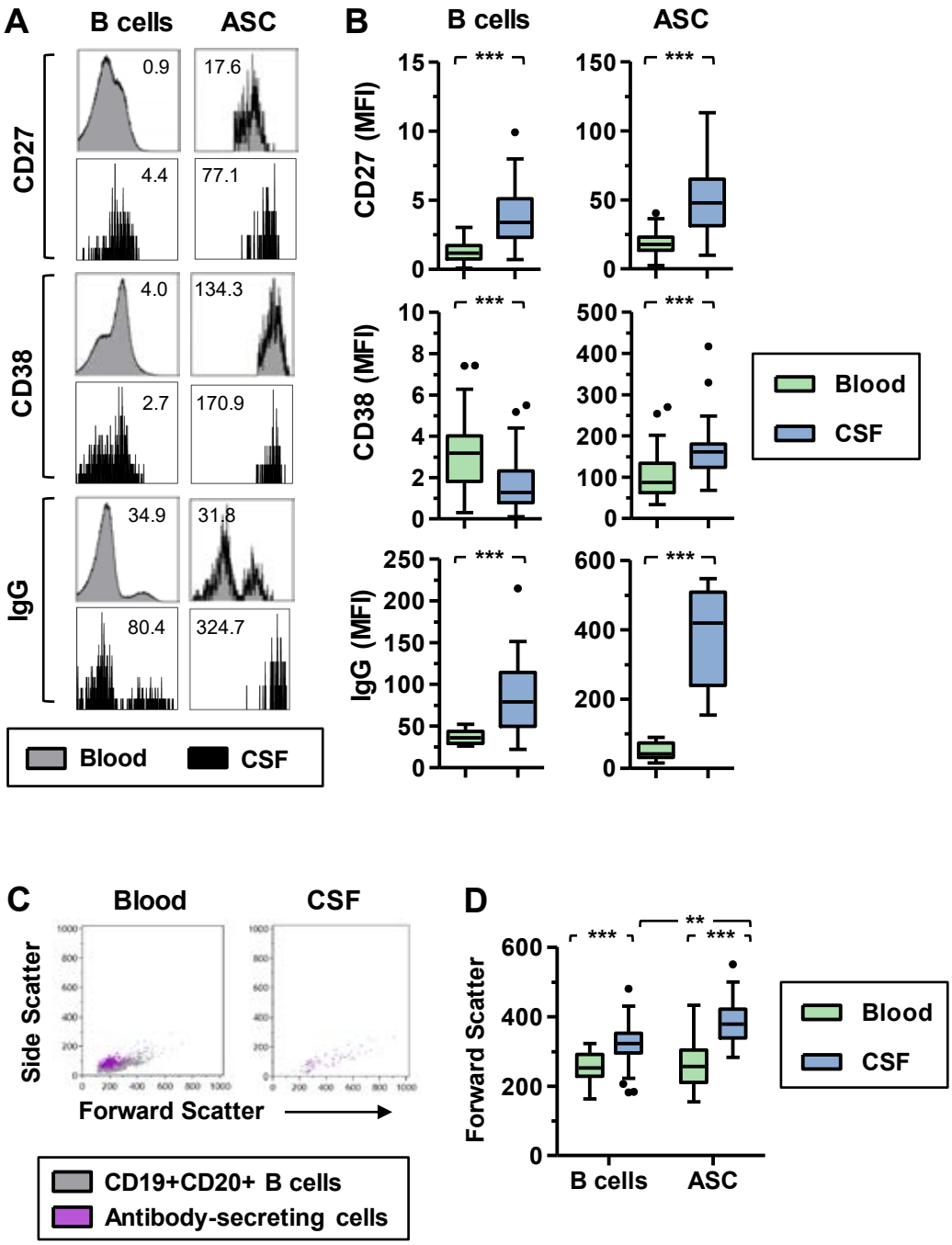

Figure 3.6 CSF B cells and ASC show features of recent activation. Representative histograms showing CD27, CD38 and IgG MFI values in CD19+CD20+ B cells and antibody-secreting cells in the blood (grey) and CSF (black) **(A)** and quantification of CD27, CD38 and IgG MFI values **(B)**. Data are significant to *** (P<0.001) using Mann-Whitney test (n= 12 to 62). Representative flow plots **(C)** and comparison **(D)** of forward scatter in the blood and CSF. Data are significant to ** (P<0.01) and *** (P<0.001) using Mann-Whitney test (n=52).

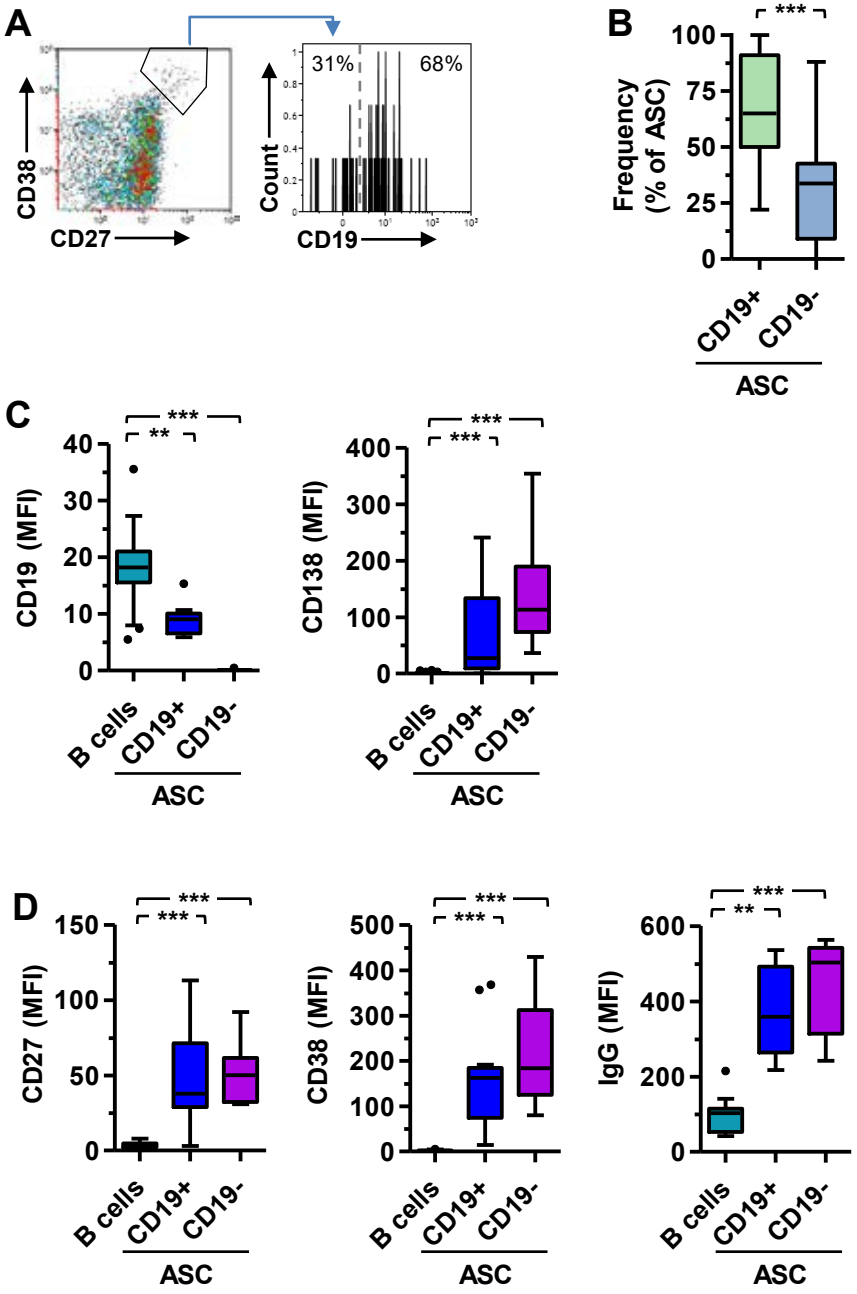

Figure 3.7 Identification of CD19+ and CD19- ASC subsets in MS CSF. Representative plot of a CSF sample from an individual with MS, gated on viable lymphocytes **(A)**. Blue arrow represents gating. The proportion of CD19+ and CD19- antibody-secreting cells in MS CSF **(B)**. Data are significant to *** (P<0.001) using Mann-Whitney test (n=15). Tukey box and whisker plot showing median values. Differential expression of CD19 and CD138 **(C)** and CD27, CD38 and IgG **(D)** by CD19+ and CD19- ASC compared to CD19+CD20+ B cells in MS CSF. Data are significant to ** (P<0.01) and *** (P<0.001) using Kruskal-Wallis test. Tukey box and whisker plots showing median values.

3.2.5 B cell and ASC numbers correlate with CSF inflammation in MS

lymphocyte counts, total FLC (kappa and lambda) and CXCL13 levels (**Fig. 3.8**). CSF lymphocyte counts (**Fig. 3.8A**) significantly correlated with the number of B cells (r = 0.88, p = <0.0001), CD19+ ASC (r = 0.75, p = <0.0001) and CD19- ASC (r = 0.70, p = <0.0001). Although the CSF FLC concentration (**Fig. 3.8B**) did not correlate with the CSF B cell frequency (r = 0.15, p = 0.36), it did correlate with CD19+ ASC (r = 0.36, p = 0.027) and CD19- ASC (r = 0.37, p = 0.022) frequencies. Finally, CSF CXCL13 levels (**Fig. 3.8C**) significantly correlated with the frequency of B cells (r = 0.5, p = 0.027), CD19+ ASC (r = 0.58, p = 0.01) and CD19- ASC (r = 0.65, p = 0.0034).

3.2.6 CSF ASC, but not B cells, are predominantly IgG+ in MS

The correlation of ASC numbers with the CSF CXCL13 concentration could suggest increased ASC migration to the CSF, increased intrathecal generation due to higher B cell numbers, or both. To investigate the possible origins of B cells and ASC in the CSF, immunoglobulin isotype expression was determined. The results showed that in MS, CSF B cells are significantly biased towards IgG compared to those in the blood (blood: 13.27%, CSF: 31.82%) (**Fig. 3.9A**). This trend was also observed in OND and ONID controls (blood: 11.28%, CSF: 29.57%). Though IgM-expressing B cells were decreased compared to the blood, IgM remained the dominant immunoglobulin isotype expressed by CSF B cells in both MS and control groups. In contrast to B cells, ASC in MS CSF were almost exclusively IgG+ (blood: 17.88%, CSF: 96.77%) with very little IgA, which is the dominant peripheral blood isotype, or IgM, detected (**Fig. 3.9B**).

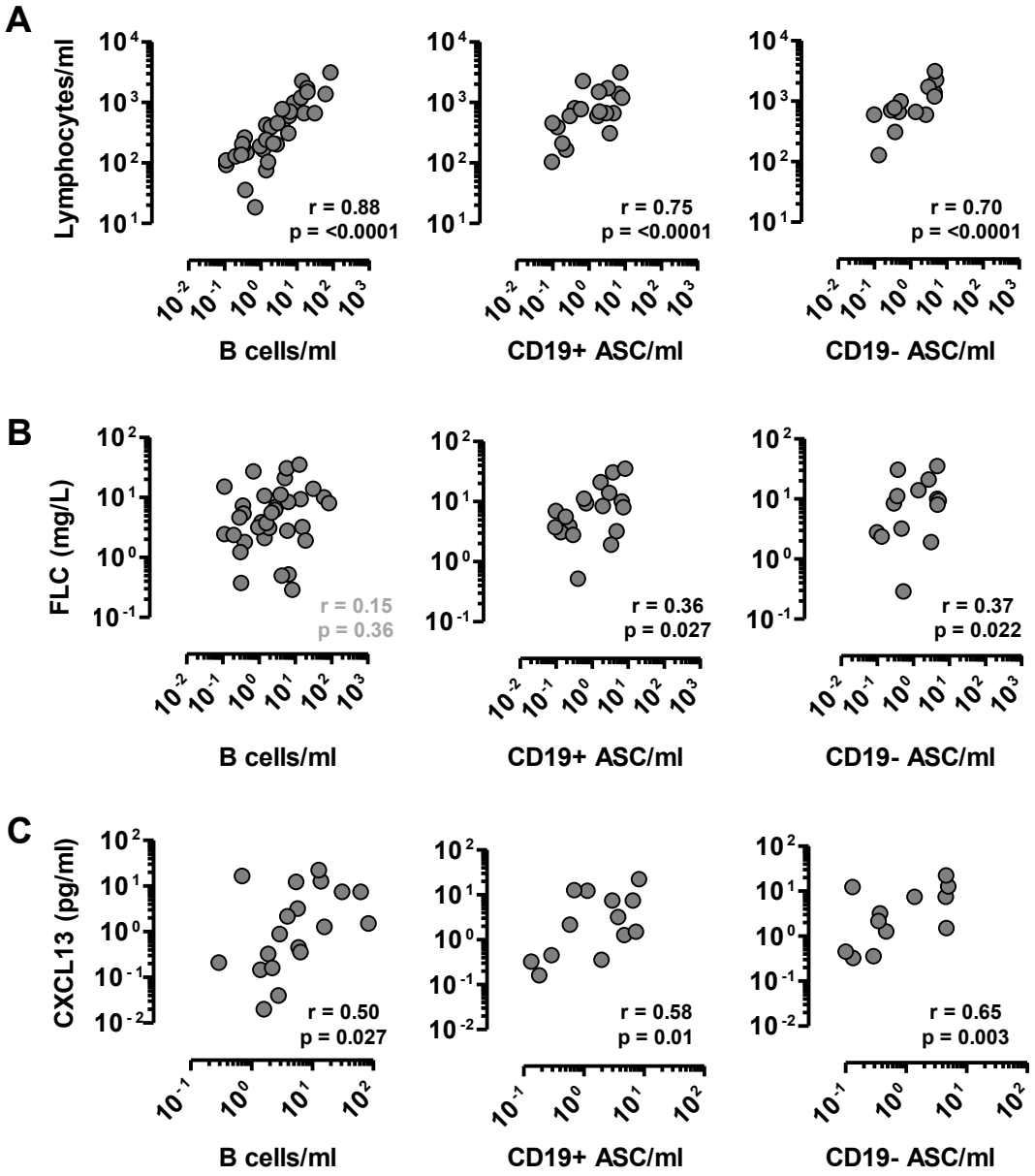

Figure 3.8. B cells and ASC correlate with inflammatory parameters in MS CSF. The number of CD19+CD20+B cells , CD19+CD138+ASC and CD19-CD138+ ASC per ml CSF was correlated with lymphocyte count per ml **(A)**, FLC concentration **(B)** and CXCL13 concentration **(C)**. Spearman correlation from all MS groups (lymphocyte count and FLC concentration, n=38; CXCL13 concentration, n=19). Non-significant associations are shown in grey font. Only matches with two positive values are displayed on the correlation plots, i.e. those with values of 0 are not displayed.

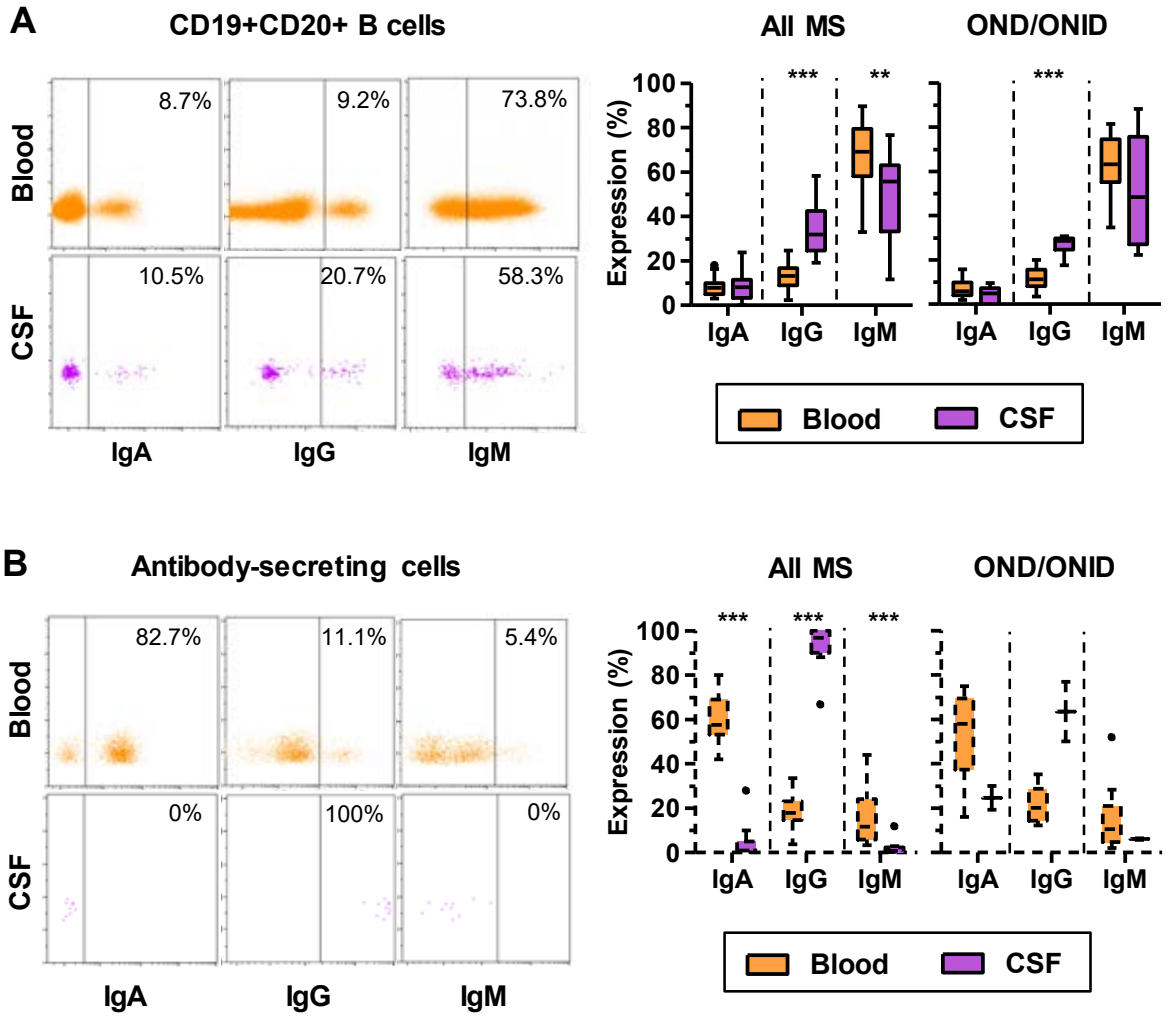

Figure 3.9 IgG is the dominant immunoglobulin isotype expressed by ASC, but not CD19+CD20+B cells, in MS CSF. Representative flow plots from an individual with MS, and corresponding quantification of immunoglobulin isotype expression in CD19+CD20+ B cells **(A)** and ASC **(B)** in the blood and CSF of MS and control (OND/ONID) groups. Data are significant to * ($P<0.05$), ** ($P<0.01$) and *** ($P<0.001$) using Mann-Whitney test (n=13-30 for peripheral blood analysis, n= 2-11 for CSF analysis).

3.2.7 CSF ASC, but not B cells, are Igκ-biased in MS

The predominance of IgG+ ASC in MS CSF could suggest these cells may have arisen following an antigen-specific response, however, it is known that IgG+ ASC express specific chemokines that may direct their homing to sites of inflammation (Kunkel and Butcher, 2003). To provide more clues as to the origins of CSF ASC, and also B cells, Igκ and Igλ expression was analysed and compared to those in the periphery (**Fig. 3.10B**). Amongst MS groups, CSF B cells were no different in their Igκ:Igλ ratio compared to peripheral blood B cells, except in the CIS group which displayed a slightly elevated Igκ-bias (blood 1.44:1, CSF 2.21:1) (**Fig. 3.10B**). MS CSF displayed a significantly biased Igκ:Igλ ratio in ASC (blood 1.12:1, CSF 9.33:1), with a trend towards this bias in CIS and following natalizumab treatment, which unfortunately was hampered by low sample numbers (**Fig. 3.10C**). In ONID but not MS CSF, the ASC Igκ:Igλ ratio was biased in either direction (range 0.13:1 – 3.73:1).

Analysis of the Igκ:Igλ ratio within CD19+ and CD19- CSF ASC populations demonstrated that CD19- ASC are preferentially associated with a stronger Igκ bias than CD19+ ASC (15.5:1 vs 4.6:1, respectively), although both ASC populations are clearly biased towards Igκ (**Fig. 3.10D**).

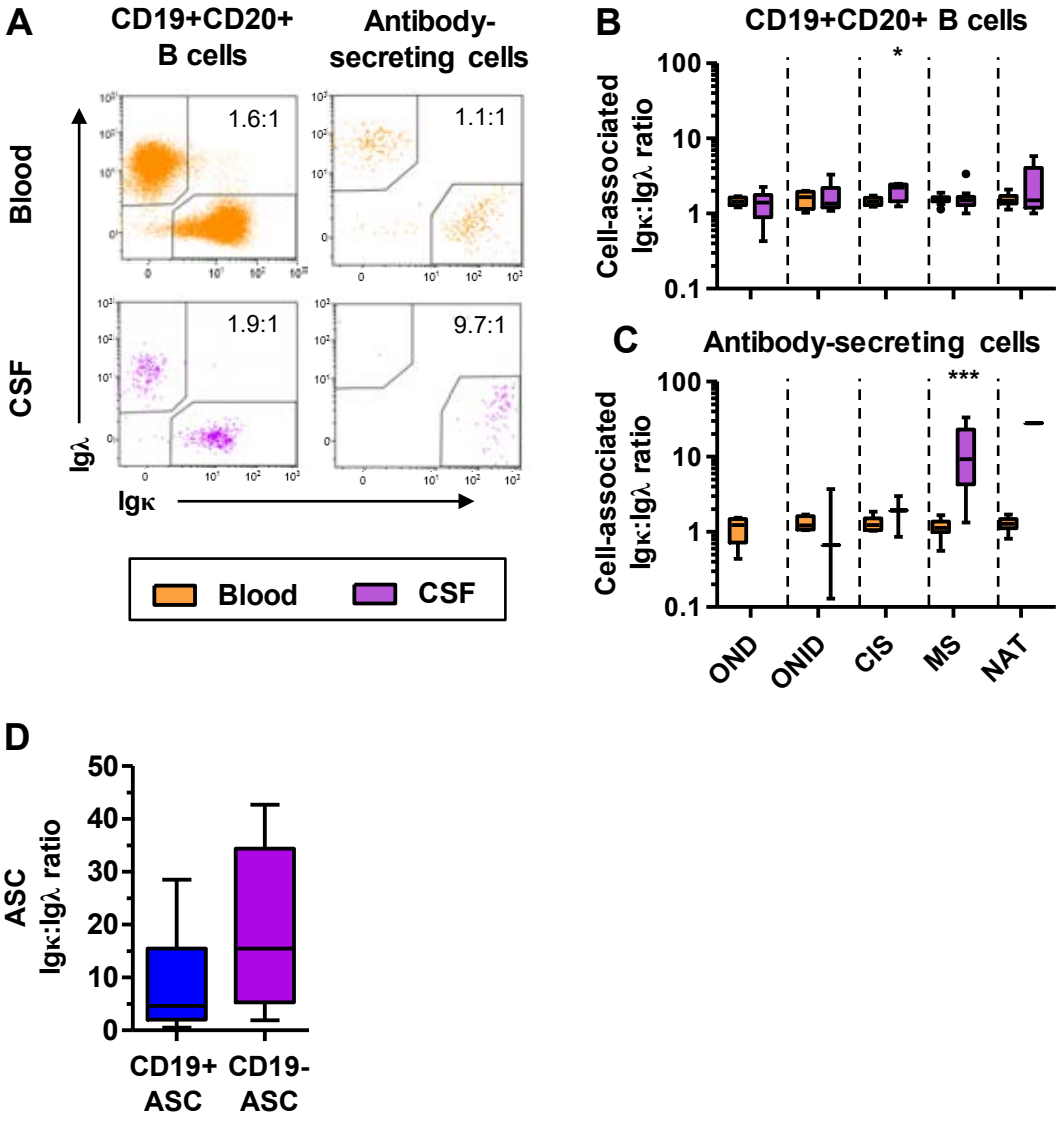

Figure 3.10 Elevated kappa light chain expression by ASC, but not CD19+CD20+ B cells, in MS CSF. Representative flow plots show the Igκ:Igλ ratio of CD19+CD20+ B cells and ASC in the blood (upper plots), compared to the CSF (lower plots), in an individual with MS **(A)**. Quantification of kappa and lambda light chain ratios of CD19+CD20+B cells and ASC in the blood **(B)** and CSF **(C)**. Data are significant to * ($P<0.05$) and *** ($P<0.001$) using Mann-Whitney test (n=5-17 for peripheral blood analysis, n= 1-9 for CSF analysis). The median Igκ:Igλ ratio in CD19+ and CD19- CSF ASC in MS **(D)**. Comparisons were not significant using Mann-Whitney test (n=7).

The Igκ:Igλ ratios on CSF B cells or ASC were compared to the CSF FLC Igκ:Igλ ratio within each MS CSF sample, cell numbers permitting. An arbitrary minimum of 10 cells were chosen to be required for analysis, as unlike with MFI analysis where the entire population was analysed, this analysis required the cells to be further subdivided into Igκ and Igλ populations before the ratio was obtai ned. FLC testing was blindly performed by an external company (The Binding Site, Birmingham) on CSF which was banked and stored at -80°C following removal of CSF cells. Results showed that the FLC Igκ:Igλ ratio did not correlate with the frequency of CD19+CD20+ B cells in the CSF ($r = 0.12$, $p = 0.55$) (**Fig. 3.11A**). However, within the IgG+ B cell population there appeared to be an association with the FLC Igκ:Igλ ratio in some of the samples ($r = 0.19$, $p = 0.51$) (**Fig. 3.11B**). The Igκ bias observed in some IgG+ B cells did not appear to be specific to any particular MS subtype, and was seen in samples from CIS (15.5:1, 7:1), established MS (5.6:1) and natalizumab-treated individuals (5.75:1). Finally, it was shown that the FLC ratio correlated significantly with the CSF ASC Igκ:Igλ ratio ($r = 0.65$, $p = 0.03$) (**Fig. 3.11C)**. Comparison of the CSF FLC Igκ:Igλ ratio between disease groups demonstrated significantly elevated ratios in all MS groups compared to OND (1:1), with CIS (12.5:1), MS (6.3:1) and natalizumab (4:1), thus indicating the presence of elevated CSF Igκ light chains in those with MS (**Fig. 3.12**).

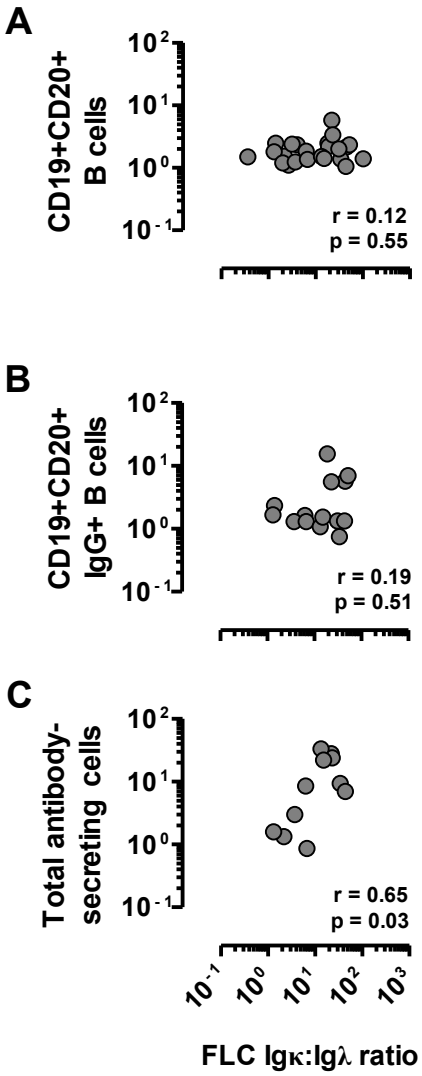

Figure 3.11 The ASC Igκ:Igλ ratio correlates with the FLC ratio in MS CSF. Relationship between the Igκ:Igλ ratio on CD19+CD20+ B cells **(A)**, CD19+CD20+IgG+ B cells **(B)** and total ASC **(C)** compared to the FLC Igκ:Igλ ratio in MS. Spearman correlation (all MS groups).

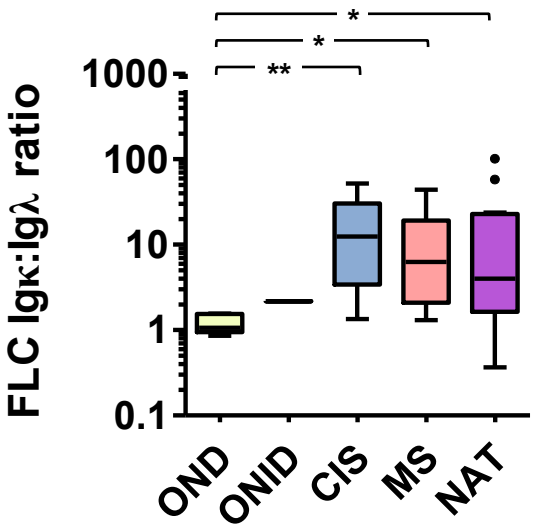

Figure 3.12 Comparison of the CSF FLC Igκ:Igλ ratio between disease groups. The CSF FLC Igκ:Igλ ratio in control groups (OND, ONID) and MS groups (CIS, MS, NAT). Data are significant to * ($P<0.05$), or ** ($P<0.01$) using Dunn's multiple comparisons test. Tukey box and whisker plot showing median values (n = 1 – 13).

3.2.8 Serial CSF analysis of B cell and ASC populations

An informative approach into the B cell response in MS is to analyse repeat CSF samples from the same individual; this could provide some information on the dynamics of the B cell response rather than a momentary snapshot offered by single sample analysis. Since LPs are performed as part of the diagnostic pathway for people with suspected neurological diseases, obtaining repeat samples is difficult in this context. However, in one individual who had recently ceased natalizumab therapy, a repeat LP was obtained, allowing comparison between the initial CSF sample (referred to as 'day 0') with a follow up sample obtained 62 days later. **(Fig. 3.13**). The CSF samples were analysed for B cell and ASC frequency, Igκ:Igλ ratio and FLC concentration. Compared to the day 0 sample, the day 62 sample displayed a more than four-fold increase in the proportion of ASC (0.7% to 2.9%); in contrast, a similar proportion of B cells was observed between samples (0.8% vs 1.0%), despite the hugely increased CSF cellularity (**Fig. 3.13A**). The Igκ:Igλ ratio in CSF B cells was 5.8:1 on first LP, compared to 2.2:1 on the second LP (**Fig. 3.13B**). In CSF ASC, the Igκ:Igλ ratio was more than 28:1 (i.e. 28 Igκ-expressing cells but no Igλ-expressing cells were identified) on first LP, which was 35:1 on subsequent LP (**Fig. 3.13B**).

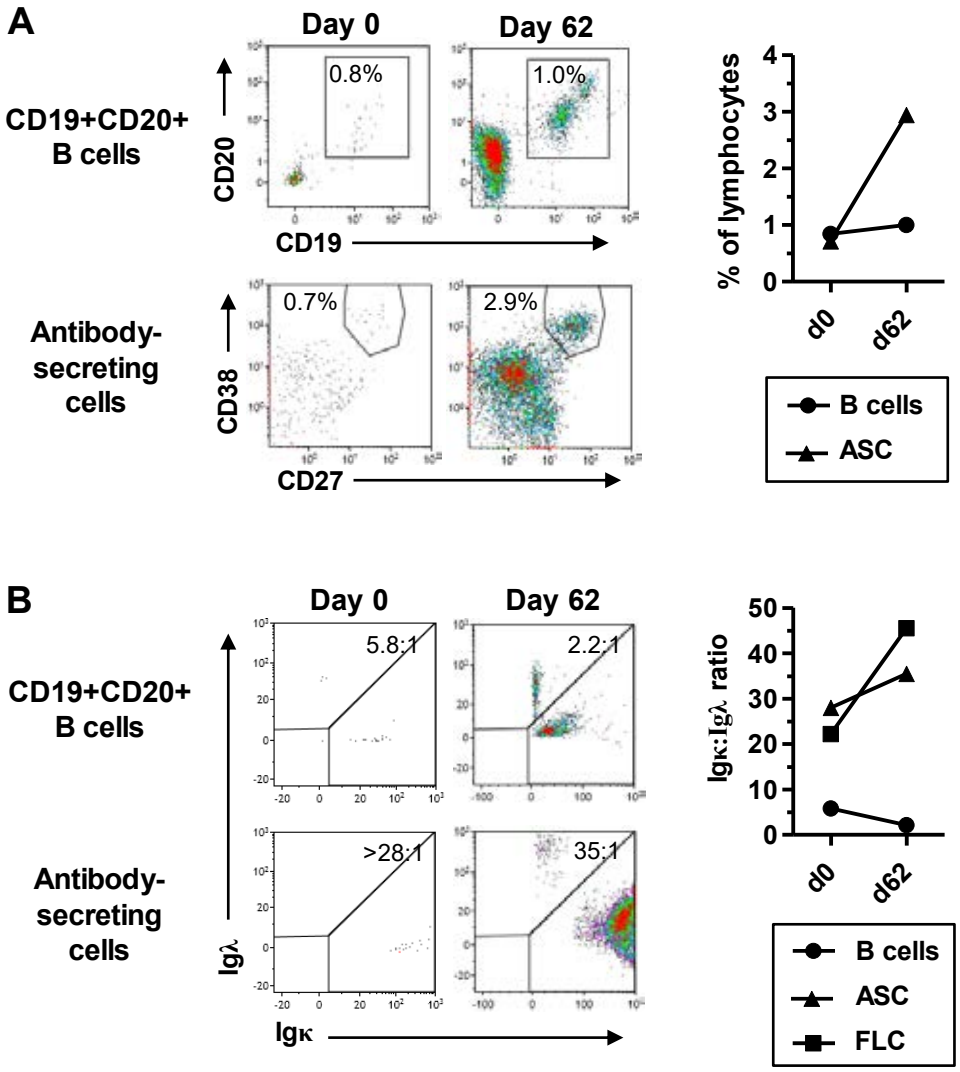

Figure 3.13 Increased frequency and kappa light chain bias of ASC, but not CD19+CD20+ B cells, in the CSF of an individual with MS following cessation of natalizumab therapy. Frequency of CD19+CD20+ B cells and ASC as a percentage of total CSF lymphocytes in an individual with MS on first (day 0; left plots) and second (day 62; right plots) lumbar puncture following cessation of natalizumab therapy **(A)**. The Igκ:Igλ ratio of CD19+CD20+ B cells and ASC was compared on first and second lumbar puncture **(B).** Natalizumab treatment was stopped prior to the first lumbar puncture (day 0).

3.3 Discussion

Despite decades of research, the CS F B cell compartment in MS remains largely elusive. In this chapter, the frequency and phenotype of CSF B cells and ASC, and their possible association with MS pathogenesis, was investigated.

3.3.1 Features and frequencies of CSF B lineage cells

Based on previous studies, peripheral ASC can be distinguished from B cells through their increased CD27, CD38 and CD138, and decreased CD19 and CD20 expression (Fig. 3.1A, B) (Ellebedy et al., 2016; Fink, 2012). This was supported by observations in this chapter by comparing MFI values to differentiate these populations (Fig. 3.2).

Peripheral ASC express low levels of CD19, and since the absence of peripheral CD19- ASC was confirmed in this chapter, it can be assumed that these circulating CD19+ ASC are plasmablasts (Fig. 3.1A, Fig. 3.2). Plasmablasts are recently generated cells that survive for up to a week in the periphery before apoptosis or migration to stromal niches, where they undergo terminal differentiation into long-lived plasma cells; therefore, it is not surprising that these cells demonstrate low, but not negative, CD19 expression (Radbruch et al., 2006; Nutt et al., 2015; Ellebedy et al., 2016). As pointed out by others, circulating ASC are heterogeneous for CD138, therefore this marker cannot be relied upon to identify these cells in the periphery (Costes et al., 1999; Medina et al., 2002; Fink, 2012). This could reflect differences in the potential of plasmablasts to adhere to a niche and differentiate into plasma cells (McCarron et al., 2017). Despite this heterogeneity in peripheral ASC, those in the CSF were highly positive for CD138 (Fig. 3.1B); this was in accordance with other studies, which use CD138 to identify ASC in the CSF (Cepok et al., 2005a; Winges et al., 2007). This

phenomenon could reflect the strong survival potential of CSF ASC, possibly driven by CNS-derived survival factors, which could in turn suggest that CSF ASC are derived from the CNS and not the periphery.

Several key phenotypic features were confirmed between B cells and ASC (Fig. 3.2, Fig. 3.3), most notably the location of immunoglobulin, definitively distinguishing the differential phenotype of these cells and confirming the gating strategy.

A significant increase in peripheral B cells was observed in the natalizumab group (Fig. 3.4A). This mirrors previous observations of altered peripheral immune cell composition following natalizumab, which is particularly pronounced in B cells compared to other immune subsets (Planas et al., 2012; Warnke et al., 2015). This could be a due to a greater dependency of B cells on α4 integrin, which when blocked leads to disrupted B cell homing and adhesion to niches (Warnke et al., 2015). In accordance with other studies, no differences were seen in peripheral blood B cells or ASC in MS or control groups (Cepok et al., 2005a; Harp et al., 2007).

Several studies have investigated the frequency of CSF B cells in MS. Although highly variable between individuals, this frequency generally constitutes around 4-5% of CSF lymphocytes (Cepok et al., 2001; Cepok et al., 2005a; Winges et al., 2007; Kuenz et al., 2008; Kowarik et al., 2012). In this chapter, CSF B cells were found to represent around 1% of CSF lymphocytes. Even using the mean (MS = 1.4%, CIS = 1.7%), as in previous studies, rather than the median (MS = 1.07%, CIS = 0.99%), my findings were still lower than previously described (Fig. 3.4A). Similarly, ASC have been reported to constitute 1.59-2% of total lymphocytes but in this chapter represented less than 1% of CSF lymphocytes (Fig. 3.4B) (Winges et al., 2007; Cepok et al., 2005a; Kowarik et al., 2012). These discrepancies may be

due to sample timing (e.g. the time from onset of symptoms to LP may differ between studies) or in sample processing. Rapid sample processing is critical as the number of viable CSF lymphocytes decreases significantly just 30 minutes following LP, but due to the clinical nature of these studies this is not always possible (de Graaf et al., 2011). CSF does not contain the appropriate factors to support long-term cell survival; this is particularly crucial for ASC, which are highly susceptible to apoptosis (Cenci and Sitia, 2007). Additionally, the already low cellularity of CSF makes these studies technically challenging. Despite these challenges, a significant elevation in CSF B cells was observed in CIS and MS groups compared to controls, consistent with previous studies (Cepok et al., 2005; Kuenz et al., 2008). Furthermore, CSF ASC were significantly elevated in MS compared to OND and natalizumab-treated groups, and in CIS compared to OND. In the group recently coming off natalizumab, CSF B cells and ASC were dramatically reduced but not absent, which could suggest that these cells have recently migrated to the CNS; alternatively, these cells may be CNS-resident and may reflect the failure of natalizumab to fully deplete these cells. Natalizumab can access the CSF, but at a 100- to 400-fold lower concentration than in the serum, and the persistence of OCB in 18% of individuals following 2 years of treatment suggests that CNS-resident B lineage cells may exist in these individuals (Harrer et al., 2015; Sehr et al., 2016; Mancuso et al., 2014).

Different frequencies in the B cell compartment between groups may provide clues as to the dynamics of the B cell response in MS. Harp et al (2007) found elevated CSF B cell frequencies in CIS compared to CDMS (Harp et al., 2007). A similar (but not significant) trend was also observed in this chapter, and although the median values between CIS and CDMS were essentially the same, more CIS samples contained a higher frequency of B cells than MS samples (Fig. 3.4A). Conversely, in the CSF, a lower frequency of ASC was

identified in CIS compared to MS (Fig. 3.4B). With the assumption that those who have had more than one clinical attack (i.e. CDMS) are further along in the disease process than those who have had one clinical attack (i.e. CIS), this could reflect evolution of the B cell response during disease, beginning with an influx of peripheral B cells, some of which may differentiate into ASC and set up residence within the CNS. This may explain the elevated B cells but lower ASC in CIS, as survival niches for ASC have not been established yet, and the decreased B cells but elevated ASC in MS (Fig. 3.4B). Conversely, Kuenz et al (2008) observed no significant difference in CSF B cell frequency between CIS or RRMS groups, although there was an increase in comparison to progressive MS, which was also shown by Wurth et al (2017) (Kuenz et al., 2008; Wurth et al., 2017). This could suggest that the B cell response in progressive MS is more compartmentalised within the CNS, consistent with the findings of ectopic follicles in progressive MS brains and the lower frequency of gadolinium-enhancing lesions, suggestive of fewer breaches of the BBB (Serafini et al., 2004; Magliozzi et al., 2007; Pikor et al., 2017; Pérez-Cerdá et al., 2016). With this in mind, a limitation of this chapter is that the CDMS group contained individuals with both RRMS and PPMS; larger sample sizes would allow these groups to be separated so that a more detailed investigation could be conducted.

An attractive therapeutic approach in MS is the specific targeting of pathogenic immune cell populations that may contribute to disease; therefore, comparing the features of B cell populations between disease groups may be beneficial. In this chapter, the expression of CD27 and CD38 in B cells and ASC were compared between disease groups (Fig. 3.5A, B). CD27 is a marker of memory B (and T) cells and its elevation in soluble form has been linked with a higher relapse rate; similarly, the ectoenzyme CD38 is associated with increased proliferation, and both markers have been used to define activation (Agematsu et al., 1997;

van der Vuurst de Vries et al., 2017; Funaro et al., 1997). No significant differences were observed in peripheral or CSF marker expression between disease groups, except in the natalizumab group, which displayed elevated CD38 expression on CSF B cells (Fig. 3.5A, B). To my knowledge, this phenomenon has not previously been reported. Natalizumab is known to perturb the peripheral B cell compartment by promoting the release of haematopoietic progenitor cells from the bone marrow; this may also occur in MS CNS, as ASC are highly dependent on α4 integrin for adherence to survival niches (Planas et al., 2012; Khan et al., 2016). In the mature B cell compartment, CD38 is highly expressed on germinal centre and post-germinal centre B cells, where it protects against apoptosis by upregulating bcl-2 proto-oncogenes (Zupo et al., 1994; Kumagai et al., 1995). Low levels of natalizumab can cross the BBB and may therefore disrupt CNS B cell development; however, a survival advantage by germinal centre B cells expressing high levels of CD38 may result in their over-representation in the CNS, due to the concomitant depletion of memory B cells by natalizumab, which express low levels of CD38 (Harrer et al., 2015; Sanz et al., 2008). This scenario is also in line with the detection of $CD38^{high}$ centroblasts in MS CSF, which are normally found within secondary lymphoid organs, and also supports the concept of the MS CNS as a B cell-fostering environment (Corcione et al., 2004, Pollok et al., 2017).

Data in this chapter demonstrated that CSF B cells and ASC display elevated CD27, IgG and increased size compared to their peripheral blood counterparts (Fig. 3.6A, B). Although this does not necessarily link these cells to disease pathogenesis, these features are suggestive of recent activation. In an investigation of the human B cell response following an immunological challenge, Ellebedy et al (2016) identified recently activated, antigen-specific B cells and ASC in the periphery (Ellebedy et al., 2016). In comparison to naïve B cells, recently activated B cells expressed elevated levels of CD27, which was even higher in

circulating ASC, 7 days after immunisation. Using forward scatter as a measure of cell size, Ellebedy et al (2016) also found that activated B cells were increased in size compared to naïve B cells (Ellebedy et al., 2016). This data therefore suggests that CSF B cells and ASC are recently activated. Increased IgG expression in CSF B cells and ASC was also observed compared to their peripheral blood counterparts. This compares to findings by Sandberg et al (1986), who showed that CSF B cells from those with MS secreted higher levels of IgG than peripheral blood B cells, suggesting that these cells may be highly activated in the CSF (Sandberg et al., 1986).

Although CD38 expression was increased in CSF ASC compared to those in the blood, suggesting a higher level of activation, the converse was true for CSF B cells, which expressed lower CD38 than those in the blood (Fig. 3.6A, B). Although this appears to contradict the idea that CSF B cells are more activated than those in the periphery, B cell maturation into memory B cells is associated with downregulation of CD38, therefore this phenomenon could result from the increased proportion of memory B cells in the CSF (Perez-Andres et al., 2010; Flores-Montero et al., 2016). Taken together, the features of CSF B cells and ASC in MS compared to those in the periphery suggest a highly activated phenotype.

Previous studies have disagreed on the frequencies of CD19- ASC in the CSF. Where some studies describe this population as largely absent, Corcione and co-authors (2004) identified CD19- ASC as the dominant ASC subset in MS CSF (Corcione et al., 2004; Cepok et al., 2005a; Kuenz et al., 2008). Additionally, Winges et al (2007) showed that CD19- ASC contribute a significant proportion (11±2%) of the CSF ASC population (Winges et al., 2007). In agreement with most previous studies, data from this chapter identified CD19+ ASC as the dominant ASC subset, constituting 64% of CSF ASC, although this frequency was highly variable (Fig. 3.7A, B). Some of the discrepancies in previous studies could have been due to

low cell numbers skewing the analysis, or differential survival of these populations in CSF following LP; for example, CD19- ASC dislodged from their survival niche will undergo rapid apoptosis, probably before CD19+ ASC, as they are dependent on continual pro-survival signals from the niche (Radbruch et al., 2006). Detection of CD19- ASC supports evidence for a continuum of ASC development in the MS CNS, since these cells are non-migratory and non-proliferating, indicating their *in situ* generation (Odendahl et al., 2005; Radbruch et al., 2006).

It is considered that mature ASC display a CD19- phenotype due to their gradual downregulation throughout the differentiation from B cell to long-lived plasma cell. This is supported by evidence that long-lived bone marrow ASC with a lifespan of over 40 years do not express CD19 (Halliley et al., 2015). In addition, ASC were shown to persist in the inflamed mouse CNS over a period of 5 weeks, and non-proliferating CD19- ASC have also been identified in MS brain lesions (Corcione et al., 2004; Pollok et al., 2017). Not only did the ASC populations identified in this chapter differ in their expression of CD19, suggesting different stages of differentiation, but ASC of a mature phenotype appeared to express higher levels of CD138, CD27, CD38 and IgG than CD19+ ASC (Fig. 3.7C, D). Caraux et al (2010) showed that in peripheral blood ASC, elevated CD38, CD27 and cytoplasmic immunoglobulin was seen in CD138+ ASC compared to CD138- ASC, suggesting that these markers could be a feature of increasing differentiation to a terminal ASC phenotype (Caraux et al., 2010; Perez-Andres et al., 2010). APRIL, a ligand for CD138, is critical for the transition of circulating plasmablasts to plasma cells following arrival at bone marrow niches; indeed, circulating plasmablasts in APRIL-deficient mice fail to become established within survival niches (Belnoue et al., 2008). It is considered that higher CD138 expression reflects a greater survival advantage, and that CD138 therefore mediates selection of mature ASC;

therefore, the elevated CD138 expression by mature ASC may allow greater responsiveness to the survival factor APRIL, and extracellular matrix molecules, which are ligands for CD138 (McCarron et al., 2017).

3.3.2 CSF B lineage cells correlate with inflammatory parameters

In agreement with previous observations, findings from this chapter demonstrated a strong correlation between the frequency of CSF B cells and ASC with the CSF lymphocyte count and CSF CXCL13 concentration (Fig. 3.8A-C) (Krumbholz et al., 2006; Kowarik et al., 2012; Puthenparampil et al., 2017). CXCL13 is markedly increased in the CNS during EAE, and its expression has been identified in ectopic follicle-like structures in EAE CNS tissue (Serafini et al., 2004; Magliozzi et al., 2004). Inflammatory cytokines such as lymphotoxin-β and TNFα can induce CXCL13 expression; therefore, exacerbation of inflammation by infiltrating peripheral lymphocytes may lead to elevated CXCL13 expression and B cell retention within the CNS (Irani, 2016). However, an association between ASC and CXCL13 does not necessarily reflect their increased migration to the CNS; it is possible that ASC may instead arise from the differentiation of recruited peripheral B cells within ectopic CNS follicles.

In this chapter, both CD19+ and CD19- ASC frequencies significantly correlated with CSF FLC (Fig. 3.8B). This is hardly surprising, since FLC are a by-product of rapid antibody production (Solling et al., 1981). The lack of correlation with CSF B cells potentially suggests that only a small proportion of these cells are disease-specific and as a whole are not necessarily related to the ASC population.

3.3.3 CSF B cells, but not ASC, are largely peripherally derived

Lymphocyte recruitment is not necessarily driven by antigen, as both antigen-specific and non-antigen specific lymphocytes are often observed at sites of inflammation (Ely et al., 2003; Chen et al., 2005). As inflammation subsides, non-antigen specific bystander lymphocytes are removed whereas the antigen-specific lymphocytes are retained (Zhang and Lakkis, 2015). In this chapter, comparison of the immunoglobulin isotype of CSF B cells to those in the periphery was performed to obtain clues as to the dynamics of B cell migration in MS. The similar immunoglobulin profile between peripheral blood and CSF B cells (Fig. 3.9A) implies that most of these cells are derived from the periphery. Indeed, sequencing studies have shown that CSF B cells are largely peripherally derived in that founding CNS B cell clones are often found within cervical lymph nodes, and that this immune response then evolves and continues within the CNS, since more mature clones are often found there (Stern et al., 2014).

Increased CSF IgG+ B cells agrees with previous reports that class-switched B cells are enriched within the CSF during neuroinflammation, however in both studies, non-inflammatory controls were not analysed (Cepok et al., 2006; Eggers et al., 2017). In this chapter, elevated CSF IgG+ B cells was observed for both MS and control groups, including non-inflammatory controls, suggesting that the increased proportion of memory B cells in the CSF is at least in part a biological phenomenon that is not specific to inflammation (Fig. 3.9B). Much like how memory T cells are preferentially found in the normal and inflamed CSF, it appears that memory B cells also show this trend; this is likely due to differential expression of chemokine and adhesion receptors that allow memory lymphocytes to enter non-lymphoid tissues (de Graaf et al., 2011). It was also found that CSF B cells were generally not Igκ-biased, and that this phenotype was comparable to peripheral blood B cells; this was true for all disease groups except for CIS, which showed a small increase, and

although not significant, clearly some individuals coming off natalizumab also showed an Igκ bias, suggesting a level of clonal expansion of CSF B cells in some individuals (Fig. 3.10A, B). Overall, the majority of CSF B cells in MS appear to be peripherally derived based on their similar immunoglobulin heavy and light chain expression.

In the periphery, most ASC are derived from mucosal responses and are therefore IgA+; however in the CSF, the overwhelming majority of these cells express IgG (Fig. 3.9B) (Mei et al., 2009). This striking difference to the peripheral blood profile has been suggested by CSF analysis in sequencing studies, and the fact that most CSF antibody in MS is IgG1κ; this phenomenon could therefore indicate clonal expansion of IgG+ ASC (Zeman et al.,2012; von Budingen et al., 2012; Stern et al., 2014). However, as the immunoglobulin isotype is also related to the homing capability of ASC, it is possible that CSF ASC have non-specifically migrated from the periphery and are not directly related to MS pathogenesis. Migration of peripherally derived ASC has been observed in NMO, where IgG+CXCR3+ plasmablasts are elevated in the periphery and enriched in the CSF during relapse (Chihara et al., 2013). Similarly, in a mouse model of viral encephalomyelitis, CXCR3+ plasmablasts were expanded in the draining cervical lymph nodes prior to their accumulation in the CNS, supporting the concept of peripheral expansion of antigen-specific plasmablasts prior to CNS infiltration (Marques et al., 2011).

3.3.4 CSF ASC, but not B cells, show features of clonal expansion

In this chapter, the frequency of CSF IgG+ ASC was increased in the MS group compared to the control group, where IgA+ ASC were increased in comparison (Fig. 3.9B). Despite the limited sample size, it is possible that this phenomenon reflects at least some peripheral ASC

migration in these individuals, since IgA is the dominant isotype in the periphery. The ASC Igκ:Igλ ratio was elevated in MS to varying degrees (Fig. 3.10A-C). In two ONID samples, CSF ASC were biased in both directions (Igκ-biased or Igλ-biased), which could reflect expansion towards the disease-causing agent; however, in MS, all of the individuals were Igκ-biased. This bias was also observed in an individual following natalizumab cessation (Fig. 3.10C). Since natalizumab blocks lymphocyte trafficking into the CNS, an obvious explanation is that at least some clonally expanded ASC are CNS-resident and remain unaffected by natalizumab therapy; this has also been suggested by the observation of residual OCB in 40% of natalizumab cases (Mancuso et al., 2014).

A light chain bias suggests antigen-driven selection, which could occur if CSF ASC are retained and fostered within the CNS. The novel observation that CD19- ASC are generally more Igκ-biased than CD19+ ASC indicates that this population possess a more limited antigen diversity, and may therefore have been generated from an earlier CNS response (Fig. 3.10D). As CD19- ASC are non-migratory, their presence in the CSF suggests they were dislodged from one of the limited number of CNS survival niches in favour of recently generated ASC, ending up in the CSF where their rapidly produced antibodies are detected prior to apoptosis (Radbruch et al., 2006). It is feasible to suggest that CNS survival niches are initially occupied by ASC generated earlier in the disease, and that with disease evolution, these cells may be out-competed by more recently generated CD19+ ASC, which have a broader antigen repertoire due to epitope and/or antigen spreading, therefore a lower Igκ:Igλ ratio.

Biologically, an elevated Igκ:Igλ ratio suggests clonal expansion of B cells specific for an antigen inducing an IgGκ response, leading to a skewed light chain ratio. These data

demonstrate the intimate relationship between FLC and ASC by showing a strong correlation between the FLC Igκ:Igλ ratio and the ASC Igκ:Igλ ratio in the CSF, which was not observed for CSF B cells (3.11A-C). IgG+ CSF B cells also showed no correlation, however a small number of samples appeared to show some relationship, indicating some intrathecal expansion in these samples. A previous study showed that CSF B lineage cells are the source of CSF OCB by demonstrating a strong overlap between CSF cell immunoglobulin mRNA, and the Ig proteome from OCB (Obermeier et al., 2008). Observations in this chapter extended these findings by showing that CSF ASC, but not CSF B cells, are strongly related to secreted CSF immunoglobulin through their strong relationship with the FLC Igκ:Igλ ratio.

A hypothesis of this work was that the FLC Igκ:Igλ ratio relates to the broadness of the humoral response in MS (Fig. 3.14). This suggests that the antibody response in MS spreads to additional epitopes and/or additional antigenic targets, becoming more diverse with time. This then presumably translates to disease duration; i.e. the disease begins with few (or even one) antigen specificities, and therefore a high FLC Igκ:Igλ ratio, which progresses to a low ratio comparable to that in the periphery due to a broad array of targets. Therefore, it is possible that those with CIS, who have had one clinical relapse, have a higher FLC Igκ:Igλ ratio than those with MS, who have experienced multiple clinical relapses. Comparison of the FLC Igκ:Igλ ratio between disease groups revealed significant Igκ bias in all MS groups compared to OND controls (Fig. 3.12). Despite the lack of a significance between CIS and MS, which could have been due to high variation and small group sizes, the CIS group shows a trend for an elevated ratio compared to the MS group (12.5:1 vs 6.3:1); additionally, the CIS group showed more significant difference against OND than the MS group, suggesting a greater increase compared to MS. Clearly, great variation exists within groups, which could

also represent the difficulty of categorising individuals as CIS or MS at diagnosis, since it is very difficult to estimate the duration of sub-clinical disease, which may have started years before clinical symptoms begin. As such, lack of a significant difference between CIS and MS does not necessarily invalidate the concept that the FLC Igκ:Igλ ratio is associated with epitope/antigen spreading and/or disease progression, and further work is required to investigate this in a larger cohort.

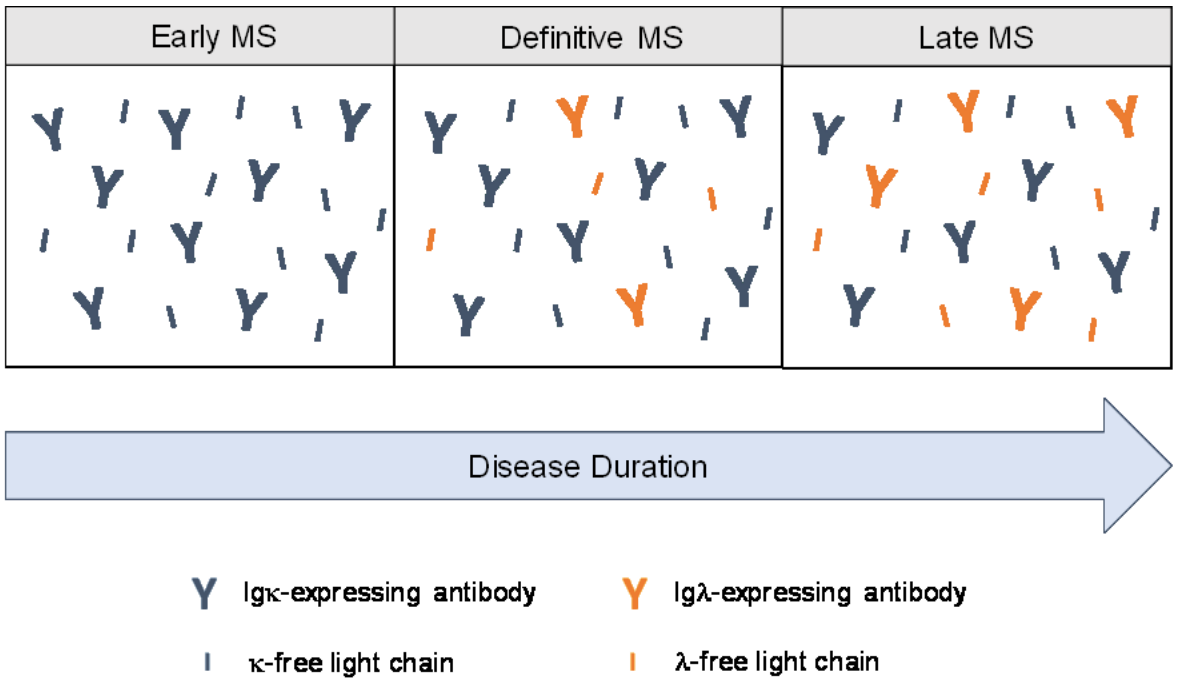

Figure 3.14 Proposed model for the spreading of the humoral response in MS. It was hypothesised that the humoral response in MS is initiated against a single immunodominant Igκ-inducing antigen in all individuals (left panel). With increasing disease duration, a combination of epitope spreading and the influx of peripheral B cells, which are retained within the inflamed CNS, causes the presence of Igλ-expressing antibodies in established MS (middle panel). In late MS (right panel) the ratio equilibrates to around 1.6:1, reflecting that seen in the periphery.

Repeat CSF samples were investigated for their potential insight into the dynamics of CSF B cells and ASC. These were obtained from an individual coming off natalizumab therapy at day 0 (i.e. CSF obtained at first LP) and day 62**.** Despite the strikingly huge lymphocytic presence in the CSF, the CD19+CD20+ B cell population represented a similar frequency at both timepoints, possibly suggesting non-specific recruitment; in contrast, the ASC frequency had quadrupled on day 62, indicating their expansion (Fig. 3.13A). The high cellularity at day 62 suggests an increase in CNS inflammation, and the preferential increase in ASC could indicate their active contribution to disease.

The lower Igκ:Igλ ratio in B cells on day 62 suggests a broader antibody repertoire, which in association with the increased cellularity suggests influx from the periphery (Fig. 3.13B). Conversely, ASC appear to display a higher Igκ-bias in the presence of increased inflammation, based on both ASC and FLC ratios, suggesting an antigen-driven response by Igκ-expressing ASC. Although these observations are based on low cellularity (for the 'day 0' sample) and are from only one individual, they provide some insight into B cell-related pathogenesis. Longitudinal analysis of the CSF antibody response would be required to fully investigate the dynamics of epitope and/or antigen spreading in MS, which is partly investigated in chapter 4, however as a final note, these data support the findings throughout this chapter that the CSF ASC population is largely independent from the CSF B cell population.

3.4 Chapter Summary

In summary, I identified and characterised both CD19+ and CD19- ASC populations in MS CSF, supporting the concept that the CNS is conducive to B cell survival and development. Phenotypic characterisation confirmed the distinct differences between these CSF ASC populations, which along with CSF B cells displayed an activated phenotype compared to their peripheral counterparts. These data support a pathological involvement of B cells and ASC in MS through their association with inflammation-related parameters, further supporting their depletion with anti-CD20 therapies (Hauser et al., 2008; Kappos et al., 2011; Krumbholz et al., 2014).

The hypothesis of this chapter, that clonally expanded B lineage cells can be detected in MS CSF, was confirmed; CSF ASC appear to be clonally expanded, based on their predominant IgGκ expression, whereas CSF B cells appear to be largely non-selective and derived from the periphery, based on their similar immunoglobulin expression profiles between the periphery and CSF. Though no significant differences were observed between CIS and MS groups, the possibility remains that the Igκ:Igλ ratio relates to epitope/antigen spreading, and thus warrants further investigation.

CHAPTER 4

INVESTIGATION OF CSF ANTIBODY SPECIFICITY IN MULTIPLE SCLEROSIS

Chapter 4: Investigation of CSF antibody specificity in multiple sclerosis

4.1. Introduction

A hallmark of MS is the presence of CSF antibodies (Walsh and Tourtellotte, 1986, Kabat et al., 1950; Giovannoni, 2014). The key pathological feature of demyelination, and the induction and functional demyelinating properties of anti-myelin antibodies in EAE, has led to the extensive investigation of myelin antigens as primary autoantibody targets in human MS (Reindl et al., 1999; Walsh and Murray, 1998; Sadler et al., 1991; Marín et al., 2014). However, antibodies to non-myelin antigens have also been identified; these include damage-related proteins, such as neurofilament light chains and neurofascin, inflammation-related proteins, such as prostaglandins and complement components, and microbial proteins, such as EBNA-1, human endogenous retroviruses (HERVs) and the so-called MRZ reaction towards measles, rubella and Varicella-zoster viruses (Puentes et al., 2017; Mathey et al., 2007; Farias et al., 2014; Santiago et al., 2010; Morandi et al., 2017; Derfuss et al., 2005; Chmielewska-Badora et al., 2000).

The strong Igκ-bias by MS CSF antibodies, and the elevated Igκ FLC concentration compared to controls, is suggestive of clonal expansion towards a common antigen; indeed, sequencing studies have demonstrated the presence of clonally expanded B cells and ASC in MS CNS (Lovato et al., 2011; Ligocki et al., 2010). However, despite decades of investigation, no single antigen has been identified thus far that is unique to MS, or that is commonly found within affected individuals (Levin et al., 2013; Hohlfeld et al., 2015a; Hohlfeld et al., 2015b). The broad antibody repertoire of MS contrasts with that of NMO, in

which a robust and specific CSF antibody response is mounted against the water channel aquaporin-4 (Takahashi et al., 2007). It is therefore possible that a unifying autoantigen responsible for the frequently observed Igκ-bias in MS is yet to be identified.

Proteomic techniques have revolutionised the search for candidate autoantigens, allowing high-throughput processing with the potential for hypotheses-free investigations. A 2014 review identified 2D gel electrophoresis as the historical basis of proteomic analysis in MS, which has been largely superseded by shotgun mass spectrometry techniques, despite its limited use of samples (Farias et al., 2014). Although several studies have since utilised high-density antigen arrays in the field of MS, large-scale analysis of the CSF autoantibody repertoire has not frequently been assessed using these methods and plenty of scope remains for further investigation (Somers et al., 2008; Häggmark et al., 2013; Bystrom et al., 2014; Quintana et al., 2014; Hecker et al., 2016; Ayoglu et al., 2016). High-density arrays allow the screening of large sample sizes and the analysis of large numbers of target antigens. Furthermore, the use of different array formats provides the opportunity to cross-validate findings of antigen reactivity. Large scale characterisation of the human proteome is a continuing initiative of the Human Protein Atlas (HPA) project (www.proteinatlas.org), which produces recombinant protein fragments for the systematic exploration of the human proteome (Sjoberg et al., 2016). These proteins represent sequences of lowest homology to other proteins and are validated using specific polyclonal antibodies (Sjoberg et al., 2016).

In this chapter, we collaborated with Professor Peter Nilsson and colleagues in Stockholm to assess CSF antibody reactivity of MS and control groups using planar and bead-based array platforms, including using the largest available planar microarray platform to date, hosting HPA-validated antigens (Sjoberg et al., 2016). Additionally, a novel aspect of this project was the investigation of antigen reactivity by antibodies bearing kappa (Igκ) and lambda (Igλ)

light chains in MS CSF, with the aim of unravelling any potential differences in antigen reactivities, the identities of which may provide clues to their involvement in MS pathogenesis. The hypothesis of this chapter was that that antibodies bearing Igκ light chain recognise a distinct antigen, which is responsible for the Igκ bias in MS.

4.1.1 Chapter Objectives

1. Identify potential autoantigen targets recognised by CSF antibodies from MS (CIS, RRMS, PPMS and natalizumab-treated) and control (OND, ONID) groups using planar arrays
2. Verify any observed autoantibody reactivity using bead-based antigen arrays
3. Identify any differences in CSF reactivity across different disease groups
4. Investigate whether antigen reactivity relates to FLC concentration and/or the Igκ:Igλ FLC ratio
5. Determine whether common MS candidate autoantigens (MAG and MBP) are identified as antigen targets in MS CSF
6. Assess whether certain antigens can induce a kappa-biased antibody response, and whether this may be related to MS pathogenesis

4.2 Results

4.2.1 Unbiased assessment of CSF reactivity using planar 21k arrays

The initial discovery phase was conducted using planar antigen arrays. The first array format employed 21,120 human protein fragments, termed '21k arrays', allowing unbiased screening of 12,412 protein encoding genes.

Due to the interest in potential autoantigens during the early phases of disease, CSF samples from six individuals with CIS were assessed for antigen reactivity using 21k arrays (**Fig. 4.1A**). These samples were selected based on their strong FLC bias towards Igκ (**Appendix II table B**) with a median ratio of 86:1, based on the hypothesis that these individuals demonstrate more antigen restriction and are earlier on in the disease course. For this phase of the study, pooled CSF from six RRMS and six OND individuals was also used (**Fig. 4.1B**). The RRMS samples used for planar arrays were also subject to selection bias; these were selected based on their non-biased Igκ:Igλ ratio (median 1.47:1) with the idea that these samples contain antibodies recognising multiple antigen specificities (**Appendix II table B**).

As in previous studies by Professor Peter Nilsson and colleagues, an arbitrary threshold for each sample or group was determined to allow the number of antigens recognised, termed 'positive hits', to be quantified (**Fig. 4.2A**). The threshold was set based on visual inspection of the antigen array data and a calculation was applied to allow distinction between positive and negative hits; this calculation was then applied to all samples. These cut-offs were sample-specific to account for the varying background reactivity between samples, allowing any antigen above this threshold to be identified as a positive hit. Defining a cut-off allowed the data to be transformed into binary values (1 or 0) to inform whether or not the cut-off value was exceeded, thus denoting positive or negative reactivity. Positive controls such as

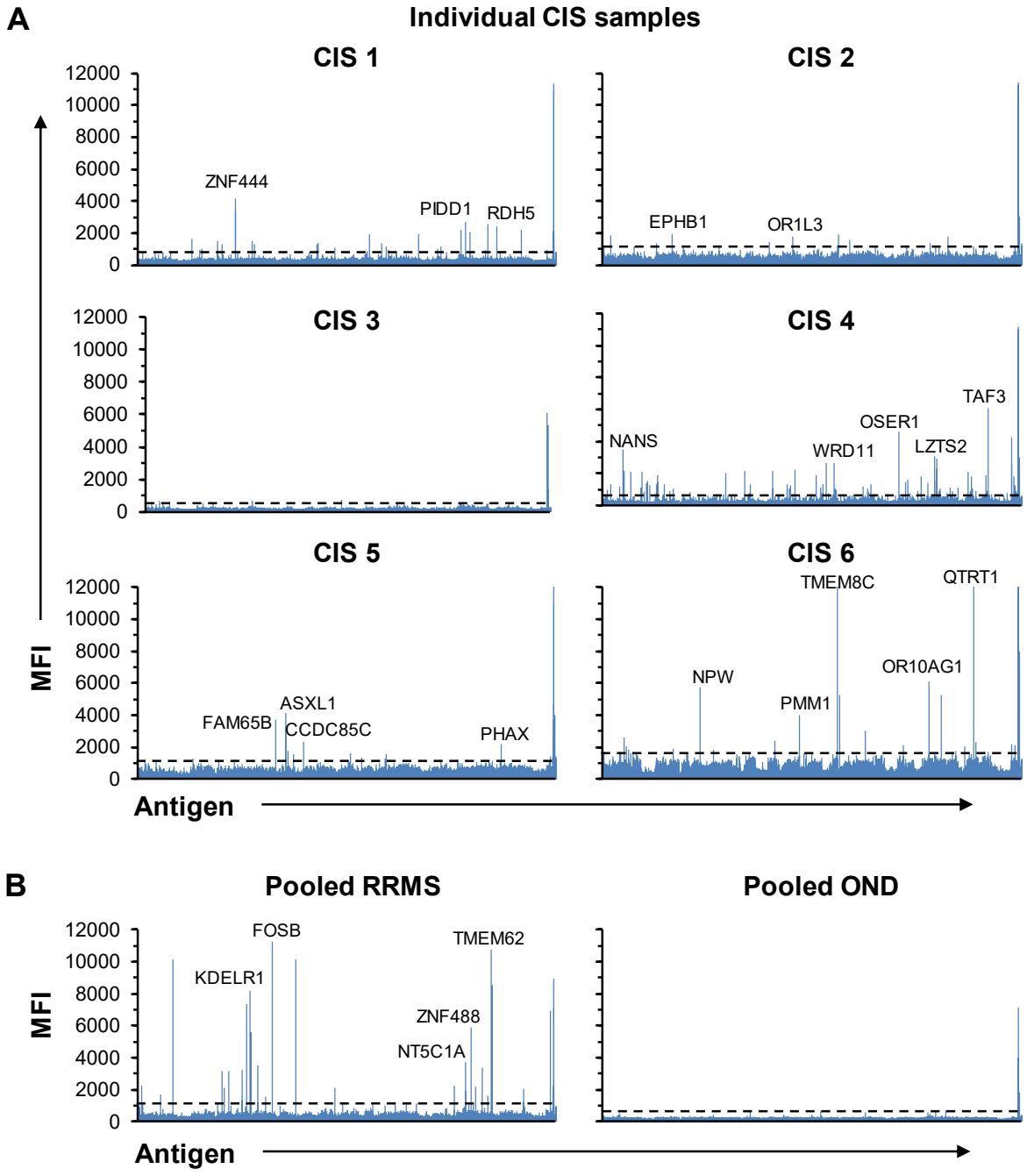

Figure 4.1 CSF reactivity using 21k planar arrays (i). CSF samples from six CIS individuals with a biased Igk:Igl FLC ratio **(A)**, and pooled CSF from six RRMS individuals with a non-biased Igk:Igl FLC ratio and six individuals with OND **(B)**, were ran on large planar arrays to determine reactivity towards 21,120 antigens. Dotted lines represent cut-offs determined for each assay based on the level of background reactivity, and was calculated by multiplying the median fluorescence intensity (MFI) of each group + 4x median absolute deviation (MAD). The rabbit anti-human IgG control is shown at the end of each graph.

A

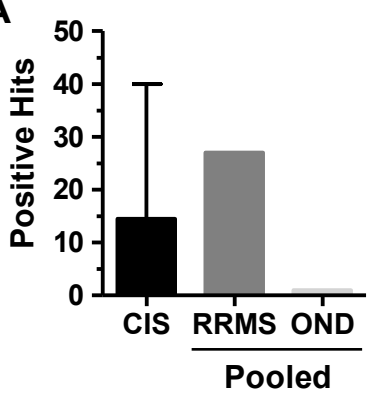

B

Gene	Gene Description	UniProt	Samples
USP13	ubiquitin-specific peptidase 13	Q92995	CIS 1, CIS 5
NT5C1A	5-nucleotidase, cytosolic 1A	Q9BXI3	CIS 1, CIS 2, RRMS pool
TAF3	TAF3 RNA polymerase II, TATA box binding protein-associated factor	Q5VWG9	CIS 4, CIS 6
CCDC85C	coiled coil domain containing 85C	A6NKD9	CIS 4, CIS 5, OND pool

C

Gene	Gene Description	UniProt
NENF	neudesin neurotrophic factor	Q9UMX5
ANO2	anoctamin 2	Q9NQ90
NPW	neuropeptide W	Q8N729
ASTN1	astrotactin 1	O14525
OR10AG1	olfactory receptor, family 10, subfamily AG, member 1	Q8NH19
PMM1	phosphomannomutase 1	Q92871
SNPH	Syntaphilin	O15079
LINGO4	Leucine-rich repeat and Ig domain-containing 4	Q6UY18

Figure 4.2 CSF reactivity using 21k planar arrays (ii). The number of positive hits for each sample was quantified following application of sample-specific cut-offs **(A)**. Data shows the median and range (for CIS group). Details of the positive hits shared between different samples **(B)** and of interesting candidate antigens identified **(C)**.

rabbit anti-human IgG were omitted from these calculations, since it was expected that these would produce a positive hit, but negative controls such as empty beads (i.e. beads alone) or His6-ABP were included to ensure the calculated threshold was above these signals. Quantification of the positive hits between groups indicated that CIS and RRMS samples identified a higher number of hits compared to OND samples (**Fig. 4.2A**). Several antigens were identified as common targets between a number of samples and/or groups (**Fig. 4.2B**), and a number of positive hits with potential relevance to MS were also identified (**Fig. 4.2C**).

4.2.2 CSF reactivity using 384 planar arrays

Following initial screening using 21k arrays, smaller arrays hosting 384 proteins were used (referred to as '384 arrays'). Although they are biased, since they host pre-determined proteins, the 384 arrays are more suited to screening a larger sample size. The 384 arrays can be custom designed based on organs or tissues of interest, or on diseases of interest, based on previously reported and/or suspected antigen targets associated with a certain disease; in this case, arrays hosting 384 antigens were selected, based on previous in-house studies by the collaborating laboratory.

Six CSF samples from individuals with CIS (**Fig. 4.3A**), RRMS (**Fig. 4.3B**) and OND (**Fig. 4.3C**) were applied to 384 planar arrays to reveal the MFI intensity profiles of each sample. Following application of sample-specific cut-offs, CIS samples (black dots) were found to identify a median of 12 (range 7-16) antigens, whereas RRMS samples (grey dots) identified 12.5 (range 4-26) and OND samples (white dots) identified 4 (range 1-6; **Fig. 4.4A**). Collectively, the extent of antigen reactivity correlated significantly with total FLC ($r= 0.807$, $p= <0.001$) (**Fig. 4.4B**). Additionally, the Igκ:Igλ FLC ratio was collectively compared with

the number of positive hits recognised by each sample (**Fig. 4.4C**). This also revealed a significant correlation ($r= 0.735$, $p= <0.001$).

In addition to calculating a threshold to define positive reactivity, high and low sample-specific cut-offs were calculated, and a heat map generated to analyse reactivity towards common antigens between samples (**Fig. 4.4D**). This was performed based on the median reactivity per sample + 0.5x the median absolute deviation (MAD) for the lower cut-off (pink boxes), and the median reactivity per sample + 4x the MAD for the higher cut-off (red boxes). Several antigens common to more than one sample were identified, including interferon-α inducible protein 27 (IFI27), B cell lymphoma/leukaemia 10 (BCL10) and phosphoglycerate mutase family member 5 (PGAM5), which were positively recognised by several CIS and RRMS CSF samples.

Following this initial investigation, a total of 55 candidate target antigens were selected using both 21k and 384 planar arrays (**Appendix IV**), which were combined with a series of candidate MS target antigens identified from the literature (**Appendix V**) as well as those identified in-house to yield 301 antigen targets which were taken forward to the verification stage of the project using bead-based antigen arrays.

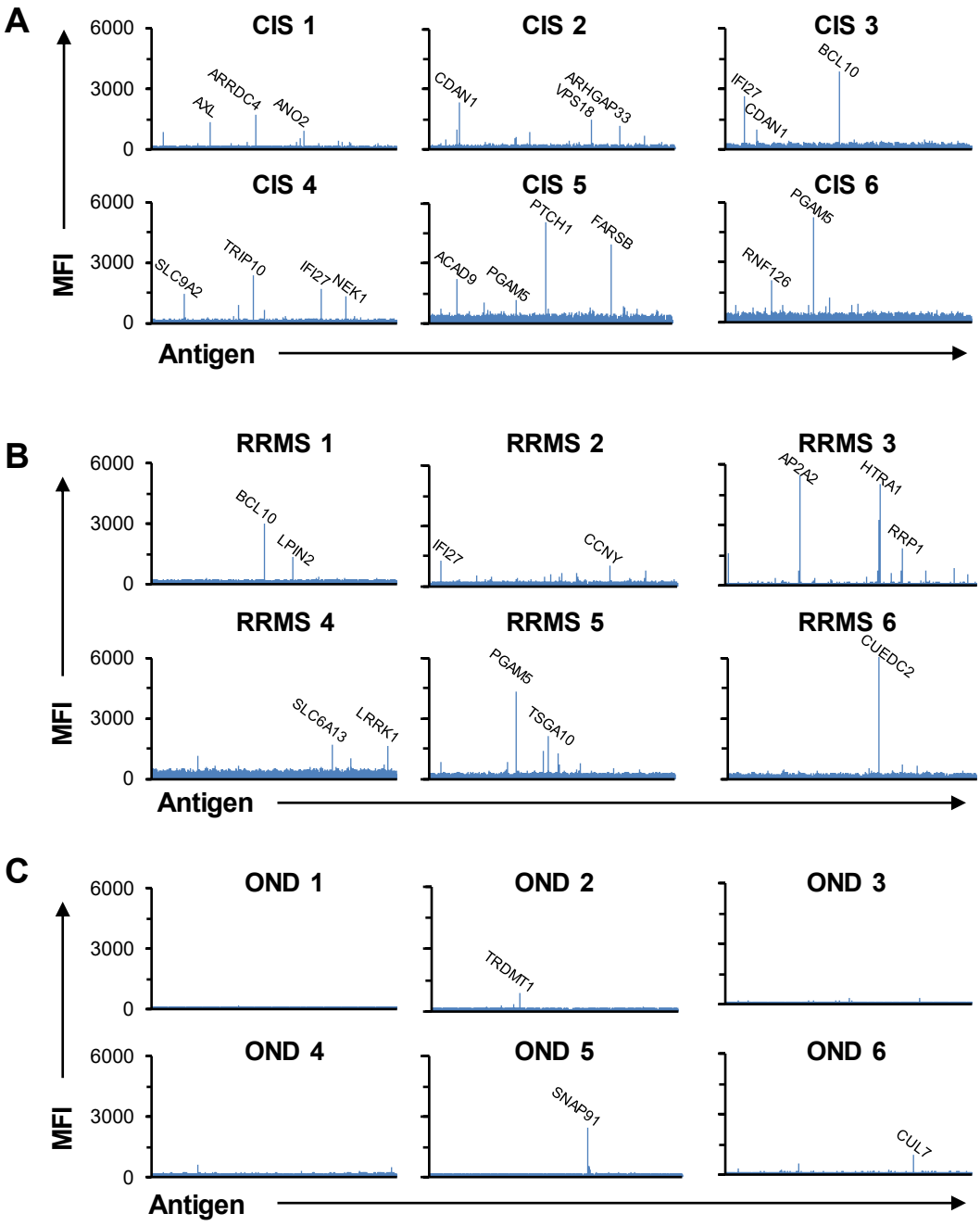

Figure 4.3 CSF reactivity on planar arrays towards 384 antigens (i). CSF samples from six CIS **(A)**, six RRMS **(B)** and six OND **(C)** individuals were ran on planar arrays to determine reactivity towards 384 antigens. Sample-specific cut-offs not shown.

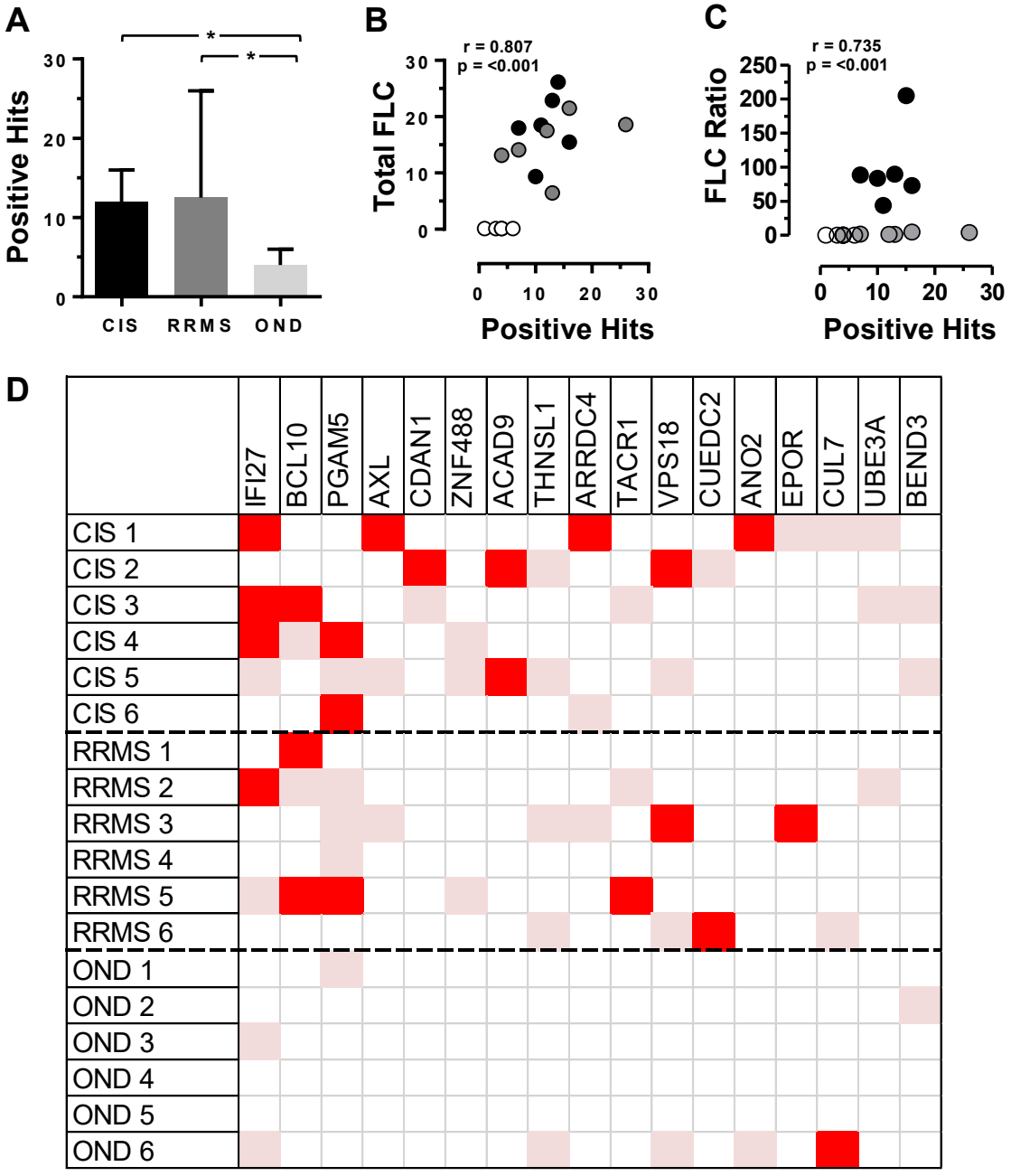

Figure 4.4 CSF reactivity on planar arrays towards 384 antigens (ii). The number of positive hits for each CSF sample was quantified following application of arbitrary sample-specific cut-offs, calculated by combining the median reactivity per sample + 0.5x the median **(A)**. Data shows the median and range, and were significant to * ($P<0.05$) using Dunn's multiple comparisons test. Spearman correlation of total CSF FLC (mg/l) **(B)** or the FLC Igκ:Igλ ratio **(C)** compared to the number of positive hits obtained for CIS (black), RRMS (grey) and OND (white) samples. Heatmap showing common antigen reactivities **(D)**. The heatmap was generated by calculating low and high sample-specific cut-offs by combining the median reactivity per sample + 0.5x the median (low cut-off; pink) or multiplying the median by 4 (high cut-off; red).

4.2.3 Buffer and antibody optimisation

Successful identification of reactive antigen targets relies on the measurement of a distinct signal which allows differentiation from the background signal. To optimise the assay conditions by reducing background signal, two assay buffers were tested; a standard buffer containing PBS + 0.1% tween, and the same buffer with 5% milk. The two assay buffers were compared for CSF pools using the anti-human IgG control, and demonstrated a modest signal reduction with the addition of 5% milk (**Fig. 4.5**). Controls used in these assays were 'empty' beads (i.e. beads which were not incubated with CSF) to show any non-specific signal derived from the beads, beads with anti-His_6-ABP to demonstrate blocking of any exogenous ABP antibodies within CSF, and anti-human IgG as the positive control. Results demonstrated a level of total signal reduction with the addition of milk.

For further optimisation, the anti-human Igκ antibody was incubated with CSF pools in both buffers at a 1/100 (**Fig. 4.6A**) and 1/500 (**Fig. 4.6B**) dilution. Similarly, this process was repeated for the anti-human Igλ antibody (**Fig. 4.7A, B**). Based on the lower signal intensity from the anti-human Igλ antibody, and the loss in signal intensity at 1/500, a 1/100 dilution was selected for both antibodies. Because of the relatively low background reactivity observed in CSF, assay buffer without milk was selected for use in the suspension bead arrays to allow greater detection of binding.

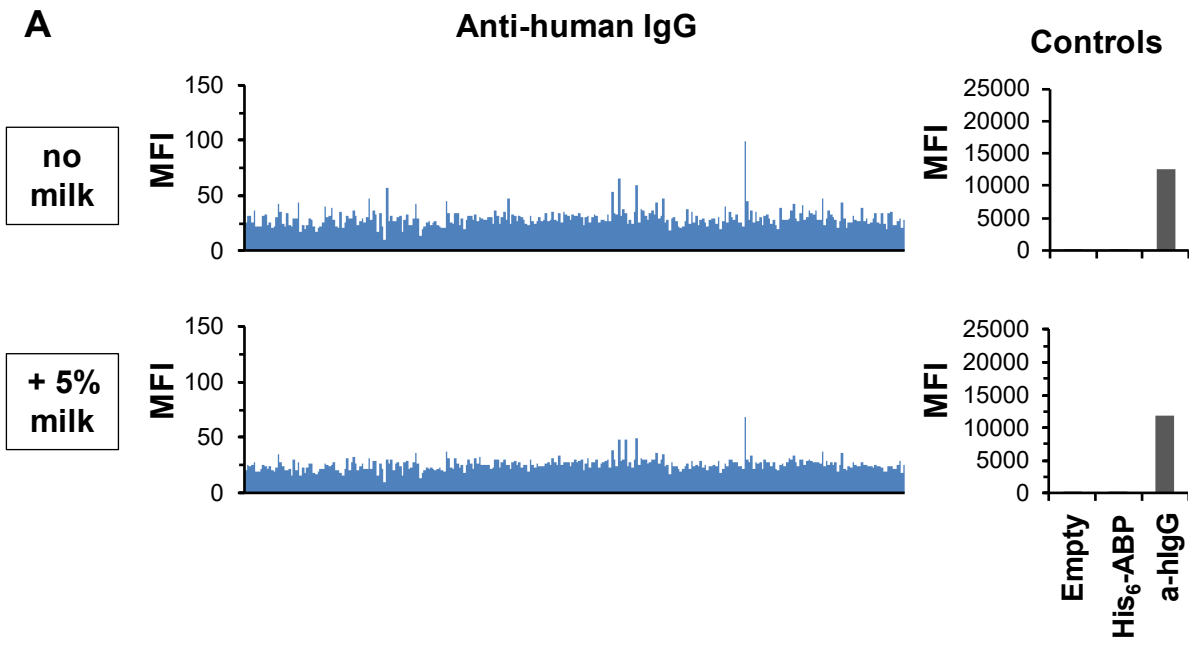

Figure 4.5 Buffer optimisation using the anti-human IgG antibody. Reactivity of pooled CSF using the anti-human IgG detection antibody in the presence of assay buffer with or without 5% milk. The corresponding controls are shown on the right (grey bars). Controls used were 'empty' beads (i.e. beads without CSF), beads with anti-His6-ABP (to demonstrate blocking of any exogenous His_6-ABP) and beads with anti-human IgG (positive control).

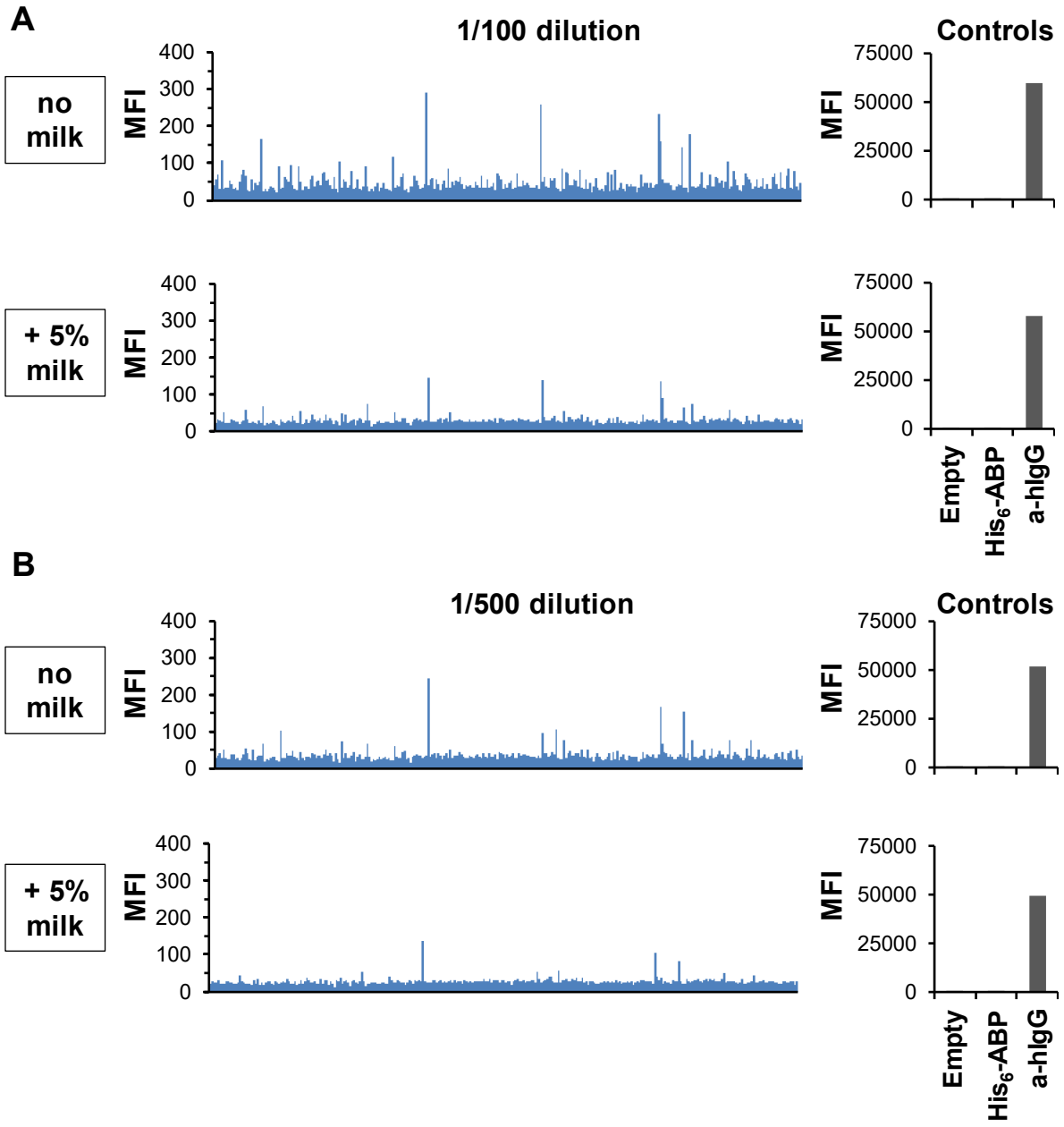

Figure 4.6 Optimisation of anti-human kappa light chain antibody. Test of anti-κ light chain antibody at 1/100 **(A)** and 1/500 **(B)** dilutions using pooled CSF, with or without the addition of 5% milk to the assay buffer.

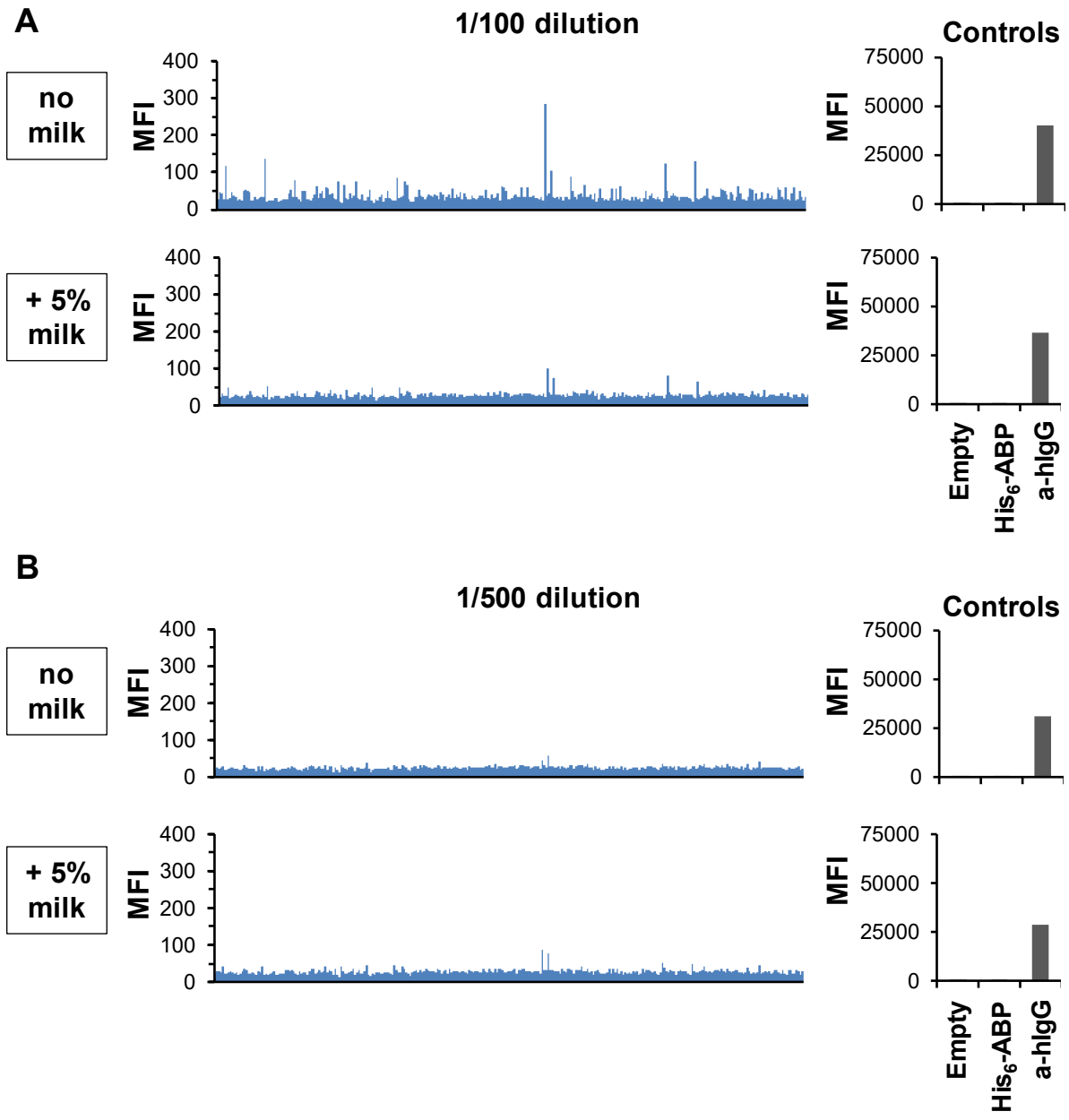

Figure 4.7 Optimisation of anti-human lambda light chain antibody. Test of anti-λ light chain antibody at 1/100 **(A)** and 1/500 **(B)** dilutions using pooled CSF, with or without the addition of 5% milk to the assay buffer.

4.2.4 Quality control testing of the suspension bead array

Suspension bead arrays were generated by first conjugating target antigens to magnetic beads labelled with a specific bead ID. To ensure pairing of the correct antigen with its corresponding bead ID, two antigens (MBP and ANO2) were selected and incubated with anti-MBP or anti-ANO2 antibodies. Binding to the correct bead IDs were confirmed, demonstrating successful pairings with the correct IDs and validating the bead IDs against their expected conjugated antigens (**Fig. 4.8A**). Incubation of antigen-conjugated beads with anti-rabbit IgG demonstrated reactivity for the correct bead IDs with no cross-reactivity with human antigens; similarly, non-specific binding was not observed following incubation of antigen-conjugated beads with anti-chicken IgY (**Fig. 4.8B**). The beads were also incubated with anti-His_6-ABP antibody to demonstrate successful antigen conjugation, binding to the His_6-ABP tagged to the antigens (**Fig. 4.8C**).

Each bead ID was representative of a single antigen, and beads were pooled following conjugation. However, beads may have been lost during the conjugation process or they may have aggregated due to sticky antigens. Therefore, an important step was to assess the bead count corresponding to each antigen to ensure that conjugation was successful and that a high enough signal would be achieved. A low bead count would also mean low antigen levels in the assay which may misleadingly result in low signals, even in the presence of saturating antibody concentrations. For each antigen, the median number of beads were determined, and a minimum count of 30 beads was chosen as the cut-off (**Fig. 4.9A**). All except 8 beads passed the bead count test; these 8 bead IDs and their corresponding antigens were excluded from further analysis, on the assumption that the conjugation step was unsuccessful (**Fig. 4.9B**).

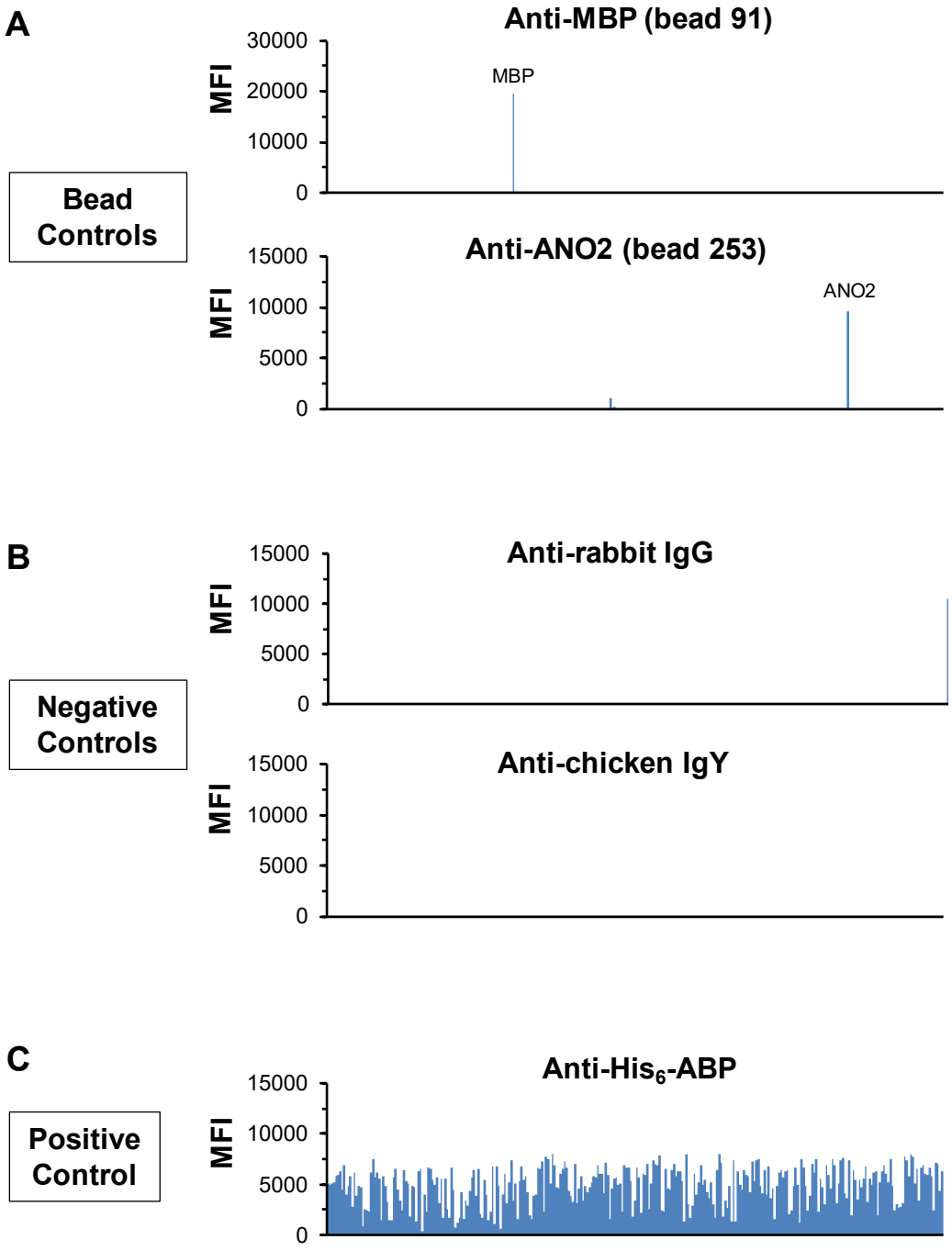

Figure 4.8 Coupling test for the suspension bead array. Antibodies against two selected bead IDs (MBP and ANO2) were used to ensure correct coupling to their corresponding IDs **(A)**. Anti-rabbit IgG and anti-chicken IgY antibodies were incubated with antigen-conjugated beads for the negative control **(B)**. The beads were incubated with an anti-His_6-ABP antibody to demonstrate successful antigen conjugation **(C)**.

A

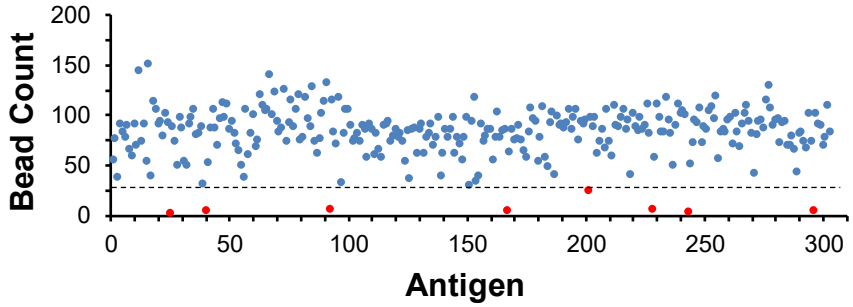

B

Bead No.	Gene	Gene Description	UniProt
25	CNTN2	Contactin 2 (axonal)	Q02246
40	IFNLR1	Interferon, lambda receptor 1	Q8IU57
92	KIF15	Kinesin family member 15	Q9NS87
167	HERC2	HECT and RLD domain-containing E3 ubiquitin protein ligase 2	O95714
201	ASTN1	Astrotactin 1	O14525
228	NCOA2	Nuclear receptor coactivator 2	Q15596
243	CNTN2	Contactin 2 (axonal)	Q02246
298	UBEA	Ubiquitin protein ligase E3A	Q05086

Figure 4.9 Exclusion of antigens with low bead counts. As part of the analysis, the median number of beads was determined for each antigen **(A)**. A minimum cut-off of 30 beads per antigen was chosen; antigens with bead numbers below this cut-off were excluded from the analysis **(B)**.

Finally, for each suspension bead array, several quality control steps were assessed. Like the CSF samples, controls were processed in a randomised fashion to avoid any plate effects. Using the anti-human IgG detection antibody, the MFI values of empty beads and beads with anti-His_6-ABP showed very little background reactivity, with median values of 27 and 23 (**Fig. 4.10A**). The anti-human IgG-conjugated beads in the presence of CSF had a median MFI of 19,431, demonstrating the presence of CSF antibody which is detectable using this assay. The consistency between the controls and across CSF samples also demonstrated reliability of the assay.

A final check after running CSF samples on the suspension bead array was to analyse the bead count for each CSF sample (**Fig. 4.10B**). This ensured consistent distribution between CSF samples to inform the reliability of the MFI values obtained from these beads during analysis. These analyses were performed for the anti-human IgG suspension bead array (shown in **Fig. 4.10**) and also for the anti-human Igκ and anti-human Igλ suspension bead arrays (data not shown).

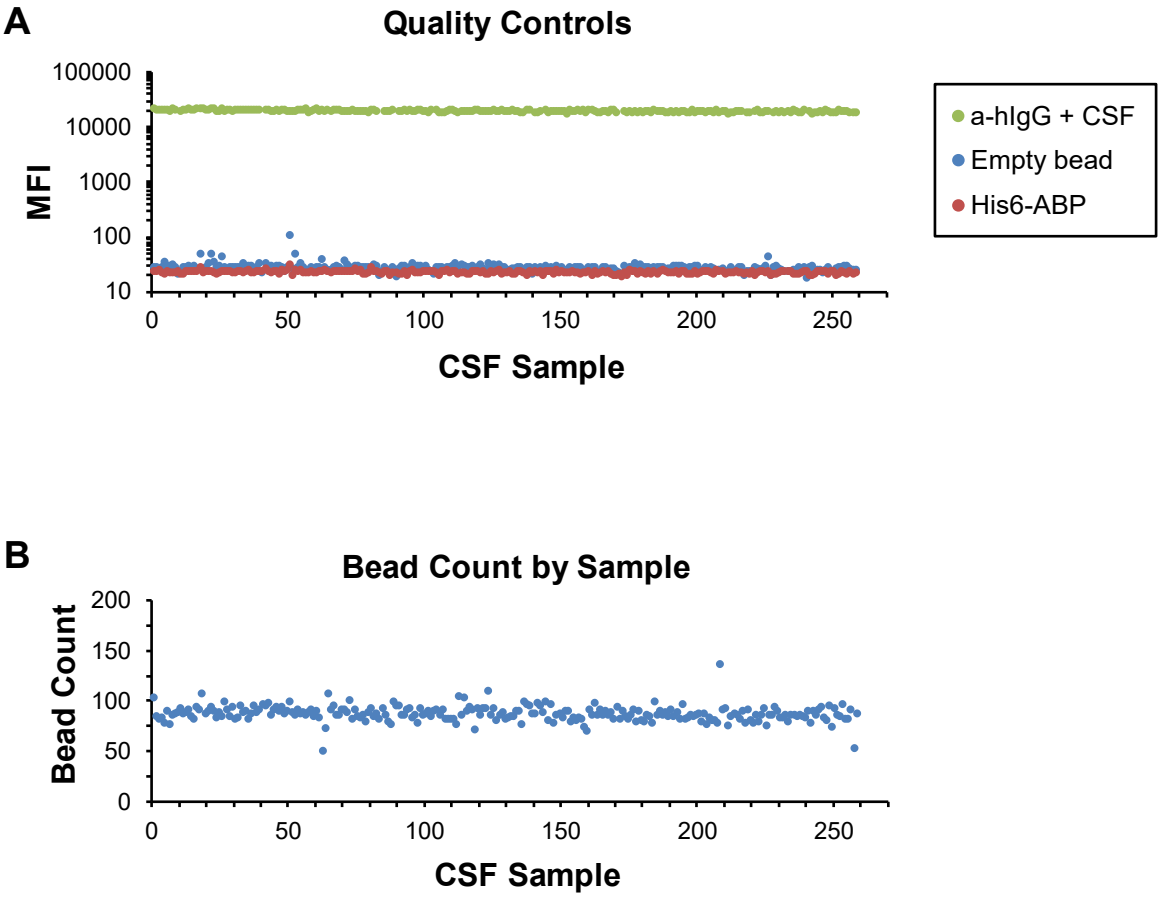

Figure 4.10 Quality controls for the anti-human IgG suspension bead array. Quality controls employed for the suspension bead array assessed MFI values for the empty bead, His_6-ABP bead and the anti-human IgG bead in the presence of CSF **(A)**. The same quality controls were also performed for the Igκ and Igλ suspension bead arrays (data not shown). For the anti-human IgG suspension bead array, the median number of beads incubated with each CSF sample was determined to ensure consistent distribution **(B)**.

4.2.5 Comparative antigen reactivity profiles between both array platforms

As two alternative antigen array platforms, planar and bead-based, were used for this project, it was possible to compare the antigen reactivity of the same CSF sample using both technologies. The antigen reactivities of six CIS samples that were used on the 21k arrays were compared to reactivities using the bead-based arrays (**Fig. 4.11**). Antigens identified as a positive hit on the bead-array were then compared to the planar array data, and if positive using both methods, were coloured in red. In half of the samples (CIS 4, 5 and 6) almost all the antigens identified as positive on the bead-based array were also identified as positive on the planar array, even in weakly identified antigens.

4.2.6 Comparative antigen reactivity profiles of repeat CSF samples

To further investigate the reproducibility of these assays, comparison of antigen reactivity profiles of repeat CSF samples from the same individual, taken at different time points, were compared for two different individuals with MS, labelled CIS-1 and NAT-1 (**Fig. 4.12A**). Samples from CIS-1 were taken 418 days apart, whereas samples from NAT-1 were taken 62 days apart. Very similar antigen reactivity profiles in terms of the magnitude of response and the identity of antigen targets were obtained for both samples; additionally, for each individual, comparison of MFI values from both samples revealed very strong correlations (**Fig. 4.12B**; CIS-1: $r = 0.933$, $p = <0.001$; NAT-1: $r = 0.925$, $p = <0.0001$).

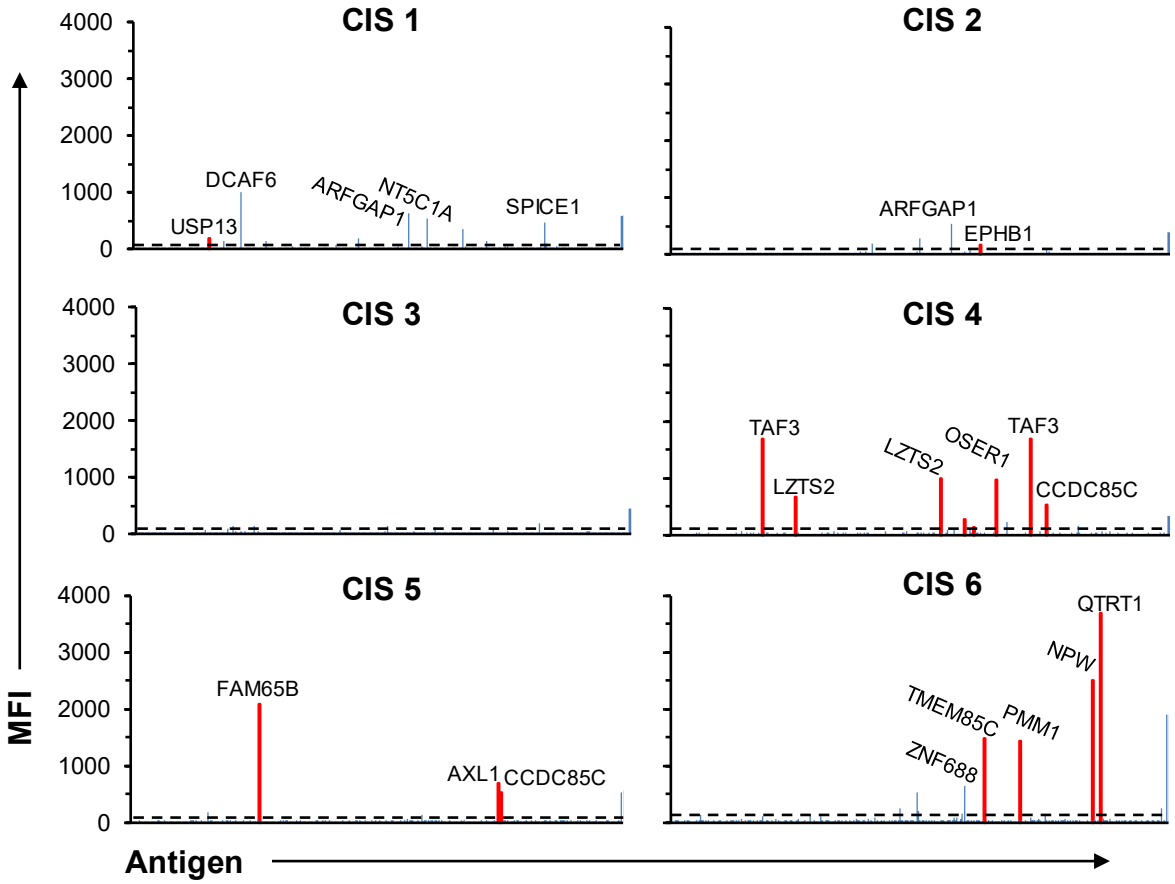

Figure 4.11 Consistent antigen reactivity profiles across both planar and bead-based array platforms. For 6 individuals with CIS, antigen reactivity of CSF was compared for planar arrays containing 21,120 antigens, and suspension bead arrays containing 301 antigens. Antigens identified as a positive hit on both arrays are shown in red. Dotted lines represent sample-specific cut-offs calculated as the median fluorescent intensity (MFI) plus 10x the median absolute deviation (MAD). The rabbit anti-human IgG control is shown at the end of each graph.

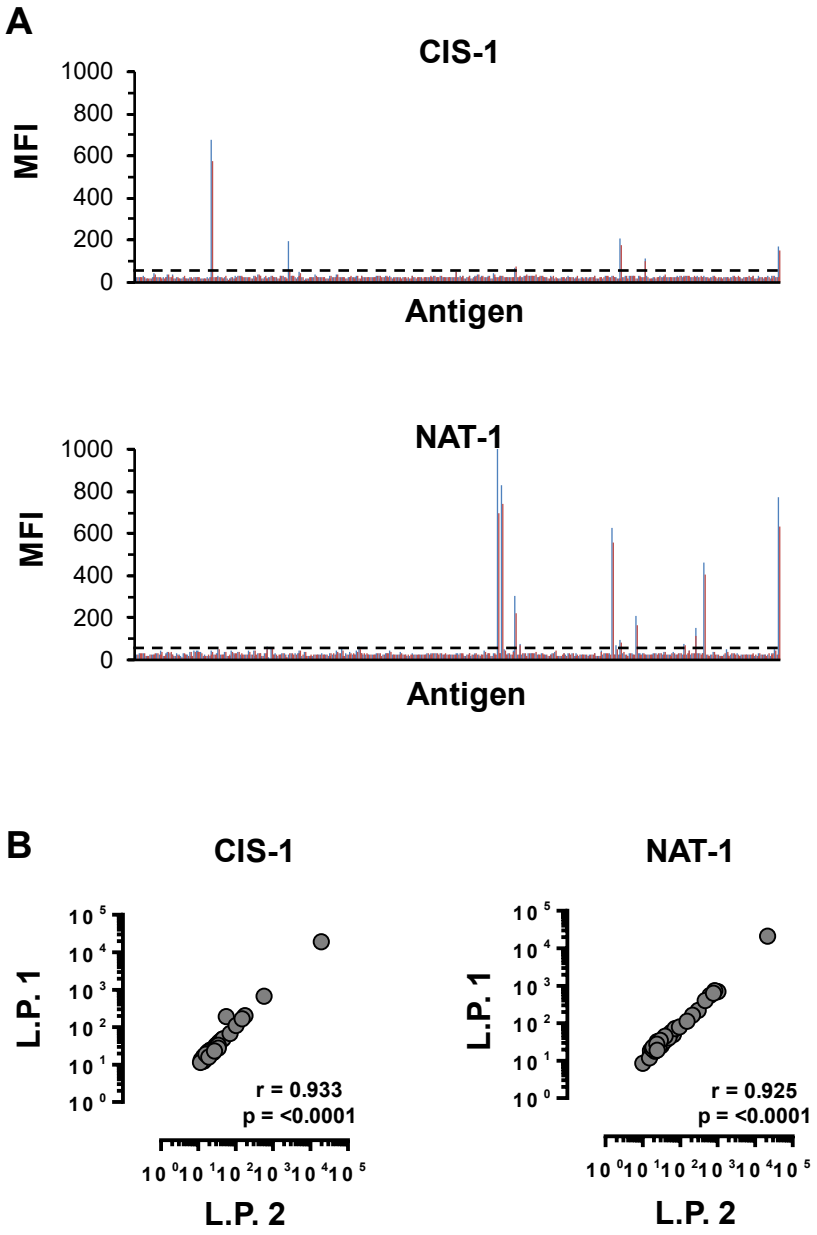

Figure 4.12 Antigen reactivity of CSF samples from the same individual using the suspension bead array. Reactivity of CSF from an individual with CIS (CIS-1) and an individual with MS treated with natalizumab (NAT-1) taken at different time points **(A)**. The second L.P. was taken at 418 days (CIS-1) or 62 days (NAT-1) following initial L.P. Blue represents the first L.P., orange represents the second L.P. Spearman correlation of antigen reactivity from CSF samples taken at the first (L.P. 1) and second (L.P. 2) time point **(B)**.

4.2.7 CSF reactivity using suspension bead arrays

As in the planar arrays, the number of positive hits identified by each CSF sample was compared with the total FLC concentration (**Fig. 4.13A**) and the Igκ:Igλ ratio (**Fig. 4.13B**). Both of these parameters showed that no association with antigen reactivity was detectable.

Data was grouped by disease classification to compare the number of positively recognised antigens for each sample; this analysis was performed for all three bead-based arrays which were carried out using different detection antibodies; anti-IgG (**Fig. 4.14A**), anti-Igκ (**Fig. 4.14B**) and anti-Igλ (**Fig. 4.14C**). No distinct differences were apparent between disease groups in the number of positive hits recognised, and in contrast to the planar arrays, differential reactivity between MS groups and control groups was not observed; however, grouping these data by disease group revealed a slightly higher number of positive hits in the CIS group compared to OND (anti-Igκ assay) (**Fig. 4.14C**).

4.2.8 Global CSF reactivity using suspension bead arrays

To identify the top reactive antigens using the suspension bead arrays, the total number of positive hits identified across all CSF samples was determined for each assay using anti-IgG (**Fig. 4.15A**), anti-Igκ (**Fig. 4.15B**) and anti-Igλ (**Fig. 4.15C**) detection antibodies. Findings revealed that similar antigens were recognised using all three detection antibodies, with top antigens including EBNA-1, coiled-coil domain containing 85C (CCDC85C), and zinc finger protein 688 (ZNF688). In addition, Igκ and Igλ antibodies showed differential reactivity towards certain antigens; for example, CCDC85C was identified by Igκ but not Igλ antibodies, whereas ARFGAP1 was identified by Igλ but not Igκ antibodies.

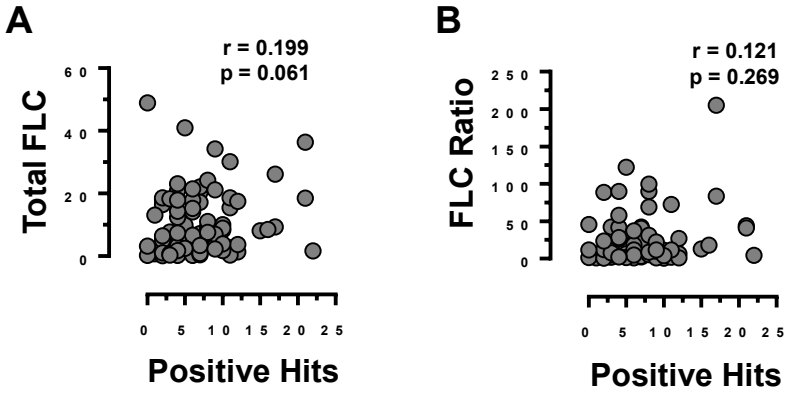

Figure 4.13 No correlation between FLC and reactivity parameters using the suspension bead array. Spearman correlation of the total FLC concentration (mg/L) **(A)** and the Igκ:Igλ FLC ratio **(B)** compared to the number of positive hits identified by each sample. The positive hits were determined using sample-specific cut-offs which were calculated by multiplying the MFI of each group + 10x median absolute deviation (MAD).
Controls were excluded from the analysis. Samples from MS groups only.

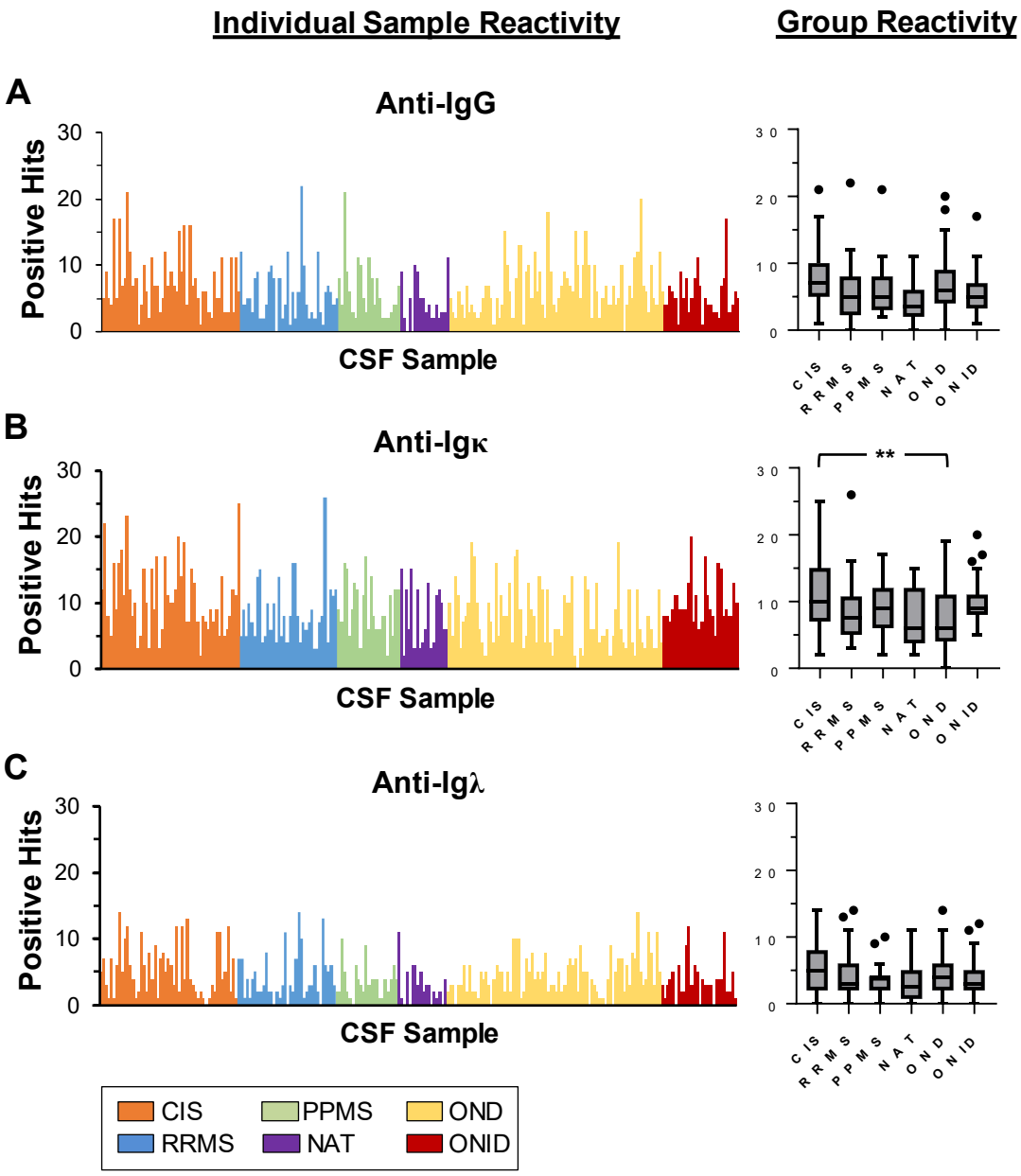

Figure 4.14 Individual and grouped sample reactivity for the suspension bead arrays. The number of positive hits per sample and per disease group were determined for the anti-IgG **(A)**, anti-Igκ **(B)** and anti-Igλ **(C)** suspension bead arrays. Tukey box and whisker plots showing median values. Comparisons were significant to ** (P=0.01) using Dunn's multiple comparisons test. CIS (n=51), RRMS (n=36), PPMS (n=23), NAT (n=18), OND (n=79) and ONID (n=28).

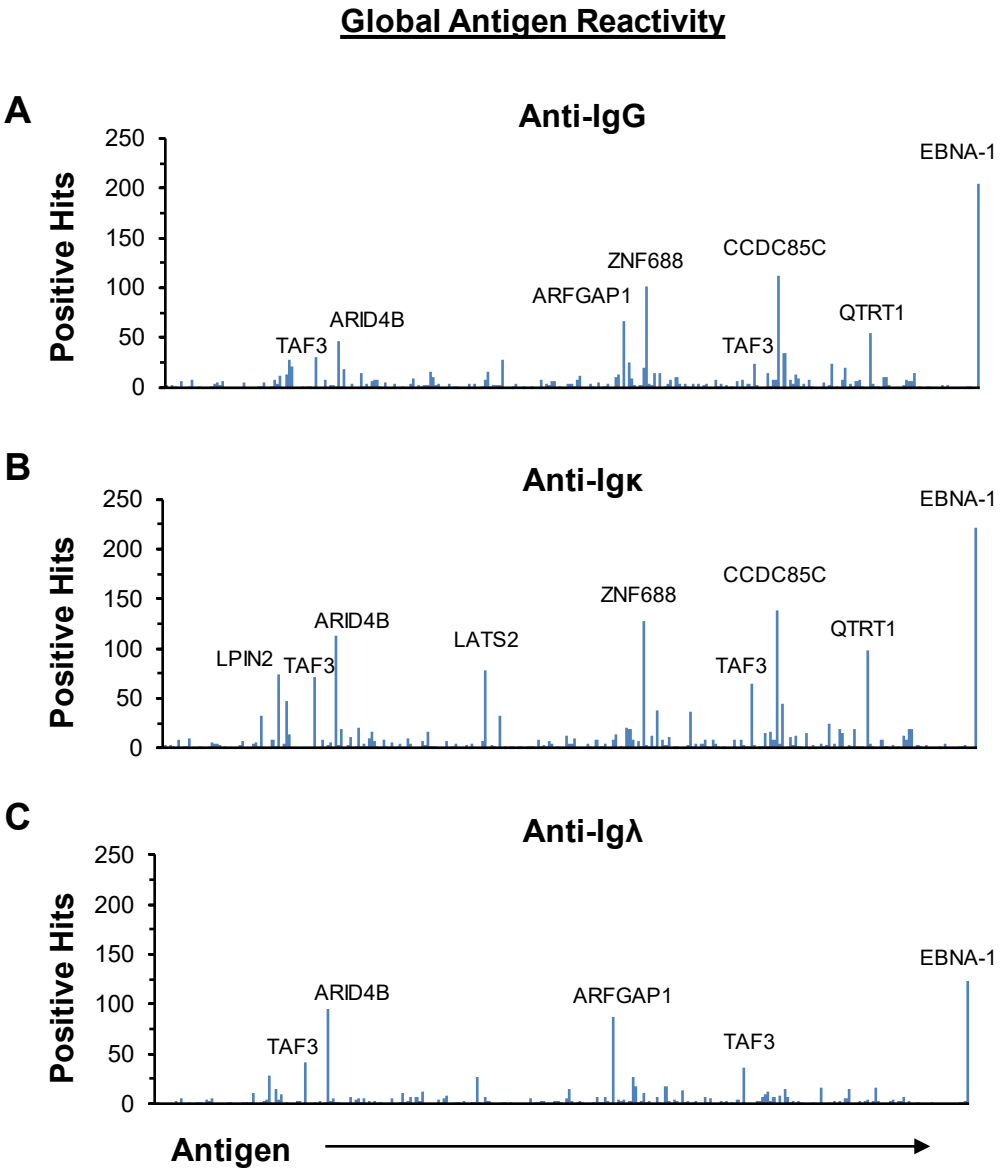

Figure 4.15 Global antigen reactivity of IgG, Igκ and Igλ using suspension bead arrays. Following the application of an arbitrary sample-specific cut-off value to define positive antigen reactivity, the number of positive hits per antigen for the anti-IgG **(A)**, anti-Igκ **(B)** and anti-Igλ **(C)** suspension bead arrays were determined.

4.2.9 Interrogation of candidate autoantigens

For the anti-IgG bead array, the top twenty hits were evaluated for the frequency they were recognised (**Fig. 4.16A**). EBNA-1 was identified by over 87% of all CSF samples, with the following most antigenic proteins being CCDC85C and ZNF688, which were recognised by almost 50% of CSF samples. For the top six most antigenic proteins, which were all deemed positive hits in at least 20% of samples, their antigen reactivity profiles for each disease group was determined (**Fig. 4.16B**). Only EBNA-1 was differentially recognised between groups, showing significantly higher reactivity in all MS groups, particularly CIS, compared to OND controls. In conjunction with the higher EBNA-1 reactivity in MS, a higher proportion of MS samples (94.4 – 97.2%) showed positive reactivity following application of sample-specific cut-offs compared to OND (74.7%) and ONID (82.1%) samples (**Fig. 4.16C**).

Antigen reactivity towards two major MS candidate autoantigens, MAG (**Fig. 4.17A**) and MBP (**Fig. 4.17B**), were also investigated. Three bead IDs were available for each of these, representing different parts of each protein. No significant reactivity was identified to any of these, although some individuals appeared to show some elevated antibody activity, particularly in the CIS group towards 91_MBP (**Fig. 4.17B**, lower middle graph).

A Anti-IgG - Top Hits

Bead ID/Antigen	Hits	%
304_EBNA-1	205	87.2
227_CCDC85C	112	47.6
178_ZNF688	101	42.9
170_ARFGAP1	67	28.5
262_QTRT1	55	23.4
65_ARID4B	47	20.0
230_KIF15	35	14.9
57_TAF3	30	12.7
125_UBE3A	28	11.9
47_TNNT2	27	11.5
172_KRTAP17-1	25	10.6
218_TAF3	24	10.2
248_BCL10	23	9.7
48_USP13	21	8.9
177_SEC63	19	8.1
253_ANO2	19	8.1
67_DCAF6	18	7.6
99_CUEDC2	15	6.4
120_LATS2	15	6.4
73_TACR1	14	5.9

C EBNA-1 Reactivity

Group	Hits	%
CIS	48	94.1
RRMS	35	97.2
PPMS	22	95.7
NAT	17	94.4
OND	59	74.7
ONID	23	82.1

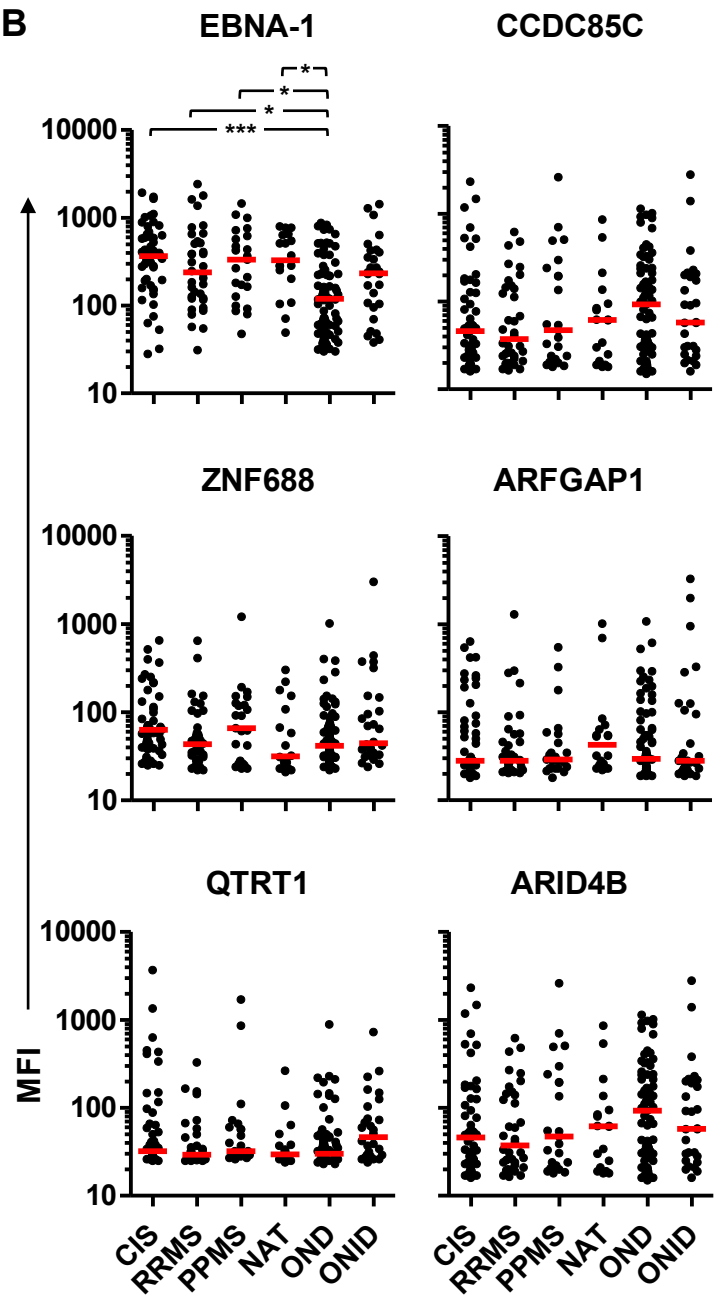

Figure 4.16 Top reactive antigens using anti-IgG in the suspension bead array. Top 20 reactive antigens recognised by CSF IgG in all disease groups **(A)**. Antigens are listed alongside their corresponding bead identification number, the frequency of hits and the percentage of CSF samples identifying the antigen as a positive hit. Comparison of antigen reactivity between groups for the 6 highest reactive antigens **(B)**. Comparisons were significant to *** ($P<0.05$) and * ($P<0.01$) using Dunn's multiple comparisons test. Reactivity towards EBNA-1 was quantified and expressed as a percentage of reactivity for each disease group **(C)**.

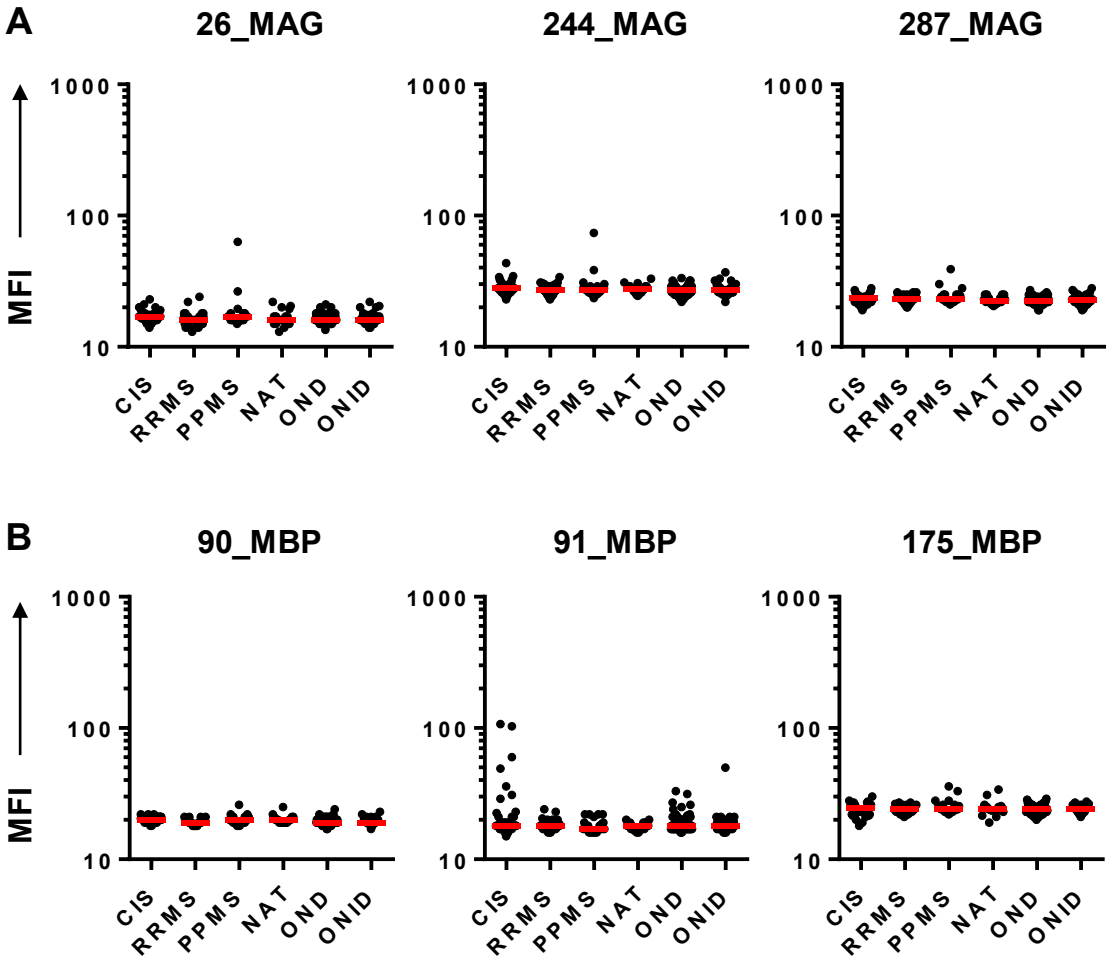

Figure 4.17 Absence of CSF IgG reactivity towards MAG and MBP proteins. Using the suspension bead array, no significant reactivity of CSF IgG was observed in response to three MAG proteins **(A)** or three MBP proteins **(B)** in any of the disease groups. Comparisons were not significant using Dunn's multiple comparisons test.

4.2.10 Differential light chain binding to antigens

A question during this project was the antigen specificity of Igκ and Igλ light chains. Using the suspension bead array, reactivity of Igκ- and Igλ-expressing CSF antibodies was assessed and converted to an Igκ:Igλ ratio to identify whether a kappa bias could have been induced by any of these antigens (**Fig. 4.18**). Several antigens appeared to elicit such responses; notably EBNA-1, CCDC85C, ZNF688 and queuine tRNA-ribosyltransferase 1 (QTRT1). For each disease group, the Igκ:Igλ ratio was compared for each of these antigens (**Fig. 4.19A**). EBNA-1 elicited the strongest Igκ bias, with the following median values: CIS (9.8:1), RRMS (7.6:1), PPMS (8.24:1), NAT (9.8:1), OND (5.8:1), ONID (5.4:1). Although the ratio was higher in MS groups than controls, this was not statistically significant. The relationship between the kappa and lambda light chain response was confirmed by correlation analysis, demonstrating that despite the higher kappa light chain reactivity towards these antigens, lambda light chain reactivity generally increases with kappa (**Fig. 4.19B**).

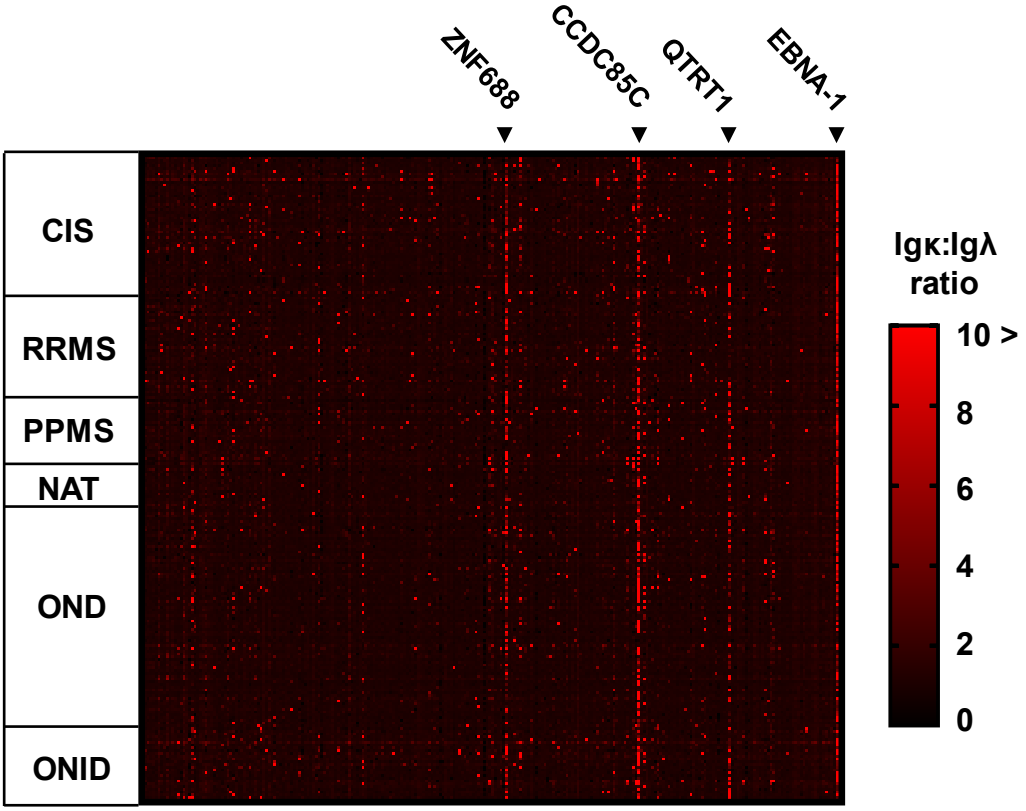

Figure 4.18 Some antigens induce a kappa-biased antibody response. The Igκ:Igλ ratio, calculated from the MFI for both Igκ and Igλ,was determined in response to each antigen and compared across disease groups. Igκ:Igλ ratios of 10:1 or above are in red.

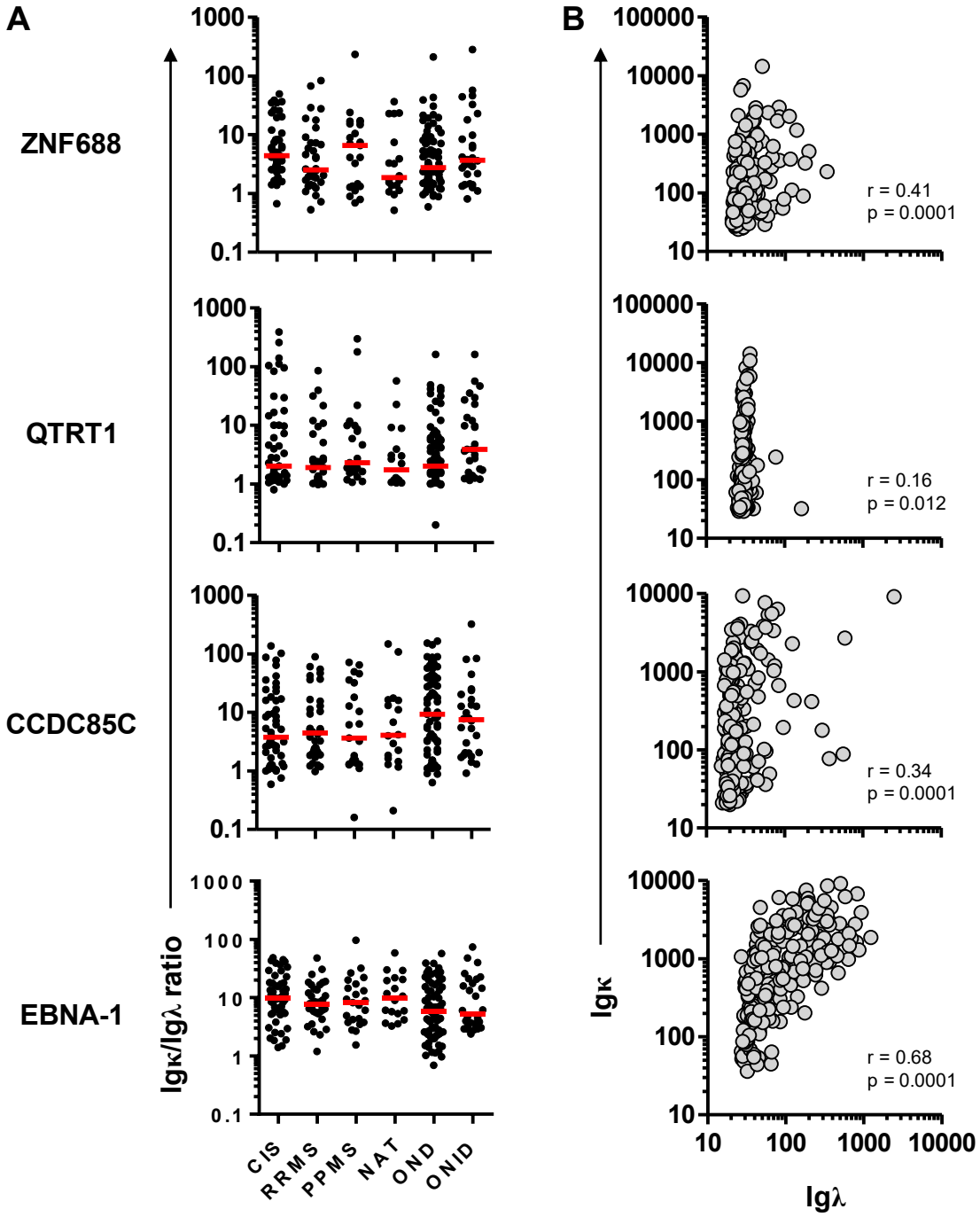

Figure 4.19 Comparison of antigens between disease groups that induce a biased kappa light chain response. The ratio of Igκ MFI to Igλ MFI in disease groups towards the top four antigens demonstrating a biased kappa light chain response **(A)**. Group comparisons were not significant using Dunn's multiple comparisons test. Relationship of Igκ and Igλ reactivity for ZNF688, QTRT1, CCDC85C and EBNA-1 **(B)**.

4.3 Discussion

4.3.1 A broad CSF antibody repertoire is an early feature of disease

For the initial part of this chapter where 21k planar arrays were used, CSF samples were selected based on their diagnostic categorisation (CIS vs RRMS) and their CSF FLC Igκ:Igλ ratio to investigate potential spreading of the humoral response throughout the disease. As in chapter 3, a diagnosis of CIS was used to represent 'early' MS, as by definition, CIS is characterised by one clinical relapse at the time of diagnosis. Selecting CIS samples with a high FLC Igκ:Igλ ratio was intended to identify individuals with restricted antibody specificity to a limited number of antigens (due to the high Igκ bias) and are therefore assumed to be at the earliest stages of the disease process. This was compared with RRMS samples with a low FLC Igκ:Igλ ratio, as by definition, RRMS represents individuals who have experienced more than one clinical relapse at diagnosis, and a less biased FLC Igκ:Igλ ratio potentially indicates broader spreading of the antibody response in MS (Fig. 3.14).

Despite the selection bias of CSF samples used for the planar arrays, a key finding was the highly heterogeneous antibody responses between individuals. This was true using both planar (Fig. 4.1 – Fig. 4.4) and bead-based (Fig. 4.14 – Fig. 4.19) arrays, and was observed within and between disease groups. This is in line with findings from other studies using antigen arrays, and is clearly a fundamental feature of MS, demonstrating the complexity of the intrathecal antibody repertoire in this disease, even during apparently early stages (Haggmark et al., 2013; Quintana et al., 2014; Hecker et al., 2016; Ayoglu et al., 2016).

An initial screen of six CIS samples using 21k planar arrays identified specificities that were highly unique to each individual (Fig. 4.1); this phenomenon was also observed using 384 planar arrays (Fig. 4.3). Most CIS samples displayed reactivity towards multiple antigens,

although some CIS samples failed to respond to any antigens (Fig. 4.1A); this is an interesting observation, as differential CSF antibody responses could potentially allow disease outcomes to be distinguished. Reactivity towards multiple antigens was also observed in pooled and individual RRMS CSF (Fig. 4.1B, Fig. 4.3B); in contrast, pooled OND CSF effectively showed no reactivity on 21k planar arrays (Fig. 4.1B), and individual OND samples on 384 arrays also showed little reactivity (Fig. 4.3C), demonstrating the relative absence of high affinity antibodies under normal physiological conditions, despite the presence of antibodies in the sample, as demonstrated by a positive signal for the rabbit anti-human IgG control (Fig. 4.1B).

4.3.2 Identification of common antigens using planar arrays

The identification of common target antigens between individuals may suggest common destructive processes mediated by the humoral response in MS. Despite the large variation between samples, quantification of the positive hits between groups following application of sample-specific cut-offs revealed several antigens common to more than one sample for both 21k (Fig. 4.2B) and 384 (Fig. 4.4D) planar arrays. Of interest, reactivity towards 5'-nucleotidase, cytosolic 1A (NT5C1A), identified as a positive hit on 21k planar arrays, has been observed previously (Fig. 4.2B); circulating autoantibodies to NT5C1A have been identified in 21% of MS cases (Lloyd 2016). However, its common association with other inflammatory or autoimmune conditions such as inclusion body myositis, systemic lupus erythematosus and Sjögren's syndrome suggests this reactivity is a consequence of general inflammation, rather than a disease-specific phenomenon (Lloyd et al., 2016; Tawara et al., 2017). Reactivity towards CCDC85C (Fig. 4.2B) in MS has also been observed previously. In a screen of SPMS plasma, 2 of 8 samples showed CCDC85C reactivity using the same planar

array platform as in this chapter (Sjoberg et al., 2016). CCDC85C is highly expressed in the cerebellum and is thought to play an important role in cortical development, therefore it is a potentially interesting neurological target (Mori et al., 2012; Uhlen et al., 2015).

Common antigens were also identified using 384 planar arrays, where six CSF samples were included per disease group (Fig. 4.4D). Zinc finger protein 488 (ZNF488) is an oligodendrocyte-specific transcriptional regulator important for the maturation of oligodendrocytes, and its depletion leads to myelin gene downregulation and subsequent impairment of myelination (Wang et al., 2006). Other common targets included mitochondrial proteins, such as IFI27, PGAM5 and Acyl-CoA dehydrogenase family member 9, mitochondrial (ACAD9), and proteins involved in apoptosis, such as IFI27 and BCL10. Of note, increased PGAM5 activity was previously observed in MS serum compared to OND controls (Ayoglu et al., 2013; Ayoglu et al., 2016). The presence of autoantibodies against such proteins is suggestive of their increased abundance; many of these proteins are not normally accessible to antibodies as they are located intracellularly, but accumulation of dead cells following tissue damage and inflammation may lead to their release.

4.3.3 Identification of several antigens with potential relevance to MS pathology

In addition to identifying several common antigens using planar arrays, several CNS-associated proteins were identified (Fig. 4.2C). The nature of these targets may provide clues as to the pathological processes underpinning antibody-mediated damage in MS. Neuropeptide W (NPW) is a brain-associated antigen that is highly expressed throughout the CNS and is thought to play a role in energy homeostasis; its depletion may contribute to

dysregulation and energy failure, and is a potential mechanism of axonal injury (Takenoya et al., 2012; Haider, 2015). In this chapter, reactivity was also observed towards FBJ murine osteosarcoma viral oncogene homolog B (FOSB) in pooled RRMS CSF. FOSB is a proto-oncogene which has previously been identified as part of an autoimmunity signature due to its involvement in regulating the matrix metalloproteinase (MMP) pathway by activating tissue inhibitor of metalloproteinase-1 (TIMP-1); its dysregulation contributes to enhanced lymphocyte trafficking through the BBB and promotes tissue destruction in the CNS (Botelho et al., 1998; Mandel et al., 2004; Mirshafiey and Kianiaslani, 2013). Increased reactivity was also observed towards phosphomannomutase-1 (PMM1); this glycosylation factor is upregulated in the MS brain, particularly in acute lesions compared to chronic active lesions, therefore its over-abundance may lend itself to becoming an autoimmune target (Tajouri et al., 2003). Another interesting target was syntaphilin, released as a stress-response to prohibit mitochondria transport and provide a stable source of adenosine triphosphate (ATP) for neurons; accordingly, syntaphilin is increased in MS brains, therefore, autoantibody-mediated depletion of this molecule may contribute to loss of compensatory mechanisms employed to preserve CNS function in MS (van den Berg et al., 2017; Mahad et al., 2009). Finally, reactivity towards the chloride channel ANO2 was observed on both planar and suspension bead arrays (Fig. 4.2C, Fig. 4.16A). A study analysing the reactivity of 2,169 plasma samples to 11,520 antigens demonstrated differential reactivity in MS towards ANO2, which was also associated with HLA-DRB1*15, and was present in MS brain tissue (Ayoglu et al., 2016). Its localisation on the cell membrane makes it freely accessible for autoimmune attack and its fundamental role in olfactory transduction may underpin the high frequency of olfactory dysfunction in MS, in which 70% of post-mortem olfactory bulbs show evidence of demyelination (Stephan et al., 2009; Pifferi et al., 2012; DeLuca et al., 2015). Consistent with

this, various olfactory family members, including OR10AG1 and OR1L3, were also identified as MS-associated autoimmune targets during the planar array screen, suggesting autoantibody-mediated damage as a contributor to olfactory dysfunction (Fig. 4.1A, Fig. 4.2C).

4.3.4 Strong reactivity of EBNA-1 using the suspension bead arrays

Following on from the broad exploration using planar arrays, suspension bead arrays were employed to interrogate candidate autoantigens in MS, which were selected based on findings from the planar arrays in addition to a literature search (see Appendices IV and V). CSF reactivity of six CIS samples on both 21k planar arrays (Fig. 4.1) and the anti-human IgG suspension bead array (Fig. 4.11) identified comparable positive hits across both technologies, confirming the reproducibility of the suspension bead arrays. Additionally, the recognition of almost identical antigens by repeat CSF samples from two individuals using the suspension bead array confirmed this technical reproducibility (Fig. 4.12). These findings also offer an insight into the kinetics of the humoral response in MS, which are particularly striking considering the long duration between LPs (62 days and 418 days respectively); this not only indicates a level of stability in the antigens recognised over time, but also suggests very slow evolution of the humoral response in at least some individuals (Fig. 4.12). Considering that a broad antibody response is already established at the time of CIS, it therefore appears likely that at this stage, the humoral response has already been in progress for many years before the onset of clinical symptoms.

Comparison of the number of positive hits identified across individual samples using the suspension bead arrays showed a high level of variation, regardless of the disease group, and

appeared to show little distinction between disease groups (Fig. 4.14A). When these samples were grouped according to their disease categorisation, significantly increased reactivity was observed in CIS compared to OND using the anti-Igκ detection antibody, but apart from this, little difference was observed overall (Fig. 4.14B). This contrasts with the planar arrays, which showed a clear distinction between disease groups, and suggests a limitation of the bead array technology. It is possible that the bead arrays were subjected to higher levels of non-specific antibody binding due to their overnight incubation with CSF, compared to the 2-hour incubation using planar arrays. It may also have been the case that most of the 301 antigens used in the suspension bead arrays did not allow enough distinction between MS and control groups, whereas the higher number of antigens used in the planar arrays allowed greater differences to be observed. Although steps were performed to optimise the assay (Fig. 4.6 – 4.8) and to eliminate bead IDs with low counts (Fig. 4.9, Fig. 4.10), time limitations prevented further exploration of this issue.

Despite the apparent lack of differential reactivity between MS and control groups using the suspension bead arrays, identifying the top reactive antigens allowed for their more detailed investigation as potential autoantigens. Almost every positive hit identified by CSF IgG was also identified by Igκ and Igλ antibodies, since targets identified by IgG (Fig. 4.15A) were also collectively identified by Igκ and Igλ antibodies (Fig. 4.15B, C). This suggests that most CSF antibodies are IgG, as the Igκ and Igλ antibodies would also represent targets identified by other heavy chain specificities. For the top reactive antigens recognised using suspension bead arrays, some were also identified as potential autoantigens using the planar arrays, such as CCDC85C and QTRT1, and interestingly, some antigens were preferentially recognised by Igκ, whereas others were preferentially recognised by Igλ (Fig. 4.15). Although the presence of a broad antibody repertoire is clear, the strongly Igκ-biased repertoire in MS CSF suggests

that one or more of the antigens preferentially recognised by Igκ may be specific MS autoantigens.

EBV is the strongest infectious agent linked to MS pathogenesis. Anti-EBNA-1 antibodies are elevated in MS serum and CSF compared to controls, and increased EBNA-1 reactivity of MS antibodies has been widely demonstrated in other antigen array studies (Santiago et al., 2010; Nociti et al., 2010; Lindsey et al., 2010; Hecker et al., 2016; Ayoglu et al., 2016). In this chapter, EBNA-1 was by far the most frequently identified of the 301 candidate autoantigens analysed using the suspension bead arrays; this was true using the anti-IgG detection antibody (Fig. 4.16) and the anti-Igκ and anti-Igλ antibodies (data not shown). This has also been shown by other antigen array studies, such as by Hecker et al, who identified EBNA-1 as the strongest candidate autoantigen using arrays hosting 3,991 peptides; importantly, these peptides were not synthesised by the HPA, demonstrating reproducible findings with different technologies (Hecker et al., 2016; Ayoglu et al., 2016).

CSF IgG from all MS groups was significantly higher than the OND group, however, the lack of a significant difference over ONID controls indicates a degree of elevated EBNA-1 reactivity during inflammation. This may be due to the exaggerated inflammatory activity in the CNS; a significant proportion (up to 2%) of the peripheral lymphocyte pool is specific for EBV, and broad antibody repertoires are a common feature of inflammatory neurological conditions, where around 80% of intrathecal antibody is not specific for the causative agent (Bonnan, 2014; Hatton et al., 2014). Nevertheless, the frequency of EBNA-1 positive CSF samples was clearly increased in all MS groups compared to ONID, and even more so, OND (Fig. 4.16C).

The distinctions between MS and controls are not dramatic because EBV seropositivity in the general population is 80-95%, but is thought to be present in over 99%, if not 100%, of those with MS (Pakpoor et al., 2013; Burnard et al., 2017). This increased EBV prevalence of around 20% in MS compared to controls is comparable to findings from this chapter, albeit with a slightly lower sensitivity using the arrays, since the average frequency in all MS groups was 95.4% compared to 74.7% in the OND group (Fig. 4.16C). These comparable frequencies to those in the literature demonstrates the reliability of these arrays and, importantly, implicate the involvement of EBV in MS. Unfortunately, however, these findings do not confirm that the elevated anti-EBNA-1 antibodies in MS are CSF-derived; as serum titres to EBNA-1 are elevated in MS, the lack of matched serum samples in this chapter means that the source of this elevated CSF reactivity cannot be confirmed. It therefore cannot be ruled out that the elevated anti-EBNA-1 antibody titre in the CSF is serum-derived, particularly under inflammatory conditions when the BBB may be compromised.

4.3.5 The Igκ bias in relation to antibody reactivity

A key question of this thesis was whether the Igκ:Igλ FLC ratio has relevance to MS pathogenesis. In this study it was postulated that the level of bias could reflect the extent of oligoclonality, with a low bias reflecting a broader range of antigen specificities, indicative of disease progression, and a high bias reflecting a restricted antibody response. Despite the large variations between individuals within each disease classification, comparable levels of antibody reactivity were observed in both CIS and RRMS using planar arrays (Fig. 4.2A, Fig. 4.4A). The similar antigen reactivity between Igκ-biased CIS CSF and unbiased RRMS CSF suggests that at diagnosis, the humoral response is well-developed and features multiple

antigen targets recognised by antibodies bearing both Igκ and Igλ. The similar level of reactivity between CIS and RRMS on 21k planar arrays was confirmed by demonstrating a significant correlation between antigen reactivity and CSF FLC concentration (Fig. 4.4B), and therefore antibody concentration; this confirms that increased antibody synthesis, for example during inflammation, leads to more diverse antigen recognition by CSF antibodies. As CSF FLC are prognostic indicators of disease severity, with increased levels predicting CIS conversion to MS and correlating with disability accumulation, its association with the number of antigen targets recognised by MS CSF suggests that the latter is also pathologically relevant (Makshakov et al., 2015). The relationship between total FLC and positive hits was not reproduced using suspension bead arrays (Fig. 4.13A), which was likely due to technical issues causing a lack of distinction between MS and control samples, as discussed.

In addition to the clear relationship between FLC concentration and antibody reactivity, these arrays appeared to demonstrate some relationship between the number of hits and the FLC ratio (Fig. 4.4C). This is in contrast to what was expected, since increased antigen reactivity has been shown to relate to disease progression, and it would be hypothesised that CSF with a high Igκ:Igλ ratio would have fewer antibody specificities as this is related to a less severe disease course (Quintana et al., 2014; Rathbone et al., 2018). However, the comparison between the Igκ:Igλ FLC ratio and antibody reactivity may have been obscured by the misrepresentation of total antibody reactivity on the arrays; i.e. it is unlikely that every single antibody reactivity in the CSF will be represented on these arrays, so any differential antibody reactivity may not be accurately represented. Additionally, the analysis was performed on small sample sizes and may have been skewed by one CSF sample with a particularly high Igκ ratio, since removal of this sample causes loss of significance. As this question has never

before been investigated, further work is required to elucidate the antigen reactivities of CSF samples with high and low ratios.

In addition to MS, biased light chain usage is a feature of several autoimmune conditions including Hashimoto thyroiditis, Sjögren's disease and rheumatoid arthritis, implicating an Igκ or Igλ preference in autoantibody formation (Chen et al., 2006; Nakayama et al., 2012; Gottenberg et al., 2007; Barnridge et al., 2014). In this chapter, several antigens were identified that preferentially induce an Igκ-biased antibody response (Fig. 4.18, 4.19). This analysis was performed by calculating the ratio between the Igκ MFI and Igλ MFI for each antigen. For the top antigens inducing an Igκ-biased response, increasing levels of kappa-bearing antibodies was generally associated with a proportional increase in lambda-bearing antibodies, suggesting that the kappa bias towards these antigens could represent a biological phenomenon rather than pathological monoclonal expansion (Fig. 4.19B). The strongest bias identified was towards EBNA-1 at a median ratio of 8.5:1 in all MS groups; however, the kappa bias towards EBNA-1, and several other antigens, was also observed in controls (Fig. 4.18, Fig. 4.19). Although the peripheral blood Igκ:Igλ ratio is approximately 1.6:1 in favour of Igκ, light chain bias in healthy donors has been observed towards certain antigens, particularly small antigens with limited epitopes (Perez-Andres et al., 2010; Smith et al., 2016). Indeed, this has been shown to be the case for EBNA-1 reactivity in the serum of healthy donors, which has a median ratio of 7.6:1 (Smith et al., 2016). This bias is considered to be caused by reactivity towards a highly antigenic part of the protein which carries a glycine-alanine repeat domain (Rumpold et al., 1987). Despite the significant hindrance of antibody diffusion into the brain, at least in part due to the widespread distribution of high affinity neonatal Fc receptors (FcRn), normal CSF contains a very low but detectable concentration of passively transferred serum-derived antibodies under physiological

conditions (Okun et al., 2010; Wolak et al., 2015; Diamond et al., 2013). This is also supported by the scarcity of CSF B cells and ASC in OND CSF, as identified by ourselves and others, which is indicative of these antibodies being peripherally derived (Cepok et al., 2005a; Kuenz et al., 2008). Therefore, the kappa bias towards certain antigens in OND is likely a physiological phenomenon which would have been observed in the serum; this is in conjunction with the overall CSF FLC Igκ:Igλ ratio in OND controls being closely related to the serum FLC ratio (Perez-Andres et al., 2010). In conclusion, the widely reported Igκ FLC bias in MS CSF is likely a consequence of B cell activation and expansion towards an antigen with limited epitopes, and it remains possible that one or several kappa bias-inducing antigen(s) identified in this chapter is responsible for the increased Igκ FLC in MS CSF (Fig. 4.19).

4.3.6 Technical considerations

Despite the identification of several antigens with potential relevance to MS pathogenesis, this study, and many others, have failed to identify a single unifying autoantigen linked to MS. Even if such antigen does not exist, discrepancies in the literature regarding other antigens, notably the classic MS autoantigens of the myelin sheath, are widespread. Data in this chapter did not identify any significant differential reactivity towards MBP or MAG proteins in MS, despite the elevated reactivity in some samples (Fig. 4.17). Other microarray studies have shown contrasting evidence for antibody reactivity towards myelin proteins; notably, while Ayoglu et al (2013) did not observe preferential binding by MS antibodies, Hecker et al (2013) observed significantly elevated reactivity in MS compared to OND (Hecker et al., 2016; Ayoglu et al., 2013). Inconsistencies throughout published literature may be partly due

to the source and format of the antigens used. Antigens produced in bacterial expression systems, such as *E. coli* as in this study, are not subjected to the same range and complexity of post-translational modifications as in eukaryotic cells and their structure may not be sufficiently representative of the native form to allow autoantibody binding. Additionally, protein modification may occur spontaneously or in response to environmental triggers, such as inflammation, and may alter various aspects of protein structure and function which may subsequently alter protein antigenicity (Doyle and Mamula, 2012). For example, MBP ordinarily contains several post-translational modifications, and aberrant post-translational modifications in MBP from MS brains has been identified; in addition, studies have demonstrated that MOG reactivity is conformation dependent, requiring correct folding for antibody binding (Kim et al., 2003; Harauz et al., 2009; Zhang et al., 2012; O'Connor et al., 2007; Menge et al., 2011). As such, autoantibodies towards modified antigens may not be identified using this approach.

In addition to these considerations, protein length may also affect the outcome of these assays. Different antibody reactivity to full-length proteins and protein fragments was observed in a study using the same antigens and planar array platform as in this chapter (Sjoberg et al., 2016). The antigens used this chapter were 25-150 amino acids long (average length of 80) and thus do not necessarily represent the full length native protein. Therefore, protein folding may be altered, and normally exposed epitopes may be hidden, or normally hidden epitopes may be exposed. Conformational epitopes, comprising discontinuous amino acid sequences brought together by protein folding, make up most epitopes recognised by antibodies and could also be disrupted, which could potentially abrogate antibody binding (Barlow et al., 1986; Sivalingam and Shepherd, 2012). Therefore, many technical aspects must be considered in the interpretation of array data.

4.4 Chapter Summary

This chapter confirmed that the intrathecal antibody response in MS is highly variable within and between disease subtypes. Whether the antibody response in early MS is more restricted than in those with established disease still remains to be elucidated, since there was no apparent difference in antibody reactivity between CSF with a high Igκ:Igλ ratio and a low Igκ:Igλ ratio. However, this relies on the assumption that all CSF antibody reactivities are represented on these arrays, which may not be the case considering the technical limitations of this technology, and requires further investigation.

Importantly, this chapter identified several common candidate autoantigens in MS, and also identified several antigens of potential relevance to MS pathology. The strongest antigen recognised was EBNA-1, which in combination with its elevated frequency in MS compared to control groups, and its preference for inducing Igκ-bearing antibodies, could mean it is at least partly responsible for inducing the FLC Igκ:Igλ bias in MS CSF.

CHAPTER 5

INVESTIGATION OF THE PHENOTYPE AND FUNCTION OF CD20+ T CELLS IN MULTIPLE SCLEROSIS AND CONTROLS

Chapter 5: Investigation of the phenotype and function of CD20+ T cells in multiple sclerosis and controls

5.1. Introduction

CD20 is a highly conserved cell-surface phosphoprotein identified in 1980 as one of the first human B cell markers (Stashenko et al., 1980; Tedder and Engel, 1994). CD20 belongs to the membrane-spanning 4 domains, subfamily A (MS4A) family of molecules and contains four transmembrane regions which form multimeric complexes on the cell surface (Tedder and Engel, 1994; Liang et al., 2001). This molecule is expressed at high levels by over 95% of B cells, and is present from the pre-B cell stage up until their terminal differentiation into ASC (Klein et al., 2013). The widespread expression of CD20 has led to its use as a highly effective therapeutic target in MS, with a single course of rituximab inducing rapid and complete depletion of peripheral CD20+ B cells, leading to a significant reduction in relapses and brain lesions (Hauser et al., 2008). Rituximab mediates a significant reduction (90%) in CSF B cells, though intriguingly, there is also a marked reduction (55%) in CSF T cells (Cross et al., 2006). Moreover, in EAE, a largely T cell-mediated disease, rituximab administration ameliorates disease in transgenic mice expressing human CD20 (Monson et al., 2011).

The identification of T cells expressing CD20, and the findings that these cells are skewed towards a pro-inflammatory memory phenotype, has led to their investigation as a possible pathogenic subset in several diseases (Hultin et al., 1993; Wilk et al., 2009, Palanichamy et al., 2014b; de Bruyn et al., 2015; Alunno et al., 2016). The depletion of these cells by rituximab in rheumatoid arthritis and MS, followed by improved clinical features, implies a

possible link with disease (Wilk et al., 2009; Palanichamy et al., 2014b; Alunno et al., 2016). Reports on the frequency of these cells in the blood of those with MS are contradictory, with one study reporting elevated frequencies in MS, and others reporting similar frequencies to OND controls (Palanichamy et al., 2014b; Holley et al., 2014; Schuh et al., 2016). In addition, Th17-like characteristics of CD20+ T cells have been reported by some (Eggleton et al., 2011; Holley et al., 2014) but not others (Wilk et al., 2009; de Bruyn et al., 2015).

The question of how CD20+ T cells acquire CD20 has been investigated previously, with conflicting results. Data exists for the expression of CD20 mRNA by these cells, however another study suggested that CD20 is acquired through trogocytosis; the transfer of cell membrane fragments, including surface molecules, to other cells following interaction (Wilk et al., 2009; Palanichamy et al., 2014b; Schuh et al. 2016; de Bruyn et al., 2015). Therefore, further investigation into this elusive subset is required to further understand their biology and potential role in disease.

Based on the hypothesis that CD20+ T cells are a pro-inflammatory population which are present in MS CSF, I sought to first investigate the phenotype and frequency of CD20+ T cells in MS and control groups in both the peripheral blood and CSF. The functional aspects of CD20+ T cell biology were investigated to ascertain any possible functions in disease pathogenesis by culturing purified CD20+ and CD20- T cells from healthy subjects.

5.1.1. Chapter Objectives

1. Confirm the phenotype of CD20+ T cells in the blood of healthy donors
2. Investigate the frequency of CD20+ T cells in CSF and blood from MS and OND groups and determine their phenotype using a selection of markers

3. Investigate the proliferation and survival of sorted CD20+ T cells from healthy subjects *in vitro*

4. Determine expression of selected surface and intracellular markers

5. Determine whether CD20+ T cells possess cytotoxic function

6. Investigate the antigen specificity of CD20+ T cells using tetramers containing common viral peptides

5.2 Results

5.2.1 Identification of CD20+ T cells in the peripheral blood

A gating strategy was established to identify CD20+ T cells within T cell subsets. Because of interference with compensation, which can cause problems particularly when identifying rare cells, a CD4+ antibody was omitted from the panel and CD8- T cells were gated on as an equivalent subset. Although this was not necessarily ideal, it was preferable to prioritise the identification of CD20+ T cells. After gating on CD3+ viable lymphocytes, and CD8+ or CD8- T cells, CD45RA and CCR7 antibodies were used to gate naïve (CCR7+CD45RA+), central memory (CM; CCR7+CD45RA-) and effector memory (EM; CCR7-CD45RA-) subsets for the CD8- fraction, and naïve, CM, EM and revertant effector memory (EMRA; CCR7-CD45RA+) for the CD8+ fraction (**Fig. 5.1A**). Although CD4+ EMRA cells do exist, their frequencies were far too low to reliably identify CD20+ T cells from this subset (Moro-Garcia 2013).

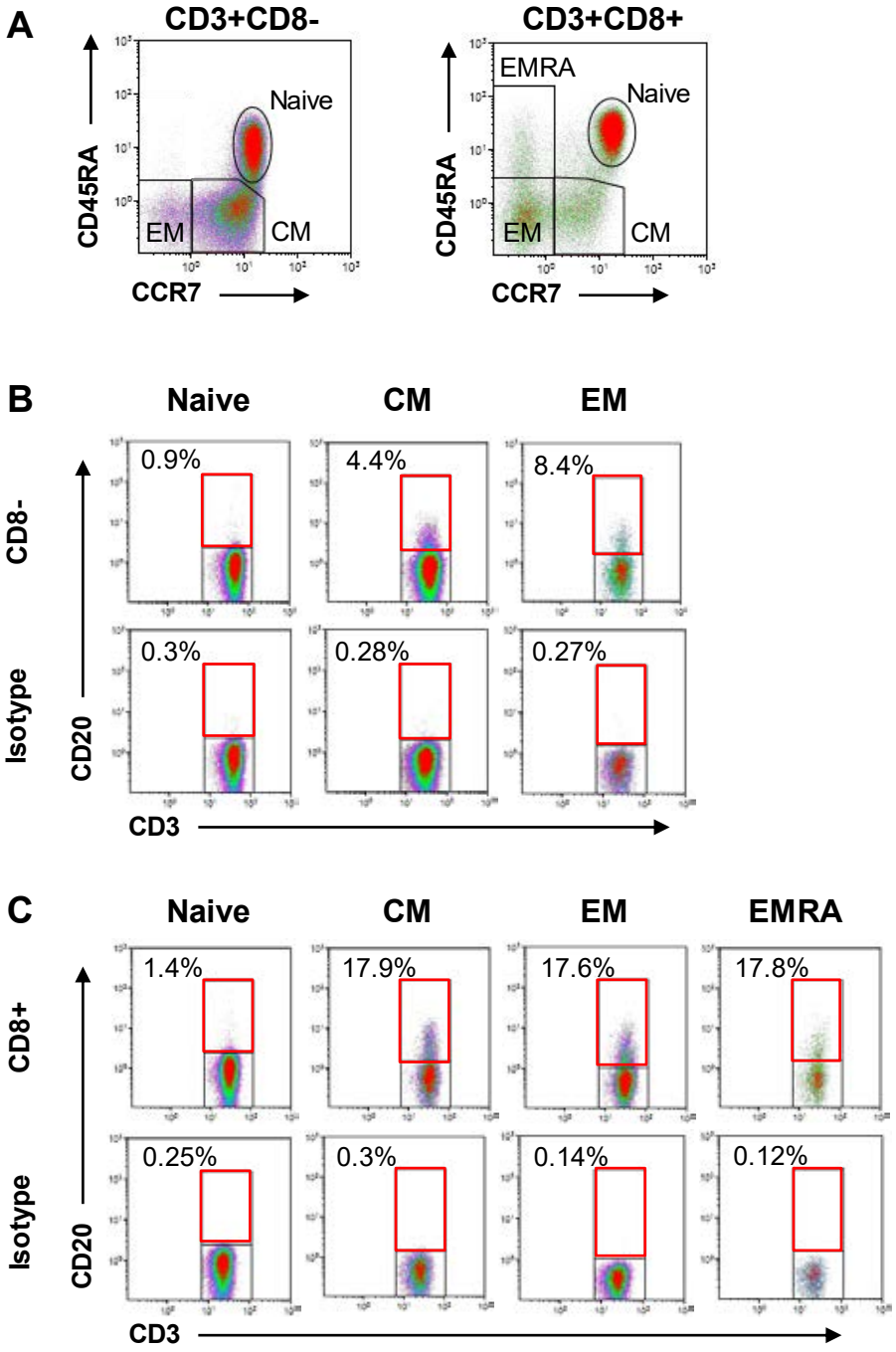

Figure 5.1 Gating strategy to identify CD20+ T cells within T cell subsets. Gating strategy for determination of naïve (CCR7+CD45RA+), central memory (CM; CCR7+CD45RA-), effector memory (EM; CCR7-CD45RA-) and revertant effector memory (EMRA; CCR7-CD45RA+) T cell subsets within CD8- and CD8+ compartments **(A)**. Gated on viable CD3+ lymphocytes with doublet exclusion. Gating strategy from a representative sample showing CD20+ T cell frequencies in CD8- **(B)** and CD8+ **(C)** T cell subsets, and isotype control staining (bottom plots). Gates were set at 0.5% positivity or less on the isotype control.

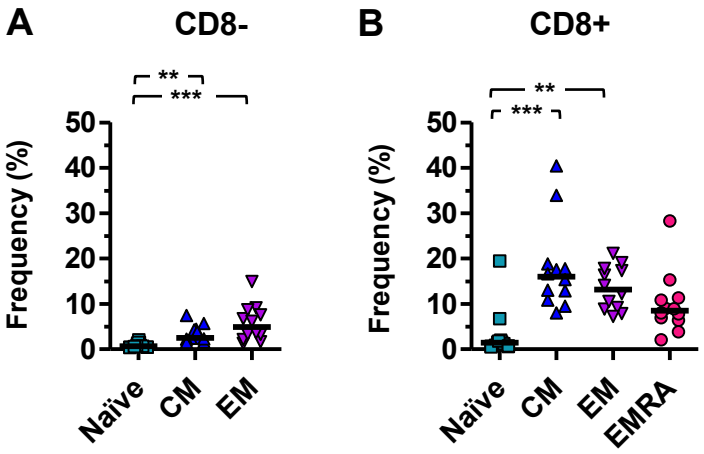

Figure 5.2 CD20+ T cells are enriched in memory T cell subsets in the peripheral blood of healthy subjects. Percentage of CD20+ T cells within CD8- **(A)** and CD8+ **(B)** T cell subsets. Data are significant to ** (P<0.01) and *** (P<0.01) using Dunn's multiple comparisons test (n=12).

CD3 was plotted against CD20 to identify CD20+ T cells in CD8- (**Fig. 5.1B**) and CD8+ subsets (**Fig. 5.1C**; upper panel of each Figure). An isotype control was used to set the gates at 0.5% positivity or less for each subset (lower panel of each Figure). Apart from CD20, where an isotype control was used, gates were set based on differential marker expression of each lymphocyte population.

5.2.2 Frequency and stability of CD20+ T cell subsets in healthy subjects

Using the gating strategy established in Figure 5.1, the frequency of CD20+ T cells using PBMC from healthy subjects was assessed. Within the CD8- population (**Fig. 5.2A**), CD20+ T cells were significantly increased in CM (2.5%) and EM (4.9%) subsets compared to the naïve subset (0.7%). A similar trend was observed in the CD8+ population (**Fig. 5.2B**), with CD20+ T cells preferentially exhibiting a CM (15.9%), EM (13.2%) and to a lesser extent EMRA (8.5%) phenotype, compared to a naïve phenotype (1.4%).

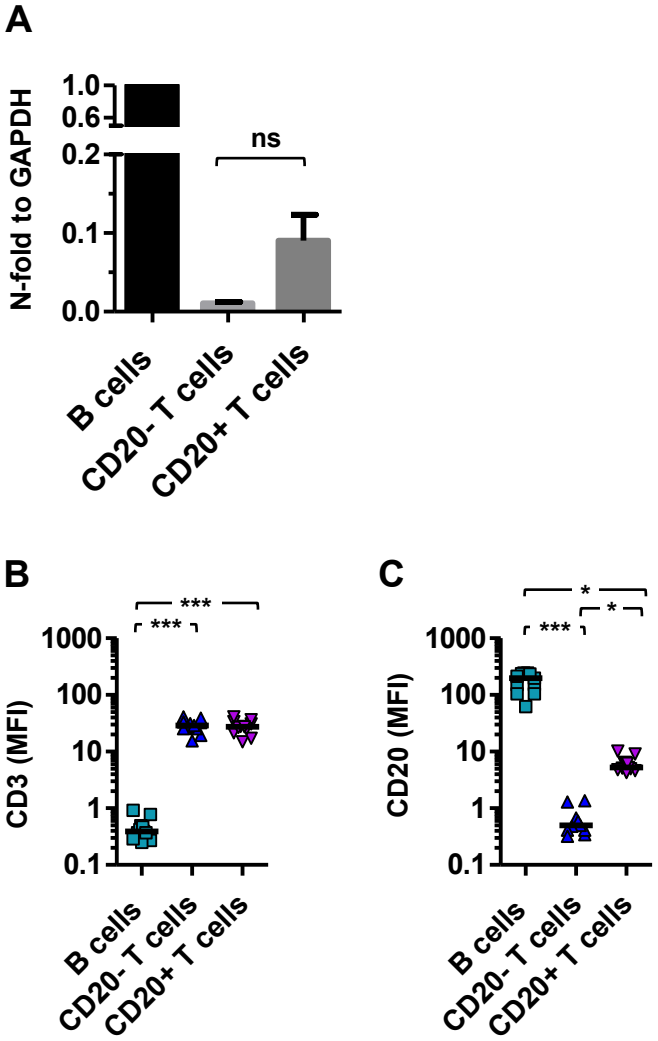

Figure 5.3 CD20+ T cells co-express CD3 and CD20 at the mRNA and protein level. Sorted CD20+ T cells and CD20- T cells were analysed for their expression of CD20 by qPCR in comparison to B cells **(A)**. CD20 expression was normalised to the housekeeping gene, GAPDH. Comparisons were not significant using Dunn's multiple comparisons test (n=2). Relative intensities of CD3 **(B)** and CD20 **(C)** expression determined by flow cytometry. Data are significant to * ($P<0.05$) and *** ($P<0.001$) using Dunn's multiple comparisons test (n=11). MFI; median fluorescence intensity.

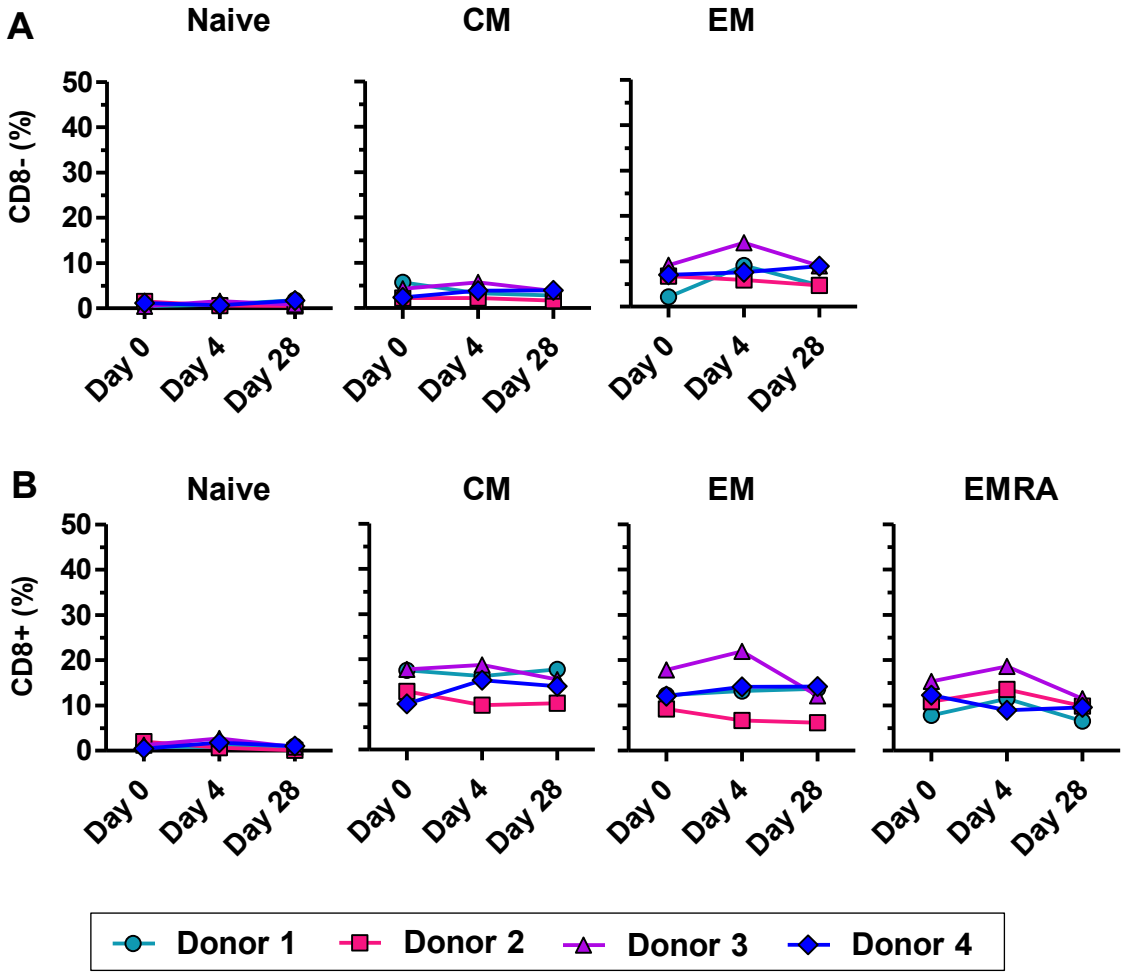

Figure 5.4 Peripheral blood CD20+ T cell frequencies are stable *in vivo* across a prolonged time period. Longitudinal analysis of CD20+ T cell frequencies within CD8- **(A)** and CD8+ **(B)** subsets in healthy subjects over 28 days (n=4).

In addition to characterising their subset distribution, longitudinal assessment of the frequency of CD20+ T cells was achieved by repeat sampling from four donors (**Fig. 5.4A, B**). For both CD8- and CD8+ populations, their frequencies appeared to be relatively consistent with time.

In addition to quantifying CD20+ T cells in the blood of healthy donors, their characteristics were also investigated. CD20 mRNA was detected for CD20+ T cells but not CD20- T cells, with around 80-85% less CD20 mRNA than in B cells; however, these findings were not significant, probably due to lack of replicates (**Fig. 5.3A**). Using the gating strategy from Fig. 5.1, MFI values were obtained for CD3 and CD20, using CD20- (conventional) T cells and CD20+ B cells as a comparison. Comparable levels of CD3 was identified in both T cell subsets, which was significantly higher than CD20+ B cells, confirming the T cell nature of these cells (**Fig. 5.3B**); conversely, elevated CD20 expression was observed in CD20+ T cells compared to CD20- T cells, which was also lower than B cells (**Fig. 5.3C**).

5.2.3 CD20+ T cells are present in the CSF of both MS and OND groups

Matched peripheral blood and CSF was obtained from MS and OND groups (see **Appendix III** for demographics). The presence of CD20+ T cells and their subset distribution in matched blood and CSF is shown from a person with MS (**Fig. 5.5A**). This was subsequently quantified and compared to the subset distribution of CD20- T cells, and was calculated as the percentage of CD20+ or CD20- T cells within each major CD8- or CD8+ T cell subset (**Fig. 5.5B**). Compared to CD20- T cells, peripheral CD20+ T cells were significantly over-represented in the effector memory compartments and reduced in the naïve compartments in both CD8- and CD8+ subsets. For the CD8- subset, the effector bias in CD20+ T cells was

also observed in the CSF, where CD20- T cells displayed a central memory bias (**Fig. 5.5B**). No significant differences in subset distribution between CD20- and CD20+ T cells were observed for CD8+ cells in the CSF.

The CD4:CD8 ratio represents the level of CD8 bias in a T cell population. In the peripheral blood, CD20- T cells were heavily biased towards CD8- (70.3% vs 28.2%), whereas CD20+ T cells displayed a CD8+ bias (41.7% CD8- vs 55.6% CD8+) (**Fig. 5.5C**). These findings were extended to the CSF, where the CD8- bias was retained for CD20- T cells, and the CD8+ bias retained by CD20+ T cells, though the latter was no longer significant.

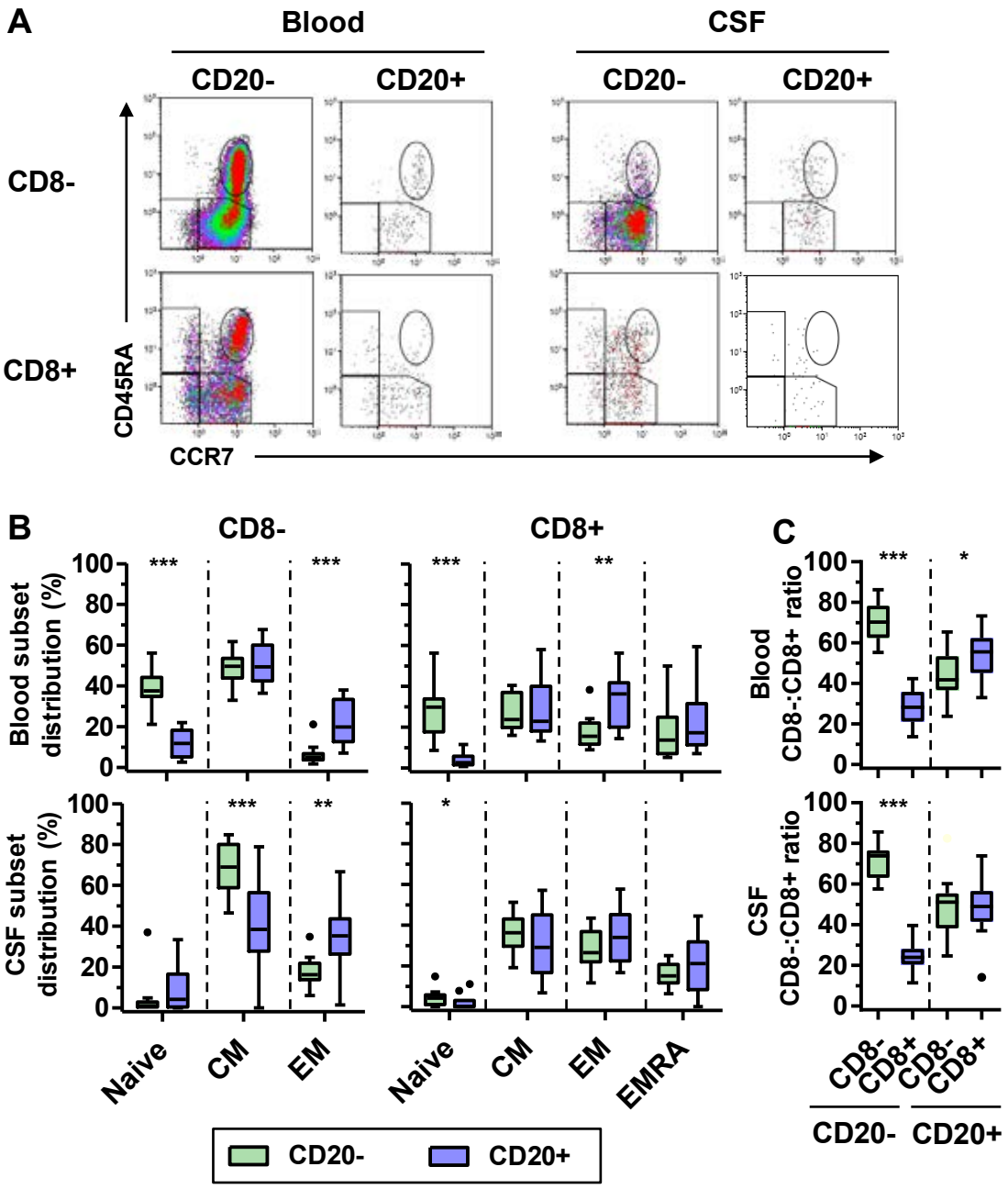

Figure 5.5 Identification of CD20+ T cells in the CSF. Representative gating strategy showing subset distribution of CD20- and CD20+ T cells in the blood and CSF of MS and OND groups **(A)**. Tukey box and whisker plots showing the distribution of CD20- and CD20+ T cells in naïve, central memory, effector memory and revertant effector memory (for CD8+ T cells only) populations in the peripheral blood and CSF of OND and MS groups **(B)**. Data are significant to * ($P<0.05$), ** ($P<0.01$) and *** ($P<0.001$) using Mann-Whitney test (n=12-13). Ratio of CD8- and CD8+ T cells for CD20- and CD20+ subsets in the blood and CSF **(C)**. Data are significant to * ($P<0.01$) and *** ($P<0.001$) using Mann-Whitney test.

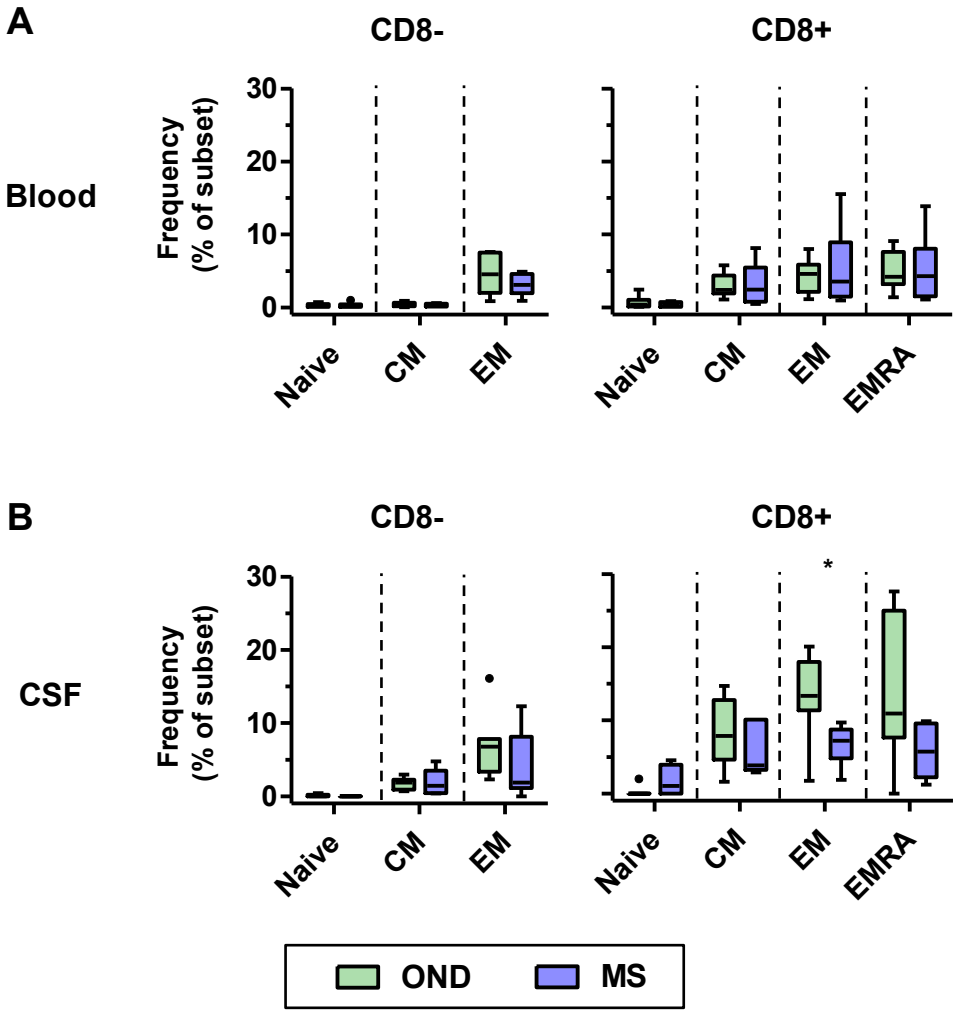

Figure 5.6 Frequency of CD20+ T cells within each T cell subset in the CSF and peripheral blood of MS and OND disease groups. Tukey box and whisker plot showing the frequency of CD20- and CD20+ T cells in the blood **(A)** and CSF **(B)** of MS and OND groups. Data are significant to * ($P<0.05$) using the Mann-Whitney test (n=6-7 samples per group).

In this chapter, the frequency of CD20+ T cells within each T cell subset was determined for both OND and MS groups (**Fig. 5.6**). Within the peripheral blood, there was no significant difference in the frequency of CD20+ T cells between MS and OND groups for both CD8- and CD8+ subsets (**Fig. 5.6A**). There was also little difference in the CSF, although OND CSF appeared to have a higher frequency of CD20+ T cells than MS CSF (**Fig. 5.6B**).

5.2.4 CD20+ T cells express elevated IFNγ and CCR6 in the CSF

Since CD20+ T cells in the CSF have not previously been phenotypically characterised, at least not in MS, it was investigated whether these cells might possess Th17-like features or other pro-inflammatory features. Intracellular cytokine (IFNγ and IL-17) and CCR6 expression was assessed following 3 hours of *ex vivo* stimulation with PMA and ionomycin in the presence of brefeldin A. Marker expression was then analysed for total memory (T_{CM}, T_{EM} and T_{EMRA}) cells within both CD20- and CD20+ T cell subsets.

Elevated IFNγ expression was observed in peripheral CD8-CD20+ T cells in both OND and MS groups (**Fig. 5.7A**). In the CSF, IFNγ expression was increased in all cell populations and was again significantly elevated in CD20+ T cells in both MS and OND groups. Within the CD8+ T cell population, CD20+ T cells also secreted significantly elevated IFNγ in the peripheral blood and CSF of both MS and OND groups (**Fig. 5.7B**). In the CSF, virtually all CD8+CD20+ T cells expressed IFNγ.

Very little IL-17 secretion was observed in CD20- or CD20+ T cells in the blood and CSF of MS and OND groups, though some high IL-17-secreting cells were observed (**Fig. 5.8A, B**). Within the CD8- compartment, no differential CCR6 expression in CD20- or CD20+ T cells was not observed in either the blood or CSF (**Fig. 5.9A**). This was also true in peripheral

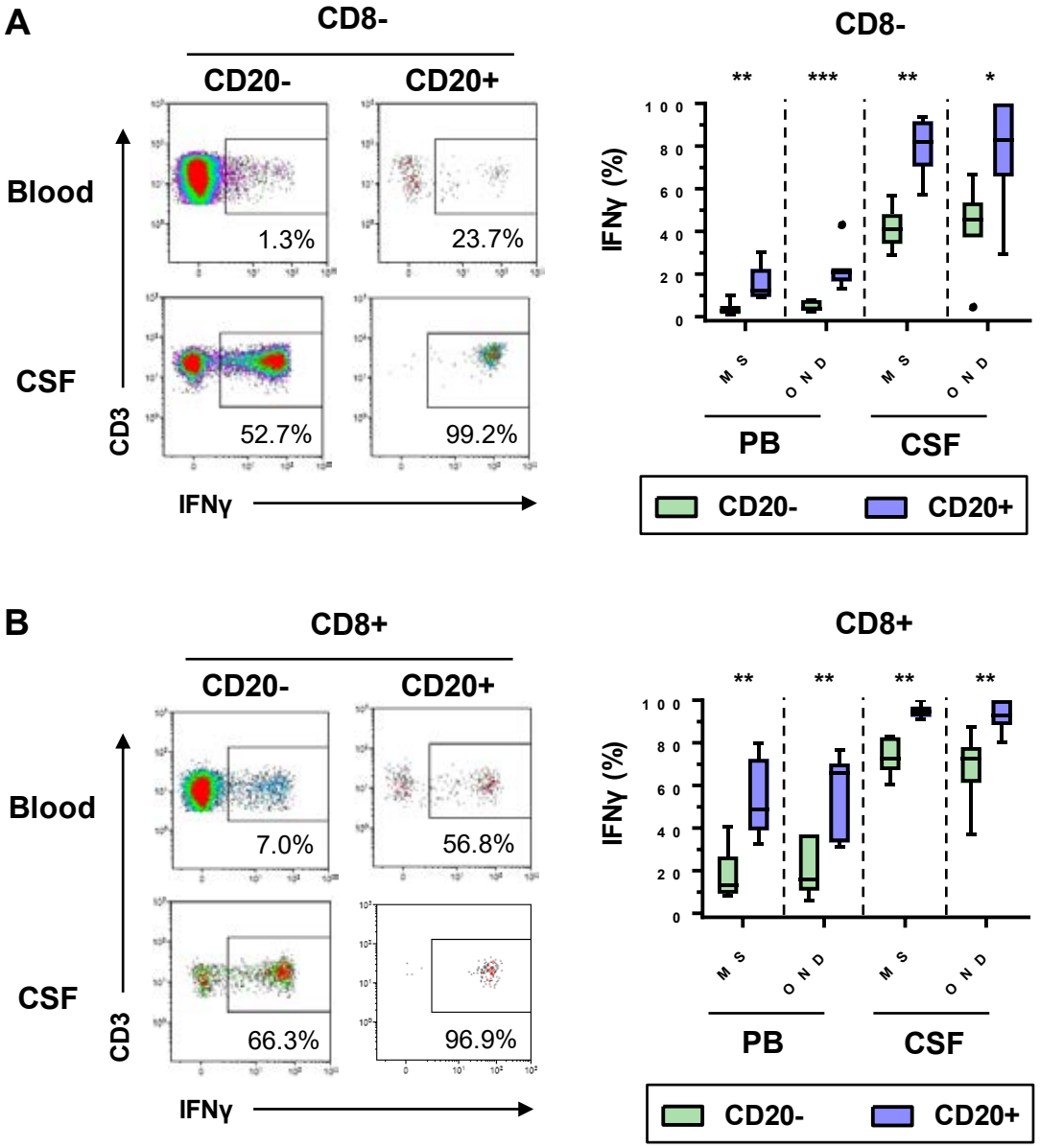

Figure 5.7 CD20+ T cells express higher levels of IFNγ in the blood and CSF. Representative flow plots and Tukey box and whisker plots showing the expression of IFNγ in total memory CD20- and CD20+ T cells in CD8- **(A)** and CD8+ **(B)** subsets for MS and OND groups. PBMC were stimulated for 3 hours with PMA and ionomycin. Data are significant to * ($P<0.05$), ** ($P<0.01$) and *** ($P<0.001$) using Mann-Whitney test (n=6-7 samples per group). PB; peripheral blood.

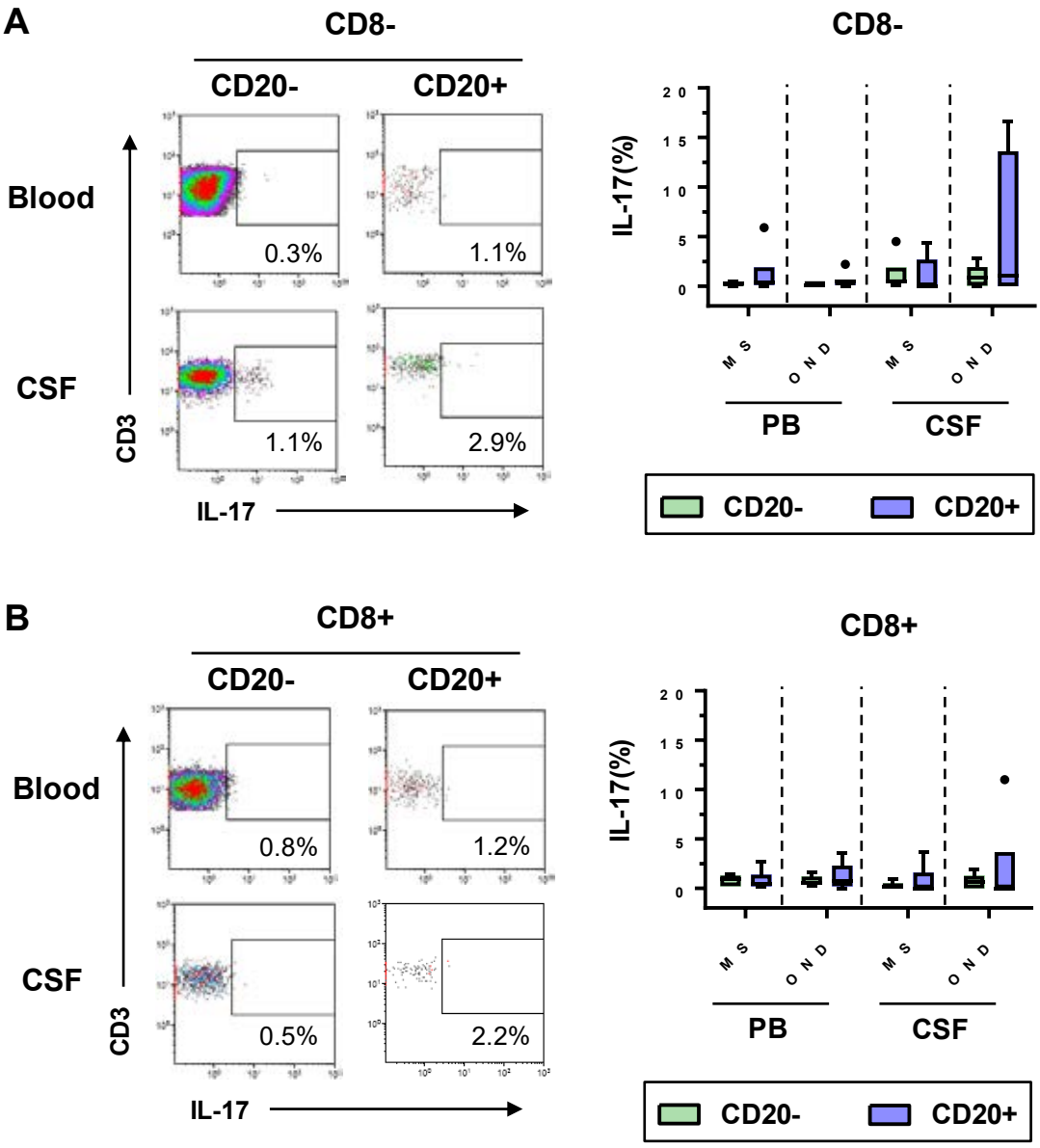

Figure 5.8 IL-17 expression in CD20+ T cells in the blood or CSF. Representative flow plots and Tukey box and whisker plots showing the expression of IL-17 in total memory CD20- and CD20+ T cells in CD8- **(A)** and CD8+ **(B)** subsets for MS and OND groups. PBMC were stimulated for 3 hours with PMA and ionomycin. No significant comparisons were made using Mann-Whitney test (n=6-7 samples per group). PB; peripheral blood.

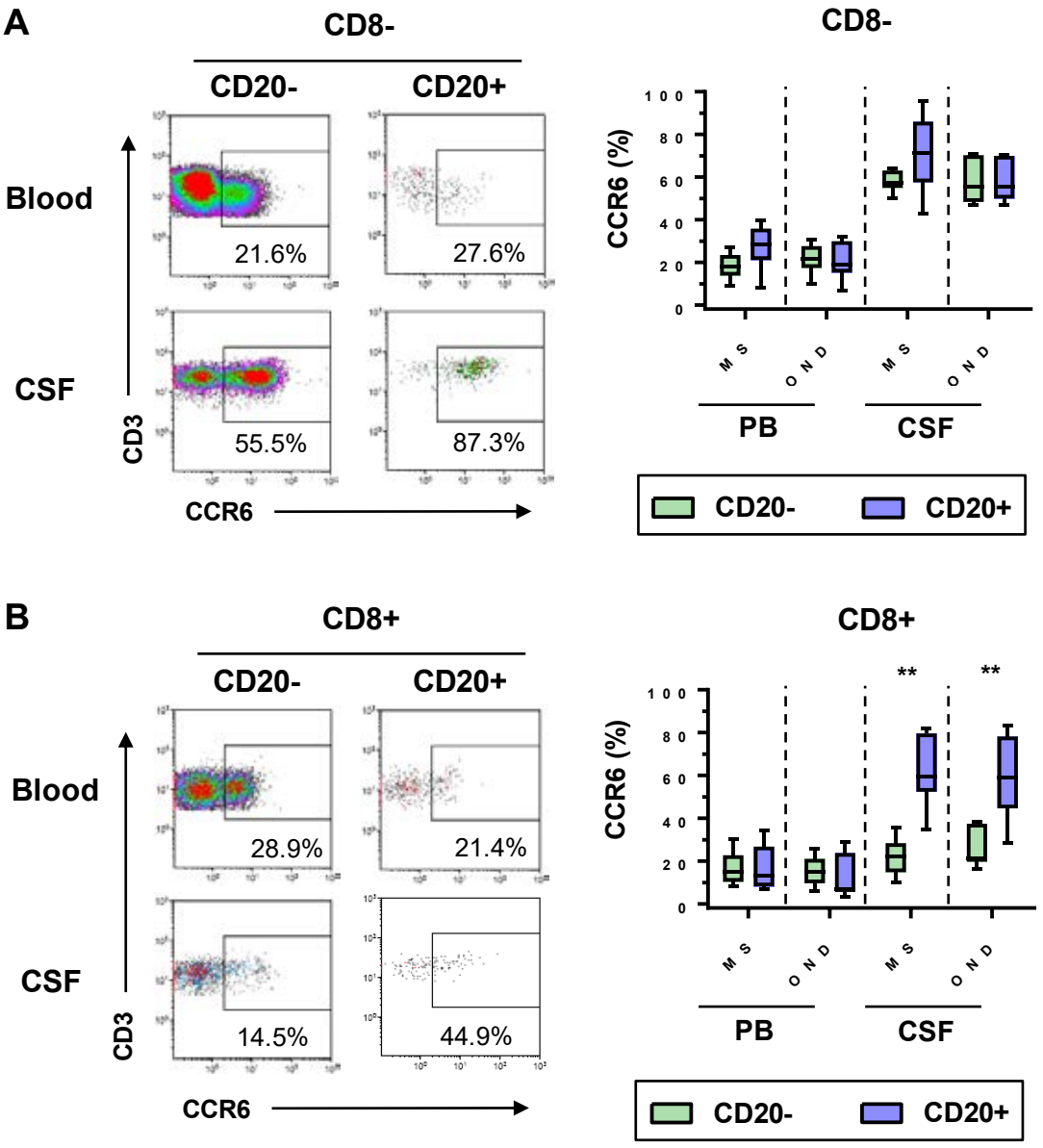

Figure 5.9 CD20+CD8+ T cells in the CSF express higher levels of CCR6 than in the peripheral blood. Representative flow plots and Tukey box and whisker plots showing the expression of CCR6 in total memory CD20- and CD20+ T cells in CD8- **(A)** and CD8+ **(B)** subsets for MS and OND groups. PBMC were stimulated for 3 hours with PMA and ionomycin. Data are significant to ** ($P<0.01$) using Mann-Whitney test (n=6-7 samples per group). PB; peripheral blood.

CD8+ T cells; however in the CSF, CD20+ T cells displayed significantly elevated CCR6 expression in both MS and OND groups (**Fig. 5.9B**).

5.2.5 CD20 is maintained by CD20+ T cells in culture, but is downregulated in the presence of PBMC

The features of CD20+ T cells were investigated with a series of *in vitro* assays. Because CD20+ T cells are enriched within the CD8+ memory pool, CD8+CD20+ T cells were focussed on for these assays. Prior to cell sorting, the CD8+ memory preparation was enriched by first passing PBMC through a magnetic negative selection column and collecting the negative fraction (**Fig. 5.10A**). This fraction was then cell sorted, with CD8+, CD45RA- and CD20+ gates applied, and CD20- and CD20+ subsets collected (**Fig. 5.10B**). Analysis of CD20 expression immediately post-sort identified 79% positivity in the CD20+ subset (**Fig. 5.10C**).

To assess the stability of CD20 expression over a 4-day period, Cell Proliferation Dye-stained CD20+ T cells were cultured with or without Dynabeads® Human T-Activator CD3/CD28 beads, or soluble tetrameric antibody (ImmunoCult™) to mimic physiological T cell activation, which was compared to CD20- T cells. CD20+ T cells maintained expression of CD20 for 4 days, regardless of whether they were unstimulated (77.7%) or stimulated via CD3/CD28 (Dynabeads® 75.8%, ImmunoCult™ 82.8%) (**Fig. 5.11A, B**). In the presence of PBMC, a significant reduction in CD20 expression was observed in all conditions (unstimulated 46.5%, Dynabeads® 38.2%, ImmunoCult™ 38.9%). Despite this reduction, CD20 was still maintained at significantly higher levels than CD20- T cells. CD20- T cells cultured alone failed to express CD20 over 4 days, although co-culture with PBMC led to an

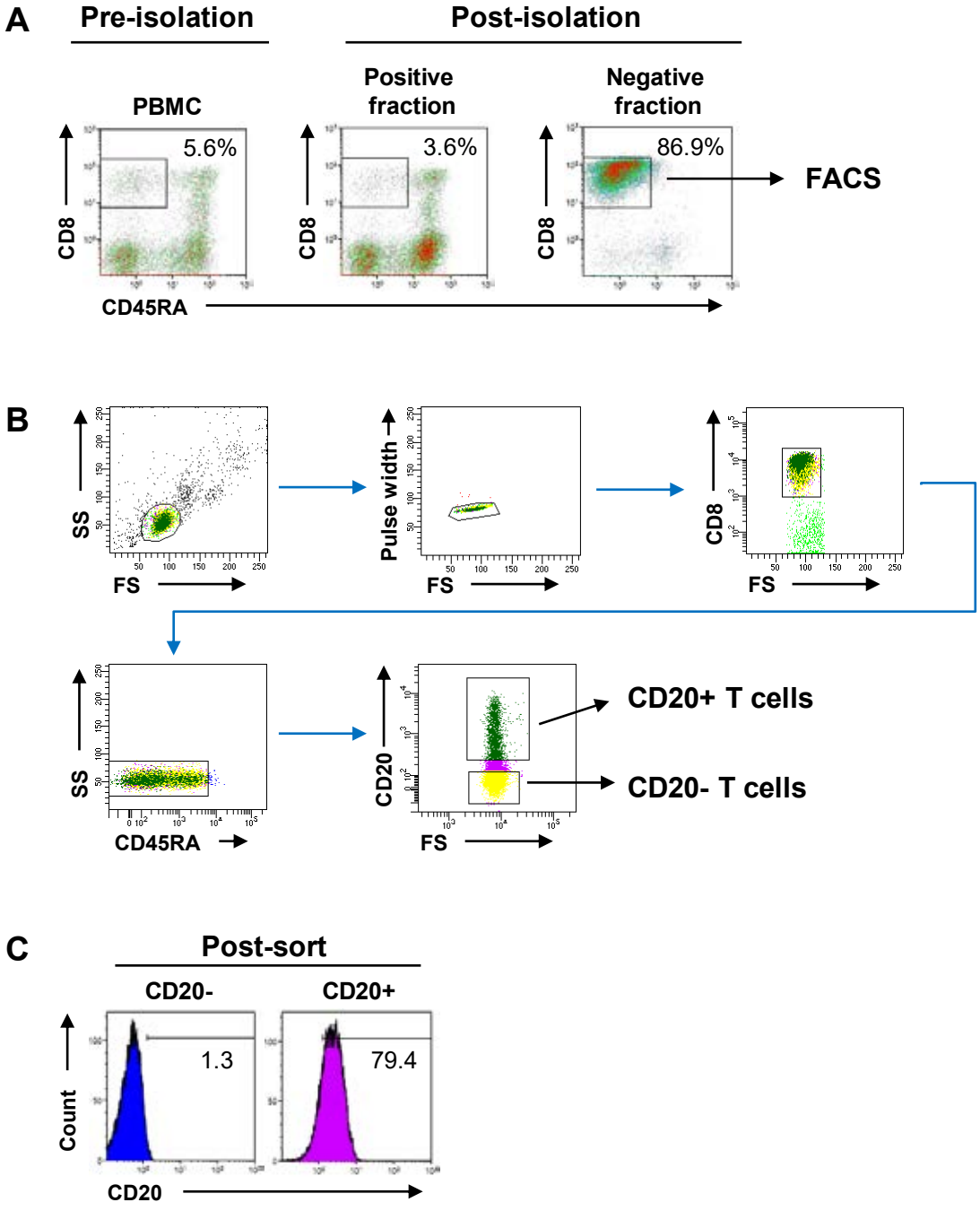

Figure 5.10 Isolation of peripheral CD20+ T cells from healthy subjects for *in vitro* assays. Following enrichment of CD8+ memory T cells using magnetic bead isolation **(A)**, cells were subjected to fluorescence activated cell sorting (FACS) to isolate CD20+ and CD20- T cell populations **(B)**. Blue arrows represent gating. CD20 expression of sorted subsets immediately following sorting **(C)**. SS; side scatter. FS; forward scatter.

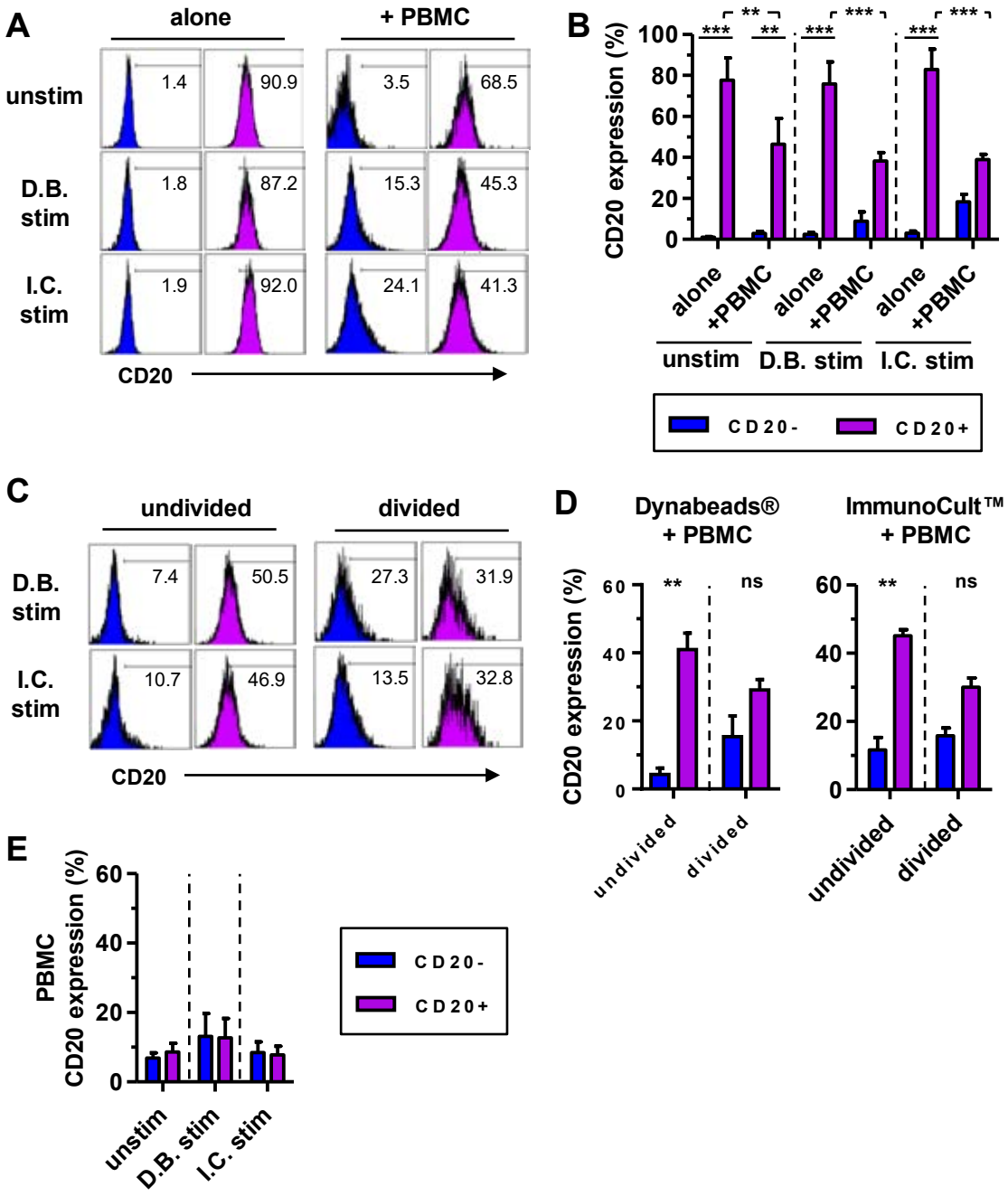

Figure 5.11 CD20+ expression by CD20+ T cells is maintained in culture, but is downregulated in the presence of PBMC. CD20 expression on CD20- (blue) and CD20+ (purple) cells, in the presence or absence of PBMC, was assessed after 4 days with or without stimulation **(A, B)**. CD20 expression on undivided and divided cells within each T cell population, cultured in the presence of PBMC **(C, D)**. CD20 expression on PBMC following T cell culture **(E)**. Data were significant to ** ($P<0.01$) and *** ($P<0.001$) using Bonferroni test and show the mean ± SEM (n=3 independent donors, duplicate wells). All other comparisons were not significant. Gates were set to 1% positivity on unstimulated or stimulated PBMC stained with an isotype control. Unstim; unstimulated, D.B; Dynabeads®, I.C; ImmunoCult™

.

increase in CD20 expression, particularly following stimulation (unstimulated 2.9%, Dynabeads® 8.8%, ImmunoCult™ 18.3%), however, this was not significant.

To investigate whether CD20 was specifically being lost by proliferating cells, CD20 expression was determined for undivided and divided cells following stimulation (**Fig. 5.11C, D**). This was achieved by gating on Cell Proliferation Dye-high cells (undivided) and on those that had lost Cell Proliferation Dye following proliferation (divided), then determining CD20 expression for each population. Undivided CD20+ T cells retained significantly higher CD20 expression than undivided CD20- T cells, however following proliferation, induced by either Dynabead® or ImmunoCult™ stimulation, CD20 was reduced by CD20+ T cells and increased by CD20- T cells (**Fig. 5.11D**). As such, no significant differences in CD20 expression were seen between CD20+ T cells and CD20- T cells following proliferation.

Finally, CD20 expression was investigated on PBMC following co-culture with sorted CD20- T cells and CD20+ T cells. This showed no significant differences in CD20 expression by PBMC for each condition (**Fig. 5.11E**).

5.2.6 CD20+ T cells display diminished proliferative capacity

The proliferative capacity of CD20+ T cells was assessed by determining the percentage of cells that had lost Cell Proliferation Dye following 4 days of culture. Results showed that CD20+ T cells displayed significantly diminished proliferative capabilities compared to CD20- T cells after both Dynabead® stimulation (30.9% CD20- vs 17.5% CD20+) and ImmunoCult™ stimulation (71.1% CD20- vs 40.9% CD20+) in the presence of PBMC (**Fig. 5.12A, B**). Both CD20+ and CD20- T cell populations failed to proliferate in the absence of PBMC.

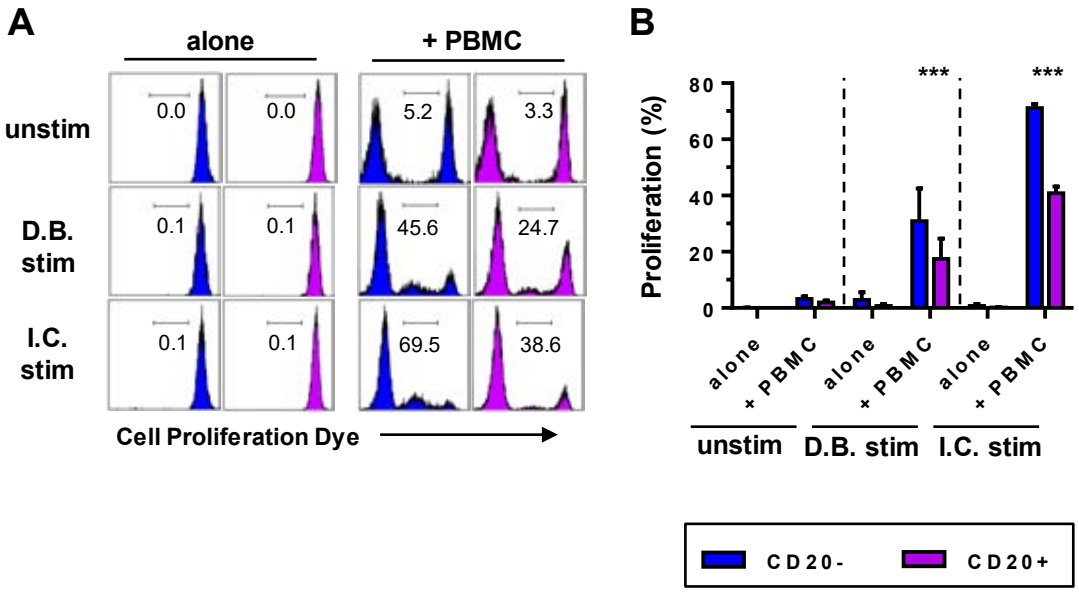

Figure 5.12 CD20+ T cells display diminished proliferative capacity. Following 4 days of culture with or without anti-CD3/CD28 stimulation, CD20- and CD20+ T cells were assessed for proliferation **(A, B)**. Data are significant to *** ($P<0.001$) using Bonferroni test and show the mean ± SEM (n=3 independent donors, duplicate wells). All other comparisons were not significant. Unstim; unstimulated, stim; stimulated, D.B; Dynabeads®, I.C; ImmunoCult™.

5.2.7 Altered marker expression by CD20+ T cells

By analysing the expression of several markers on total CD8- and CD8+ memory cells, some interesting differences were observed between CD20- and CD20+ T cells (**Fig. 5.13**). These markers were selected based on their involvement in cell activation, cytotoxicity, immune checkpoint inhibition and chemokine responsiveness. Because of the high over-representation of CD20+ T cells in the memory compartment, naïve cells were excluded from this analysis to allow like-for-like comparisons between memory CD20- and memory CD20+ T cells. Gates were set for each subset on isotype control/fluorescence minus one (FMO) samples, which were then applied to the full panel. Of note, there was a significant reduction in CD38 expression in both CD8- and CD8+ CD20+ T cell subsets, and a significant reduction in granzyme B expression in CD8+CD20+ T cells. In addition, significantly elevated PD-1 expression was observed in CD8- and CD8+ memory CD20+ T cells. Investigation of intracellular cytokine expression demonstrated elevated IL-4 secretion by CD8-CD20+ T cells, however no other comparisons were significant (**Fig. 5.14**).

5.2.8 CD20+ T cells express elevated PD-1

The novel observation of significantly elevated PD-1 expression by CD20+ T cells was further investigated. Using isotype control staining, PD-1 expression was determined for total CD8- and CD8+ memory T cells (**Fig. 5.15A**); this expression was compared to that of naïve T cells, which was very low in comparison (**Fig. 5.15B**). For both CD8- and CD8+ subsets, PD-1 expression was significantly increased, although this was not observed for the MFI values (**Fig. 5.15C**). On further analysis, PD-1 expression on central memory and effector memory CD8-CD20+ subsets failed to show a significant difference to CD8-CD20- T cells,

		CD8- memory			CD8+ memory		
Marker	n	CD20-	CD20+	P value	CD20-	CD20+	P value
CD25	7	11.08	8.47	ns	4.61	4.63	ns
CD27	7	88.29	87.99	ns	80.40	97.34	ns
CD38	6	17.98	7.21	**	17.62	6.74	**
CD69	6	6.51	6.81	ns	8.18	10.42	ns
Perforin	7	22.75	50.92	ns	72.99	53.39	ns
CXCR5	7	4.87	3.65	ns	5.30	7.57	ns
Granzyme B	7	20.06	11.51	ns	44.56	19.59	*
Granzyme A	7	34.02	30.17	ns	33.34	40.10	ns
Granulysin	8	15.04	7.73	ns	12.65	5.20	ns
FAS ligand	6	1.51	1.65	ns	2.42	1.67	ns
CTLA-4	5	31.99	19.74	ns	10.46	3.92	ns
PD-1	7	43.36	66.7	*	35.42	58.09	***
TIM-3	6	2.66	1.93	ns	2.42	2.42	ns

Figure 5.13 Investigation of marker expression by CD20+ T cells. Expression levels of selected markers were analysed for CD20- and CD20+ T cells within the CD8- memory and CD8+ memory compartments. Cells were stained *ex vivo* except for CTLA-4 and FAS ligand, which were first stimulated for 3h using PMA and ionomycin in the presence of brefeldin A. Staining was intracellular for granzyme A, granzyme B, granulysin and CTLA-4. Data are significant to * ($P<0.05$), ** ($P<0.01$) or *** ($P<0.001$) using Mann-Whitney test.

		CD8- memory			CD8+ memory		
Cytokine	n	CD20-	CD20+	P value	CD20-	CD20+	P value
GM-CSF	6	16.57	14.79	ns	16.82	18.16	ns
IL-4	7	3.55	5.92	*	2.63	0.77	ns
IL-5	6	1.51	1.80	ns	2.76	2.79	ns
IL-10	6	1.28	1.37	ns	1.56	0.88	ns
IL-13	6	2.37	1.74	ns	2.37	3.49	ns
IL-2	5	17.74	22.39	ns	11.02	10.87	ns
LTα	4	3.34	5.09	ns	3.76	2.87	ns

Figure 5.14 Investigation of cytokine expression by CD20+ T cells. Following 3h stimulation with PMA and ionomycin in the presence of brefeldin A, cytokine expression was analysed by intracellular staining. Data are significant to * ($P<0.05$) using Mann-Whitney test. LTα; lymphotoxin alpha.

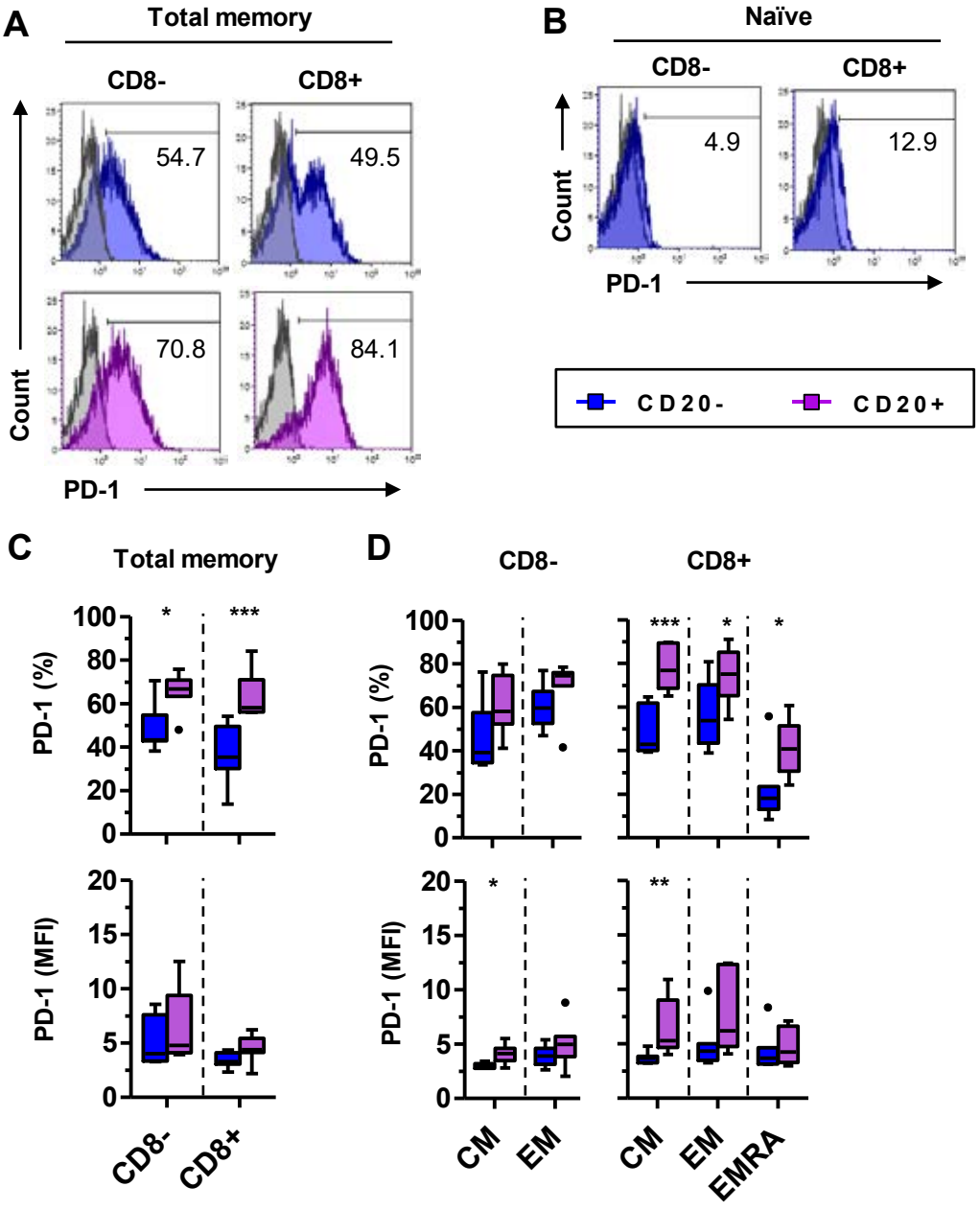

Figure 5.15 Elevated PD-1 expression in CD20+ memory subsets. Representative flow plots showing PD-1 expression in resting memory **(A)** and naive **(B)** T cells. Tukey box and whisker plots showing PD-1 expression and MFI values in CD8- and CD8+ total memory T cells **(C)** and memory T cell subsets **(D)**. Data are significant to * ($P<0.05$), ** ($P<0.01$) and *** ($P<0.001$) using Mann-Whitney test (n=7).

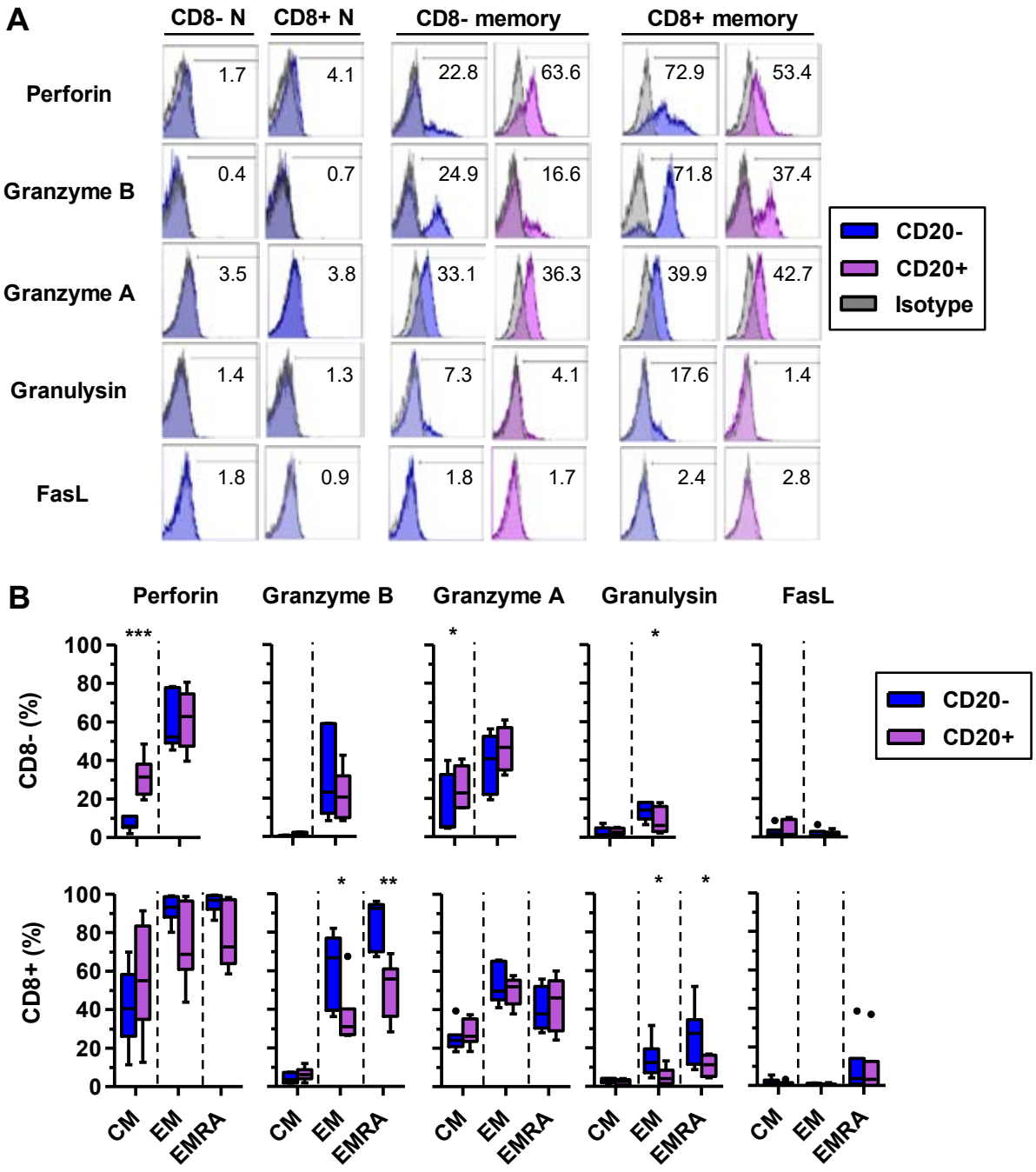

Figure 5.16 Expression of cytotoxic molecules by CD20+ T cells. Representative frequency histograms of intracellular perforin, granzyme B, granzyme A, granulysin and FASL expression by CD20- (blue) and CD20+ (purple) T cells **(A)**. Isotype control staining is shown in grey. N; naïve T cells. Tukey box and whisker plots showing percent expression of cytotoxic molecules in CD20- and CD20+ T cells within central memory, effector memory and effector memory RA compartments **(B)**. Data are significant to * ($P<0.05$), ** ($P<0.01$) or *** ($P<0.001$) using Mann-Whitney test (n=7). FasL; Fas ligand.

however there was a significantly increased MFI when comparing central memory CD8- subsets (**Fig. 5.15D**). For CD8+ T cells, PD-1 expression was significantly elevated within each memory subset, with the strongest increase in the central memory compartment; this was also reflected by a significantly increased MFI for central memory CD20+ T cells but no other memory subset (**Fig. 5.15D**).

5.2.9 CD20+ T cells retain cytotoxic potential despite diminished cytotoxic marker expression

The CD8+ memory bias of CD20+ T cells warranted further investigation into the cytotoxic functions of these cells, therefore, the *ex vivo* expression of cytotoxic molecules was investigated. Perforin expression was generally increased in CD8- memory but decreased in CD8+ memory subsets (**Fig. 5.16A**). Overall, perforin expression appeared to be increased in CM (especially CD8-) but decreased in EM and EMRA subsets (**Fig. 5.16A, B**). Granzyme B (second column) and granulysin (fourth column) expression was decreased in CD20+ T cells, which for both markers was significant in CD8+ effector memory and EMRA subsets. Granzyme A expression (third column) appeared slightly elevated in central memory subsets, which was significant for CD8-CD20+ T cells, and the low levels of FasL (fourth column) failed to show any differences between CD20- and CD20+ subsets.

Following the observation of perturbed cytotoxic molecule expression in CD20+ T cells, the ability of these cells to degranulate in response to PMA and ionomycin stimulation was assessed over a 3-hour time course (**Fig. 5.17A, B**). This assay was performed by stimulating total PBMC, with subsequent gating to identify CD20- and CD20+ T cells, and identification of degranulation was achieved by analysing intracellular perforin and surface CD107a, also

known as LAMP-1, a functional marker of degranulation (Alter et al., 2004). Both CD20- and CD20+ T cells showed decreased perforin expression over the time course, which was associated with a concomitant increase in surface CD107a by both subsets, which appeared higher in CD20+ T cells (**Fig. 5.17A, B**).

5.2.10 CD20+ T cells are present within the EBV-specific CD8+ T cell compartment

Because of the high seroprevalence of EBV infection in the general population, and its strong association with MS, the EBV specificity of CD20+ T cells was investigated by tetramer staining (Hatton et al., 2014). Using PBMC, gates were applied to CD3+CD8+ T cells, which were split based on CD20 expression, and tetramer positive gates were applied based on FMO staining (**Fig. 5.18A**). Reactivity towards GLC and YVL, two common EBV lytic cycle peptides, were then analysed in three HLA-A*02-positive donors (**Fig. 5.18B**). CD20+ T cells displayed clear reactivity for EBV, and interestingly, appeared to represent a higher frequency of tetramer positive cells than CD20- T cells; however, a larger number of donors would be required to confirm this.

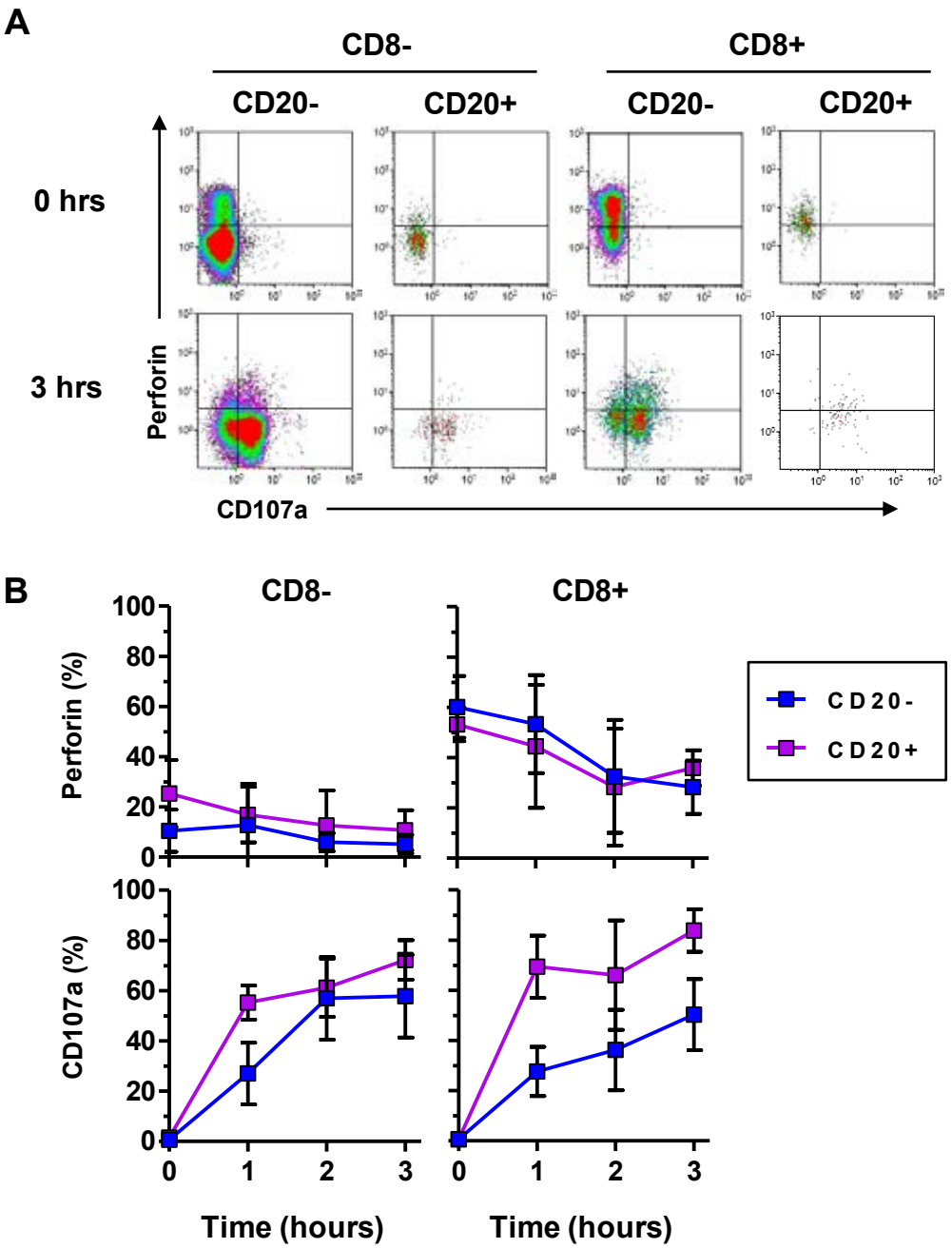

Figure 5.17 CD20+ T cells express cytolytic granules. Representative flow plots of perforin and CD107a expression at 0 hours and 3 hours post-stimulation with PMA and ionomycin **(A)**. Kinetics of intracellular perforin and surface CD107a expression of memory T cells with (purple) and without (blue) CD20 expression **(B)**. Mean values ± standard deviation (n=4).

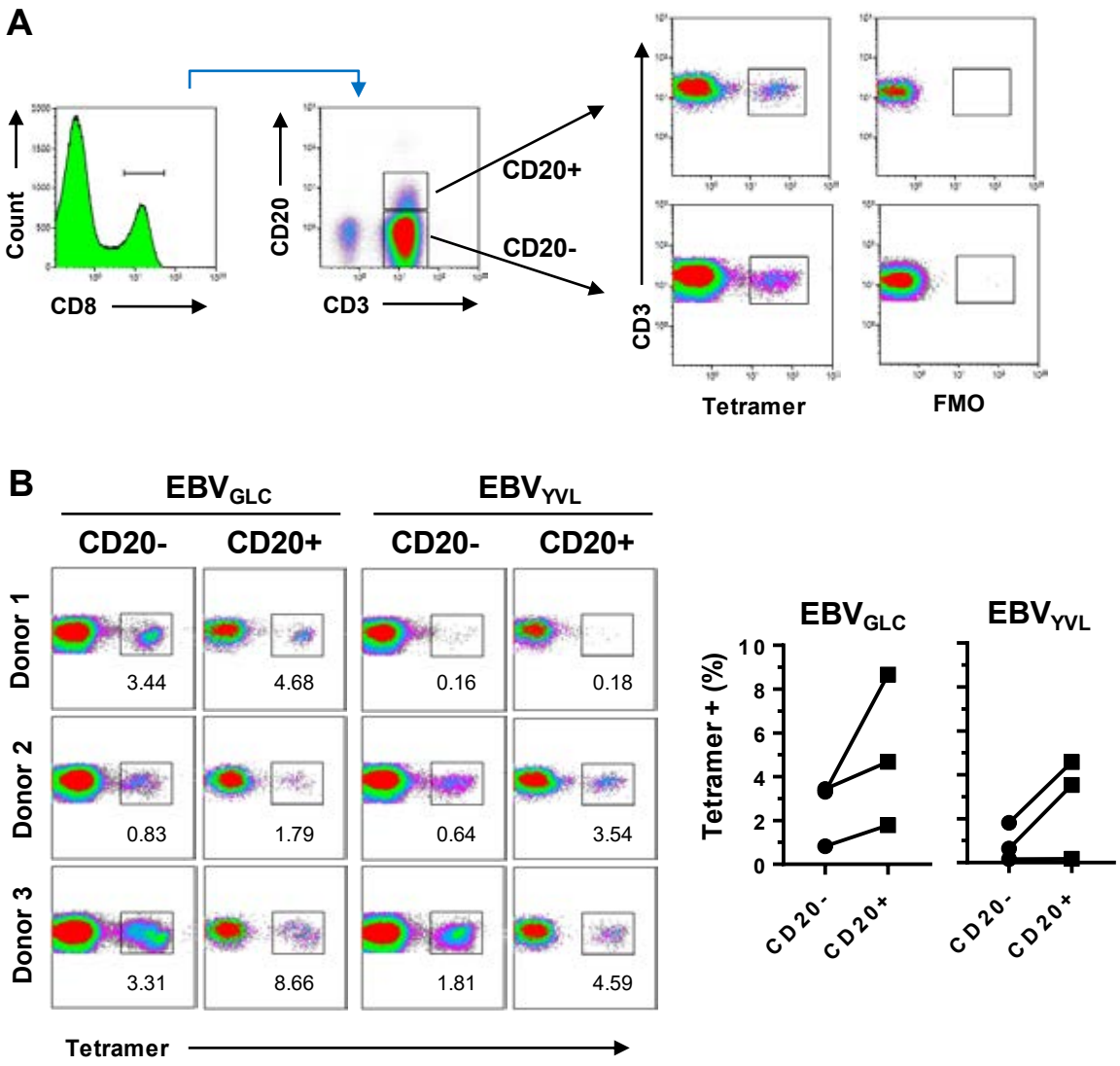

Figure 5.18 CD20+ T cells are present within the EBV-specific CD8+ T cell compartment. Representative gating strategy to determine the frequency of EBV-specific T cells, and comparison with FMO **(A)**. From total viable lymphocytes with doublets excluded, CD3+CD8+ cells were divided into CD20- and CD20+ and then assessed for tetramer positivity. Flow plots and quantification of the frequency of CD3+CD8+CD20- or CD3+CD8+CD20+ T cells from healthy HLA-A*02-positive donors that show specificity towards two common EBV lytic cycle peptides, GLC and YVL (n=3) **(B)**. FMO; fluorescence minus one.

5.3 Discussion

Despite their initial description 25 years ago, there has been recent interest in CD20+ T cells due to their reported associations with several inflammatory conditions, including MS (Hultin et al., 1993; Palanichamy et al., 2014b). In conjunction with previous reports, data from this chapter confirmed the presence of a T cell population in the blood and CSF that co-express low levels of CD20, secrete elevated levels of pro-inflammatory cytokines and are over-represented in the CD8 memory compartment.

5.3.1 Identification and characterisation of CD20+ T cells

In this chapter, a gating strategy was established that clearly identified CD20+ T cells within peripheral blood T cell populations (Fig. 5.1A-C). CD20+ T cells have been shown to express lower levels of CD20 than B cells, and are sometimes referred to as $CD20^{dim}$, therefore a bright fluorochrome (PE or Bv421 depending on the panel) was used for their identification. Isotype control staining (Fig. 5.1C) revealed very little non-specific staining, indicating that the gated cells truly express CD20, which has previously been contested (Henry et al., 2010).

The expression of CD20 by T cells has been investigated by others. In a co-culture assay with B cell and T cell lines, de Bruyn and colleagues (2015) found that CD20 was acquired by around 30% of T cells following a 1-hour incubation, which was also associated with acquisition of HLA-DR (de Bruyn et al., 2015). In contrast, a more recent report demonstrated that CD20+ T cells do not display HLA-DR, or any other typical B cell molecules, suggesting that trogocytosis is not the reason for CD20 expression by these cells (Schuh et al., 2016). In addition, other studies have demonstrated low but detectable levels of CD20 mRNA in CD20+ T cells (Wilk et al., 2009; Palanichamy et al., 2014b; Schuh et al., 2016). Findings

from this chapter agree with others that CD20+ T cells transcribe CD20 at the gene level, implicating *de novo* CD20 synthesis as the primary (if not only) mechanism by which these cells express CD20 (Fig. 5.3A).

Although the validity of the CD20+ T cell population was previously challenged, with the suggestion they may be an artefact of flow cytometry, the equivalent levels of CD3 expressed by CD20+ and CD20- T cells confirmed the T cell nature of these cells (Henry et al., 2010). Additionally, despite the lack of significance, the mRNA data mirrored the level of CD20 surface expression by CD20+ T cells compared to B cells, which was around a tenth lower, suggesting that the mRNA data is reliable (Fig. 5.3A-C). This also compares to published data, where CD20+ B cells carried 10-15-fold higher levels of CD20 mRNA than CD20+ T cells; further to this, the lack of CD19 mRNA in CD20+ T cells, as demonstrated by others, confirms that these are truly T cells (Wilk et al., 2009; Schuh et al., 2016).

5.3.2 Frequency and stability of CD20+ T cell populations in healthy donors

That only memory T cells express CD20 suggests that it could be acquired following activation, and its absence on naïve T cells demonstrates that this population do not inherently express CD20 throughout their lifespan (Fig. 5.2, Fig. 5.5). The lower frequency of CD20+ T cells in the CD8+ EMRA subset compared to central and effector memory subsets indicates that CD20 is not a feature associated with terminal T cell differentiation. That CD20+ T cell frequencies are preferentially higher in the CD8+ than the CD8- population supports the previously reported CD8+ memory bias in these cells, and point to a cytotoxic role for these cells (Wilk et al., 2009; Schuh et al., 2016). The relatively stable frequencies of CD20+ T

cells observed over 28 days indicates either stable expression over time, or continual induction under homeostatic conditions (Fig. 5.4). Taken together, these data suggest that CD20 is a physiological marker induced by a specific event occurring only in memory cells, but which can also occur in any other memory T cell subset, leading to a heterogeneous CD20+ T cell population.

5.3.3 CD20+ T cell frequencies in MS and controls

In the periphery, the CD8- (i.e. CD4+):CD8+ ratio showed that CD20- T cells were heavily biased towards CD8- at approximately 2:1 (Fig. 5.5C), agreeing with published data (McBride 2017). This also validates the gating strategy for identifying CD4+ T cells using a CD3+CD8- phenotype instead of a CD3+CD4+ phenotype. Similar ratios between CD8- and CD8+ subsets were observed in CD20+ T cells, agreeing with previous findings, and confirming the CD8+ T cell bias in this cohort of individuals (Wilk et al., 2009). Data from this chapter also identified CD20+ T cells in the CSF, where they retained their subset composition and CD8-:CD8+ ratio compared to CD20+ T cells in the periphery; this similarity could suggest the absence of selective CD20+ T cell recruitment into the CSF (since the populations are comparable to the periphery), or that the stimuli responsible for inducing CD20 expression on T cells is also present in the CSF (Fig. 5.5). The presence of CD20+ T cells in MS CSF has also been reported recently; furthermore, these cells have been identified in chronic white matter lesions in MS brain tissue but not in control tissue, suggesting that these cells may contribute to disease (Schuh et al., 2016; Holley et al., 2014).

Previous reports on the frequency of CD20+ T cells in MS peripheral blood have been conflicting (Palanichamy et al., 2014b; Holley et al., 2014; Schuh et al., 2016). Though

overall frequencies as a proportion of total T cells was not performed in this chapter, as analysis within each subset was favoured to omit any potential subset bias between individuals, I observed CD20+ T cells at similar frequencies within T cell subsets for both MS and OND groups (Fig. 5.6A). This agrees with two previous studies, but disagrees with Palanichamy et al (2014b), who found that peripheral CD20+ T cells are increased in MS (7.2%) compared to OND controls (5.4%) (Palanichamy et al., 2014b; Holley et al., 2014, Schuh et al., 2016). Considering the lack of association in other studies, this small increase seen by Palanichamy et al (2014b) could be a statistical artefact caused by biological variation, or alternatively, may be correct; as such, further work with a larger sample size (these studies analysed 8-12 samples per group) may shed more light on this.

In this chapter, CD20+ T cells were identified in the CSF of both OND and MS groups where the CSF frequency, particularly in the OND group, appeared higher than their peripheral blood counterparts (Fig. 5.6). Furthermore, the frequency of CD20+ T cells in OND CSF appeared increased compared to MS CSF, with a significant difference observed in the CD8+ effector memory subset (Fig. 5.6B). Interestingly, the only other study which has investigated the frequency of CD20+ T cells in the CSF reported similar findings, with almost double the frequency in OND versus MS; this may therefore suggest that these cells are not positively associated with disease pathogenesis (Schuh et al., 2016).

5.3.4 Phenotype of CD20+ T cells in the CSF

Although several reports describe these cells as pro-inflammatory, elevated IFNγ following stimulation has been reported by some (Holley et al., 2014; de Bruyn et al., 2015; Schuh et al., 2016) but not others (Wilk et al., 2009). It was confirmed in this chapter that CD20+ T

cells in the peripheral blood express elevated intracellular IFNγ in both CD8- and CD8+ subsets following PMA/ionomycin stimulation for 3 hours, which was higher in the CD8+ subset, in accordance with their cytotoxic role (Fig. 5.7). In the CSF, CD20+ T cells expressed even higher levels compared to those in the periphery, which was significantly higher than CD20- T cells for both CD8- and CD8+ subsets. The enhanced secretion of IFNγ by CSF CD20+ T cells may support a variety of pathological functions leading to exacerbation of disease activity, as seen in people with MS treated with IFNγ, potentially linking these cells with pathology (Vartanian et al., 1995; Panitch et al., 1987). However, the comparable levels of IFNγ between both MS and OND suggests that this is probably a general feature of these cells. It must also be considered that IFNγ can play protective roles in the CNS, such as ameliorating EAE severity and limiting T cell proliferation; therefore, it cannot be excluded that these cells play a protective role (Balashov et al., 1995; Chen et al., 2009).

A previous report suggested that CD20+ T cells preferentially secrete IL-17 compared to CD20- T cells following 4-hour stimulation with PMA and ionomycin (Schuh et al., 2016). IL-17-secreting CD20+ T cells were also reportedly expanded in rheumatoid arthritis compared to controls, and IL-17+CD20+ T cells have been identified in MS brain tissue (Eggleton et al., 2011; Holley et al., 2014). In this chapter, very little IL-17 secretion was observed in both CD20- and CD20+ T cell subsets in both MS and OND groups after 3 hours of stimulation, although a slight elevation was observed in CSF OND CD8-CD20+ T cells (Fig. 5.8). In line with these findings, other studies, which also stimulated their cells for 4 hours as in the study by Schuh et al (2016), failed to identify significantly elevated IL-17 production from peripheral CD20+ T cells compared to CD20- T cells due to low cell frequencies (Wilk et al., 2009; Holley et al., 2014; de Bruyn et al., 2015). Although Schuh et al (2016) do not report the exact frequencies of IL-17+CD20+ T cells, they appear to be

around 3% for CD20+ T cells compared to around 1% for CD20- T cells, and represent the mean rather than the median, despite the absence of a normal distribution (Schuh et al., 2016). The presence of some high outliers, and the likelihood of low cell numbers as reported by others, may have caused this difference to be exaggerated.

Within the CD8+ subset, CD20+ T cells in the CSF expressed higher levels of CCR6 than CD20- T cells, which was not observed in the peripheral blood (Fig. 5.9). This novel finding appears to suggest the active migration of these cells into the CSF, as CCR6 regulates the migration of T cells into the CNS (Yamazaki et al., 2008). The abrogation of CCR6 ameliorates disease severity in EAE models, pointing to a possible pathological role of these cells, however as with IFNγ, the lack of distinction between OND and MS suggests that this increased expression is not necessarily an indicator of disease (Reboldi et al., 2009; Arellano et al., 2015). Conversely, an alternative phenomenon may exist in that CCR6+ T cells preferentially become CD20+ after entering the CSF. IFNγ-secreting T cells in the CSF is strongly associated with CCR6 expression, and it may be the elevated IFNγ secretion by CCR6+ CSF T cells that leads to CD20 induction, possibly as a protective response to limit immune cell activation, which could have serious consequences in the CNS (Restorick et al., 2017).

5.3.5 *In vitro* characterisation of CD20+ T cells

The features of CD20+ T cells were further investigated with a series of *in vitro* assays following their isolation from the peripheral blood of healthy subjects (Fig. 5.10). In contrast to the conventional gating strategy established in Fig. 5.1, it was important for the gates to identify CD20+ and CD20- T cells to be set apart to reduce the risk of cross-contamination

between populations. Analysis of CD20 expression immediately following cell sorting suggested that only 79% CD20+ T cells expressed CD20; however, the difficulty to obtain truly separate peaks with no overlap is a likely artefact of analysing weakly expressed markers by flow cytometry.

To investigate the dynamics of CD20 expression by T cells, CD20+ T cells were cultured in the presence or absence of PBMC with or without stimulation (Fig. 5.11). Extending a previous report that CD20 is maintained for 48 hours in culture, it was shown here that CD20 expression was maintained for 4 days when cells were cultured in isolation; in addition, CD20- T cells remained CD20-negative. However, in the presence of PBMC, CD20 was lost by around 50% of CD20+ T cells; conversely, CD20 appeared to be upregulated by some CD20- T cells (Fig. 5.11A, B). This implies that CD20 is regulated by interaction with other cells, either directly through cell-cell contact or indirectly through cytokine signals. As the effects of CD20 loss were greater following stimulation, CD20 expression was analysed for both undivided and divided cells (Fig. 5.11C, D). Loss of CD20 by CD20+ T cells was observed following proliferation, with some increased CD20 expression by CD20- T cells, suggesting that CD20 could be modulated by cell proliferation. Thus, CD20 expression appears to be induced but also reversible.

Although acquisition by trogocytosis was effectively ruled out based on the presence of CD20 mRNA in CD20+ T cells, this was further confirmed by analysing CD20 expression on PBMC following co-culture with each T cell subset (Fig. 5.11E). Loss of CD20 by CD20+ T cells was not associated with increased expression by PBMC in the same co-culture; accordingly, acquisition of CD20 by CD20- T cells was not associated with decreased CD20 expression by PBMC. This therefore suggests that CD20 is not transferred by trogocytosis, at least in this *in vitro* model.

Further supporting the concept that CD20 may be involved in cell proliferation, I demonstrated that CD20+ T cells displayed a diminished proliferative capacity compared to CD20- T cells (Fig. 5.12). T cell populations alone did not proliferate despite the addition of recombinant IL-2, possibly due to the low cell numbers used (20,000 per well). Of note, Wilk et al (2009) also demonstrated a diminished proliferative capacity of CD20+ T cells using a ^{3}H-thymidine incorporation assay (Wilk et al., 2009). The group also identified that CD20 is functional, as CD20+ T cells can mobilise calcium ions, and that these cells were four-fold more susceptible to activation-induced apoptosis than CD20- T cells (Wilk et al., 2009). These are interesting observations, because although the precise function of CD20 has not been determined and no natural ligand has been described thus far, its structure has been compared to that of an ion channel (Kanzaki et al., 1997). Consistent with this comparison, evidence suggests that CD20 plays a role in calcium conductance, as transfection of CD20 cDNA into non-lymphoid cells induces calcium transmembrane conductance identical to that observed in B cells (Bubien et al., 1993). Calcium is known to play a role in cell death; increased cytosolic levels occur during apoptosis and very high levels can promote necrosis (Rizzuto et al., 2003). In B cells, CD20 cross-linking can induce calcium-dependent cell death via activation of caspase 3 (Hofmeister et al., 2000). Although a role for CD20 in activation-induced apoptosis seems possible, observations in this chapter that CD20 is maintained on isolated CD20+ T cells suggests it is not directly involved in cell death, since these cells were still viable following 4 days of culture. Alternatively, CD20 may be a precursor of apoptosis, whereby removal of the proliferative stimulus rescues the cell from apoptosis.

5.3.6 Marker expression by CD20+ T cells

Marker expression and cytokine secretion were analysed in peripheral CD20+ T cells from healthy subjects to further characterise this population. As previously reported, decreased CD38 expression, and elevated IL-4 expression, were both observed (Fig. 5.13 & Fig. 5.14) (Wilk et al., 2009, Schuh et al., 2016). CD38 participates in many cellular functions such as signal transduction and calcium signalling; as an explanation to why CD20+ T cells express lower levels of CD38, Wilk et al (2009) hypothesised that CD20 may serve as an alternative calcium signalling molecule (Wilk et al., 2009). The elevated IL-4 expression observed in the CD8-CD20+ population is interesting, as its functions include promoting a Th2 response, which seems contradictory considering the elevated IFNγ secretion by these cells. Despite this, other Th2 cytokines (IL-5 and IL-13) were not elevated (Fig. 5.14), and the lack of significantly elevated CXCR5 in CD20+ T cells suggests that these cells do not provide B cell help in the context of functioning as follicular T cells. This then could suggest an alternative purpose for CD20+ T cell-derived IL-4. If CD20 plays a role in limiting T cell activation, IL-4 may be simultaneously upregulated as a regulatory mechanism to counteract the proinflammatory features of these cells. Indeed, IL-4 is involved in regulating inflammation and promoting tissue repair, and in the CNS can protect against autoimmune demyelination (Choi and Reiser, 1998; Furlan et al., 1998; Luzina et al., 2012).

Though not of statistical significance, there was a trend towards increased CD27 expression in CD8+CD20+ T cells, suggesting that these cells have been recently activated by antigen presenting cells (Borst et al., 2005). Contrary to previous findings, we did not observe any difference in CD69, CD25 or IL-10 in these cells (Wilk et al., 2009; Schuh et al., 2016). In this chapter, the over-representation of CD20+ T cells in the memory compartment was corrected for by comparing them to CD20- memory cells, rather than the whole CD20- T cell

population, so as not to bias the analysis; others did not do this, which may have led to apparent differences in these cells based on the fact they are memory cells, rather than the fact they express CD20 (Wilk et al., 2009; Schuh et al., 2016).

The strongest difference was seen in PD-1 expression, where significantly elevated levels were observed by CD20+ T cells in both CD8- and CD8+ subsets (Fig. 5.13). On further interrogation, it was clear that this increased frequency was largely in the CD8+ central memory subset; this was also observed for the MFI value, also suggesting an increased intensity of expression (Fig. 5.15A-D). PD-1 is an immune checkpoint inhibitor which negatively regulates T cell responses, and although often associated with exhaustion, all T cells express PD-1 following activation (Sharpe and Pauken, 2018). Considering the features of CD20+ T cells, such as their functional cytokine-secreting capacity, it seems likely that these cells are highly activated rather than exhausted.

As CD20+ T cells are biased towards a CD8 memory phenotype, the cytotoxic properties of these cells were investigated. Although perforin expression was greater in the CD8-CD20+ central memory compartment, demonstrating their increased cytotoxic potential compared to CD20- T cells, it was reduced in CD8+ effector memory and EMRA compartments (Fig. 5.16A, B). Granzyme B expression was also significantly reduced, as was granulysin to a lesser extent, whereas granzyme A expression appeared similar to CD20- T cells. These features suggest that CD8-CD20+ T cells possess increased cytolytic potential compared to CD8-CD20- T cells, whereas CD8+CD20+ T cells may have recently purged their cytolytic contents due their decreased expression of perforin. Despite these features, degranulation assays indicated that CD8+CD20+ T cells not only retain their cytolytic capacity, but the level of degranulation appeared even higher than in CD20- T cells (Fig. 5.17A, B). CD8-CD20+ T cells were also able to degranulate, as demonstrated by the increased surface expression of

CD107a over time, thus indicating a functional cytolytic response. These findings could indicate a different cytotoxic profile of CD20+ T cells compared to conventional T cells; other granzymes (H, K and M) exist in humans which were not studied in this chapter, and their possible expression by CD20+ T cells could explain how these cells retain potent cytolytic capacity despite their significantly reduced granzyme B expression (Voskoboinik et al., 2015).

The findings in this chapter of comparable IL-2 production (Fig. 5.14) and functional lytic capacity (Fig. 5.17) again suggest that these cells are not exhausted, despite their elevated PD-1 expression, since these key functions are lost early in the exhaustion process (Wherry et al., 2003). The ability to produce IL-2 also suggests that these cells have not undergone anergy in response to persistent antigen (Mescher et al., 2007). Based on the features of these cells identified thus far, it appears that CD20 expression is induced on highly activated memory T cells which show some functional loss but retain their cytokine-secreting capacity.

5.3.7 EBV reactivity of CD20+ T cells

The crucial anti-viral role of CD8+ T cells led to the investigation of antigen specificity in CD20+ T cells. Because of the high prevalence of EBV infection in the general population, and its strong association with MS, EBV reactivity was investigated (Almohmeed et al., 2013; Pakpoor et al., 2013; Laurence and Benito-Leon, 2017). Indeed, data in this chapter identified CD20+ T cells within the circulating EBV-specific CD8+ T cell pool of healthy donors, where they even appear to be enriched (Fig. 5.18). Although time constraints prevented further investigation into this phenomenon, one might speculate that, since these cells are involved in curtailing EBV infection during the lytic cycle (i.e. active replication) and appear

to enter the CSF, CD20+ T cells could play a role in controlling CNS viral responses under homeostatic conditions. Interestingly, a recent study revealed a decreased CD8+ T cell response to EBV lytic phase antigens at the onset of MS, which might lead to the accumulation of EBV-infected B cells in the CNS; the authors postulated this as a potential predisposing factor to the disease (Pender et al., 2017). Reduced frequency or a functional defect of CD20+ T cells in MS could therefore lead to inadequate viral clearance, potentially explaining a link with MS pathogenesis that remains to be explored.

5.4 Chapter Summary

Data in this chapter identify CD20+ T cells in the CSF, where they express significantly elevated IFNγ and CCR6, however no difference in frequencies were observed between MS and OND. These cells possess a highly activated phenotype but are limited in their cytotoxic potential due to reduced cytotoxic molecules, and proliferative capacity, possibly due to elevated PD-1 expression. These features suggest that CD20 may regulate activation and/or proliferation and may therefore play a protective role. So, although some studies have reported an increased frequency of these cells in several pathological conditions, such as MS, rheumatoid arthritis and ovarian cancer, a direct contributing effect has not yet been demonstrated and the possibility that they function to dampen the immune response in the presence of inflammation cannot be excluded (Palanichamy et al., 2014b; Eggleton et al., 2011; de Bruyn et al., 2015).

CHAPTER 6

GENERAL DISCUSSION

Chapter 6: General Discussion

The contributions of B cells to MS pathogenesis remain unclear. Clonal B cell populations have been identified in multiple CNS compartments, where they show features of an antigen-driven response through somatic hypermutation and VH4 segment bias (Baranzini et al., 1999; Colombo et al., 2010; Lovato et al., 2011; Rounds et al., 2015). B cells can traffic between the CNS and periphery where they may undergo clonal expansion on both sides of the BBB; however, the relative contributions of recently recruited peripheral B cells versus CNS-expanded B cells remains unclear (von Budingen et al., 2012; Palanichamy et al., 2014a). Furthermore, a pathogenic role for the humoral response in MS is also unclear. Intrathecal antibodies are a hallmark of MS, and anti-neuronal antibodies can cause neuronal damage or disease progression in animal models (Kabat et al., 1950; Puentes et al., 2017; Amor et al., 2014). However, the rapid clinical benefits mediated by anti-CD20 therapies suggests that B cells predominantly contribute to disease through antibody-independent mechanisms (Harp et al., 2010; Parker Harp et al., 2015; Hauser et al., 2008). Additionally, the possibility remains that the benefits of anti-CD20 therapies result from CD20+ T cell depletion rather than B cell depletion. In this thesis I attempted to address some of these unanswered questions by investigating multiple aspects of B cells in MS, including their phenotype and antibody repertoire in the CSF. I also carried out investigations into the phenotype and function of CD20+ T cells in MS, control groups and healthy controls.

6.1 What are the dynamics of the B cell response in MS?

A summary schematic showing a model for the development of the humoral response in MS is shown in Fig. 6.1. In early MS, the humoral response is initiated following abnormal

recognition of self-antigen in the periphery (Stern et al., 2014). One or a small number of these autoreactive B cells then migrate to the CNS, arriving at the perivascular or leptomeningeal spaces. These cells will not be permitted into the CNS proper unless they are re-activated by autoreactive T cells expressing their cognate antigen, allowing their specific migration through the glia limitans where the humoral response against self is initiated (Engelhardt et al., 2017). Following local reactivation, these autoreactive B cells may also produce plasmablasts in the perivascular space. In addition to this, autoreactive peripheral plasmablasts generated from the initial reaction could also gain access to the CNS. At this stage, CSF antibodies are largely IgGκ as they are directed towards the initiating autoantigen, however, a low level of antibodies of alternative isotypes, with reactivity towards other antigens, may be detected due to their non-specific diffusion into the CSF. Based on the heterogeneous antigen reactivity of CSF from those with CIS, it appears that the initial stages of the humoral response in MS occur some time before clinical symptoms appear.

During the early stages of disease it is likely that there is limited space for CNS residency. Ectopic lymphoid organ formation relies on the presence of other cell types and inflammatory cytokines, such as IL-17 and IL-22, and is generally associated with chronic inflammation (Zhang and Lu, 2012; Barone et al., 2015; Corsiero et al., 2016). Therefore, some of these CNS-specific memory B cells will then exit the CNS, probably via efferent lymphatics, where they can be detected in the periphery (Louveau et al., 2015b; von Budingen et al., 2012; Palanichamy et al., 2014a). Upon re-encounter with their cognate antigen in the secondary lymphoid organs, particularly the cervical lymph nodes, these cells will become re-activated and undergo subsequent germinal centre reactions, producing B cells with high affinity BCRs (Stern et al., 2014). Although this is a relatively small magnitude response, being highly diluted compared to all the other peripheral antigen specificities, clonal B cells from the CNS

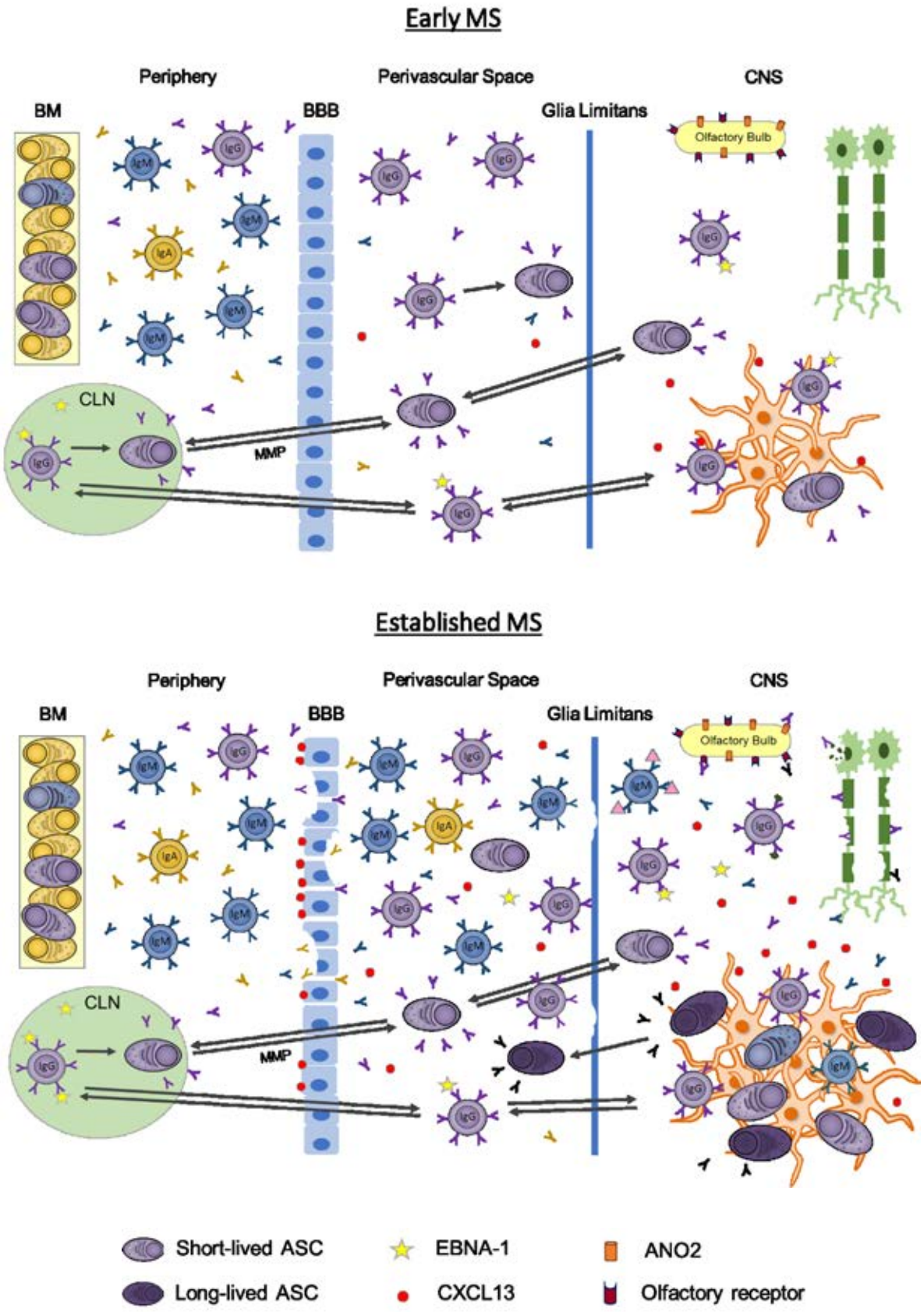

Figure 6.1. Model for the development of the humoral response in multiple sclerosis. *(continued overleaf)*

Figure 6.1. Model for the development of the humoral response in multiple sclerosis. In early MS, autoreactive IgGκ+ B cells, which have been activated in the periphery against an unknown self-antigen migrate to the perivascular space (upper panel). Local reactivation by cognate T cells (not shown) leads to their re-activation where they may differentiate into plasmablasts or migrate into the CNS. Autoreactive IgGκ+ plasmablasts generated from the initial response in the periphery may also enter the CNS compartment with the aid of molecules such as MMPs. At this stage, only IgGκ antibodies are secreted within the CNS and CSF, leading to a strong Igκ-bias, but bidirectional exchange of CNS-specific B cells and plasmablasts, and their prolonged stimulation on both sides of the BBB, allows evolution of the immune response. In established MS, inflammation at the blood-brain barrier generates a CXCL13 gradient and allows the influx of peripheral B cells of various antibody isotypes with multiple specificities, which may overcome the inflamed glia limitans and establish an increasingly diverse antibody response within the CNS (lower panel). These are often towards damage-associated antigens, such as neuronal and olfactory components (e.g. ANO2), and the resulting antibodies possess various heavy and light chain combinations, leading to a low Igκ:Igλ ratio. These infiltrating B cells may then set up residency within established CNS niches, which also permit the generation of long-lived plasma cells, although they may be out-competed by more recently generated plasmablasts and expelled into the CSF.

may be still detected in the periphery, and resulting antibodies from this reaction may occasionally be detected in the periphery as a biased light chain ratio. These cells may then be permitted access to the CNS compartment once again, where their higher affinity for antigen may permit their retention, or they may again exit the CNS via efferent lymphatics. Repeated rounds of affinity maturation may eventually lead to divergence from the original initiating autoantigen, causing spreading of the antibody response to other epitopes and/or antigens as time progresses.

Despite this memory B cell enrichment, most B cells entering the CSF at time of diagnostic sampling appear to not be disease-specific and are likely present as a consequence of inflammatory activity, based on their similar immunoglobulin isotype to those in the periphery. The relatively high proportion of IgM+ B cells in MS CSF suggests that unswitched memory B cells and possibly naïve B cells also gain access to the CSF compartment; this is likely a consequence of inflammation and increased migratory activity at the BBB, in which pro-inflammatory cytokines disrupt endothelial cell-cell junctions

(Kermode et al., 1990; Minagar and Alexander, 2003). Indeed, B cell arrival at the inflamed CNS is facilitated by chemokines, particularly CXCL13; this thesis along with other studies have demonstrated the relationship between intrathecal CXCL13 and CSF B cell frequencies (Krumbholz et al., 2006; Kowarik et al., 2012; Puthenparampil et al., 2017). Inflammatory conditions also promote the formation and expansion of CNS survival niches, and elevated pro-inflammatory cytokines such as IL-6 promote plasma cell survival and maturation (Radbruch et al., 2006). Therefore, since the inflamed CNS is conducive for B cell survival, at least some of these IgM+ B cells may be retained, where they differentiate into ASC; in support of this, it has been shown that switched IgM+ B cells may undergo bidirectional exchange and affinity maturation in both peripheral and CNS compartments (Palanichamy et al., 2014a). This scenario may also apply to switched B cells expressing other immunoglobulin isotypes that are not specific for CNS antigens, and this sequence of events explains the heterogeneous antibody repertoire in MS, which recognises multiple ubiquitous targets that are not specific to the CNS (Brändle et al., 2016). Mechanisms favouring the retention and differentiation of B cells in the CNS could result from affinity for their specific antigen; animal studies have shown that high affinity germinal centre B cells have lower death rates compared to low affinity B cells, and that only those with high affinity for their antigen can differentiate into ASC (Phan et al., 2006; Anderson et al., 2009). Therefore, in the very early stages, only disease-specific B cells may be retained within the limited number of CNS survival niches, but with increasing duration, an increasing number of B cells with multiple specificities are retained.

So, while the memory B cell response in established disease appears to be characterised by a relatively high turnover, the ASC response may be less dynamic, as suggested by the distinct differences in immunoglobulin isotypes between peripheral and CSF ASC. It also appears that

this isotype distribution is maintained throughout the disease course, as other studies identified almost all ASC as IgG+ in post-mortem MS brain tissue (Esiri, 1977, Stern et al., 2014). Additionally, sequencing studies have demonstrated little clonal overlap between CD19+ B cells and CD138+ ASC in MS CSF, indicating that the CNS ASC compartment is largely sustained independently of B cells. Studies have shown that CD19+ B cell sequences are more diverse and contain less clonal populations than CD138+ ASC; in contrast, there are strong clonal relationships between CD19+ plasmablasts and CD19- plasma cells in MS CSF (Ritchie et al., 2004; Winges et al., 2007). This concept is supported by Vh segment analysis, showing that CSF ASC are strongly Vh4-biased, which is not always present in the IgG+ CSF B cell repertoire (Owens et al., 2007). In line with our own findings, which identified mature, IgGκ-biased CD19- ASC in MS CSF, this confirms that the MS CNS has the capacity to sustain an evolving B cell response.

Although evidence demonstrates a strong CNS component of the ASC response, migration of peripheral ASC (i.e. plasmablasts) into the CNS remains a possibility (Piccio et al., 2010). In addition to CNS infiltration by B cells not specific to MS, this phenomenon could contribute to the broad reactivity of CSF antibodies. Furthermore, that CSF OCB are reduced or eliminated in around 45% of individuals treated with natalizumab indicates that antibody production is at least partly driven by peripherally-derived B-lineage cells (Mancuso et al., 2014). Several studies have demonstrated evidence of clonally related ASC in both the CNS and peripheral blood, including the production of matched OCB and the identification of related sequences by deep sequencing in both compartments (Obermeier et al., 2008; Bankoti et al., 2014; Palanichamy et al., 2014a). Aside from the migration of IgG+ ASC to inflammatory sites, ASC can secrete MMP-2 and MMP-9 under inflammatory conditions, which are specifically required for the cleavage of dystroglycan at the BBB, permitting

migration across the parenchymal basement membrane (Kunkel and Butcher, 2003; Di Girolamo et al., 1998; Trocme et al., 1998; Agrawal et al., 2006; Song et al., 2015). Accordingly, CSF levels of MMP-9 significantly correlate with ASC frequency, and are increased during acute relapse, pointing to their possible migration into the CNS (Kuenz et al., 2008). Therefore, it seems likely that ASC, generated in the cervical lymph nodes from post-CNS B cells, could migrate to the CNS and continue the immune response (Stern et al., 2014).

6.2 Is the FLC Igκ:Igλ ratio a marker of epitope spreading in MS?

A novel undertaking of this thesis was the investigation of the Igκ:Igλ ratio as a potential marker of epitope spreading in MS; a biological phenomenon in which the antibody repertoire becomes diversified following an initial dominant epitope-specific response (Vanderlugt and Miller, 2002). Several lines of evidence support B cell epitope spreading in MS. In a relapsing-remitting EAE model, interaction of MOG-reactive B cells with transgenic autoimmune T cells bearing a specific MOG peptide induced their expansion towards other MOG epitopes (Pollinger et al., 2009). In myelin proteolipid protein (PLP)-induced EAE, epitope spreading was shown to correlate with disease progression; the initial antibody response towards PLP expanded to multiple epitopes over the course of 67 days (Kidd et al., 2008). In a study of childhood MS, consecutive serum antibody profiles indicated spreading of the immune response to CNS antigens up to twelve months after disease onset compared to those with a monophasic CNS event (Quintana et al., 2014). And finally, it was observed that

CSF containing a single band progressed to an oligoclonal response in MS but not in other conditions following subsequent LP (Davies et al., 2003). In addition, there is also evidence for T cell-mediated epitope spreading in both EAE and MS, which correlates with disease severity (Ellmerich et al., 2004; Davies et al., 2005).

In this thesis, a biased Igκ:Igλ ratio of around 10:1 was identified in MS CSF. In contrast, a 1977 study identified Igκ-biased ASC in post-mortem MS brain tissue with an average ratio of 2.3:1 in active lesions; this significantly lower ratio compared to the relatively early (diagnostic) stages of MS, as investigated in this thesis, supports the concept of epitope spreading with disease progression (Esiri, 1977).

The heterogeneous nature of MS and the benefits of early therapeutic intervention highlight the value of reliable prognostic markers in MS (Kappos et al., 2006; Comi et al., 2009; Ziemssen et al., 2015). Although some promising biomarkers have been identified thus far, such as CSF neurofilament light chains or chitinase 3-like 1, they appear to represent CNS damage, which may not necessarily be consistent with the disease course, and their ability to predict longer term disability remains to be seen (Canto et al., 2015; Puentes et al., 2017; Soelberg Sorensen and Sellebjerg, 2016). Findings from this thesis that the CSF FLC Igκ:Igλ ratio is specifically elevated in MS groups compared to OND and ONID controls, is intrinsically linked to CSF ASC, and is stable following repeat sampling could make this an attractive potential biomarker. Although no significant difference in the FLC Igκ:Igλ ratio was seen between CIS and established MS in the small sample size used in this thesis, our larger study has shown a more marked difference, which was indicative of disease accumulation. It was shown that those with an FLC Igκ:Igλ ratio of >10:1 had significantly lower accumulation of disability at 5-year follow-up, as measured by EDSS, compared to

those with a ratio below 10:1 (Rathbone et al., 2018). These findings, which link antibody diversification with disease progression, agree with studies from the Monson group which used the accumulation of somatic hypermutations in MS CSF B cells to predict conversion from CIS to CDMS with 91% accuracy (Cameron et al., 2009; Ligocki et al., 2010).

This scenario then suggests that Igκ-expressing B cells, specific for an elusive common antigen, populate the CNS first due to their re-activation by antigen-specific T cells, where they differentiate into short-lived plasmablasts. Some of these cells then undergo terminal differentiation into long-lived plasma cells, where they cease migratory capacity and become dependent on the CNS niche for survival (Radbruch et al., 2006). With disease evolution, an expanding CNS B cell population will lead to competition from recently generated ASC for a space within the niche, and long-lived ASC may be expelled and replaced (Odendahl et al., 2005). Findings in this thesis of CD19- ASC in MS CSF, which are generally more Igκ-biased than CD19+ ASC, support this hypothesis.

6.3 What are the potential mechanisms of MS pathogenesis?

Analysis of post-mortem MS brain tissue showed a Igκ:Igλ ratio of 2.3:1 in active lesions compared to a lower ratio of 1.6:1 in inactive lesions and non-lesional tissue (Esiri, 1977). This could suggest that re-appearance of the Igκ-inducing antigen within the CNS contributes to acute inflammatory activity. Periodic reactivation of EBV within the CNS may account for this, which may also partly explain some of the discrepancies in the literature regarding the small proportion of individuals with intrathecal synthesis of anti-EBV antibodies (Bonnan, 2014; Burnard et al., 2017). An anti-EBV response in MS is also supported by findings in this

thesis, which identified higher EBNA-1 reactivity in MS CSF compared to OND controls, in accordance with several other studies (Cepok et al., 2005b; Hecker et al., 2016; Ayoglu et al., 2016). This could then support the concept of molecular mimicry, in which the Igκ-biased response towards EBV cross-reacts with self-proteins; this could include the N-terminal of alpha B-crystallin, which is homologous to a region of EBNA-1 (Hecker et al., 2016).

An interesting hypothesis relates to alpha B-crystallin, a small heat-shock protein and candidate MS autoantigen (van Noort et al., 1995). EBV infection of B cells has been shown to induce alpha B-crystallin expression, which is then presented via HLA-DR to T cells; furthermore, unlike other stress-induced heat-shock proteins, alpha B-crystallin is not constitutively expressed in human lymphoid tissues under normal conditions, but is found in all other animal species examined, potentially explaining why MS is a uniquely human disease (van Sechel et al., 1999). This constitutive lack of expression could prevent the formation of immunological tolerance towards alpha B-crystallin, which also serves as an immunodominant myelin antigen, where its presentation by EBV-infected B cells to autoreactive T cells may lead to CNS damage; accordingly, alpha B-crystallin accumulates in the MS brain (van Noort et al., 1995; van Noort et al., 2010; van Noort et al., 2012). This scenario is consistent with Pender's hypothesis, in which defective clearance of EBV-infected B cells leads to their persistence and subsequent accumulation in the CNS (Pender, 2011; Pender et al., 2017). EBV preferentially infects memory B cells, and through altering the expression of chemokine receptors – for example, increasing CCR6 expression – may promote their migration to the CNS (Cepok et al., 2005b; Joseph et al., 2000; Nakayama et al., 2002; Reboldi et al., 2009). As shown in this thesis, the sustained elevation of CSF Igκ following inhibition of lymphocyte trafficking with natalizumab indicates the long-term survival of ASC in these individuals, which is independent of peripheral B cell recruitment.

Similarly, another study found that Igκ FLC was increased following intrathecal rituximab treatment, and that CSF B cells were not depleted, despite the significant reduction in peripheral B cells (Topping et al., 2016). This could implicate a role for EBV in transforming CNS-resident B cells and in maintaining the Igκ-biased antibody response which persists in the absence of peripheral lymphocyte trafficking. Additionally, the preferential association of EBV-infected B cells with ectopic follicles in MS CNS could suggest that these follicles have resulted from their expansion (Serafini et al., 2007). ASC derived from infected memory B cells can sustain a functional EBV pool, and this differentiation activates the replicative cycle of EBV (Laichalk and Thorley-Lawson, 2005; Al Tabaa et al., 2009). Shedding of the virus from infected ASC may then infect memory B cells arriving from the periphery, leading to their subsequent transformation, and allowing their prolonged survival where they can provide co-stimulation to autoreactive T cells arriving at the CNS (Pender, 2011).

6.4 Could CD20+ T cells be involved in MS pathology?

Since CD20+ T cells are also depleted by rituximab, we asked whether these cells might be associated with MS pathogenesis (Wilk et al., 2009; Palanichamy et al., 2014b). The novel findings in this thesis that CD20+ T cells may enter the CSF, based on their elevated CCR6 expression, where they retain their ability to secrete high levels of IFNγ, could indicate that these cells are pathogenic; however, their presence in OND CSF suggests that CD20+ T cells are likely part of a normal physiological response. Including the CSF and peripheral blood, as investigated in this thesis, CD20+ T cells have also been identified in other bodily compartments, such as the liver, lymph node, thymus, bone marrow, brain, synovial fluid and ascites (Algino et al., 1996; Wilk et al., 2009; Holley et al., 2014; de Bruyn et al., 2015;

Schuh et al., 2016). Features of these cells, including elevated IFNγ expression and reduced granzyme B and perforin expression, suggest they have recently been activated and have purged their cytolytic contents; although these cells still retain functional cytolytic capacity, their reduced proliferation and elevated PD-1 expression suggests that CD20 may act to limit potentially damaging T cell responses by curtailing activation. For example, in B cells, CD20 becomes heavily phosphorylated following PMA stimulation, which occurs in conjunction with abnormally high intracellular calcium levels; CD20 on T cells is also associated with calcium flux, suggesting the two processes are related and that CD20 may modulate T cell functions in response to stimulation (Valentine et al., 1987; Genot et al., 1991; Wilk et al., 2009).

Another observation in this thesis was the apparent decrease in CD20+ T cells in MS CSF; interestingly, this was also observed in another study (Schuh et al., 2016). If CD20 expression is induced on highly activated T cells to limit their activation, their lower frequency in MS could suggest that this protective mechanism is faulty, leading to loss of control and exacerbated inflammation. Alternatively, the presence of CD20+ T cells may be a remnant of a prior anti-viral response, including towards EBV; this is in line with the observation that CD20+ T cells appear to be over-represented in the normal CD8+ memory T cell pool towards EBV lytic antigens. Interestingly, a recent study identified decreased CD8+ T cell responses to EBV lytic antigens in MS (Pender et al., 2017). It is therefore tempting to speculate that the defective response of MS T cells towards EBV-infected B cells manifests as a reduced frequency of CD20+ T cells.

6.5 A case for neuro-protective B cells in MS?

The use of immunomodulators have offered insights into the role of immune cells in MS. Memory B cells are the major contributing B cell subset to MS pathogenesis, as demonstrated by their depletion observed with all current MS therapies, many of which were believed to act via T cell inhibition (Baker et al., 2017a; Baker et al., 2017b). In this instance, sparing naïve B cells may prove beneficial, since central tolerance checkpoints remain intact in MS and therefore autoreactive B cells will not be found in this pool (Kinnunen et al., 2013). It therefore seems important for new immunotherapies to consider sparing non-pathogenic subsets, particularly considering the potentially damaging consequences of widespread targeting of immune populations. A prime example is the increased inflammatory activity seen following depletion of BAFF and APRIL by atacicept in two MS clinical trials, where the harmful effects of blocking ASC function appears to indicate some protective function for these cells (Kappos et al., 2014; Sergott et al., 2015). Another therapeutic failure in MS resulted from TNFα blockade; a seemingly contradictory outcome, considering the positive effects in RA and EAE (Lenercept MS study group, 1999; Moreland et al., 1997; Selmaj et al., 1991). Development of ectopic lymphoid structures, a characteristic pathological feature of RA, is abrogated following anti-TNFα treatment, and in a mouse model of atherosclerosis, TNFα was shown to be critical for tertiary lymphoid organ development (Canete et al., 2009; Furtado et al., 2014). Therefore, it can be speculated that the removal of ectopic lymphoid follicles by TNFα blockade in MS also depletes protective ASC. Indeed, Matsumoto et al showed that protective compensatory mechanisms arise during inflammation to limit further damage (Matsumoto et al., 2014). It was demonstrated that in EAE but not control mice, plasmablasts generated in the draining lymph nodes following disease induction

predominantly expressed IL-10 and contributed to curtailing autoimmunity, and genetic ablation of the ASC transcription factors IRF4 and BLIMP-1 led to exacerbated disease (Matsumoto et al., 2014).

In addition to a protective role via cytokine secretion, ASC may also secrete protective antibodies. It has also been shown that ASC generated from regulatory B10 cells rapidly produced polyreactive IgG and IgM antibodies which may promote the clearance of common antigens, such as those associated with apoptotic debris (Maseda et al., 2012; Schwartz-Albiez et al., 2009). Natural autoreactive antibodies are reported to promote CNS repair via several mechanisms, such as preventing neuron apoptosis or activating intracellular repair-promoting signals in CNS cells; remyelinating antibodies have also been investigated clinically for their therapeutic potential (Paz Soldan et al., 2003; Wright et al., 2009; Eisen et al., 2017). B cells may also provide CNS protection under homeostatic conditions; it was recently shown that B cells are the predominant infiltrating lymphocyte subset in the developing mouse brain, where they promote oligodendrogenesis (Tanabe and Yamashita, 2018). These data collectively indicate that the balance between regulatory and pathogenic ASC may modulate disease severity and raise the possibility that regulatory ASC may generate protective antibodies in MS.

In all, the heterogeneity of the B cell response, and their multiple and sometimes contradictory contributions to MS, raises the possibility that MS may be preferentially driven by certain lymphocyte subsets which varies between individuals. MS lesions demonstrate immunological heterogeneity between individuals, for example showing signs of T cell-mediated (pattern I) or antibody-mediated (pattern II) damage, and these lesion patterns remained consistent in consecutive biopsies from the same individuals (Lucchinetti et al., 2000; Metz et al., 2014). This implicates different pathological mechanisms between

individuals, and may allow for more targeted immunomodulators to be administered based on the underlying immunopathology; immunological heterogeneity may also explain the variable responses to anti-CD20 therapy, which although beneficial for many, some individuals continue to accumulate disability (Cross et al., 2006). As such, these variable immunophenotypes are an important consideration and may have important implications for the development of personalised therapies.

6.6 Further Work

Following on from this thesis, investigating the diagnostic and prognostic relevance of the CSF Igκ:Igλ ratio in a large cohort over an extended time period could determine the extent of its association with disability accumulation, and whether it has use as a biomarker in MS. Longitudinal analysis of the Igκ:Igλ ratio, for example, in response to relapse or infectious agents, may provide evidence of its involvement in epitope spreading and/or disease progression. Further investigating the CSF antibody reactivity of Igκ and Igλ in a larger cohort, against unconventional and full-length proteins, may help to identify the specificity of the dominant IgGκ antibodies found in MS. This could be achieved by immunohistochemistry of CSF antibodies on fresh-frozen MS brain sections and detection with anti-Igκ or anti-Igλ antibodies. Or, column purification of CSF IgG antibodies following incubation with MS brain lysate, and performing mass spectrometry on antibody-antigen complexes. Understanding the molecular trigger(s) of MS could allow the development of antigen-specific tolerance mechanisms, antigen-specific adoptive immunotherapy or even vaccination. In relation to EBV, phase I clinical trials are currently underway into an EBV-specific adoptive immunotherapy in MS (Pender et al., 2014). The therapies involve expanding and

infusing EBV-specific T cells, as performed in a proof of principle study by Pender et al., and are reportedly showing positive results thus far (Pender et al., 2014; Pender, 2017).

As discussed, the presence of B cells in MS CSF is not necessarily indicative of their involvement in disease; intracellular cytokine analysis by CSF B lineage cells could shed more light on the involvement of B cell subsets in MS. It is known that peripheral B cells in MS express lower IL-10 and higher pro-inflammatory cytokines such as IL-6 and GM-CSF, but the cytokine-secreting properties of CSF-derived B cells have not been explored thus far (Barr et al., 2012; Li et al., 2015; Guerrier et al., 2018). In line with this, developing safer and more focussed therapies which specifically deplete pathogenic memory B cells will potentially be important; future therapies may be able to predict disease progression and response to therapy based on the immunophenotype by analysing CSF or blood lymphocyte populations, for example, by using mass cytometry to analyse up to 42 parameters, or using next generation sequencing to identify disease-associated SNPs (Kay et al., 2016; Vrijenhoek et al., 2015).

Finally, although this thesis unravelled several novel aspects of CD20+ T cell biology, many questions remain unanswered. The precise function of CD20 on T cells, if any, and its dynamics on these cells, remain elusive. Observations in this thesis suggest that CD20 is inducible in these cells; therefore, analysis of methylation status may inform whether CD20 is regulated at the epigenetic level. Importantly, a potential role for these cells in MS remains elusive; a larger scale study, including CSF analysis, and the response of these cells towards EBV peptides *in vitro* may provide more information.

Appendix I Demographics for Chapter 3.

Disease group (n)	Age	Sex ratio (F:M)
OND (17)	50 (25 – 74)	1.28:1
ONID (7)	57 (35 – 78)	0.75:1
CIS (10)	49.5 (30 – 69)	2.3:1
MS (14)	41.5 (20 – 66)	1:1
NAT (14)	38 (25 – 54)	6:1

Appendix I. Demographics for Chapter 3. Matched blood and CSF samples were obtained from MS groups and those with OND and ONID as controls. The median age and range and female to male sex ratio is shown where information was available.
OND; other neurological disease, ONID; other neurological inflammatory disease, CIS; clinically isolated syndrome, NAT; MS patients recently ceasing natalizumab therapy. The MS group consisted of 9 RRMS and 5 PPMS cases.

Appendix II Demographics for Chapter 4.

A

Disease group (n)	Age
OND (6)	34.5 (22 – 65)
CIS (6)	43.5 (33 – 70)
RRMS (6)	34 (19 – 46)

B

CSF sample	Total FLC (mg/L)	Igκ:Igλ FLC ratio
CIS 1	26.158	204.97
CIS 2	22.892	89.84
CIS 3	17.988	88.49
CIS 4	9.386	83.56
CIS 5	15.474	72.69
CIS 6	18.499	43.90
RRMS 1	13.162	0.34
RRMS 2	21.511	4.80
RRMS 3	18.622	4.03
RRMS 4	14.097	1.73
RRMS 5	6.452	1.24
RRMS 6	17.536	1.20
OND 1	<0.112	N/A
OND 2	<0.112	N/A
OND 3	<0.112	N/A
OND 4	<0.112	N/A
OND 5	<0.112	N/A
OND 6	<0.112	N/A

C

Disease group (n)	Age
OND (79)	41 (17 – 66)
ONID (28)	53 (24 – 83)
CIS (51)	45 (21 – 70)
RRMS (36)	42.5 (19 – 72)
PPMS (23)	53.5 (35 – 71)
NAT (18)	36 (24 – 54)

Appendix II. Demographics and FLC data for Chapter 4. For the first part of the project using planar antigen arrays, six CSF samples from individuals with OND, CIS and RRMS were selected **(A)**. The number of sample per group and median age and range is shown. MS samples were selected based on their high (CIS) or low (RRMS) Igκ:Igλ FLC ratios **(B)**. CSF samples used in the second part of the project using suspension bead arrays **(C)**. These samples were solely selected based on their diagnosis. The number of sample per group and median age and range is shown. The CIS group consisted of 4 individuals with a diagnosis of radiologically isolated syndrome (RIS).

Appendix III Demographics for Chapter 5.

Disease group (n)	Age	Sex ratio (F:M)
OND (7)	70 (28 – 74)	1:1
MS (6)	45 (36 – 55)	5:1

Appendix III. Demographics for Chapter 5. Matched blood and CSF samples were obtained from MS (2 CIS and 4 RRMS) and OND groups. The number of samples, median age and range, and the female to male sex ratio is shown.

Appendix IV

Positive hits identified using planar arrays were selected for verification using suspension bead arrays *(continued overleaf).*

Gene (n)	Gene Description	UniProt
ACAD9 (3)	acyl-CoA dehydrogenase family, member 9	Q9H845
ANO2 (3)	anoctamin 2, calcium activated chloride channel	Q9NQ90
AP2A2 (2)	adaptor-related protein complex 2, alpha 2 subunit	O94973
ARID4B (4)	AT rich interactive domain 4B (RBP1-like)	Q4LE39
ARRDC4 (2)	arrestin domain containing 4	Q8NCT1
ASTN1 (6)	astrotactin 1	O14525
ASXL1 (3)	additional sex combs like transcriptional regulator 1	Q8IXJ9
AXL (3)	AXL receptor tyrosine kinase	P30530
BCL10 (3)	B-cell CLL/lymphoma 10	O95999
CCDC137 (2)	coiled-coil domain containing 137	Q6PK04
CCDC85C (2)	coiled-coil domain containing 85C	A6NKD9
CCNY (2)	cyclin Y	Q8ND76
CDAN1 (2)	codanin 1	Q8IWY9
CUEDC2 (3)	CUE domain containing 2	Q9H467
DCAF6 (4)	DDB1 and CUL4 associated factor 6	Q58WW2
EIF4E3 (2)	eukaryotic translation initiation factor 4E family member 3	Q8N5X7
EPHB1 (4)	EPH receptor B1	P54762
EPOR (5)	erythropoietin receptor	P19235
FAM65B (3)	family with sequence similarity 65, member B	Q9Y4F9
FOSB (2)	FBJ murine osteosarcoma viral oncogene homolog B	P53539
GRINA (3)	glutamate receptor, ionotropic, N-methyl D-aspartate-associated protein 1	Q7Z429
HERC2 (5)	HECT and RLD domain containing E3 ubiquitin protein ligase 2	O95714
IFI27 (2)	interferon, alpha-inducible protein 27	
IFNLR1 (3)	interferon, lambda receptor 1	Q8IU57
KDELR1 (1)	KDEL (Lys-Asp-Glu-Leu) endoplasmic reticulum protein retention receptor 1	P24390
KDELR2 (1)	KDEL (Lys-Asp-Glu-Leu) endoplasmic reticulum protein retention receptor 2	P33947
KLK9 (2)	kallikrein-related peptidase 9	Q9UKQ9
LPIN2 (3)	lipin 2	Q92539
LZTS2 (3)	leucine zipper, putative tumour suppressor 2	Q9BRK4
NANS (2)	N-acetylneuraminic acid synthase	Q9NR45
NPW (2)	neuropeptide W	Q8N729
NT5C1A (2)	5'-nucleotidase, cytosolic IA	Q9BXI3
OR10AG1 (3)	olfactory receptor, family 10, subfamily AG, member 1	Q8NH19
OR11H1;OR11H12;OR11H2 (1)	olfactory receptor, family 11, subfamily H, member 1; olfactory receptor, family 11, subfamily H, member 12; olfactory receptor, family 11, subfamily H, member 2	Q8NG94;B2RN74;Q8NH07
OR1L3 (1)	olfactory receptor, family 1, subfamily L, member 3	Q8NH93
OSER1 (2)	oxidative stress responsive serine-rich 1	Q9NX31
PGAM5 (2)	PGAM family member 5, serine/threonine protein phosphatase, mitochondrial	Q96HS1

PMM1 (3)	phosphomannomutase 1	Q92871
QTRT1 (3)	queuine tRNA-ribosyltransferase 1	Q9BXR0
RDH5 (2)	retinol dehydrogenase 5 (11-cis/9-cis)	Q92781
RRM1 (4)	ribonucleotide reductase M1	P23921
SMAD7 (3)	SMAD family member 7	O15105
SPICE1 (3)	spindle and centriole associated protein 1	Q8N0Z3
TACR1 (4)	tachykinin receptor 1	P25103
TAF3 (5)	TAF3 RNA polymerase II, TATA box binding protein (TBP)-associated factor, 140kDa	Q5VWG9
THNSL1 (3)	threonine synthase-like 1	Q8IYQ7
TMEM62 (3)	transmembrane protein 62	Q0P6H9
TMEM8C (2)	transmembrane protein 8C	A6NI61
TRA2A (1)	transformer 2 alpha homolog (Drosophila)	Q13595
TRA2B (2)	transformer 2 beta homolog (Drosophila)	P62995
TTC39C (5)	tetratricopeptide repeat domain 39C	Q8N584
USP13 (3)	ubiquitin specific peptidase 13 (isopeptidase T-3)	Q92995
VPS18 (2)	vacuolar protein sorting 18 homolog (S. cerevisiae)	Q9P253
ZNF488 (3)	zinc finger protein 488	Q96MN9
ZNF688 (3)	zinc finger protein 688	P0C7X2

Appendix IV. Positive hits identified using planar arrays were selected for verification using suspension bead arrays. Based on the initial discovery phase, antigens were selected for the verification phase using suspension bead arrays. Depending on the size and complexity, one or multiple PrESTs were generated for each antigen.

Appendix V

Antigens from the literature were included in the suspension bead arrays *(continued overleaf).*

Gene (n)	Gene Description	UniProt
ACTA2;ACTG2;POTEF;POTEI;POTEJ;POTEE;ACTG1;ACTB;ACTC1;ACTA1;ACTBL2 (3)	actin, alpha 2, smooth muscle, aorta; actin, gamma 2, smooth muscle, enteric;POTE ankyrin domain family, member F;POTE ankyrin domain family, member I;POTE ankyrin domain family, member J;POTE ankyrin domain family, member E; actin gamma 1;actin, beta; actin, alpha, cardiac muscle 1;actin, alpha 1, skeletal muscle; actin, beta-like 2	P62736;P63267;A5A3E0;P0CG38;P0CG39;Q6S8J3;P63261;P60709;P68032;P68133;Q562R1
ACTN1 (2)	actinin, alpha 1	P12814
ACTN4;ACTN1;ACTN3;ACTN2 (1)	actinin, alpha 4; actinin, alpha 1; actinin, alpha 3 (gene/pseudogene); actinin, alpha 2	O43707;P12814;Q08043;P35609
ARFGAP1 (2)	ADP-ribosylation factor GTPase activating protein 1	Q8N6T3
ARID3B (3)	AT rich interactive domain 3B (BRIGHT-like)	Q8IVW6
ARRB1 (2)	arrestin, beta 1	P49407
ATF4 (4)	activating transcription factor 4	P18848
ATP10A (3)	ATPase, class V, type 10A	O60312
ATP5SL (2)	ATP5S-like	Q9NW81
BEX4 (2)	brain expressed, X-linked 4	Q9NWD9
CDKL1 (3)	cyclin-dependent kinase-like 1 (CDC2-related kinase)	Q00532
CDS1 (2)	CDP-diacylglycerol synthase (phosphatidate cytidylyltransferase) 1	Q92903
CKB (1)	creatine kinase, brain	P12277
CNTN2 (3)	contactin 2 (axonal)	Q02246
COL5A1 (5)	collagen, type V, alpha 1	P20908
CRYAB (3)	crystallin, alpha B	P02511
DRD5 (4)	dopamine receptor D5	P21918
EHMT2 (3)	euchromatic histone-lysine N-methyltransferase 2	Q96KQ7
ENO3;ENO2;ENO1 (4)	enolase 3 (beta, muscle); enolase 2 (gamma, neuronal); enolase 1, (alpha)	P13929;P09104;P06733
GABRE (3)	gamma-aminobutyric acid (GABA) A receptor, epsilon	P78334
GFM2 (3)	G elongation factor, mitochondrial 2	Q969S9
GPR62 (1)	G protein-coupled receptor 62	Q9BZJ7
HHEX (4)	haematopoietically expressed homeobox	Q03014
IFNB1 (3)	Interferon, beta 1, fibroblast	P01574
INSM2 (2)	Insulinoma-associated 2	Q96T92
KCNJ10 (5)	potassium channel, inwardly rectifying subfamily J, member 10	P78508
KIAA1614 (3)	KIAA1614 (uncharacterised protein)	Q5VZ46
KIF15 (3)	kinesin family member 15	Q9NS87
LATS2 (4)	large tumor suppressor kinase 2	Q9NRM7
MAG (3)	myelin associated glycoprotein	P20916
MBP (3)	myelin basic protein	P02686
MED6 (4)	mediator complex subunit 6	O75586
MOG (1)	myelin oligodendrocyte glycoprotein	Q16653
MRPL43 (2)	mitochondrial ribosomal protein L43	Q8N983

MYDGF (2)	myeloid-derived growth factor	Q969H8
NCOA2 (5)	nuclear receptor coactivator 2	Q15596
NEFL (1)	neurofilament, light polypeptide	P07196
NRXN1 (6)	neurexin 1	P58400;Q9ULB1
PAGE2B;PAGE2;PAGE5 (2)	P antigen family, member 2B;P antigen family, member 2 (prostate associated);P antigen family, member 5 (prostate associated)	Q5JRK9;Q7Z2X7;Q96GU1
PARP3 (7)	poly (ADP-ribose) polymerase family, member 3	Q9Y6F1
QSOX1 (3)	quiescin Q6 sulfhydryl oxidase 1	O00391
RABEP2 (2)	rabaptin, RAB GTPase binding effector protein 2	Q9H5N1
RBPJ (6)	recombination signal binding protein for immunoglobulin kappa J region	Q06330
S100A1 (1)	S100 calcium binding protein A1	P23297
SEC63 (3)	SEC63 homolog, protein translocation regulator	Q9UGP8
TKT (2)	transketolase	P29401
TMEM134 (2)	transmembrane protein 134	Q9H6X4
TNNT2 (2)	troponin T type 2 (cardiac)	P45379
TUBB1;TUBB8;TUBB2A;TUBB2B;TUBB;TUBB4A;TUBB6;TUBB4B;RP11-566K11.2;TUBB3 (2)	tubulin, beta 1 class VI; tubulin, beta 8 class VIII ;tubulin, beta 2A class IIa; tubulin, beta 2B class IIb; tubulin, beta class I; tubulin, beta 4A class IVa; tubulin, beta 6 class V; tubulin, beta 4B class IVb; tubulin, beta 3 class III	Q9H4B7;Q3ZCM7;Q13885;Q9BVA1;P07437;P04350;Q9BUF5;P68371;Q13509
TUBB8;TUBB2A;TUBB2B;TUBB;TUBB4A;TUBB6;TUBB4B;RP11-566K11.2;TUBB3 (1)	tubulin, beta 8 class VIII; tubulin, beta 2A class IIa; tubulin, beta 2B class IIb; tubulin, beta class I; tubulin, beta 4A class IVa; tubulin, beta 6 class V; tubulin, beta 4B class IVb; tubulin, beta 3 class III	Q3ZCM7;Q13885;Q9BVA1;P07437;P04350;Q9BUF5;P68371;Q13509

Appendix V. Antigens from the literature were included in the suspension bead arrays. Antigens identified in the literature, including those previously identified by the group, were selected for the verification phase using suspension bead arrays. Depending on the size and complexity, one or multiple PrESTs were generated for each antigen.

References

Agahozo, M. C., Peferoen, L., Baker, D., et al. 2016. CD20 therapies in multiple sclerosis and experimental autoimmune encephalomyelitis - Targeting T or B cells? *Mult Scler Relat Disord,* 9**,** 110-7.

Agematsu, K., Nagumo, H., Yang, F. C., et al. 1997. B cell subpopulations separated by CD27 and crucial collaboration of CD27+ B cells and helper T cells in immunoglobulin production. *Eur J Immunol,* 27**,** 2073-9.

Agrawal, S., Anderson, P., Durbeej, M., et al. 2006. Dystroglycan is selectively cleaved at the parenchymal basement membrane at sites of leukocyte extravasation in experimental autoimmune encephalomyelitis. *J Exp Med,* 203**,** 1007-19.

Aharoni, R. 2013. The mechanism of action of glatiramer acetate in multiple sclerosis and beyond. *Autoimmun Rev,* 12**,** 543-53.

Ahuja, A., Anderson, S. M., Khalil, A., et al. 2008. Maintenance of the plasma cell pool is independent of memory B cells. *PNAS USA,* 105**,** 4802-4807.

Al Tabaa, Y., Tuaillon, E., Bollore, K., et al. 2009. Functional Epstein-Barr virus reservoir in plasma cells derived from infected peripheral blood memory B cells. *Blood,* 113**,** 604-11.

Alcina, A., Abad-Grau, M. D. M., Fedetz, M., et al. 2012. Multiple Sclerosis Risk Variant HLA-DRB1*1501 Associates with High Expression of DRB1 Gene in Different Human Populations. *PLoS One,* 7**,** e29819.

Algino, K. M., Thomason, R. W., King, D. E., et al. 1996. CD20 (pan-B cell antigen) expression on bone marrow-derived T cells. *Am J Clin Pathol,* 106**,** 78-81.

Allen, C. D. C., Okada, T. & Cyster, J. G. 2007. Germinal Center Organization and Cellular Dynamics. *Immunity,* 27**,** 190-202.

Almohmeed, Y. H., Avenell, A., Aucott, L., et al. 2013. Systematic Review and Meta-Analysis of the Sero-Epidemiological Association between Epstein Barr Virus and Multiple Sclerosis. *PLoS One,* 8**,** e61110.

Alter, A., Duddy, M., Hebert, S., et al. 2003. Determinants of human B cell migration across brain endothelial cells. *J Immunol,* 170**,** 4497-505.

Alter, G., Malenfant, J. M. & Altfeld, M. 2004. CD107a as a functional marker for the identification of natural killer cell activity. *J Immunol Meth,* 294**,** 15-22.

Alunno, A., Carubbi, F., Bistoni, O., et al. 2016. Interleukin (IL)-17-producing pathogenic T lymphocytes co-express CD20 and are depleted by rituximab in primary Sjogren's syndrome: a pilot study. *Clin Exp Immunol,* 184**,** 284-92.

Amor, S., Van Der Star, B. J., Bosca, I., et al. 2014. Neurofilament light antibodies in serum reflect response to natalizumab treatment in multiple sclerosis. *Mult Scler,* 20**,** 1355-62.

Andersen, M. H., Schrama, D., Thor Straten, P., et al. 2006. Cytotoxic T cells. *J Invest Dermatol,* 126**,** 32-41.

Anderson, M. S., Venanzi, E. S., Klein, L., et al. 2002. Projection of an immunological self shadow within the thymus by the aire protein. *Science,* 298**,** 1395-401.

Anderson, S. M., Khalil, A., Uduman, M., et al. 2009. Taking advantage: high-affinity B cells in the germinal center have lower death rates, but similar rates of division, compared to low-affinity cells. *J Immunol,* 183**,** 7314-25.

Anthony, I. C., Crawford, D. H. & Bell, J. E. 2003. B lymphocytes in the normal brain: contrasts with HIV-associated lymphoid infiltrates and lymphomas. *Brain,* 126**,** 1058-67.

Arellano, G., Ottum, P. A., Reyes, L. I., et al. 2015. Stage-Specific Role of Interferon-Gamma in Experimental Autoimmune Encephalomyelitis and Multiple Sclerosis. *Frontiers in Immunology,* 6**,** 492.

Artyomov, M. N., Lis, M., Devadas, S., et al. 2010. CD4 and CD8 binding to MHC molecules primarily acts to enhance Lck delivery. *Proc Natl Acad Sci U S A,* 107**,** 16916-21.

Ascherio, A. & Munger, K. L. 2007. Environmental risk factors for multiple sclerosis. Part I: the role of infection. *Ann Neurol,* 61**,** 288-99.

Ashton-Rickardt, P. G. 2012. An Emerging Role for Serine Protease Inhibitors in T Lymphocyte Immunity and Beyond. *ISRN Immunology,* 2012**,** 15.

Attaf, M., Legut, M., Cole, D. K., et al. 2015. The T cell antigen receptor: the Swiss army knife of the immune system. *Clin Exp Immunol,* 181**,** 1-18.

Ayoglu, B., Haggmark, A., Khademi, M., et al. 2013. Autoantibody profiling in multiple sclerosis using arrays of human protein fragments. *Mol Cell Proteomics,* 12**,** 2657-72.

Ayoglu, B., Mitsios, N., Kockum, I., et al. 2016. Anoctamin 2 identified as an autoimmune target in multiple sclerosis. *Proc Natl Acad Sci U S A,* 113**,** 2188-93.

Babbe, H., Roers, A., Waisman, A., et al. 2000. Clonal expansions of CD8(+) T cells dominate the T cell infiltrate in active multiple sclerosis lesions as shown by micromanipulation and single cell polymerase chain reaction. *J Exp Med,* 192**,** 393-404.

Baker, D., Herrod, S. S., Alvarez-Gonzalez, C., et al. 2017a. Both cladribine and alemtuzumab may effect MS via B-cell depletion. *Neuro Neuroimmunol & Neuroinflamm,* 4**,** e360.

Baker, D., Marta, M., Pryce, G., et al. 2017b. Memory B Cells are Major Targets for Effective Immunotherapy in Relapsing Multiple Sclerosis. *EBioMedicine,* 16**,** 41-50.

Balashov, K. E., Khoury, S. J., Hafler, D. A., et al. 1995. Inhibition of T cell responses by activated human CD8+ T cells is mediated by interferon-gamma and is defective in chronic progressive multiple sclerosis. *J Clin Invest,* 95**,** 2711-2719.

Bankoti, J., Apeltsin, L., Hauser, S. L., et al. 2014. In multiple sclerosis, oligoclonal bands connect to peripheral B-cell responses. *Ann Neurol,* 75**,** 266-76.

Bar-Or, A., Calabresi, P. A., Arnold, D., et al. 2008. Rituximab in relapsing-remitting multiple sclerosis: a 72-week, open-label, phase I trial. *Ann Neurol,* 63**,** 395-400.

Baranzini, S. E., Jeong, M. C., Butunoi, C., et al. 1999. B cell repertoire diversity and clonal expansion in multiple sclerosis brain lesions. *J Immunol,* 163**,** 5133-44.

Barber, D. L., Andrade, B. B., Sereti, I., et al. 2012. Immune reconstitution inflammatory syndrome: the trouble with immunity when you had none. *Nat Rev Micro,* 10**,** 150-156.

Barlow, D. J., Edwards, M. S. & Thornton, J. M. 1986. Continuous and discontinuous protein antigenic determinants. *Nature,* 322**,** 747-8.

Barnidge, D. R., Dasari, S., Ramirez-Alvarado, M., et al. 2014. Phenotyping polyclonal kappa and lambda light chain molecular mass distributions in patient serum using mass spectrometry. *J Proteome Res,* 13**,** 5198-205.

Barone, F., Nayar, S., Campos, J., et al. 2015. IL-22 regulates lymphoid chemokine production and assembly of tertiary lymphoid organs. *Proc Natl Acad Sci U S A,* 112**,** 11024-9.

Barr, T. A., Shen, P., Brown, S., et al. 2012. B cell depletion therapy ameliorates autoimmune disease through ablation of IL-6–producing B cells. *J Exp Med,* 209**,** 1001-1010.

Bartholomaus, I., Kawakami, N., Odoardi, F., et al. 2009. Effector T cell interactions with meningeal vascular structures in nascent autoimmune CNS lesions. *Nature,* 462**,** 94-8.

Basten, A. & Silveira, P. A. 2010. B-cell tolerance: mechanisms and implications. *Curr Opin Immunol,* 22**,** 566-74.

Beecham, A. H., Patsopoulos, N. A., Xifara, D. K., et al. 2013. Analysis of immune-related loci identifies 48 new susceptibility variants for multiple sclerosis. *Nat Genet,* 45**,** 1353-60.

Belnoue, E., Pihlgren, M., Mcgaha, T. L., et al. 2008. APRIL is critical for plasmablast survival in the bone marrow and poorly expressed by early-life bone marrow stromal cells. *Blood,* 111**,** 2755-64.

Bennett, J. L., Haubold, K., Ritchie, A. M., et al. 2008. CSF IgG Heavy-Chain Bias in Patients at the Time of a Clinically Isolated Syndrome. *J neuroimmunol,* 199**,** 126-32.

Beresford, P. J., Zhang, D., Oh, D. Y., et al. 2001. Granzyme A activates an endoplasmic reticulum-associated caspase-independent nuclease to induce single-stranded DNA nicks. *J Biol Chem,* 276**,** 43285-93.

Berge, T., Leikfoss, I. S., Brorson, I. S., et al. 2016. The multiple sclerosis susceptibility genes TAGAP and IL2RA are regulated by vitamin D in CD4+ T cells. *Genes Immun*.

Blalock, J. E., Zhou, S. R., Maier, C. C., et al. 1999. Highly related immunoglobulin light chain sequences in different multiple sclerosis patients. *J Neuroimmunol,* 100**,** 98-101.

Blauth, K., Owens, G. P. & Bennett, J. L. 2015. The Ins and Outs of B Cells in Multiple Sclerosis. *Front Immunol,* 6**,** 565.

Blum, J. S., Wearsch, P. A. & Cresswell, P. 2013. Pathways of antigen processing. *Annu Rev Immunol,* 31**,** 443-73.

Bonnan, M. 2014. Does disease-irrelevant intrathecal synthesis in multiple sclerosis make sense in the light of tertiary lymphoid organs? *Front Neurol,* 5**,** 27.

Borst, J., Hendriks, J. & Xiao, Y. 2005. CD27 and CD70 in T cell and B cell activation. *Curr Opin Immunol,* 17**,** 275-81.

Bostrom, I., Stawiarz, L. & Landtblom, A. M. 2013. Sex ratio of multiple sclerosis in the National Swedish MS Register (SMSreg). *Mult Scler,* 19**,** 46-52.

Botelho, F. M., Edwards, D. R. & Richards, C. D. 1998. Oncostatin M stimulates c-Fos to bind a transcriptionally responsive AP-1 element within the tissue inhibitor of metalloproteinase-1 promoter. *J Biol Chem,* 273**,** 5211-8.

Bradwell, A. R., Carr-Smith, H. D., Mead, G. P., et al. 2001. Highly sensitive, automated immunoassay for immunoglobulin free light chains in serum and urine. *Clin Chem,* 47**,** 673-80.

Brändle, S. M., Obermeier, B., Senel, M., et al. 2016. Distinct oligoclonal band antibodies in multiple sclerosis recognize ubiquitous self-proteins. *PNAS USA,* 113, 7864-9.

Brennan, K. M., Galban-Horcajo, F., Rinaldi, S., et al. 2011. Lipid arrays identify myelin-derived lipids and lipid complexes as prominent targets for oligoclonal band antibodies in multiple sclerosis. *J Neuroimmunol,* 238**,** 87-95.

Briney, B. S. & Jr, J. E. C. 2013. Secondary mechanisms of diversification in the human antibody repertoire. *Frontiers in Immunology,* 4**,** 42.

Brinkman, C. C., Rouhani, S. J., Srinivasan, N., et al. 2013. Peripheral tissue homing receptors enable T cell entry into lymph nodes and affect the anatomical distribution of memory cells. *J immunol,* 191**,** 2412-2425.

Bubien, J. K., Zhou, L. J., Bell, P. D., et al. 1993. Transfection of the CD20 cell surface molecule into ectopic cell types generates a Ca2+ conductance found constitutively in B lymphocytes. *J Cell Biol,* 121**,** 1121-32.

Burnard, S., Lechner-Scott, J. & Scott, R. J. EBV and MS: Major cause, minor contribution or red-herring? *Multiple Sclerosis and Related Disorders,* 16**,** 24-30.

Bystrom, S., Ayoglu, B., Haggmark, A., et al. 2014. Affinity proteomic profiling of plasma, cerebrospinal fluid, and brain tissue within multiple sclerosis. *J Proteome Res,* 13**,** 4607-19.

Calabrese, M., Magliozzi, R., Ciccarelli, O., et al. 2015. Exploring the origins of grey matter damage in multiple sclerosis. *Nat Rev Neurosci,* 16**,** 147-58.

Cameron, E. M., Spencer, S., Lazarini, J., et al. 2009. Potential of a unique antibody gene signature to predict conversion to clinically definite multiple sclerosis. *J Neuroimmunol,* 213**,** 123-30.

Canete, J. D., Celis, R., Moll, C., et al. 2009. Clinical significance of synovial lymphoid neogenesis and its reversal after anti-tumour necrosis factor alpha therapy in rheumatoid arthritis. *Ann Rheum Dis,* 68**,** 751-6.

Canto, E., Tintore, M., Villar, L. M., et al. 2015. Chitinase 3-like 1: prognostic biomarker in clinically isolated syndromes. *Brain,* 138**,** 918-31.

Cao, Y., Goods, B. A., Raddassi, K., et al. 2015. Functional inflammatory profiles distinguish myelin-reactive T cells from patients with multiple sclerosis. *Sci Transl Med,* 7**,** 287ra74.

Caraux, A., Klein, B., Paiva, B., et al. 2010. Circulating human B and plasma cells. Age-associated changes in counts and detailed characterization of circulating normal CD138- and CD138+ plasma cells. *Haematologica,* 95**,** 1016-20.

Cenci, S. & Sitia, R. 2007. Managing and exploiting stress in the antibody factory. *FEBS Lett,* 581**,** 3652-7.

Cepok, S., Jacobsen, M., Schock, S., et al. 2001. Patterns of cerebrospinal fluid pathology correlate with disease progression in multiple sclerosis. *Brain,* 124**,** 2169-2176.

Cepok, S., Rosche, B., Grummel, V., et al. 2005a. Short-lived plasma blasts are the main B cell effector subset during the course of multiple sclerosis. *Brain,* 128**,** 1667-76.

Cepok, S., Von Geldern, G., Grummel, V., et al. 2006. Accumulation of class switched IgD−IgM− memory B cells in the cerebrospinal fluid during neuroinflammation. *J Neuroimmunol,* 180**,** 33-39.

Cepok, S., Zhou, D., Srivastava, R., et al. 2005b. Identification of Epstein-Barr virus proteins as putative targets of the immune response in multiple sclerosis. *J Clin Invest,* 115**,** 1352-60.

Cerutti, A., Cols, M. & Puga, I. 2013. Marginal zone B cells: virtues of innatelike antibody-producing lymphocytes. *Nature reviews. Immunology,* 13**,** 118-32.

Chen, A. M., Khanna, N., Stohlman, S. A., et al. 2005. Virus-specific and bystander CD8 T cells recruited during virus-induced encephalomyelitis. *J Virol,* 79**,** 4700-8.

Chen, D., Ireland, S. J., Davis, L. S., et al. 2016a. Autoreactive CD19+CD20- Plasma Cells Contribute to Disease Severity of Experimental Autoimmune Encephalomyelitis. *J Immunol*. 196:1541-9.

Chen, H. I., Akpolat, I., Mody, D. R., et al. 2006. Restricted kappa/lambda light chain ratio by flow cytometry in germinal center B cells in Hashimoto thyroiditis. *Am J Clin Pathol,* 125**,** 42-8.

Chen, J., Chia, N., Kalari, K. R., et al. 2016b. Multiple sclerosis patients have a distinct gut microbiota compared to healthy controls. *Sci Rep,* 6**,** 28484.

Chen, M. L., Yan, B. S., Kozoriz, D., et al. 2009. Novel CD8+ Treg suppress EAE by TGF-beta- and IFN-gamma-dependent mechanisms. *Eur J Immunol,* 39**,** 3423-35.

Chihara, N., Aranami, T., Oki, S., et al. 2013. Plasmablasts as migratory IgG-producing cells in the pathogenesis of neuromyelitis optica. *PLoS One,* 8**,** e83036.

Chmielewska-Badora, J., Cisak, E. & Dutkiewicz, J. 2000. Lyme borreliosis and multiple sclerosis: any connection? A seroepidemic study. *Ann Agric Environ Med,* 7**,** 141-3.

Choi, P. & Reiser, H. 1998. IL-4: role in disease and regulation of production. *Clin Exp Immunol,* 113**,** 317-319.

Chorny, A., Puga, I. & Cerutti, A. 2010. Innate Signaling Networks in Mucosal IgA Class Switching. *Advan Immunol,* 107**,** 31-69.

Chowdhury, D. & Lieberman, J. 2008. Death by a thousand cuts: granzyme pathways of programmed cell death. *Annu Rev Immunol,* 26**,** 389-420.

Chu, V. T., Fröhlich, A., Steinhauser, G., et al. 2011. Eosinophils are required for the maintenance of plasma cells in the bone marrow. *Nat Immunol,* 12**,** 151.

Cobaleda, C., Schebesta, A., Delogu, A., et al. 2007. Pax5: the guardian of B cell identity and function. *Nat Immunol,* 8**,** 463-70.

Colombo, M., Dono, M., Gazzola, P., et al. 2000. Accumulation of clonally related B lymphocytes in the cerebrospinal fluid of multiple sclerosis patients. *J Immunol,* 164**,** 2782-9.

Comi, G., Martinelli, V., Rodegher, M., et al. 2009. Effect of glatiramer acetate on conversion to clinically definite multiple sclerosis in patients with clinically isolated syndrome (PreCISe study): a randomised, double-blind, placebo-controlled trial. *Lancet,* 374**,** 1503-11.

Compston, A. & Coles, A. 2008. Multiple sclerosis. *Lancet,* 372**,** 1502-17.

Constantinescu, C. S., Farooqi, N., O'brien, K., et al. 2011. Experimental autoimmune encephalomyelitis (EAE) as a model for multiple sclerosis (MS). *Br J Pharmacol,* 164**,** 1079-106.

Corcione, A., Casazza, S., Ferretti, E., et al. 2004. Recapitulation of B cell differentiation in the central nervous system of patients with multiple sclerosis. *Proc Natl Acad Sci U S A,* 101**,** 11064-9.

Corsiero, E., Nerviani, A., Bombardieri, M., et al. 2016. Ectopic Lymphoid Structures: Powerhouse of Autoimmunity. *Front Immunol,* 7**,** 430.

Corthay, A. 2009. How do regulatory T cells work? *Scand J Immunol,* 70**,** 326-36.

Costes, V., Magen, V., Legouffe, E., et al. 1999. The Mi15 monoclonal antibody (anti-syndecan-1) is a reliable marker for quantifying plasma cells in paraffin-embedded bone marrow biopsy specimens. *Hum Pathol,* 30**,** 1405-11.

Crawford, M. P., Yan, S. X., Ortega, S. B., et al. 2004. High prevalence of autoreactive, neuroantigen-specific CD8+ T cells in multiple sclerosis revealed by novel flow cytometric assay. *Blood,* 103**,** 4222-31.

Crome, S. Q., Wang, A. Y. & Levings, M. K. 2010. Translational Mini-Review Series on Th17 Cells: Function and regulation of human T helper 17 cells in health and disease. *Clin Exp Immunol,* 159**,** 109-19.

Cross, A. H., Stark, J. L., Lauber, J., et al. 2006. Rituximab reduces B cells and T cells in cerebrospinal fluid of multiple sclerosis patients. *J neuroimmunol,* 180**,** 63-70.

Crotty, S. 2014. T follicular helper cell differentiation, function, and roles in disease. *Immunity,* 41**,** 529-42.

Das, S., Nikolaidis, N. & Nei, M. 2009. Genomic organization and evolution of immunoglobulin kappa gene enhancers and kappa deleting element in mammals. *Mol Immunol,* 46**,** 3171-3177.

Davies, G., Keir, G., Thompson, E. J., et al. 2003. The clinical significance of an intrathecal monoclonal immunoglobulin band. *A follow-up study,* 60**,** 1163-6.

Davies, S., Nicholson, T., Laura, M., et al. 2005. Spread of T Lymphocyte Immune Responses to Myelin Epitopes With Duration of Multiple Sclerosis. *Journal of Neuropath & Exp Neuro,* 64**,** 371-7.

De Bruyn, M., Wiersma, V. R., Wouters, M. C., et al. 2015. CD20 T cells have a predominantly Tc1 effector memory phenotype and are expanded in the ascites of patients with ovarian cancer. *Oncoimmunol,* 4**,** e999536.

De Graaf, M. T., De Jongste, A. H., Kraan, J., et al. 2011. Flow cytometric characterization of cerebrospinal fluid cells. *Cytometry B Clin Cytom,* 80**,** 271-81.

De Jager, P. L. 2011. Genome-wide association study of severity in multiple sclerosis: International Multiple Sclerosis Genetics Consortium. *Gen and Immu,* 12**,** 615-25.

Deenick, E. K., Hasbold, J. & Hodgkin, P. D. 2005. Decision criteria for resolving isotype switching conflicts by B cells. *Eur J Immunol,* 35**,** 2949-55.

Defranco, A. L. 1996. The two-headed antigen. B-cell co-receptors. *Curr Biol,* 6**,** 548-50.

Deluca, G. C., Joseph, A., George, J., et al. 2015. Olfactory Pathology in Central Nervous System Demyelinating Diseases. *Brain Path,* 25**,** 543-51.

Dendrou, C. A., Fugger, L. & Friese, M. A. 2015. Immunopathology of multiple sclerosis. *Nat Rev Immunol,* 15**,** 545-58.

Derbinski, J., Schulte, A., Kyewski, B., et al. 2001. Promiscuous gene expression in medullary thymic epithelial cells mirrors the peripheral self. *Nat Immunol,* 2**,** 1032-9.

Derfuss, T., Hohlfeld, R. & Meinl, E. 2005. Intrathecal antibody (IgG) production against human herpesvirus type 6 occurs in about 20% of multiple sclerosis patients and might be linked to a polyspecific B-cell response. *J Neurol,* 252**,** 968-71.

Di Girolamo, N., Tedla, N., Lloyd, A., et al. 1998. Expression of matrix metalloproteinases by human plasma cells and B lymphocytes. *Eur J Immunol,* 28**,** 1773-84.

Diamond, B., Honig, G., Mader, S., et al. 2013. Brain-reactive antibodies and disease. *Ann Rev Immunol,* 31**,** 345-85.

Didonna, A. & Oksenberg, J. R. 2015. Genetic determinants of risk and progression in multiple sclerosis. *Clin Chim Acta,* 449**,** 16-22.

Disanto, G., Berlanga, A. J., Handel, A. E., et al. 2011. Heterogeneity in Multiple Sclerosis: Scratching the Surface of a Complex Disease. *Autoimmune Diseases,* 2011.

Doyle, H. A. & Mamula, M. J. 2012. Autoantigenesis: The evolution of protein modifications in autoimmune disease. *Current Opinion in Immunology,* 24**,** 112-118.

Duddy, M., Niino, M., Adatia, F., et al. 2007. Distinct effector cytokine profiles of memory and naive human B cell subsets and implication in multiple sclerosis. *J Immunol,* 178**,** 6092-9.

Earl, L. A. & Baum, L. G. 2008. CD45 glycosylation controls T-cell life and death. *Immunol Cell Biol,* 86**,** 608-15.

Edwards, L. J., Robins, R. A. & Constantinescu, C. S. 2010. Th17/Th1 phenotype in demyelinating disease. *Cytokine,* 50**,** 19-23.

Eggers, E. L., Michel, B. A., Wu, H., et al. 2017. Clonal relationships of CSF B cells in treatment-naïve multiple sclerosis patients. *JCI Insight.* 16, pii: 92724.

Eggleton, P., Bremer, E., Tarr, J. M., et al. 2011. Frequency of Th17 CD20+ cells in the peripheral blood of rheumatoid arthritis patients is higher compared to healthy subjects. *Arthritis Res Ther,* 13**,** R208.

Eisen, A., Greenberg, B. M., Bowen, J. D., et al. 2017. A double-blind, placebo-controlled, single ascending-dose study of remyelinating antibody rHIgM22 in people with multiple sclerosis. *Mult Scler J Exp Transl Clin,* 3**,** 2055217317743097.

Ellmerich, S., Takacs, K., Mycko, M., et al. 2004. Disease-related epitope spread in a humanized T cell receptor transgenic model of multiple sclerosis. *Eur J Immunol,* 34**,** 1839-48.

Ely, K. H., Cauley, L. S., Roberts, A. D., et al. 2003. Nonspecific recruitment of memory CD8+ T cells to the lung airways during respiratory virus infections. *J Immunol,* 170**,** 1423-9.

Engelhardt, B. & Ransohoff, R. M. 2012. Capture, crawl, cross: the T cell code to breach the blood-brain barriers. *Trends Immunol,* 33**,** 579-89.

Engelhardt, B., Vajkoczy, P. & Weller, R. O. 2017. The movers and shapers in immune privilege of the CNS. *Nat Immunol,* 18**,** 123-131.

Esiri, M. M. 1977. Immunoglobulin-containing cells in multiple-sclerosis plaques. *Lancet,* 2**,** 478.

Falschlehner, C., Schaefer, U. & Walczak, H. 2009. Following TRAIL's path in the immune system. *Immunol,* 127**,** 145-54.

Farez, M. F., Mascanfroni, I. D., Mendez-Huergo, S. P., et al. 2015. Melatonin Contributes to the Seasonality of Multiple Sclerosis Relapses. *Cell,* 162**,** 1338-52.

Farias, A. S., Pradella, F., Schmitt, A., et al. 2014. Ten years of proteomics in multiple sclerosis. *Proteomics,* 14**,** 467-80.

Felgenhauer, K., Schadlich, H. J., Nekic, M., et al. 1985. Cerebrospinal fluid virus antibodies. A diagnostic indicator for multiple sclerosis? *J Neurol Sci,* 71**,** 291-9.

Ferber, I. A., Brocke, S., Taylor-Edwards, C., et al. 1996. Mice with a disrupted IFN-gamma gene are susceptible to the induction of experimental autoimmune encephalomyelitis (EAE). *The J Immunol,* 156**,** 5-7.

Fernandez-Menendez, S., Fernandez-Moran, M., Fernandez-Vega, I., et al. 2016. Epstein-Barr virus and multiple sclerosis. From evidence to therapeutic strategies. *J Neurol Sci,* 361**,** 213-9.

Fidler, J. M., Dejoy, S. Q. & Gibbons, J. J. 1986. Selective immunomodulation by the antineoplastic agent mitoxantrone. I. Suppression of B lymphocyte function. *The J Immunol,* 137**,** 727-32.

Fink, K. 2012. Origin and Function of Circulating Plasmablasts during Acute Viral Infections. *Front Immunol,* 3**,** 78.

Fisniku, L. K., Brex, P. A., Altmann, D. R., et al. 2008. Disability and T2 MRI lesions: a 20-year follow-up of patients with relapse onset of multiple sclerosis. *Brain,* 131**,** 808-17.

Fletcher, J. M., Lalor, S. J., Sweeney, C. M., et al. 2010. T cells in multiple sclerosis and experimental autoimmune encephalomyelitis. *Clin Exp Immunol,* 162**,** 1-11.

Flores-Montero, J., De Tute, R., Paiva, B., et al. 2016. Immunophenotype of normal vs. myeloma plasma cells: Toward antibody panel specifications for MRD detection in multiple myeloma. *Cytometry B Clin Cytom,* 90**,** 61-72.

Ford, M. L. & Evavold, B. D. 2005. Specificity, magnitude, and kinetics of MOG-specific CD8+ T cell responses during experimental autoimmune encephalomyelitis. *European J Immunol,* 35**,** 76-85.

Franciotta, D., Columba-Cabezas, S., Andreoni, L., et al. Oligoclonal IgG band patterns in inflammatory demyelinating human and mouse diseases. *J Neuroimmunol,* 200**,** 125-128.

Fraussen, J., De Bock, L. & Somers, V. 2016. B cells and antibodies in progressive multiple sclerosis: Contribution to neurodegeneration and progression. *Autoimmun Rev,* 15**,** 896-9.

Fuertes Marraco, S. A., Neubert, N. J., Verdeil, G., et al. 2015. Inhibitory Receptors Beyond T Cell Exhaustion. *Fronti Immunol,* 6**,** 310.

Fujimoto, M., Fujimoto, Y., Poe, J. C., et al. 2000. CD19 regulates Src family protein tyrosine kinase activation in B lymphocytes through processive amplification. *Immunity,* 13**,** 47-57.

Funaro, A., Morra, M., Calosso, L., et al. 1997. Role of the human CD38 molecule in B cell activation and proliferation. *Tissue Antigens,* 49**,** 7-15.

Furlan, R., Poliani, P. L., Galbiati, F., et al. 1998. Central Nervous System Delivery of Interleukin 4 by a Nonreplicative Herpes Simplex Type 1 Viral Vector Ameliorates Autoimmune Demyelination. *Human Gene Therapy,* 9**,** 2605-17.

Furtado, G. C., Pacer, M. E., Bongers, G., et al. 2014. TNFα-dependent development of lymphoid tissue in the absence of RORγt(+) Lymphoid Tissue Inducer cells. *Mucosal Immunol,* 7**,** 602-14.

Gajofatto, A. & Benedetti, M. D. 2015. Treatment strategies for multiple sclerosis: When to start, when to change, when to stop? *World J Clin Cases : WJCC,* 3**,** 545-555.

Gandoglia, I., Ivaldi, F., Laroni, A., et al. 2017. Teriflunomide treatment reduces B cells in patients with MS. *Neuro Neuroimmunol & Neuroinflamm,* 4**,** e403.

Geland, J.M., Cree, B.A., Hauser, S.L. 2017. Ocrelizumab and other CD20+ B cell-depleting therapies in multiple sclerosis. *Neurotherapeutics,* 14, 835-41.

Genot, E., Valentine, M. A., Degos, L., et al. 1991. Hyperphosphorylation of CD20 in hairy cells. Alteration by low molecular weight B cell growth factor and IFN-alpha. *J Immunol,* 146**,** 870-8.

Germain, R. N. 2002. T-cell development and the CD4-CD8 lineage decision. *Nat Rev Immunol,* 2**,** 309-22.

Giovannoni, G. 2014. Cerebrospinal fluid analysis. *Handb Clin Neurol,* 122**,** 681-702.

Good, K. L. & Tangye, S. G. 2007. Decreased expression of Kruppel-like factors in memory B cells induces the rapid response typical of secondary antibody responses. *PNAS USA,* 104**,** 13420-5.

Goodnow, C. C., Crosbie, J., Adelstein, S., et al. 1988. Altered immunoglobulin expression and functional silencing of self-reactive B lymphocytes in transgenic mice. *Nature,* 334**,** 676-82.

Gottenberg, J. E., Aucouturier, F., Goetz, J., et al. 2007. Serum immunoglobulin free light chain assessment in rheumatoid arthritis and primary Sjögren's syndrome. *Ann Rheum Dis,* 66**,** 23-27.

Goverman, J. 2009. Autoimmune T cell responses in the central nervous system. *Nat Rev Immunol,* 9**,** 393-407.

Gran, B., Gestri, D., Sottini, A., et al. 1998. Detection of skewed T-cell receptor V-beta gene usage in the peripheral blood of patients with multiple sclerosis. *J Neuroimmunol,* 85**,** 22-32.

Grawunder, U., Leu, T. M., Schatz, D. G., et al. 1995. Down-regulation of RAG1 and RAG2 gene expression in preB cells after functional immunoglobulin heavy chain rearrangement. *Immunity,* 3**,** 601-8.

Groves, A., Kihara, Y. & Chun, J. 2013. Fingolimod: direct CNS effects of sphingosine 1-phosphate (S1P) receptor modulation and implications in multiple sclerosis therapy. *J Neurol Sci,* 328**,** 9-18.

Guerrier, T., Labalette, M., Launay, D., et al. 2018. Proinflammatory B-cell profile in the early phases of MS predicts an active disease. *Neuro Neuroimmunol & Neuroinflamm,* 5**,** e431.

Gururajan, M., Sindhava, V. & Bondada, S. 2014. B Cell Tolerance in Health and Disease. *Antibodies,* 3**,** 116.

Gyülvészi, G., Haak, S. & Becher, B. 2009. IL-23-driven encephalo-tropism and Th17 polarization during CNS-inflammation in vivo. *European J Immunol,* 39**,** 1864-1869.

Haak, S., Croxford, A. L., Kreymborg, K., et al. 2009. IL-17A and IL-17F do not contribute vitally to autoimmune neuro-inflammation in mice. *The J Clin Invest* 119**,** 61-69.

Häggmark, A., Byström, S., Ayoglu, B., et al. 2013. Antibody-based profiling of cerebrospinal fluid within multiple sclerosis. *Proteomics,* 13**,** 2256-2267.

Haider, L. 2015. Inflammation, Iron, Energy Failure, and Oxidative Stress in the Pathogenesis of Multiple Sclerosis. *Ox Med Cell Longev,* 2015**,** 10.

Haider, L., Fischer, M. T., Frischer, J. M., et al. 2011. Oxidative damage in multiple sclerosis lesions. *Brain,* 134**,** 1914-24.

Halliley, J. L., Tipton, C. M., Liesveld, J., et al. 2015. Long-Lived Plasma Cells Are Contained within the CD19(-)CD38(hi)CD138(+) Subset in Human Bone Marrow. *Immunity,* 43**,** 132-45.

Harauz, G., Ladizhansky, V. & Boggs, J. M. 2009. Structural polymorphism and multifunctionality of myelin basic protein. *Biochemistry,* 48**,** 8094-104.

Harp, C., Lee, J., Lambracht-Washington, D., et al. 2007. Cerebrospinal fluid B cells from multiple sclerosis patients are subject to normal germinal center selection. *J Neuroimmunol,* 183**,** 189-99.

Harp, C. T., Ireland, S., Davis, L. S., et al. 2010. Memory B cells from a subset of treatment-naive relapsing-remitting multiple sclerosis patients elicit CD4(+) T-cell proliferation and IFN-gamma production in response to myelin basic protein and myelin oligodendrocyte glycoprotein. *Eur J Immunol,* 40**,** 2942-56.

Harrer, A., Pilz, G., Wipfler, P., et al. 2015. High interindividual variability in the CD4/CD8 T cell ratio and natalizumab concentration levels in the cerebrospinal fluid of patients with multiple sclerosis. *Clin Exp Immunol,* 180**,** 383-92.

Harwood, N. E. & Batista, F. D. 2010. Early events in B cell activation. *Annu Rev Immunol,* 28**,** 185-210.

Hassan-Smith, G., Durant, L., Tsentemeidou, A., et al. 2014. High sensitivity and specificity of elevated cerebrospinal fluid kappa free light chains in suspected multiple sclerosis. *J Neuroimmunol,* 276**,** 175-9.

Hassani, A., Corboy, J. R., Al-Salam, S., et al. 2018. Epstein-Barr virus is present in the brain of most cases of multiple sclerosis and may engage more than just B cells. *PloS One,* 13**,** e0192109.

Hatton, O. L., Arnold-Harris, A., Schaffert, S., et al. 2014. The Interplay Between Epstein Barr Virus and B Lymphocytes: Implications for Infection, Immunity, and Disease. *Immunol Res,* 58**,** 268-76.

Hauser, A. E., Debes, G. F., Arce, S., et al. 2002. Chemotactic responsiveness toward ligands for CXCR3 and CXCR4 is regulated on plasma blasts during the time course of a memory immune response. *J Immunol,* 169**,** 1277-82.

Hauser, S. L., Bhan, A. K., Gilles, F., et al. 1986. Immunohistochemical analysis of the cellular infiltrate in multiple sclerosis lesions. *Ann Neurol,* 19**,** 578-87.

Hauser, S. L., Waubant, E., Arnold, D. L., et al. 2008. B-cell depletion with rituximab in relapsing-remitting multiple sclerosis. *N Engl J Med,* 358**,** 676-88.

Hauser, S. L., Bar-Or, A., Comi, G., et al. 2017. Ocrelizumab versus Interferon Beta-1a in Relapsing Multiple Sclerosis. *N Engl J Med*, 376(3);221-34.

Hawkins, S. A. & Mcdonnell, G. V. 1999. Benign multiple sclerosis? Clinical course, long term follow up, and assessment of prognostic factors. *J Neurol Neurosurg Psychiatry,* 67**,** 148-52.

He, B., Xu, W., Santini, P. A., et al. 2007. Intestinal bacteria trigger T cell-independent immunoglobulin A(2) class switching by inducing epithelial-cell secretion of the cytokine APRIL. *Immunity,* 26**,** 812-26.

Hecker, M., Fitzner, B., Wendt, M., et al. 2016. High-density peptide microarray analysis of IgG autoantibody reactivities in serum and cerebrospinal fluid of multiple sclerosis patients. *Mol Cell Proteomics*.

Hedegaard, C. J., Chen, N., Sellebjerg, F., et al. 2009. Autoantibodies to myelin basic protein (MBP) in healthy individuals and in patients with multiple sclerosis: a role in regulating cytokine responses to MBP. *Immunology,* 128**,** e451-61.

Heesters, B. A., Myers, R. C. & Carroll, M. C. 2014. Follicular dendritic cells: dynamic antigen libraries. *Nat Rev Immunol,* 14**,** 495-504.

Henry, C., Ramadan, A., Montcuquet, N., et al. 2010. CD3+CD20+ cells may be an artifact of flow cytometry: comment on the article by Wilk et al. *Arthritis Rheum,* 62**,** 2561-3; author reply 2563-5.

Henson, S. M., Riddell, N. E. & Akbar, A. N. 2012. Properties of end-stage human T cells defined by CD45RA re-expression. *Curr Opin Immunol,* 24**,** 476-81.

Hobeika, E., Nielsen, P. J. & Medgyesi, D. 2015. Signaling mechanisms regulating B-lymphocyte activation and tolerance. *J Mol Med,* 93**,** 143-58.

Hoffman, W., Lakkis, F. G. & Chalasani, G. 2016. B Cells, Antibodies, and More. *Clin J Am Soc Nephrol,* 11**,** 137-54.

Hofmeister, J. K., Cooney, D. & Coggeshall, K. M. 2000. Clustered CD20 induced apoptosis: src-family kinase, the proximal regulator of tyrosine phosphorylation, calcium influx, and caspase 3-dependent apoptosis. *Blood Cells Mol Dis,* 26**,** 133-43.

Hohlfeld, R., Dornmair, K., Meinl, E., et al. 2015a. The search for the target antigens of multiple sclerosis, part 1: autoreactive CD4+ T lymphocytes as pathogenic effectors and therapeutic targets. *Lancet Neurol*.

Hohlfeld, R., Dornmair, K., Meinl, E., et al. 2015b. The search for the target antigens of multiple sclerosis, part 2: CD8+ T cells, B cells, and antibodies in the focus of reverse-translational research. *Lancet Neurol*.

Holley, J. E., Bremer, E., Kendall, A. C., et al. 2014. CD20+inflammatory T-cells are present in blood and brain of multiple sclerosis patients and can be selectively targeted for apoptotic elimination. *Mult Scler Relat Disord,* 3**,** 650-8.

Hultin, L. E., Hausner, M. A., Hultin, P. M., et al. 1993. CD20 (pan-B cell) antigen is expressed at a low level on a subpopulation of human T lymphocytes. *Cytometry,* 14**,** 196-204.

Hurd, E. R. & Giuliano, V. J. 1975. The effect of cyclophosphamide on B and T lymphocytes in patients with connective tissue diseases. *Arthritis Rheum,* 18**,** 67-75.

Ilyas, A. A., Chen, Z. W. & Cook, S. D. 2003. Antibodies to sulfatide in cerebrospinal fluid of patients with multiple sclerosis. *J Neuroimmunol,* 139**,** 76-80.

Inglese, M. 2006. Multiple Sclerosis: New Insights and Trends. *Am J Neurorad,* 27**,** 954-57.

Ingold, K., Zumsteg, A., Tardivel, A., et al. 2005. Identification of proteoglycans as the APRIL-specific binding partners. *J Exp Med,* 201**,** 1375-83.

Irani, D. N. 2016. Regulated Production of CXCL13 within the Central Nervous System. *J Clin Cell Immunol,* 7**,** 460.

Islam, T., Gauderman, W. J., Cozen, W., et al. 2006. Differential twin concordance for multiple sclerosis by latitude of birthplace. *Ann Neurol,* 60**,** 56-64.

Iwasaki, A. & Medzhitov, R. 2015. Control of adaptive immunity by the innate immune system. *Nat Immunol,* 16**,** 343-53.

Jafari, N., Broer, L., Hoppenbrouwers, I. A., et al. 2010. Infectious mononucleosis-linked HLA class I single nucleotide polymorphism is associated with multiple sclerosis. *Mult Scler,* 16**,** 1303-7.

Jego, G., Bataille, R. & Pellat-Deceunynck, C. 2001. Interleukin-6 is a growth factor for nonmalignant human plasmablasts. *Blood,* 97**,** 1817-22.

Jilek, S., Schluep, M., Rossetti, A. O., et al. 2007. CSF enrichment of highly differentiated CD8+ T cells in early multiple sclerosis. *Clin Immunol,* 123**,** 105-13.

Joseph, A. M., Babcock, G. J. & Thorley-Lawson, D. A. 2000. EBV persistence involves strict selection of latently infected B cells. *J Immunol,* 165**,** 2975-81.

Junker, A., Ivanidze, J., Malotka, J., et al. 2007. Multiple sclerosis: T-cell receptor expression in distinct brain regions. *Brain,* 130**,** 2789-99.

Kabat, E. A., Freedman, D. A. & Et Al. 1950. A study of the crystalline albumin, gamma globulin and total protein in the cerebrospinal fluid of 100 cases of multiple sclerosis and in other diseases. *Am J Med Sci,* 219**,** 55-64.

Kabat, E. A., Wolf, A. & Bezer, A. E. 1948. Studies on acute disseminated encephalomyelitis produced experimentally in rhesus monkeys. *J Exp Med,* 88**,** 417-26.

Kanter, J. L., Narayana, S., Ho, P. P., et al. 2006. Lipid microarrays identify key mediators of autoimmune brain inflammation. *Nat Med,* 12**,** 138-43.

Kanzaki, M., Lindorfer, M. A., Garrison, J. C., et al. 1997. Activation of the calcium-permeable cation channel CD20 by alpha subunits of the Gi protein. *J Biol Chem,* 272**,** 14733-9.

Kappos, L., Hartung, H. P., Freedman, M. S., et al. 2014. Atacicept in multiple sclerosis (ATAMS): a randomised, placebo-controlled, double-blind, phase 2 trial. *Lancet Neurol,* 13**,** 353-63.

Kappos, L., Li, D., Calabresi, P. A., et al. 2011. Ocrelizumab in relapsing-remitting multiple sclerosis: a phase 2, randomised, placebo-controlled, multicentre trial. *Lancet,* 378**,** 1779-87.

Kappos, L., Polman, C. H., Freedman, M. S., et al. 2006. Treatment with interferon beta-1b delays conversion to clinically definite and McDonald MS in patients with clinically isolated syndromes. *Neuro,* 67**,** 1242-9.

Kay, A. W., Strauss-Albee, D. M. & Blish, C. A. 2016. Application of Mass Cytometry (CyTOF) for Functional and Phenotypic Analysis of Natural Killer Cells. *Meth Mol Bio,* 1441**,** 13-26.

Kermode, A. G., Thompson, A. J., Tofts, P., et al. 1990. Breakdown of the blood-brain barrier precedes symptoms and other MRI signs of new lesions in multiple sclerosis. Pathogenetic and clinical implications. *Brain,* 113**,** 1477-89.

Khan, N., Hills, R. K., Knapper, S., et al. 2016. Normal Hematopoietic Progenitor Subsets Have Distinct Reactive Oxygen Species, BCL2 and Cell-Cycle Profiles That Are Decoupled from Maturation in Acute Myeloid Leukemia. *PLoS One,* 11**,** e0163291.

Kidd, B. A., Ho, P. P., Sharpe, O., et al. 2008. Epitope spreading to citrullinated antigens in mouse models of autoimmune arthritis and demyelination. *Arthritis Res Ther,* 10**,** R119.

Kim, J. K., Mastronardi, F. G., Wood, D. D., et al. 2003. Multiple sclerosis: an important role for post-translational modifications of myelin basic protein in pathogenesis. *Mol Cell Proteomics,* 2**,** 453-62.

Kinnunen, T., Chamberlain, N., Morbach, H., et al. 2013. Specific peripheral B cell tolerance defects in patients with multiple sclerosis. *J Clin Invest,* 123**,** 2737-41.

Kirkham, P. M., Mortari, F., Newton, J. A., et al. 1992. Immunoglobulin VH clan and family identity predicts variable domain structure and may influence antigen binding. *EMBO J,* 11**,** 603-9.

Klein, C., Lammens, A., Schafer, W., et al. 2013. Epitope interactions of monoclonal antibodies targeting CD20 and their relationship to functional properties. *MAbs,* 5**,** 22-33.

Klein, L., Kyewski, B., Allen, P. M., et al. 2014. Positive and negative selection of the T cell repertoire: what thymocytes see (and don't see). *Nat Rev Immunol,* 14**,** 377-91.

Klein, U., Rajewsky, K. & Kuppers, R. 1998. Human immunoglobulin (Ig)M+IgD+ peripheral blood B cells expressing the CD27 cell surface antigen carry somatically mutated variable region genes: CD27 as a general marker for somatically mutated (memory) B cells. *J Exp Med,* 188**,** 1679-89.

Kowarik, M. C., Cepok, S., Sellner, J., et al. 2012. CXCL13 is the major determinant for B cell recruitment to the CSF during neuroinflammation. *J Neuroinflamm,* 9**,** 93.

Krumbholz, M., Theil, D., Cepok, S., et al. 2006. Chemokines in multiple sclerosis: CXCL12 and CXCL13 up-regulation is differentially linked to CNS immune cell recruitment. *Brain,* 129**,** 200-11.

Ksiazek-Winiarek, D. J., Szpakowski, P. & Glabinski, A. 2015. Neural Plasticity in Multiple Sclerosis: The Functional and Molecular Background. *Neural Plast,* 2015**,** 307175.

Kuenz, B., Lutterotti, A., Ehling, R., et al. 2008. Cerebrospinal Fluid B Cells Correlate with Early Brain Inflammation in Multiple Sclerosis. *PLoS One,* 3**,** e2559.

Kuhle, J., Pohl, C., Mehling, M., et al. 2007. Lack of association between antimyelin antibodies and progression to multiple sclerosis. *N Engl J Med,* 356**,** 371-8.

Kumagai, M., Coustan-Smith, E., Murray, D. J., et al. 1995. Ligation of CD38 suppresses human B lymphopoiesis. *J Exp Med,* 181**,** 1101-10.

Kumar, D. R., Aslinia, F., Yale, S. H., et al. 2011. Jean-Martin Charcot: the father of neurology. *Clin Med Res,* 9**,** 46-9.

Kunkel, E. J. & Butcher, E. C. 2003. Plasma-cell homing. *Nat Rev Immunol,* 3**,** 822-9.

Kurosaki, T., Kometani, K. & Ise, W. 2015. Memory B cells. *Nat Rev Immunol,* 15**,** 149-59.

Laichalk, L. L. & Thorley-Lawson, D. A. 2005. Terminal differentiation into plasma cells initiates the replicative cycle of Epstein-Barr virus in vivo. *J Virol,* 79**,** 1296-307.

Landsverk, O. J., Snir, O., Casado, R. B., et al. 2017. Antibody-secreting plasma cells persist for decades in human intestine. *J Exp Med,* 214**,** 309-17.

Langrish, C. L., Chen, Y., Blumenschein, W. M., et al. 2005. IL-23 drives a pathogenic T cell population that induces autoimmune inflammation. *J Exp Med,* 201**,** 233-40.

Laplaud, D. A., Ruiz, C., Wiertlewski, S., et al. 2004. Blood T-cell receptor beta chain transcriptome in multiple sclerosis. Characterization of the T cells with altered CDR3 length distribution. *Brain,* 127**,** 981-95.

Laschinger, M., Vajkoczy, P. & Engelhardt, B. 2002. Encephalitogenic T cells use LFA-1 for transendothelial migration but not during capture and initial adhesion strengthening in healthy spinal cord microvessels in vivo. *Eur J Immunol,* 32**,** 3598-606.

Lassmann, H., Bruck, W. & Lucchinetti, C. F. 2007. The immunopathology of multiple sclerosis: an overview. *Brain Pathol,* 17**,** 210-8.

Laurence, M. & Benito-Leon, J. 2017. Epstein-Barr virus and multiple sclerosis: Updating Pender's hypothesis. *Mult Scler Relat Disord,* 16**,** 8-14.

Legroux, L. & Arbour, N. 2015. Multiple Sclerosis and T Lymphocytes: An Entangled Story. *J Neuroimmune Pharmacol,* 10**,** 528-46.

Lehmann-Horn, K., Sagan, S. A., Bernard, C. C., et al. 2015. B-cell very late antigen-4 deficiency reduces leukocyte recruitment and susceptibility to central nervous system autoimmunity. *Ann Neurol,* 77**,** 902-8.

Lenercept MS Study Group, 1999. TNF neutralization in MS: results of a randomized, placebo-controlled multicenter study. The Lenercept Multiple Sclerosis Study Group and The University of British Columbia MS/MRI Analysis Group. *Neuro,* 53**,** 457-65.

Lesley, R., Xu, Y., Kalled, S. L., et al. 2004. Reduced competitiveness of autoantigen-engaged B cells due to increased dependence on BAFF. *Immunity,* 20**,** 441-53.

Levin, M. C., Lee, S., Gardner, L. A., et al. 2013. Autoantibodies to Non-myelin Antigens as Contributors to the Pathogenesis of Multiple Sclerosis. *J Clin Cell Immunol,* 4**,** 10.4172/2155-9899.1000148.

Li, R., Rezk, A., Miyazaki, Y., et al. 2015. Proinflammatory GM-CSF–producing B cells in multiple sclerosis and B cell depletion therapy. *Sci Trans Med,* 7**,** 310ra166-310ra166.

Liang, Y., Buckley, T. R., Tu, L., et al. 2001. Structural organization of the human MS4A gene cluster on Chromosome 11q12. *Immunogen,* 53**,** 357-368.

Liddelow, S. A. 2011. Fluids and barriers of the CNS: a historical viewpoint. *Fluids Barriers CNS,* 8**,** 2.

Ligocki, A. J., Lovato, L., Xiang, D., et al. 2010. A unique antibody gene signature is prevalent in the central nervous system of patients with multiple sclerosis. *J Neuroimmunol,* 226**,** 192-3.

Lincoln, M. R., Montpetit, A., Cader, M. Z., et al. 2005. A predominant role for the HLA class II region in the association of the MHC region with multiple sclerosis. *Nat Genet,* 37**,** 1108-12.

Lindsey, J. W., Hatfield, L. M. & Vu, T. 2010. Epstein-Barr virus neutralizing and early antigen antibodies in multiple sclerosis. *Eur J Neurol,* 17**,** 1263-9.

Linington, C., Bradl, M., Lassmann, H., et al. 1988. Augmentation of demyelination in rat acute allergic encephalomyelitis by circulating mouse monoclonal antibodies directed against a myelin/oligodendrocyte glycoprotein. *Am J Path,* 130**,** 443-454.

Link, H. & Zettervall, O. 1970. Multiple sclerosis: disturbed kappa: lambda chain ratio of immunoglobulin G in cerebrospinal fluid. *Clin Exp Immunol,* 6**,** 435-8.

Lloyd, T. E., Christopher-Stine, L., Pinal-Fernandez, I., et al. 2016. Cytosolic 5′-Nucleotidase 1A As a Target of Circulating Autoantibodies in Autoimmune Diseases. *Arthritis Care Res* 68**,** 66-71.

Louveau, A., Harris, T. H. & Kipnis, J. 2015a. Revisiting the Mechanisms of CNS Immune Privilege. *Trends Immunol,* 36**,** 569-77.

Louveau, A., Smirnov, I., Keyes, T. J., et al. 2015b. Structural and functional features of central nervous system lymphatics. *Nature,* 523**,** 337-41.

Lovato, L., Willis, S. N., Rodig, S. J., et al. 2011. Related B cell clones populate the meninges and parenchyma of patients with multiple sclerosis. *Brain,* 134**,** 534-41.

Lovett-Racke, A. E., Yang, Y. & Racke, M. K. 2011. Th1 versus Th17: are T cell cytokines relevant in multiple sclerosis? *Biochim Biophys Acta,* 1812**,** 246-51.

Lucchinetti, C., Bruck, W., Parisi, J., et al. 2000. Heterogeneity of multiple sclerosis lesions: implications for the pathogenesis of demyelination. *Ann Neurol,* 47**,** 707-17.

Lund, F. E. 2008. Cytokine-producing B lymphocytes – key regulators of immunity. *Curr Opin Immunol,* 20**,** 332-8.

Luo, Z., Ronai, D. & Scharff, M. D. 2004. The role of activation-induced cytidine deaminase in antibody diversification, immunodeficiency, and B-cell malignancies. *J Allergy Clin Immunol,* 114**,** 726-35.

Luzina, I. G., Keegan, A. D., Heller, N. M., et al. 2012. Regulation of inflammation by interleukin-4: a review of "alternatives". *J Leukoc Biol,* 92**,** 753-64.

Lyons, J. A., Ramsbottom, M. J. & Cross, A. H. 2002. Critical role of antigen-specific antibody in experimental autoimmune encephalomyelitis induced by recombinant myelin oligodendrocyte glycoprotein. *Euro J Immunol,* 32**,** 1905-13.

Macallan, D. C., Wallace, D. L., Zhang, Y., et al. 2005. B-cell kinetics in humans: rapid turnover of peripheral blood memory cells. *Blood,* 105**,** 3633-40.

Macauley, M. S. & Paulson, J. C. 2014. Siglecs induce tolerance to cell surface antigens by BIM-dependent deletion of the antigen-reactive B cells. *J Immunol,* 193**,** 4312-21.

Macrez, R., Stys, P. K., Vivien, D., et al. 2016. Mechanisms of glutamate toxicity in multiple sclerosis: biomarker and therapeutic opportunities. *Lancet Neurol,* 15**,** 1089-102.

Mader, S., Gredler, V., Schanda, K., et al. 2011. Complement activating antibodies to myelin oligodendrocyte glycoprotein in neuromyelitis optica and related disorders. *J Neuroinflamm,* 8**,** 184.

Magliozzi, R., Columba-Cabezas, S., Serafini, B., et al. 2004. Intracerebral expression of CXCL13 and BAFF is accompanied by formation of lymphoid follicle-like structures in the meninges of mice with relapsing experimental autoimmune encephalomyelitis. *J Neuroimmunol,* 148**,** 11-23.

Magliozzi, R., Howell, O., Vora, A., et al. 2007. Meningeal B-cell follicles in secondary progressive multiple sclerosis associate with early onset of disease and severe cortical pathology. *Brain,* 130**,** 1089-104.

Magliozzi, R., Howell, O. W., Reeves, C., et al. 2010. A Gradient of neuronal loss and meningeal inflammation in multiple sclerosis. *Ann Neurol,* 68**,** 477-93.

Mahad, D. J., Ziabreva, I., Campbell, G., et al. 2009. Mitochondrial changes within axons in multiple sclerosis. *Brain,* 132**,** 1161-74.

Mahnke, Y. D., Brodie, T. M., Sallusto, F., et al. 2013. The who's who of T-cell differentiation: human memory T-cell subsets. *Eur J Immunol,* 43**,** 2797-809.

Makshakov, G., Nazarov, V., Kochetova, O., et al. 2015. Diagnostic and Prognostic Value of the Cerebrospinal Fluid Concentration of Immunoglobulin Free Light Chains in Clinically Isolated Syndrome with Conversion to Multiple Sclerosis. *PLoS One,* 10**,** e0143375.

Maloney, D. G., Liles, T. M., Czerwinski, D. K., et al. 1994. Phase I clinical trial using escalating single-dose infusion of chimeric anti-CD20 monoclonal antibody (IDEC-C2B8) in patients with recurrent B-cell lymphoma. *Blood,* 84**,** 2457-66.

Mancuso, R., Franciotta, D., Rovaris, M., et al. 2014. Effects of natalizumab on oligoclonal bands in the cerebrospinal fluid of multiple sclerosis patients: a longitudinal study. *Mult Scler,* 20**,** 1900-3.

Mandel, M., Gurevich, M., Pauzner, R., et al. 2004. Autoimmunity gene expression portrait: specific signature that intersects or differentiates between multiple sclerosis and systemic lupus erythematosus. *Clin Exp Immunol,* 138**,** 164-70.

Marcus, J. F. & Waubant, E. L. 2013. Updates on Clinically Isolated Syndrome and Diagnostic Criteria for Multiple Sclerosis. *The Neurohospitalist,* 3**,** 65-80.

Marín, N., Eixarch, H., Mansilla, M. J., et al. 2014. Anti-myelin antibodies play an important role in the susceptibility to develop proteolipid protein-induced experimental autoimmune encephalomyelitis. *Clin Exp Immunol,* 175**,** 202-207.

Market, E. & Papavasiliou, F. N. 2003. V(D)J recombination and the evolution of the adaptive immune system. *PLoS Biol,* 1**,** E16.

Markovic, M., Trajkovic, V., Drulovic, J., et al. 2003. Antibodies against myelin oligodendrocyte glycoprotein in the cerebrospinal fluid of multiple sclerosis patients. *J Neurol Sci,* 211**,** 67-73.

Marques, C. P., Kapil, P., Hinton, D. R., et al. 2011. CXCR3-dependent plasma blast migration to the central nervous system during viral encephalomyelitis. *J Virol,* 85**,** 6136-47.

Márquez, A. C. & Horwitz, M. S. 2015. The Role of Latently Infected B Cells in CNS Autoimmunity. *Frontiers in Immunology,* 6**,** 544.

Maseda, D., Smith, S. H., Dilillo, D. J., et al. 2012. Regulatory B10 cells differentiate into antibody-secreting cells after transient IL-10 production in vivo. *J Immunol,* 188**,** 1036-48.

Mathey, E. K., Derfuss, T., Storch, M. K., et al. 2007. Neurofascin as a novel target for autoantibody-mediated axonal injury. *J Exp Med,* 204**,** 2363-72.

Mathias, A., Perriard, G., Canales, M., et al. 2017. Increased ex vivo antigen presentation profile of B cells in multiple sclerosis. *Mult Scler,* 23**,** 802-9.

Matsumoto, M., Baba, A., Yokota, T., et al. 2014. Interleukin-10-Producing Plasmablasts Exert Regulatory Function in Autoimmune Inflammation. *Immunity,* 41**,** 1040-1051.

Mazzoni, A., Santarlasci, V., Maggi, L., et al. 2015. Demethylation of the RORC2 and IL17A in human CD4+ T lymphocytes defines Th17 origin of nonclassic Th1 cells. *J Immunol,* 194**,** 3116-26.

Mccarron, M. J., Park, P. W. & Fooksman, D. R. 2017. CD138 mediates selection of mature plasma cells by regulating their survival. *Blood,* 129**,** 2749-59.

Medina, F., Segundo, C., Campos-Caro, A., et al. 2002. The heterogeneity shown by human plasma cells from tonsil, blood, and bone marrow reveals graded stages of increasing maturity, but local profiles of adhesion molecule expression. *Blood,* 99**,** 2154-61.

Mei, H. E., Yoshida, T., Sime, W., et al. 2009. Blood-borne human plasma cells in steady state are derived from mucosal immune responses. *Blood,* 113**,** 2461-9.

Melchers, F. 2015. Checkpoints that control B cell development. *J Clin Invest,* 125**,** 2203-10.

Menge, T., Lalive, P. H., Von Büdingen, H. C., et al. 2011. Conformational epitopes of myelin oligodendrocyte glycoprotein are targets of potentially pathogenic antibody responses in multiple sclerosis. *J Neuroinflamm,* 8**,** 161.

Mescher, M. F., Popescu, F. E., Gerner, M., et al. 2007. Activation-induced non-responsiveness (anergy) limits CD8 T cell responses to tumors. *Sem Cancer Biol,* 17**,** 299-308.

Metz, I., Radue, E. W., Oterino, A., et al. 2012. Pathology of immune reconstitution inflammatory syndrome in multiple sclerosis with natalizumab-associated progressive multifocal leukoencephalopathy. *Acta Neuropathol,* 123**,** 235-45.

Metz, I., Weigand, S. D., Popescu, B. F. G., et al. 2014. Pathologic heterogeneity persists in early active multiple sclerosis lesions. *Ann Neurol,* 75**,** 728-38.

Miller, D. H. & Leary, S. M. 2007. Primary-progressive multiple sclerosis. *Lancet Neurol,* 6**,** 903-12.

Miller, F. R. 1931. The induced development and histogenesis of plasma cells. *J Exp Med,* 54**,** 333-47.

Minagar, A. & Alexander, J. S. 2003. Blood-brain barrier disruption in multiple sclerosis. *Mult Scler,* 9**,** 540-9.

Mirshafiey, A. & Kianiaslani, M. 2013. Autoantigens and autoantibodies in multiple sclerosis. *Iran J Allergy Asthma Immunol,* 12**,** 292-303.

Miyazaki, Y. & Niino, M. 2015. Epigenetics in multiple sclerosis. *Clin Exp Neuroimmunol,* 6**,** 49-58.

Mokry, L. E., Ross, S., Ahmad, O. S., et al. 2015. Vitamin D and Risk of Multiple Sclerosis: A Mendelian Randomization Study. *PLoS Med,* 12**,** e1001866.

Molnarfi, N., Schulze-Topphoff, U., Weber, M. S., et al. 2013. MHC class II-dependent B cell APC function is required for induction of CNS autoimmunity independent of myelin-specific antibodies. *J Exp Med,* 210**,** 2921-37.

Monson, N. L., Cravens, P., Hussain, R., et al. 2011. Rituximab Therapy Reduces Organ-Specific T Cell Responses and Ameliorates Experimental Autoimmune Encephalomyelitis. *PLoS One,* 6**,** e17103.

Montalban, X., Hauser, S. L., Kappos, L., et al. 2017. Ocrelizumab versus Placebo in Primary Progressive Multiple Sclerosis. *N Engl J Med,* 376**,** 209-20.

Moosmann, A., Bigalke, I., Tischer, J., et al. 2010. Effective and long-term control of EBV PTLD after transfer of peptide-selected T cells. *Blood,* 115**,** 2960-70.

Morandi, E., Tanasescu, R., Tarlinton, R. E., et al. 2017. The association between human endogenous retroviruses and multiple sclerosis: A systematic review and meta-analysis. *PLoS One,* 12**,** e0172415.

Morbach, H., Eichhorn, E. M., Liese, J. G., et al. 2010. Reference values for B cell subpopulations from infancy to adulthood. *Clin Exp Immunol,* 162**,** 271-9.

Moreland, L. W., Baumgartner, S. W., Schiff, M. H., et al. 1997. Treatment of rheumatoid arthritis with a recombinant human tumor necrosis factor receptor (p75)-Fc fusion protein. *N Engl J Med,* 337**,** 141-7.

Mori, N., Kuwamura, M., Tanaka, N., et al. 2012. Ccdc85c encoding a protein at apical junctions of radial glia is disrupted in hemorrhagic hydrocephalus (hhy) mice. *Am J Pathol,* 180**,** 314-27.

Mueller, D. L. 2010. Mechanisms maintaining peripheral tolerance. *Nat Immunol,* 11**,** 21-7.

Muramatsu, M., Sankaranand, V. S., Anant, S., et al. 1999. Specific expression of activation-induced cytidine deaminase (AID), a novel member of the RNA-editing deaminase family in germinal center B cells. *J Biol Chem,* 274**,** 18470-6.

Murphy, K. M. & Reiner, S. L. 2002. The lineage decisions of helper T cells. *Nat Rev Immunol,* 2**,** 933-44.

Nadel, B. & Feeney, A. J. 1997. Nucleotide deletion and P addition in V(D)J recombination: a determinant role of the coding-end sequence. *Mol Cell Bio,* 17**,** 3768-3778.

Nagele, E. P., Han, M., Acharya, N. K., et al. 2013. Natural IgG autoantibodies are abundant and ubiquitous in human sera, and their number is influenced by age, gender, and disease. *PLoS One,* 8**,** e60726.

Nakayama, S., Yokote, T., Hirata, Y., et al. 2012. Immunohistological analysis in diagnosis of plasma cell myeloma based on cytoplasmic kappa/lambda ratio of CD38-positive plasma cells. *Hematology,* 17**,** 317-20.

Nakayama, T., Fujisawa, R., Izawa, D., et al. 2002. Human B cells immortalized with Epstein-Barr virus upregulate CCR6 and CCR10 and downregulate CXCR4 and CXCR5. *J Virol,* 76**,** 3072-7.

Nemazee, D. 2006. Receptor editing in lymphocyte development and central tolerance. *Nat Rev Immunol,* 6**,** 728-40.

Nemazee, D. A. & Bürki, K. 1989. Clonal deletion of B lymphocytes in a transgenic mouse bearing anti-MHC class I antibody genes. *Nature,* 337**,** 562.

Nociti, V., Frisullo, G., Marti, A., et al. 2010. Epstein-Barr virus antibodies in serum and cerebrospinal fluid from multiple sclerosis, chronic inflammatory demyelinating polyradiculoneuropathy and amyotrophic lateral sclerosis. *J Neuroimmunol,* 225**,** 149-52.

Nowakowski, G. S., Call, T. G., Morice, W. G., et al. 2005. Clinical significance of monoclonal B cells in cerebrospinal fluid. *Cytometry B Clin Cytom,* 63**,** 23-7.

Nutt, S. L., Hodgkin, P. D., Tarlinton, D. M., et al. 2015. The generation of antibody-secreting plasma cells. *Nat Rev Immunol,* 15**,** 160-71.

Nylander, A. & Hafler, D. A. 2012. Multiple sclerosis. *J Clin Invest,* 122**,** 1180-8.

O'connor, K. C., Chitnis, T., Griffin, D. E., et al. 2003. Myelin basic protein-reactive autoantibodies in the serum and cerebrospinal fluid of multiple sclerosis patients are characterized by low-affinity interactions. *J Neuroimmunol,* 136**,** 140-8.

O'connor, K. C., Mclaughlin, K. A., De Jager, P. L., et al. 2007. Self-antigen tetramers discriminate between myelin autoantibodies to native or denatured protein. *Nat Med,* 13**,** 211-7.

O'gorman, C. M. & Broadley, S. A. 2016. Smoking increases the risk of progression in multiple sclerosis: A cohort study in Queensland, Australia. *J Neurol Sci,* 370**,** 219-223.

Obermeier, B., Lovato, L., Mentele, R., et al. 2011. Related B cell clones that populate the CSF and CNS of patients with multiple sclerosis produce CSF immunoglobulin. *J Neuroimmunol,* 233**,** 245-248.

Obermeier, B., Mentele, R., Malotka, J., et al. 2008. Matching of oligoclonal immunoglobulin transcriptomes and proteomes of cerebrospinal fluid in multiple sclerosis. *Nat Med,* 14**,** 688-93.

Odendahl, M., Mei, H., Hoyer, B. F., et al. 2005. Generation of migratory antigen-specific plasma blasts and mobilization of resident plasma cells in a secondary immune response. *Blood,* 105**,** 1614-21.

Okun, E., Mattson, M. P. & Arumugam, T. V. 2010. Involvement of Fc Receptors in Disorders of the Central Nervous System. *NeuroMolecular Medicine,* 12**,** 164-178.

Owens, G. P., Bennett, J. L., Lassmann, H., et al. 2009. Antibodies produced by clonally expanded plasma cells in multiple sclerosis cerebrospinal fluid. *Ann Neurol,* 65**,** 639-49.

Owens, G. P., Kraus, H., Burgoon, M. P., et al. 1998. Restricted use of VH4 germline segments in an acute multiple sclerosis brain. *Ann Neurol,* 43**,** 236-43.

Owens, G. P., Ritchie, A. M., Burgoon, M. P., et al. 2003. Single-Cell Repertoire Analysis Demonstrates that Clonal Expansion Is a Prominent Feature of the B Cell Response in Multiple Sclerosis Cerebrospinal Fluid. *J Immunol,* 171**,** 2725-33.

Owens, G. P., Winges, K. M., Ritchie, A. M., et al. 2007. VH4 Gene Segments Dominate the Intrathecal Humoral Immune Response in Multiple Sclerosis. *J Immunol,* 179**,** 6343-6351.

Pakpoor, J., Disanto, G., Gerber, J. E., et al. 2013. The risk of developing multiple sclerosis in individuals seronegative for Epstein-Barr virus: a meta-analysis. *Mult Scler,* 19**,** 162-6.

Pakpoor, J., Wotton, C. J., Schmierer, K., et al. 2016. Gender identity disorders and multiple sclerosis risk: A national record-linkage study. *Mult Scler*.

Palanichamy, A., Apeltsin, L., Kuo, T. C., et al. 2014a. Immunoglobulin class-switched B cells form an active immune axis between CNS and periphery in multiple sclerosis. *Sci Transl Med,* 6**,** 248ra106.

Palanichamy, A., Jahn, S., Nickles, D., et al. 2014b. Rituximab efficiently depletes increased CD20-expressing T cells in multiple sclerosis patients. *J Immunol,* 193**,** 580-6.

Panitch, H. S., Hirsch, R. L., Haley, A. S., et al. 1987. Exacerbations of multiple sclerosis in patients treated with gamma interferon. *Lancet,* 1**,** 893-5.

Parker Harp, C. R., Archambault, A. S., Sim, J., et al. 2015. B cell antigen presentation is sufficient to drive neuroinflammation in an animal model of multiple sclerosis. *J Immunol,* 194**,** 5077-84.

Paz Soldan, M. M., Warrington, A. E., Bieber, A. J., et al. 2003. Remyelination-promoting antibodies activate distinct Ca2+ influx pathways in astrocytes and oligodendrocytes: relationship to the mechanism of myelin repair. *Mol Cell Neurosci,* 22**,** 14-24.

Pearce, J. M. 2005. Historical descriptions of multiple sclerosis. *Eur Neurol,* 54**,** 49-53.

Pender, M. P. 2003. Infection of autoreactive B lymphocytes with EBV, causing chronic autoimmune diseases. *Trends Immunol,* 24**,** 584-8.

Pender, M. P. 2011. The Essential Role of Epstein-Barr Virus in the Pathogenesis of Multiple Sclerosis. *The Neuroscientist,* 17**,** 351-67.

Pender, M. P. 2017. Safety and clinical improvement in a phase I trial of autologous Epstein–Barr virus-specific T cell therapy in patients with progressive multiple sclerosis. ECTRIMS Online Library.

Pender, M. P., Csurhes, P. A., Burrows, J. M., et al. 2017. Defective T-cell control of Epstein-Barr virus infection in multiple sclerosis. *Clin Trans Immunol,* 6**,** e126.

Pender, M. P., Csurhes, P. A., Pfluger, C. M., et al. 2014. Deficiency of CD8+ effector memory T cells is an early and persistent feature of multiple sclerosis. *Mult Scler,* 20**,** 1825-32.

Pereira, J. P., Kelly, L. M. & Cyster, J. G. 2010. Finding the right niche: B-cell migration in the early phases of T-dependent antibody responses. *Intl Immunol,* 22**,** 413-419.

Perez-Andres, M., Paiva, B., Nieto, W. G., et al. 2010. Human peripheral blood B-cell compartments: a crossroad in B-cell traffic. *Cytometry B Clin Cytom,* 78 Suppl 1**,** S47-60.

Pérez-Cerdá, F., Sánchez-Gómez, M. V. & Matute, C. 2016. The link of inflammation and neurodegeneration in progressive multiple sclerosis. *Mult Scler Demyelin Dis,* 1**,** 9.

Phan, T. G., Paus, D., Chan, T. D., et al. 2006. High affinity germinal center B cells are actively selected into the plasma cell compartment. *J Exp Med,* 203**,** 2419-2424.

Piccio, L., Naismith, R. T., Trinkaus, K., et al. 2010. Changes in B- and T-lymphocyte and chemokine levels with rituximab treatment in multiple sclerosis. *Arch Neurol,* 67**,** 707-14.

Pieper, K., Grimbacher, B. & Eibel, H. 2013. B-cell biology and development. *J Allergy Clin Immunol,* 131**,** 959-71.

Pifferi, S., Cenedese, V. & Menini, A. 2012. Anoctamin 2/TMEM16B: a calcium-activated chloride channel in olfactory transduction. *Exp Physiol,* 97**,** 193-9.

Pikor, N. B., Cupovic, J., Onder, L., et al. 2017. Stromal Cell Niches in the Inflamed Central Nervous System. *J Immunol,* 198**,** 1775-81.

Pinkoski, M. J., Waterhouse, N. J., Heibein, J. A., et al. 2001. Granzyme B-mediated apoptosis proceeds predominantly through a Bcl-2-inhibitable mitochondrial pathway. *J Biol Chem,* 276**,** 12060-7.

Pittock, S. J., Mayr, W. T., Mcclelland, R. L., et al. 2004. Disability profile of MS did not change over 10 years in a population-based prevalence cohort. *Neurology,* 62**,** 601-6.

Pittock, S. J., Reindl, M., Achenbach, S., et al. 2007. Myelin oligodendrocyte glycoprotein antibodies in pathologically proven multiple sclerosis: frequency, stability and clinicopathologic correlations. *Mult Scler,* 13**,** 7-16.

Planas, R., Jelcic, I., Schippling, S., et al. 2012. Natalizumab treatment perturbs memory- and marginal zone-like B-cell homing in secondary lymphoid organs in multiple sclerosis. *Eur J Immunol,* 42**,** 790-8.

Pobezinskaya, Y. L. & Liu, Z. 2012. The role of TRADD in death receptor signaling. *Cell Cycle,* 11**,** 871-6.

Podbielska, M., Banik, N. L., Kurowska, E., et al. 2013. Myelin Recovery in Multiple Sclerosis: The Challenge of Remyelination. *Brain Sciences,* 3**,** 1282-324.

Pollinger, B., Krishnamoorthy, G., Berer, K., et al. 2009. Spontaneous relapsing-remitting EAE in the SJL/J mouse: MOG-reactive transgenic T cells recruit endogenous MOG-specific B cells. *J Exp Med,* 206**,** 1303-16.

Pollok, K., Mothes, R., Ulbricht, C., et al. 2017. The chronically inflamed central nervous system provides niches for long-lived plasma cells. *Acta Neuropathologica Comm,* 5**,** 88.

Polman, C. H., Reingold, S. C., Banwell, B., et al. 2011. Diagnostic criteria for multiple sclerosis: 2010 revisions to the McDonald criteria. *Ann Neurol,* 69**,** 292-302.

Presslauer, S., Milosavljevic, D., Huebl, W., et al. 2014. Kappa free light chains: diagnostic and prognostic relevance in MS and CIS. *PLoS One,* 9**,** e89945.

Puentes, F., Van Der Star, B. J., Boomkamp, S. D., et al. 2017. Neurofilament light as an immune target for pathogenic antibodies. *Immunology,* 152**,** 580-8.

Purohit, B., Ganewatte, E. & Kollias, S. S. 2016. Natalizumab-Related Progressive Multifocal Leukoencephalopathy-Immune Reconstitution Inflammatory Syndrome: A Case Report Highlighting Clinical and MRI Features. *Malay J Med Sci,* 23**,** 91-5.

Puthenparampil, M., Federle, L., Miante, S., et al. 2017. BAFF Index and CXCL13 levels in the cerebrospinal fluid associate respectively with intrathecal IgG synthesis and cortical atrophy in multiple sclerosis at clinical onset. *J Neuroinflamm,* 14**,** 11.

Qin, Y., Duquette, P., Zhang, Y., et al. 1998. Clonal expansion and somatic hypermutation of V(H) genes of B cells from cerebrospinal fluid in multiple sclerosis. *J Clin Invest,* 102**,** 1045-50.

Quintana, F. J., Patel, B., Yeste, A., et al. 2014. Epitope spreading as an early pathogenic event in pediatric multiple sclerosis. *Neurology,* 83**,** 2219-26.

Radbruch, A., Muehlinghaus, G., Luger, E. O., et al. 2006. Competence and competition: the challenge of becoming a long-lived plasma cell. *Nat Rev Immunol,* 6**,** 741-50.

Ragheb, S., Li, Y., Simon, K., et al. 2011. Multiple sclerosis: BAFF and CXCL13 in cerebrospinal fluid. *Mult Scler,* 17**,** 819-29.

Rathbone, E., Durant, L., Kinsella, J., et al. 2018. Cerebrospinal fluid immunoglobulin light chain ratios predict disease progression in multiple sclerosis. *J Neurol Neurosurg Psychiatry*, doi: 10.1136/jnnp-2018-317947.

Rauch, I., Müller, M. & Decker, T. 2013. The regulation of inflammation by interferons and their STATs. *JAK-STAT,* 2**,** e23820.

Reboldi, A., Coisne, C., Baumjohann, D., et al. 2009. C-C chemokine receptor 6-regulated entry of TH-17 cells into the CNS through the choroid plexus is required for the initiation of EAE. *Nat Immunol,* 10**,** 514-23.

Regner, M. & Mullbacher, A. 2004. Granzymes in cytolytic lymphocytes - to kill a killer? *Immunol Cell Biol,* 82**,** 161-169.

Reindl, M., Linington, C., Brehm, U., et al. 1999. Antibodies against the myelin oligodendrocyte glycoprotein and the myelin basic protein in multiple sclerosis and other neurological diseases: a comparative study. *Brain,* 122**,** 2047-56.

Rentzos, M., Cambouri, C., Rombos, A., et al. 2006. IL-15 is elevated in serum and cerebrospinal fluid of patients with multiple sclerosis. *J Neurol Sci,* 241**,** 25-9.

Restorick, S. M., Durant, L., Kalra, S., et al. CCR6+ Th cells in the cerebrospinal fluid of persons with multiple sclerosis are dominated by pathogenic non-classic Th1 cells and GM-CSF-only-secreting Th cells. *Brain, Beha Immun*, 64: 71–9.

Ritchie, A. M., Gilden, D. H., Williamson, R. A., et al. 2004. Comparative analysis of the CD19+ and CD138+ cell antibody repertoires in the cerebrospinal fluid of patients with multiple sclerosis. *J Immunol,* 173**,** 649-56.

Rizzuto, R., Pinton, P., Ferrari, D., et al. 2003. Calcium and apoptosis: facts and hypotheses. *Oncogene,* 22**,** 8619-27.

Rodriguez, M., Siva, A., Ward, J., et al. 1994. Impairment, disability, and handicap in multiple sclerosis: a population-based study in Olmsted County, Minnesota. *Neuro,* 44**,** 28-33.

Rothenberg, E. V., Moore, J. E. & Yui, M. A. 2008. Launching the T-cell-lineage developmental programme. *Nat Rev Immunol,* 8**,** 9-21.

Rounds, W. H., Salinas, E. A., Wilks, T. B., 2nd, et al. 2015. MSPrecise: A molecular diagnostic test for multiple sclerosis using next generation sequencing. *Gene,* 572**,** 191-7.

Rumpold, H., Rhodes, G. H., Bloch, P. L., et al. 1987. The glycine-alanine repeating region is the major epitope of the Epstein-Barr nuclear antigen-1 (EBNA-1). *J Immunol,* 138**,** 593-9.

Russ, B. E., Prier, J. E., Rao, S., et al. 2013. T cell immunity as a tool for studying epigenetic regulation of cellular differentiation. *Front Genet,* 4**,** 218.

Sadler, R. H., Sommer, M. A., Forno, L. S., et al. 1991. Induction of anti-myelin antibodies in EAE and their possible role in demyelination. *J Neurosci Res,* 30**,** 616-24.

Sallusto, F., Geginat, J. & Lanzavecchia, A. 2004. Central memory and effector memory T cell subsets: function, generation, and maintenance. *Annu Rev Immunol,* 22**,** 745-63.

Salou, M., Garcia, A., Michel, L., et al. 2015. Expanded CD8 T-cell sharing between periphery and CNS in multiple sclerosis. *Ann Clin Transl Neurol,* 2**,** 609-22.

Samijn, J. P. A., Te Boekhorst, P. a. W., Mondria, T., et al. 2006. Intense T cell depletion followed by autologous bone marrow transplantation for severe multiple sclerosis. *J Neurol Neurosurg Psychiatry,* 77**,** 46-50.

Samuel, C. E. 2001. Antiviral Actions of Interferons. *Clin Micro Rev,* 14**,** 778-809.

Sandberg, M., Levinson, A. I., Zweiman, B., et al. 1986. B cell activation in multiple sclerosis. *Acta Neuro Scand,* 74**,** 417-24.

Santiago, O., Gutierrez, J., Sorlozano, A., et al. 2010. Relation between Epstein-Barr virus and multiple sclerosis: analytic study of scientific production. *Eur J Clin Microbiol Infect Dis,* 29**,** 857-66.

Sanz, I., Wei, C., Lee, F. E., et al. 2008. Phenotypic and functional heterogeneity of human memory B cells. *Semin Immunol,* 20**,** 67-82.

Sarma, J. V. & Ward, P. A. 2011. The complement system. *Cell Tissue Res,* 343**,** 227-35.

Sawcer, S., Hellenthal, G., Pirinen, M., et al. 2011. Genetic risk and a primary role for cell-mediated immune mechanisms in multiple sclerosis. *Nature,* 476**,** 214-9.

Schluesener, H. J., Sobel, R. A., Linington, C., et al. 1987. A monoclonal antibody against a myelin oligodendrocyte glycoprotein induces relapses and demyelination in central nervous system autoimmune disease. *J Immunol,* 139**,** 4016-21.

Schmidt, H., Williamson, D. & Ashley-Koch, A. 2007. HLA-DR15 haplotype and multiple sclerosis: a HuGE review. *Am J Epidemiol,* 165**,** 1097-109.

Schuh, E., Berer, K., Mulazzani, M., et al. 2016. Features of Human CD3+CD20+ T Cells. *J Immunol,* 197**,** 1111-7.

Schwartz-Albiez, R., Monteiro, R. C., Rodriguez, M., et al. 2009. Natural antibodies, intravenous immunoglobulin and their role in autoimmunity, cancer and inflammation. *Clin Exp Immunol,* 158**,** 43-50.

Schwickert, T. A., Victora, G. D., Fooksman, D. R., et al. 2011. A dynamic T cell–limited checkpoint regulates affinity-dependent B cell entry into the germinal center. *J Exp Med,* 208**,** 1243-1252.

Selmaj, K., Raine, C. S. & Cross, A. H. 1991. Anti-tumor necrosis factor therapy abrogates autoimmune demyelination. *Ann Neurol,* 30**,** 694-700.

Serafini, B., Rosicarelli, B., Franciotta, D., et al. 2007. Dysregulated Epstein-Barr virus infection in the multiple sclerosis brain. *J Exp Med,* 204**,** 2899-912.

Serafini, B., Rosicarelli, B., Magliozzi, R., et al. 2004. Detection of ectopic B-cell follicles with germinal centers in the meninges of patients with secondary progressive multiple sclerosis. *Brain Pathol,* 14**,** 164-74.

Sergott, R. C., Bennett, J. L., Rieckmann, P., et al. 2015. ATON: results from a Phase II randomized trial of the B-cell-targeting agent atacicept in patients with optic neuritis. *J Neurol Sci,* 351**,** 174-8.

Sharpe, A. H. & Pauken, K. E. 2018. The diverse functions of the PD1 inhibitory pathway. *Nat Rev Immunol,* 18**,** 153-67.

Shechter, R., London, A. & Schwartz, M. 2013. Orchestrated leukocyte recruitment to immune-privileged sites: absolute barriers versus educational gates. *Nat Rev Immunol,* 13**,** 206-18.

Shiomi, A., Usui, T. & Mimori, T. 2016. GM-CSF as a therapeutic target in autoimmune diseases. *Inflamm Regen,* 36**,** 8.

Sivalingam, G. N. & Shepherd, A. J. 2012. An analysis of B-cell epitope discontinuity. *Mol Immunol,* 51**,** 304-9.

Sjoberg, R., Mattsson, C., Andersson, E., et al. 2016. Exploration of high-density protein microarrays for antibody validation and autoimmunity profiling. *N Biotechnol,* 33**,** 582-92.

Skulina, C., Schmidt, S., Dornmair, K., et al. 2004. Multiple sclerosis: brain-infiltrating CD8+ T cells persist as clonal expansions in the cerebrospinal fluid and blood. *PNAS USA,* 101**,** 2428-33.

Smith-Garvin, J. E., Koretzky, G. A. & Jordan, M. S. 2009. T cell activation. *Annu Rev Immunol,* 27**,** 591-619.

Smith, K., Shah, H., Muther, J. J., et al. 2016. Antigen nature and complexity influence human antibody light chain usage and specificity. *Vaccine,* 34**,** 2813-20.

Soelberg Sorensen, P. & Sellebjerg, F. 2016. Neurofilament in CSF—A biomarker of disease activity and long-term prognosis in multiple sclerosis. *Mult Scler,* 22**,** 1112-3.

Solling, K., Solling, J. & Romer, F. K. 1981. Free light chains of immunoglobulins in serum from patients with rheumatoid arthritis, sarcoidosis, chronic infections and pulmonary cancer. *Acta Med Scand,* 209**,** 473-7.

Somers, V., Govarts, C., Somers, K., et al. 2008. Autoantibody profiling in multiple sclerosis reveals novel antigenic candidates. *J Immunol,* 180**,** 3957-63.

Song, J., Wu, C., Korpos, E., et al. 2015. Focal MMP-2 and MMP-9 activity at the blood-brain barrier promotes chemokine-induced leukocyte migration. *Cell Rep,* 10**,** 1040-54.

Sorensen, P. S. & Blinkenberg, M. 2016. The potential role for ocrelizumab in the treatment of multiple sclerosis: current evidence and future prospects. *Ther Adv Neurol Dis,* 9**,** 44-52.

Sorensen, P. S., Lisby, S., Grove, R., et al. 2014. Safety and efficacy of ofatumumab in relapsing-remitting multiple sclerosis. *Neuro,* 82**,** 573-581.

Sriram, S., Stratton, C. W., Yao, S., et al. 1999. Chlamydia pneumoniae infection of the central nervous system in multiple sclerosis. *Ann Neurol,* 46**,** 6-14.

Stadanlick, J. E. & Cancro, M. P. 2008. BAFF and the plasticity of peripheral B cell tolerance. *Curr Opin Immunol,* 20**,** 158-61.

Stashenko, P., Nadler, L. M., Hardy, R., et al. 1980. Characterization of a human B lymphocyte-specific antigen. *J Immunol,* 125**,** 1678-85.

Stavnezer, J. & Schrader, C. E. 2014. Ig heavy chain class switch recombination: mechanism and regulation. *J Immunol,* 193**,** 5370-8.

Stenger, S., Hanson, D. A., Teitelbaum, R., et al. 1998. An antimicrobial activity of cytolytic T cells mediated by granulysin. *Science,* 282**,** 121-5.

Stephan, A. B., Shum, E. Y., Hirsh, S., et al. 2009. ANO2 is the cilial calcium-activated chloride channel that may mediate olfactory amplification. *PNAS USA,* 106**,** 11776-81.

Stern, J. N., Yaari, G., Vander Heiden, J. A., et al. 2014. B cells populating the multiple sclerosis brain mature in the draining cervical lymph nodes. *Sci Transl Med,* 6**,** 248ra107.

Stys, P. K., Zamponi, G. W., Van Minnen, J., et al. 2012. Will the real multiple sclerosis please stand up? *Nat Rev Neurosci,* 13**,** 507-14.

Sun, D., Whitaker, J. N., Huang, Z., et al. 2001. Myelin antigen-specific CD8+ T cells are encephalitogenic and produce severe disease in C57BL/6 mice. *J Immunol,* 166**,** 7579-87.

Suzuki, K., Maruya, M., Kawamoto, S., et al. 2010. The sensing of environmental stimuli by follicular dendritic cells promotes immunoglobulin A generation in the gut. *Immunity,* 33**,** 71-83.

Tajouri, L., Mellick, A. S., Ashton, K. J., et al. 2003. Quantitative and qualitative changes in gene expression patterns characterize the activity of plaques in multiple sclerosis. *Brain Res Mol Brain Res,* 119**,** 170-83.

Takahashi, T., Fujihara, K., Nakashima, I., et al. 2007. Anti-aquaporin-4 antibody is involved in the pathogenesis of NMO: a study on antibody titre. *Brain,* 130**,** 1235-43.

Takenoya, F., Kageyama, H., Hirako, S., et al. 2012. Neuropeptide W. *Front Endocrinol,* 3**,** 171.

Tanabe, S. & Yamashita, T. 2018. B-1a lymphocytes promote oligodendrogenesis during brain development. *Nat Neurosci,* 21**,** 506-16.

Tangye, S. G., Ferguson, A., Avery, D. T., et al. 2002. Isotype switching by human B cells is division-associated and regulated by cytokines. *J Immunol,* 169**,** 4298-306.

Tangye, S. G. & Tarlinton, D. M. 2009. Memory B cells: effectors of long-lived immune responses. *Eur J Immunol,* 39**,** 2065-75.

Tawara, N., Yamashita, S., Zhang, X., et al. 2017. Pathomechanisms of anti-cytosolic 5'-nucleotidase 1A autoantibodies in sporadic inclusion body myositis. *Ann Neurol,* 81**,** 512-25.

Tedder, T. F. & Engel, P. 1994. CD20: a regulator of cell-cycle progression of B lymphocytes. *Immunol Today,* 15**,** 450-4.

Tegla, C. A., Cudrici, C., Patel, S., et al. 2011. Membrane attack by complement: the assembly and biology of terminal complement complexes. *Immunol Res,* 51**,** 45-60.

Thompson, A. J., Banwell, B. L., Barkhof, F., et al. 2018. Diagnosis of multiple sclerosis: 2017 revisions of the McDonald criteria. *Lancet Neurol,* 17**,** 162-73.

Thompson, M. R., Kaminski, J. J., Kurt-Jones, E. A., et al. 2011. Pattern Recognition Receptors and the Innate Immune Response to Viral Infection. *Viruses,* 3**,** 920-40.

Thorpe, J. W., Mumford, C. J., Compston, D. A., et al. 1994. British Isles survey of multiple sclerosis in twins: MRI. *J Neurol Neurosurg Psychiatry,* 57**,** 491-6.

Topping, J., Dobson, R., Lapin, S., et al. 2016. The effects of intrathecal rituximab on biomarkers in multiple sclerosis. *Mult Scler Relat Disord,* 6**,** 49-53.

Trocme, C., Gaudin, P., Berthier, S., et al. 1998. Human B lymphocytes synthesize the 92-kDa gelatinase, matrix metalloproteinase-9. *J Biol Chem,* 273**,** 20677-84.

Turvey, S. E. & Broide, D. H. 2010. Chapter 2: Innate Immunity. *J Allergy Clin Immunol,* 125**,** S24-S32.

Uhlen, M., Fagerberg, L., Hallstrom, B. M., et al. 2015. Proteomics. Tissue-based map of the human proteome. *Science,* 347**,** 1260419.

Vafaii, P. & Digiuseppe, J. A. 2014. Detection of B-cell populations with monotypic light chain expression in cerebrospinal fluid specimens from patients with multiple sclerosis by polychromatic flow cytometry. *Cytometry B Clin Cytom,* 86**,** 106-10.

Vajkoczy, P., Laschinger, M. & Engelhardt, B. 2001. Alpha4-integrin-VCAM-1 binding mediates G protein-independent capture of encephalitogenic T cell blasts to CNS white matter microvessels. *J Clin Invest,* 108**,** 557-65.

Valentine, M. A., Cotner, T., Gaur, L., et al. 1987. Expression of the human B-cell surface protein CD20: alteration by phorbol 12-myristate 13-acetate. *PNAS USA,* 84**,** 8085-9.

Van Den Berg, R., Hoogenraad, C. C. & Hintzen, R. Q. 2017. Axonal transport deficits in multiple sclerosis: spiraling into the abyss. *Acta Neuropathol,* 134**,** 1-14.

Van Der Vuurst De Vries, R. M., Mescheriakova, J. Y., Runia, T. F., et al. 2017. Soluble CD27 Levels in Cerebrospinal Fluid as a Prognostic Biomarker in Clinically Isolated Syndrome. *JAMA Neurol,* 74**,** 286-292.

Van Noort, J. M., Baker, D. & Amor, S. 2012. Mechanisms in the development of multiple sclerosis lesions: reconciling autoimmune and neurodegenerative factors. *CNS Neurol Disord Drug Targets,* 11**,** 556-69.

Van Noort, J. M., Bsibsi, M., Gerritsen, W. H., et al. 2010. Alphab-crystallin is a target for adaptive immune responses and a trigger of innate responses in preactive multiple sclerosis lesions. *J Neuropathol Exp Neurol,* 69**,** 694-703.

Van Noort, J. M., Van Sechel, A. C., Bajramovic, J. J., et al. 1995. The small heat-shock protein alpha B-crystallin as candidate autoantigen in multiple sclerosis. *Nature,* 375**,** 798-801.

Van Oosten, B. W., Lai, M., Hodgkinson, S., et al. 1997. Treatment of multiple sclerosis with the monoclonal anti-CD4 antibody cM-T412: results of a randomized, double-blind, placebo-controlled, MR-monitored phase II trial. *Neuro,* 49**,** 351-7.

Van Sechel, A. C., Bajramovic, J. J., Van Stipdonk, M. J., et al. 1999. EBV-induced expression and HLA-DR-restricted presentation by human B cells of alpha B-crystallin, a candidate autoantigen in multiple sclerosis. *J Immunol,* 162**,** 129-35.

Vanderlugt, C. L. & Miller, S. D. 2002. Epitope spreading in immune-mediated diseases: implications for immunotherapy. *Nat Rev Immunol,* 2, 85-95.

Vantourout, P. & Hayday, A. 2013. Six-of-the-best: unique contributions of γδ T cells to immunology. *Nat Rev Immunol,* 13**,** 88-100.

Vargas, D. L. & Tyor, W. R. 2017. Update on disease-modifying therapies for multiple sclerosis. *J Investig Med,* 65**,** 883-91.

Vartanian, T., Li, Y., Zhao, M., et al. 1995. Interferon-gamma-induced oligodendrocyte cell death: implications for the pathogenesis of multiple sclerosis. *Mol Med,* 1**,** 732-43.

Villar, L. M., Costa-Frossard, L., Masterman, T., et al. 2015. Lipid-specific immunoglobulin M bands in cerebrospinal fluid are associated with a reduced risk of developing progressive multifocal leukoencephalopathy during treatment with natalizumab. *Ann Neurol,* 77**,** 447-57.

Villar, L. M., Espino, M., Costa-Frossard, L., et al. 2012. High levels of cerebrospinal fluid free kappa chains predict conversion to multiple sclerosis. *Clin Chim Acta,* 413**,** 1813-6.

Von Budingen, H. C., Harrer, M. D., Kuenzle, S., et al. 2008. Clonally expanded plasma cells in the cerebrospinal fluid of MS patients produce myelin-specific antibodies. *Eur J Immunol,* 38**,** 2014-23.

Von Budingen, H. C., Kuo, T. C., Sirota, M., et al. 2012. B cell exchange across the blood-brain barrier in multiple sclerosis. *J Clin Invest,* 122**,** 4533-43.

Von Glehn, F., Farias, A. S., De Oliveira, A. C., et al. 2012. Disappearance of cerebrospinal fluid oligoclonal bands after natalizumab treatment of multiple sclerosis patients. *Mult Scler,* 18**,** 1038-41.

Voortman, M. M., Stojakovic, T., Pirpamer, L., et al. 2017. Prognostic value of free light chains lambda and kappa in early multiple sclerosis. *Mult Scler,* 23**,** 1496-505.

Voskoboinik, I., Whisstock, J. C. & Trapani, J. A. 2015. Perforin and granzymes: function, dysfunction and human pathology. *Nat Rev Immunol,* 15**,** 388-400.

Vrijenhoek, T., Kraaijeveld, K., Elferink, M., et al. 2015. Next-generation sequencing-based genome diagnostics across clinical genetics centers: implementation choices and their effects. *Euro J Hum Genet,* 23**,** 1142.

Walsh, M. J. & Murray, J. M. 1998. Dual implication of 2',3'-cyclic nucleotide 3' phosphodiesterase as major autoantigen and C3 complement-binding protein in the pathogenesis of multiple sclerosis. *J Clin Invest,* 101**,** 1923-31.

Walsh, M. J. & Tourtellotte, W. W. 1986. Temporal invariance and clonal uniformity of brain and cerebrospinal IgG, IgA, and IgM in multiple sclerosis. *J Exp Med,* 163**,** 41-53.

Wang, H., Kadlecek, T. A., Au-Yeung, B. B., et al. 2010. ZAP-70: an essential kinase in T-cell signaling. *Cold Spring Harb Perspect Biol,* 2**,** a002279.

Wang, H., Wang, K., Zhong, X., et al. 2012. Cerebrospinal Fluid BAFF and APRIL Levels in Neuromyelitis Optica and Multiple Sclerosis Patients During Relapse. *J Clin Immunol,* 32**,** 1007-11.

Wang, S. Z., Dulin, J., Wu, H., et al. 2006. An oligodendrocyte-specific zinc-finger transcription regulator cooperates with Olig2 to promote oligodendrocyte differentiation. *Development,* 133**,** 3389-98.

Wang, W., Singh, S., Zeng, D. L., et al. 2007. Antibody structure, instability, and formulation. *J Pharm Sci,* 96**,** 1-26.

Warnke, C., Stettner, M., Lehmensiek, V., et al. 2015. Natalizumab exerts a suppressive effect on surrogates of B cell function in blood and CSF. *Mult Scler,* 21**,** 1036-44.

Weill, J. C., Weller, S. & Reynaud, C. A. 2009. Human marginal zone B cells. *Annu Rev Immunol,* 27**,** 267-85.

Weissert, R. 2013. The immune pathogenesis of multiple sclerosis. *J Neuroimmune Pharmacol,* 8**,** 857-66.

Wherry, E. J., Blattman, J. N., Murali-Krishna, K., et al. 2003. Viral persistence alters CD8 T-cell immunodominance and tissue distribution and results in distinct stages of functional impairment. *J Virol,* 77**,** 4911-27.

Wilk, E., Witte, T., Marquardt, N., et al. 2009. Depletion of functionally active CD20+ T cells by rituximab treatment. *Arthritis Rheum,* 60**,** 3563-71.

Willinger, T., Freeman, T., Hasegawa, H., et al. 2005. Molecular signatures distinguish human central memory from effector memory CD8 T cell subsets. *J Immunol,* 175**,** 5895-903.

Winges, K. M., Gilden, D. H., Bennett, J. L., et al. 2007. Analysis of multiple sclerosis cerebrospinal fluid reveals a continuum of clonally related antibody-secreting cells that are predominantly plasma blasts. *J Neuroimmunol,* 192**,** 226-34.

Wolak, D. J., Pizzo, M. E. & Thorne, R. G. 2015. Probing the extracellular diffusion of antibodies in brain using in vivo integrative optical imaging and ex vivo fluorescence imaging. *J Control Release,* 0**,** 78-86.

Wright, B. R., Warrington, A. E., Edberg, D. E., et al. 2009. Cellular Mechanisms of CNS Repair by Natural Autoreactive Monoclonal Antibodies. *Arch Neurol,* 66**,** 1456-1459.

Wurth, S., Kuenz, B., Bsteh, G., et al. 2017. Cerebrospinal fluid B cells and disease progression in multiple sclerosis - A longitudinal prospective study. *PLoS One,* 12**,** e0182462.

Xiao, B. G., Linington, C. & Link, H. 1991. Antibodies to myelin-oligodendrocyte glycoprotein in cerebrospinal fluid from patients with multiple sclerosis and controls. *J Neuroimmunol,* 31**,** 91-6.

Xing, Y. & Hogquist, K. A. 2012. T-cell tolerance: central and peripheral. *Cold Spring Harb Perspect Biol,* 4.

Yamazaki, T., Yang, X. O., Chung, Y., et al. 2008. CCR6 regulates the migration of inflammatory and regulatory T cells. *J Immunol,* 181**,** 8391-401.

Yoshida, T., Mei. H., Dorner, T., et al., 2010. Memory B and memory plasma cells. *Immunol Rev,* 237, 117-39.

Yuseff, M. I., Pierobon, P., Reversat, A., et al. 2013. How B cells capture, process and present antigens: a crucial role for cell polarity. *Nat Rev Immunol,* 13**,** 475-86.

Zang, Y. C., Li, S., Rivera, V. M., et al. 2004. Increased CD8+ cytotoxic T cell responses to myelin basic protein in multiple sclerosis. *J Immunol,* 172**,** 5120-7.

Zeman, D., Hradílek, P., Švagera, Z., et al. 2012. Detection of oligoclonal IgG kappa and IgG lambda bands in cerebrospinal fluid and serum with Hevylite™ antibodies. comparison with the free light chain oligoclonal pattern. *Fluids and Barriers of the CNS,* 9**,** 5-5.

Zhang, C., Walker, A. K., Zand, R., et al. 2012. Myelin basic protein undergoes a broader range of modifications in mammals than in lower vertebrates. *J Proteome Res,* 11**,** 4791-802.

Zhang, Q. & Lakkis, F. G. 2015. Memory T Cell Migration. *Frontiers in Immunology,* 6**,** 504.

Zhang, X. & Lu, B. 2012. IL-17 initiates tertiary lymphoid organ formation. *Cell Mol Immunol,* 9**,** 9-10.

Zhang, Y., Garcia-Ibanez, L. & Toellner, K. M. 2016. Regulation of germinal center B-cell differentiation. *Immunol Rev,* 270**,** 8-19.

Zielinski, C. E., Mele, F., Aschenbrenner, D., et al. 2012. Pathogen-induced human TH17 cells produce IFN-gamma or IL-10 and are regulated by IL-1beta. *Nature,* 484**,** 514-8.

Ziemssen, T., De Stefano, N., Sormani, M. P., et al. 2015. Optimizing therapy early in multiple sclerosis: An evidence-based view. *Mult Scler Relat Disord,* 4**,** 460-69.

Zuniga-Pflucker, J. C. 2004. T-cell development made simple. *Nat Rev Immunol,* 4**,** 67-72.

Zupo, S., Rugari, E., Dono, M., et al. 1994. CD38 signaling by agonistic monoclonal antibody prevents apoptosis of human germinal center B cells. *Euro J Immunol,* 24**,** 1218-22.